AN INVESTIGATION OF SOIL CARBON FLUXES AND POOLS IN THE THERMO-SEQUENCE OF MT. TARANAKI FOREST

A thesis presented in partial fulfilment of the requirements for the degree of

Doctor of Philosophy

In Soil Science

At Massey University, Manawatu

New Zealand

IDRI HASTUTY SIREGAR

2023

ABSTRACT

Understanding the relationship between temperature and soil carbon (C) pools and fluxes is a key aspect in determining the feedback of the global C balance to rising temperature. The overall objective of this thesis was to investigate the influence of rising temperature in the net change of soil C stocks and fluxes in a thermo-sequence of Mt. Taranaki and explore the mechanisms underlying this change if any. Taranaki region has a ca. 3.2^{o}C mean annual temperature (MAT) gradient with identical parent material, moisture (constant plant-available moisture), and vegetation type. The soil type under this study is alu-andic Andosol, which is the mineral soil group with the largest C content worldwide and characterised by its abundance in aluminium (Al)-organic matter (OM) complexes (e.g., Al^{3+}-OM and allophane-OM complexes). Yet, there is considerable uncertainty as to how rising temperatures will affect the stability of organo-mineral complexes and their formation. Together with the unique thermo-sequence available across the Taranaki slope, they offer an excellent benchmark for investigating the potential responses of soil C storage to long-term warming.

Firstly, we hypothesised that: (i) temperature rise influences the forms of reactive Al (i.e., short range order (SRO) constituents vs. organo-Al complexes), with a greater abundance of SRO constituents at warmer elevation sites as opposed to organo-Al complexes at colder elevation sites, where the weathering rate is slower; (ii) in warmer conditions, microbial-derived C is favoured, while in cooler conditions, plant fingerprints are more evident; (iii) as a result, the C preservation mechanism along the transect differs, with SRO constituents (and microbial-derived C) being more prevalent at warmer elevation sites and Al cations (and plant-derived C) being more abundant at colder elevation sites. To reveal how climatic and geochemical properties regulate soil C preservation, we conducted a field

survey to investigate the changes in: (i) soil geochemical properties including; soil pH, reactive Al and Fe (i.e., SRO constituents and organo-Al complexes); (ii) total C content, stocks, and fractions, as well as composition of OM along the gradient, in which soils at four elevation sites were sampled down to 85 cm depth. Four sampling sites were selected, with elevations ranging from 512 to 1024 m above sea level (asl) and and a mean annual temperature (MAT) of 7.3, 8.2, 9.1, and 10.5 ^{o}C (referred to as T7, T8, T9, and T10, respectively). The results showed that: (i) at colder elevation sites (T7 and T8), soil profiles were richer in well-preserved plant material and in organo-Al complexes, as opposed to (ii) warmer elevation sites (T9 and T10), which had a more microbial processed C and a higher fraction of protected C forms, along with a greater abundance of SRO Al constituents. The results revealed that climate (particularly temperature rise) and soil geochemistry interacted to regulate soil C preservation. While the study has revealed that the mechanisms that protect OM (particularly at depth) differ across the thermogradient, C stocks do not change with temperature., models projecting soil C changes over time under various climate scenarios should also consider the existing interaction with soil geochemistry (Chapter 3).

After understanding the interaction between soil geochemistry and temperature rise in relation to the soil C preservation mechanism, we investigated the long-term effect of rising temperatures on the soil C fluxes (input and output) in a mature native forest along the thermo-sequence in Mt. Taranaki. We used specific molecular markers to monitor the changes in soil C abundance and composition (i.e., carbohydrates) in order to gain a deeper understanding of the effect of temperature rise on the turnover of soil C. We hypothesised that, in the absence of a water shortage, an increase in temperature would increase forest productivity and litterfall, which in turn would increase soil C inputs; this increase in organic substrate along with higher temperatures would, in turn, generate an additional soil CO_2 efflux;

however, no net C loss would occur as the increased in soil C input would offset the increased soil CO_2 efflux. To test this, soil C pools, plant biomass C pools, soil C fluxes, and soil OM composition (i.e., carbohydrate abundance and composition), at four elevation sites along the Taranaki thermo-sequence were quantified. The outcome of this investigation demonstrated that above- and below-ground biomass C increased ca. 32% (significant at P <.05) when temperatures rose (from T7 to T10). This led to an increase in aboveground litterfall (29%), belowground C input (15%), soil respiration rate (16%, significant at P <.05), and decay intensity (as inferred from the carbohydrate preservation index (CPI)). The study showss that the increase in temperature along this quasi-thermo-sequence at Taranaki increases plant C input through enhanced net primary production, which counteracts soil C loss, resulting in no apparent detrimental effect on soil C storage (Chapter 4). This study highlights the importance of considering plant C input of an entire ecosystem along with soil OM decomposition when investigating the response to temperature rise.

To understand the effect of warming on the temperature sensitivity (Q_{10}) of soil organic matter (OM) decomposition rate along the Taranaki thermo-sequence, we collected soils from four distinct elevation sites with four different depths and incubated them in the laboratory at temperatures of 5, 15, 25, and 35^{o}C for 330 days (Chapter 5). The incubation data were then fitted with a three-component model to generate three C pools with distinct decomposition rates, followed by the calculation of their respective Q_{10} values. Using multivariate analysis, these values were then combined with a complete set of soil geochemical characteristics and OM molecular composition data to gain mechanistic insights into the biogeochemical causes of Q_{10} variations. The results of this study revealed that: (i) Q_{10} of soil OM decomposition is inclined to attenuate over a centennial scale under elevated MAT; and (ii) Q_{10} values of the bulk soil OM and the distinct C pools were differentially regulated by soil C availability, OM

molecular composition, and OM-mineral interactions (Chapter 5). These results suggest that temperature affects the distinct C pools differently; with Q_{10} values having a trend to decrease as temperature increases.All the results obtained in this thesis contribute to provide a mechanistic understanding about the effect of rising temperatures on soil C fluxes, and stocks as well as the underlying mechanism governing them, in order to accurately anticipate soil C dynamics in response to global warming.

ACKNOWLEDGMENTS

Praise upon Allah SWT for giving me the opportunity to pursue a doctorate at Massey University in New Zealand. I wouldn't have been able to get to this point without His blessing, affection, and help.

My deepest gratitude to my beloved parents, late Linen Siregar and Tinur Rohma Harahap, for your endless affection and prayers for me. Without your blessing, I would not have gotten here.

My sincere thanks to my main supervisor, Prof. Marta Camps-Arbestain, for your excellent supervision, constructive suggestions, and never-ending encouragement. The way you appreciate every little step I've taken is a very valuable motivator for me to complete my education.

My sincere thanks to my co-supervisor, Assoc. Prof. Gabor Kereszturi, for your kindness, patience, and sincerity in sharing knowledge with me. I also would like to thank you for all of your assistance during my field work.

My sincere thanks to my co-supervisor, Dr. Miko U.F. Kirschbaum, for your dedication to improving my knowledge. Your time and door are always open, and even when we meet informally, you are always enthusiastic to discuss my study.

My sincere thanks to my co-supervisor, Assoc. Prof. Alan Palmer, for your attention, motivation, and sincerity in sharing knowledge with me. You are always concerned with the development of my thesis.

My sincere thanks to my co-supervisor, Prof. Tao Wang, for your great support, sincerity, enthusiasm, and constructive ideas during my writing stage.

To all my supervisors, words are not enough to describe my gratitude. God blessed me with all of you as my supervisors. I not only gain knowledge from you, but also good values and attitudes in life that enrich my character.

My special thanks go to the New Zealand Aid Scholarship (NZAS) program for awarding me a Doctoral Scholarship.

I am also indebted to Joeri Kaal (Pyrolyscience, Santiago de Compostela, Spain) for assistant with the pyrolysis-gas chromatography/mass spectrometry.

My sincere acknowledge is extended to Dr. Qinhua Shen, Mr. Ian Furkert, Mr. Bob Toes, Dr. Neha Jha, Dr. Jim Chen for the guidance they provided me with the laboratory work.

My special thanks to Ernest Osei-Asante, almost two years we have always been hand in hand, we did a lot of work together and we shared many enjoyable times and experiences.

My special thanks to my two kind-hearted friends, Yang Li and Stanislav Aleksandrovich Garbuz, for your generosity in sharing knowledge and guidance in the laboratory work.

My big thanks also go to all of my colleagues: Chao Kong, Akinson Tumbure, Nilusha Ubeynarayana, Dhani Fadlullah Ramadhani, Romana Mbya, and many others. We shared a wonderful moments during our PhD student life.

My special thanks to the Indonesian community in Palmerston North for making me feel at home while I was there.

My special thanks to Jamie Hooper and the entire international student officer for the great work in assisting us during our study in Massey University.

Last but not least, my gratitude also extends to my husband, who always supports my progress. Thank you to my late grandfather, my younger siblings, and all of my extended family for the endless love, prayers, and support.

PUBLICATION AND PRESENTATIONS

Publication under review/to be submitted

1. **Idri Hastuty Siregar**, Marta Camps-Arbestain, Gabor Kereszturi, Alan Palmer, Miko U.F. Kirschbaum, Tao Wang. The control of soil geochemistry and temperature on soil carbon of volcanic soils under a temperate native forest (To be submitted).

2. **Idri Hastuty Siregar**, Marta Camps-Arbestain, Tao Wang, Miko U.F. Kirschbaum, Gabor Kereszturi, Alan Palmer. Higher temperature accelerates the fluxes of soil organic carbon in a mature montane forest without decreasing soil carbon stocks (To be submitted).

3. **Idri Hastuty Siregar**, Ernest Osei-Asante, Marta Camps-Arbestain, Miko U.F. Kirschbaum, Tao Wang, Gabor Kereszturi, Alan Palmer. Temperature sensitivity of soil organic matter decomposition across a thermos-sequence in a temperate montane forest (To be submitted).

Abstracts/proceedings and posters/presentations in Conference/Workshop

1. **Idri Hastuty Siregar**, Marta Camps-Arbestain, Qinhua Shen, Gabor Kereszturi, Miko U.F. Kirschbaum (2018). The control of soil geochemistry and temperature on soil carbon of volcanic soils under a temperate native forest. In 'School of Agriculture and Environment Symposium 2018 (Massey University, Palmerston North, New Zealand).

2. **Idri Hastuty Siregar**, Marta Camps-Arbestain, Qinhua Shen, Gabor Kereszturi, Miko U.F. Kirschbaum (2018). The control of soil geochemistry and temperature on soil carbon of volcanic soils under a temperate native forest. In 'NZ Society of Soil Science Conference 2018' (NZSSS: Napier, New Zealand).

3. **Idri Hastuty Siregar**, Marta Camps-Arbestain, Miko U.F. Kirschbaum, Gabor Kereszturi, Alan Palmer (2019). Higher temperature accelerates the fluxes of soil organic carbon in a mature montane forest without decreasing soil carbon stocks. In 'School of Agriculture and Environment Symposium 2019' (Massey University, Palmerston North, New Zealand).

TABLE OF CONTENTS

LIST OF TABLE AND FIGURES

among the four sites at the same depth, whereas lowercase letters indicate differences among the four different soil depths at the same site. Different letters denote a significant difference according to one-way ANOVA followed by Tukey's test (P <.05). Error bars represent the standard error of the means (n = 4).

Figure 3.3 (A) The average total C content at each sampling site and depth, and (B) cumulative soil C stocks at four different depths across sites along the Taranaki gradient. Capital letters indicate differences among the four distinct sites at the same depth, whereas lowercase letters indicate differences among the four different soil depths at the same site. Different letters denote a significant difference according to one-way ANOVA followed by Tukey's test (P <.05). Error bars represent the standard error of the means (n = 4).

Figure 3.4 The carbon fraction of total C content after demineralisation with 2% HF solution: (A) $C_{HF\text{-}residuum}$ and (B) $C_{HF\text{-}mobile}$/total C in across sites and depths along the Taranaki gradient. Capital letters indicate differences among the four sites at the same depth, whereas lowercase letters indicate the differences among the four different soil depths at the same site. Different letters denote a significant difference according to one-way ANOVA followed by Tukey's test (P <.05). Error bars represent the standard error of the means (n = 4).

Figure 3.5 Linear regression by depth (excluding the top 10 cm) across sites for: (A) total C content vs. Al_{py}, (B) $C_{HF\text{-}residuum}$ vs. Al_{py}, and (C) $C_{HF\text{-}mobile}$ vs. Al_{ox}. The square, diamond, and triangle indicate depth levels of 10–30 cm, 30–50 cm, and 50–85 cm, respectively; blue, green, yellow, and red indicate the sampling sites (T7, T8, T9, and T10, respectively). The black line is the regression line for all data points < 10 cm.

Figure 3.6 Distribution of the groups of the products of pyrolysis (pyrolysis-gas chromatography–mass spectrometry) along the altitudinal gradient on Taranaki. Capital letters indicate the differences among the four sites at the same depth, whereas lowercase letters indicate the differences among the four different soil depths at the same site. Different letters denote a significant difference according to one-way ANOVA followed by Tukey's test (P <.05). Error bars represent the standard error of the means (n = 3).

Figure 3.7 (A) The loading of soil chemical properties including the C fractions ($C_{HF\text{-}residuum}$, $C_{HF\text{-}mobile}$, and C_{py}) on the axes of PC1 and PC2 and (B) the factor scores of the data on the axes of PC1 and PC2 from all sampling sites and depths. The circle, rectangle, diamond, and triangle indicate depth levels of 0–10 cm, 10–30 cm, 30–50 cm, and 50–85 cm, respectively. Blue, green, yellow, and red indicate sites T7, T8, T9, and T10, respectively.

Figure 3.8 PC3 scores of the pyrolysis GC/MS compounds along the altitudinal gradient on Taranaki. Capital letters indicate the differences among the four sites at the same depth, whereas lowercase letters indicate the differences among the four different soil depths at the same site. Different letters denote a significant difference according to one-way

ANOVA followed by Tukey's test (P <.05). Error bars represent the standard error of the means (n = 3).

Figure S3.2.1 The average of the soil pH at each sampling site and depth. Capital letters indicate the comparison of four distinct sites at the same depth, whereas small letters indicate the comparison of four different soil depths at the same site. Different letters denote a significant difference according to one-way ANOVA followed by Tukey's test (P <.05). Error bars represent the standard error of the means (n = 4).

Figure S3.2.2 The average C:N ratio of (A) bulk soil and (B) $C_{HF\text{-}residuum}$ at each sampling site and depth. Capital letters indicate the comparison of four distinct sites at the same depth, whereas small letters indicate the comparison of four different soil depths at the same site. Different letters denote a significant difference according to one-way ANOVA followed by Tukey's test (P <.05). Error bars represent the standard error of the means (n = 4).

Figure S3.2.3 $C_{HF\text{-}mobile}$ (the organic carbon fraction of total C content that was mobilised by 2% HF solution). Capital letters indicate the comparison of four distinct sites at the same depth, whereas small letters indicate the comparison of four different soil depths at the same site. Different letters denote a significant difference according to one-way ANOVA followed by Tukey's test (P <.05). Error bars represent the standard error of the means (n = 4).

Figure S3.2.4 Pyrophosphate-extractable Carbon (C_{py}) at all sampling sites. Capital letters indicate the comparison of four distinct sites at the same depth, whereas small letters indicate the comparison of four different soil depths at the same site. Different letters denote a significant difference according to one-way ANOVA followed by Tukey's test (P <.05). Error bars represent the standard error of the means (n = 4).

Figure S3.2.5 PC1 and PC2 scores of the Pyrolysis GC/MS compound along the altitudinal gradient on Mount Taranaki. Capital letters indicate the comparison of four distinct sites at the same depth, whereas small letters indicate the comparison of four different soil depths at the same site. Different letters denote a significant difference according to one-way ANOVA followed by Tukey's test (P <.05). Error bars represent the standard error of the means (n = 3).

Figure S3.2.6 Pyrolysis product group distribution (Py-GC-MS) along the altitudinal gradient on Mount Taranaki. Capital letters indicate the comparison of four distinct sites at the same depth, whereas small letters indicate the comparison of four different soil depths at the same site. Different letters denote a significant difference according to one-way ANOVA followed by Tukey's test (P <.05). Error bars represent the standard error of the means (n = 3). MCC=methylene chain compounds (aliphatic OM), MAHs/PAHs=monocyclic/polycyclic aromatic hydrocarbons.

Figure S3.2.7 Linear regression by depth (excluding the top 10 cm) across sites between total C content and $Al_{ox.}$ The coefficient correlation (r), P value (significant at P <.05) and number of replicates (n) are given in the figure in the same colour as the trendline. The rectangle, diamond, and triangle each indicate a depth level: 10–30 cm, 30–50 cm, and 50–85 cm, respectively. The colour s blue, green, yellow, and red indicate the sampling sites T7, T8, T9, and T10, respectively.

Figure S3.2.8 The average of $Al_{ox}+1/2Fe_{ox}$ content at each sampling site and depth. Capital letters indicate the comparison of four distinct sites at the same depth, whereas small letters indicate the comparison of four different soil depths at the same site. Different letters denote the significant difference according to one-way ANOVA followed by Tukey's test (*P* <.05). Error bars represent the standard error of the mean (n = 4).

Figure 4.1 (A) The mean value of aboveground biomass (ABG) and belowground biomass (BGB) C (roots), (B) forest floor C stocks along the thermo-sequence in Taranaki. Different letters denote significant differences among sampling sites according to one-way ANOVA followed by Tukey's test (*P* <.05). Error bars represent the standard error of the mean (n = 4).

Figure 4.2 (A) The relationship between individual values of aboveground litterfall (F_{AC}) and temperature at sampling time (r = 0.77, *P* <.05) measured monthly over a 1-yr research period, (B) the relationship between average monthly F_{AC} and mean annual temperature (MAT) (r = 0.77, *P* <.05) along the thermo-sequence in Taranaki. Different letters denote significant differences among sampling sites according to one-way ANOVA followed by Tukey's test (P <.05). Error bars represent the standard error of the mean (n = 5).

Figure 4.3 (A) Monthly average air temperature (Ta, bottom graph) and soil respiration (Fs, top graph), which mirror the seasonal temperature along the thermo-sequence in Taranaki, with summer (December–February) having the highest value and winter (June–August) having the lowest, (B) monthly relationship between Fs (individual values of replicates) and Ta over a 1-yr research period (r = 0.96, 0.92, 0.89, 0.89 and 0.91 for T7, T8, T9, T10 and all data, respectively; significant at P <.05, (C) monthly mean Fs at each sampling site. Different letters denote significant differences according to one-way ANOVA followed by Tukey's test (*P* <.05). Error bars represent the standard error of the mean (n = 4).

Figure 4.4 The annual average total belowground carbon (F_{BC}) at each sampling site across a ~3.2^{o}C mean annual temperature gradient in Taranaki. Different letters denote significant differences among sampling sites according to one-way ANOVA followed by Tukey's test (*P* <.05). Error bars represent the standard error of the mean (n = 4).

Figure 4.5 (A) Total carbon (C) content and (B) cumulative soil C stocks at four different sites and depths along the thermo-sequence in Taranaki. Different letters denote significant

differences among sampling sites according to one-way ANOVA followed by Tukey's test (P <.05). Error bars represent the standard error of the means (n = 4).

Figure 4.6 Carbohydrates and carbohydrate preservation index (CPI) along the thermo-sequence in Taranaki. Capital letters show a comparison among the four soil depths at the same site, whereas small letters represent a comparison of the four different sites at the corresponding depth. Different letters denote a significant difference according to one-way ANOVA followed by Tukey's test (P <.05). Error bars represent the standard error of the mean of two to four replicates.

Figure 4.7 A summary of the response of a mature native forest ecosystem to an increasing ~3.2^{o}C MAT gradient in Taranaki, New Zealand. Coarse woody debris and dissolved organic C (DOC) leaching are in blue font, indicating that they are considered to be negligible.

Figure S4.1.1 Litterfall trap size 1 m × 1 m was set up at each sampling site.

Figure S4.1.2 (A) Four respiration chambers were inserted ca. 50 mm randomly into the soil (litter layer intact) at each sampling site, (B) A 25 mL syringe was connected to the chamber pipe for taking the gas sampling.

Figure S4.1.3 A temperature logger was installed to record air temperature at a 30 min interval during the research period at each sampling site.

Figure S4.2.1 The average of the C_{H2O} at each sampling site. Different letters denote the significant difference between sampling sites according to one-way ANOVA followed by Tukey's test (P <.05). Error bars represent the standard errors (n = 4).

Figure S4.2.2 Linear regression analysis between Fs and F_{AC}. A linear curve fitted independently to all sampling sites with $Fs = 3.45F_{AC} + 2.49$, r = 0.83, significant at P <.05. The measurement was carried out monthly over a one-year research period.

Figure S4.2.3 The turnover rate of unprotected particulate C (i.e., C that is not associated with the mineral fraction) at each sampling site. Different letters denote the significant difference between sampling sites according to one-way ANOVA followed by Tukey's test (P <.05). Error bars represent the standard errors (n = 4).

Figure 5.1 Soil C effluxes at different sites at a 25^{o}C incubation temperature during 330 days of incubation.

Figure 5.2 Cumulative C efflux (%initial total C content) of soils collected at four different sites and depths across a mean annual temperature gradient. Capital letters indicate differences among the four sites at the same temperature, whereas lowercase letters indicate differences among the four different incubation temperatures at the same site. Different letters denote a significant difference according to one-way ANOVA followed by Tukey's test (P <.05). Error bars represent the standard error of the means (n = 4).

Figure 5.3 The decomposition rates of soil organic matter (OM) of three notional C pools in response to temperature rise in all sampling sites and depths studied. Capital letters indicate the comparison of four distinct sites at the same depth, whereas small letters indicate the comparison of four different soil depths at the same site. Different letters denote the significant difference according to one-way ANOVA followed by Tukey's test (P <.05). Error bars represent the standard error of the mean (n = 4).

Figure 5.4 Temperature sensitivity of cumulative CO_2 efflux ($Q_{10\text{--cum}}$) and the three- pool C fractions ($Q_{10\text{--fast}}$, $Q_{10\text{--intermediate}}$, $Q_{10\text{-slow}}$) measured across sites and depths during a 330-day incubation period. Capital letters indicate the comparison of four distinct sites at the same depth, whereas small letters indicate the comparison of four different soil depths at the same site. Different letters denote the significant difference according to one-way ANOVA followed by Tukey's test (P <.05). Error bars represent the standard error of the mean (n = 4).

Figure S5.1.1 Pictorial representation of the steps: A) Soil sampling to a 40 cm depth at 5 cm intervals, B) Soils in columns ready to be irrigated to bring moisture content to field capacity, C) Soils acclimatised in the dark at room temperature after field capacity and prior to incubation, D) Jar with the soil column and NaOH solution in a P35 plastic vial ready for incubation, E) Samples in incubation temperature/chamber.

Figure S5.2.1 C effluxes from all sampling sites: T7, T8, T9, T10 at four distinct depths during 5, 15, and 35^{o}C incubation temperatures.

Figure S5.2.2 (A) The loading of soil OM composition on the axes of PC1 and PC2 and (B) the factor scores of the data on the axes of PC1 and PC2 across sites and depths along the Taranaki gradient. The circle, rectangle, diamond, and triangle indicate depth levels of 0–5 cm, 10–15 cm, 20–25 cm, and 35–40 cm, respectively. Blue, green, yellow, and red indicate sites T7, T8, T9, and T10, respectively. Methylene chain compounds (MCC), monocyclic aromatic hydrocarbons (MAHs), and polycyclic aromatic hydrocarbons (PAHs)).

LIST OF ABBREVIATIONS

AGB	aboveground biomass
Al	aluminium
Al_{ox}	ammonium oxalate-extractable aluminium
Al_{py}	sodium pyrophosphate-extractable aluminium
BGB	belowground biomass
C	carbon
$C_{HF\text{-}residuum}$	the C recovered in the soil residue after the HF treatment
$C_{HF\text{-}mobile}$	the C fraction mobilised by 2% HF
CO_2	carbon dioxide
C_{py}	sodium pyrophosphate-extractable carbon
OC	organic carbon
CPI	carbohydrate preservation index
CWD	coarse woody debris
DBH	diameter at breast height
DOC	dissolved organic carbon
ESM	equivalent soil mass
F_{AC}	aboveground litterfall
F_{BC}	total belowground carbon allocation
Fe_{ox}	ammonium oxalate-extractable iron

Fe_{py}	sodium pyrophosphate-extractable iron
Fs	CO_2 efflux from the soil surface
GC/MS	gas chromatography mass spectrometry
HF	hydrofluoric acid
MAHs	monocyclic aromatic hydrocarbons
MAT	mean annual temperature
MAP	mean annual precipitation
MCC	methylene chain compounds
MRT	mean residence time
N	nitrogen
NPP	net primary productivity
OC	organic carbon
OM	organic matter
PAHs	polycyclic aromatic hydrocarbons
PCA	principal component analysis
Si_{ox}	ammonium oxalate-extractable silicon
SRO	short-range order
TQPA	total quantified peak area

CHAPTER 1

GENERAL INTRODUCTION

1.1 General background

The terrestrial ecosystem contains ca. 2500 Pg of soil carbon (C) (to a depth of 2 m) and represents the largest terrestrial C reservoir (Lal, 2004). This reservoir is the result of the net balance between soil C inputs and outputs. About 60 Pg of soil C are released to the atmosphere annually through soil surface CO_2 efflux (soil respiration), and this is replenished by approximately the same amount of C through aboveground litterfall and the belowground C flux. The latter includes C as needed for the production and maintenance of roots, mycorrhizae and other symbionts and C released as root exudates, herbivory or biomass turnover (Giardina & Ryan, 2002).

There is a growing confidence that rising temperature can hasten the incoming and outgoing soil C fluxes. Soil respiration seems to respond positively to warming, as many studies have documented short-term (sub-diurnal to decadal) increases in soil organic matter (OM) decomposition with rising temperature (Kirschbaum, 2000; Schuur et al., 2015; Li et al., 2020). In the absence of other limiting factors (e.g., water limitations), net primary production (NPP) also tends to increase with warming because of the elevated atmospheric CO_2 concentration favouring photosynthesis and the increasing release of plant-available nutrients with accelerated mineralisation (Dignac, 2017), with a corresponding increase in the amount of plant-derived C available belowground. If accelerated decomposition outpaces any changes in C input from enhanced plant growth, considerable amounts of C could be lost to the atmosphere, further contributing to global warming. Therefore, understanding the the temperature sensitivity of both plant C input and soil organic matter decomposition is critical (Kirschbaum, 1995). Temperature sensitivity (Q_{10} value) refers to the rate of change in a biological or chemical system in response to a 10°C increase in temperature.

Understanding the temperature sensitivity of bulk soil C and its fractions is critical for determining the feedback between global C balance and rising temperatures (Giardina & Ryan, 2000; Conant et al., 2011; Zhu et al., 2016). Various environmental factors that are temperature sensitive (e.g., soil geochemistry, microbial abundance and community composition, among others) may mask the intrinsic temperature sensitivity of substrate decomposition (Davidson & Janssens, 2006). Temperature sensitivity (Q_{10}) of soil OM decomposition is also influenced by chemical composition, probably increasing for more chemically-resistant soil organic molecules (Conant et al., 2008), but decreasing for C protected by the soil mineral matrix (Ryan & Davidson, 2011). While several mathematical models for projecting soil C stocks have been established, such as RothC and CENTURY, they are not always applicable and may require adjustment for specific sites (Falloon & Smith, 2002). In the Taranaki region – the site where this research was carried out – there is a ~3.2^{o}C mean annual temperature (MAT) gradient under a non-plant limiting precipitation regime (>3000 mm annually). Andosol, the soil type in this volcanic region, is characterised by a high content of short range order (SRO) constituents (e.g., allophane, imogolite, ferrihydrite) and high soil C (i.e., they have andic properties) (Harsh, 2005). The high soil C stocks of these soils are related to the ability of these SRO constituents to interact with soil C, forming organo-mineral complexes, and protect C against decomposition (Kögel-Knabner & Amelung, 2014; Shen, et al., 2018). However, soils with andic properties are also more susceptible to losing C when subjected to environmental/chemical change (Kov, 2017). Moreover, there is a lack of: (i) considerable uncertainty as to how rising temperature will affect the soil geochemistry (particularly, the formation of organo-mineral complexes and their stability) (Conant et al., 2008); (ii) understanding of how temperature rise will affect the C balance

(input and output) in a mature native forest; and (iii) understanding of how warming will affect the temperature sensitivity (Q_{10}) of the soil OM decomposition rate as well as the underlying mechanisms that regulate them. This thesis aimed to fill these research gaps by testing four hypotheses as follows:

- Along the thermal gradient, SRO constituents are more abundant at warmer sites, where the weathering rate is faster.
- Soil C is likely to be more microbially processed at warmer sites than at colder sites, where the chemical composition of OM more closely resembles the chemical composition of the source plant material.
- The mechanisms of C protection differ along the transect, with more C being associated with SRO constituents at warmer sites.
- An increase in temperature under conditions of no water deficit increases above- and belowground plant biomass and litterfall, thereby increasing C inputs to soil, which drives a larger efflux of CO_2 to the atmosphere and, thus, a larger microbial processing of soil C, but does not result in a significant loss of soil C stock, as the increase in soil CO_2 efflux is offset by the increase in soil C input.
- Temperature sensitivity (Q_{10}) of soil OM decomposition decreases as MAT increases due to the smaller relative rise in the fraction of molecules with enough energy to react at higher temperature. Moreover, Q_{10} of different OM components (e.g., carbohydrates, N compounds, lignin, methylene chain compounds (MCC), monocyclic aromatic hydrocarbons (MAHs), and polycyclic aromatic hydrocarbons (PAHs)) differs in response to elevated temperature, with contrasting mechanisms driving the responses. Among them, the fact that an increase in mineral protection of soil OM at warmer sites reduces OM accessibility to microbes.

1.2 Research objectives

The main objective of this thesis is to investigate the effect of temperature rise in the soil C cycling, with special attention to C fluxes, C stocks, fractions, and composition in a thermo-sequence of Taranaki region and explore the mechanisms underlying differences in quantity and quality, if any. Three sub-objectives are associated or derived from the main objective, including the following:

- To investigate the effect of rising temperatures and soil geochemistry as well as their combined effects on soil C stocks, fractions, and composition.
- To conduct a cross-site examination of the generality of previous findings (Giardina et al., 2014) that whole-ecosystem warming accelerates soil C cycling but has no impact on the soil C stocks.
- To investigate the effect of warming on the temperature sensitivity (Q_{10}) of bulk soil OM decomposition rate and the Q_{10} of distinct OM components as well as the underlying mechanisms that govern them.

1.3 Thesis outline

This thesis comprises six chapters in total. Chapters 1 and 2 are the general introduction and literature review, respectively. Chapters 3 to 5 are research chapters, which are to be submitted as journal articles. Chapter 6 is general summary of the whole thesis and potential areas for future research.

Chapter 1 (this chapter) gives a general introduction to the entire thesis, including the background, research hypotheses and objectives, and outline of this dissertation.

Chapter 2 consists of a literature review of: (i) Mt. Taranaki; (ii) An overview of soil C; (iii) The role of soil C as a C sink and source of CO_2 emission; (iv) Soil OM decomposition; (v) Soil C preservation;

(vi) Relationship between temperature and soil C storage, (vii) Approaches to modelling soil OM decomposition, (viii) Conclusions and research gap.

Chapter 3 covers the research carried out to investigate the changes in soil geochemistry existing within the range of ~3.2^{o}C MAT gradient and their influence on soil C stocks, fractions, and composition. The results reveal how the interactions of climatic (particularly temperature) and soil geochemistry regulate the mechanisms through which soil C is stored.

Chapter 4 presents the investigation carried out in that same temperate native forest to examine the long term effect of temperature rise on the C cycling (input and output) as well as to conduct a cross-site examination of the generality of previous findings that whole-ecosystem warming accelerates soil C cycling but has no impact on the soil C stocks. This study shows that increasing the temperature along this quasi-thermo-sequence in Taranaki enhances both plant C input through increased net primary productivity and soil OM decomposition rates, rendering no discernible negative influence on soil C storage..

Chapter 5 presents a laboratory experiment that was conducted to assess the temperature sensitivity (Q_{10}) of bulk soil OM decomposition rate along the gradient in Mt. Taranaki by incubating the soils at 5, 15, 25, and 35^{o}C for 330 days. The incubation data were then fitted to a three-pool C model to determine the decomposition rate of the three notional C pools (fast, intermediate, and slow), which was then used to calculate their Q_{10}. According to the findings of this study, the Q_{10} of bulk soil OM and the Q_{10s} from the three-pool C model tended to drop as MAT increased. The Q_{10} values of the bulk soil OM and the various C pools were found to be variably regulated by soil C availability, OM molecular composition, and OM-mineral interactions using redundancy analysis (RDA) and structural equation modelling (SEM).

Chapter 6 includes a general summary of the whole thesis and suggests some potential areas for future research.

Note that the content of Chapters 3–5 is in the process of being submitted to journals for publication.

CHAPTER 2

LITERATURE REVIEW

2.1 Mt. Taranaki

Mt. Taranaki, also known as Mt. Egmont (hereafter referred to as Taranaki), is the youngest and most southerly volcano of the Taranaki Volcanic Lineament, the largest andesite volcano in New Zealand, and the second-highest mountain in the North Island after Mt. Ruapehu (Neall & Stewart, 1986; Alloway et al., 1995; Zernack et al., 2011). This stratovolcano's summit rises to an elevation of 2518 m above sea level (asl), and its nearly perfect cone shape is interrupted by the parasitic cone of Fanthams Peak on its southern flank (Neall, 1979).

2.1.1 Volcanic history

Taranaki's volcanic history is marked by episodes of cone build up to a critical height or size, followed by a catastrophic structural collapse (Neall & Stewart, 1986; Zernack et al., 2009, 2011). Cone growth is characterised by effusive, lava, and dome-forming volcanism, alternating with periods of very explosive, Plinian to sub-Plinian eruptions every 300–500 years on average, and smaller, Strombolian or vulcanian-style eruptions every 50–80 years (Alloway et al., 1995; Platz et al., 2007; Turner et al., 2011).

Taranaki's volcanic history can be divided into four periods:

- From 200 kilo annum (ka) to 14 ka, 13 edifice collapses sent debris avalanche deposits to the northeast, southeast, and southwest flanks of the current volcano, defining distinct episodes of edifice regrowth (Zernack et al., 2011). Intercalated sediments with the debris avalanche deposit document 12 edifice growth periods, including numerous explosive eruptions that deposited pyroclasts within roughly 20 tephra formations. During the first 130 ka, debris, hyper-concentrated flow deposits (Neall, 1979; Zernack et al., 2011),

shallow marine, water, and fluvial deposits were also deposited during these edifice growth periods (Alloway et al., 2005; Zernack et al., 2011).

- Between 14 and 7 ka, thick fall deposits were produced by sub-Plinian eruptions (Alloway et al., 1995). Concurrent with these occurrences, lahars began to flow down the volcano and the first dated block-and-ash flow deposits were directed to the east and west sides of the current cone (Neall, 1979).
- From <7 ka to about 1000 AD, the volcano entered an effusive phase, which is when the majority of the current cone was formed. Eight tephra formations, whose outcrops can be found in either proximal areas of the volcanic edifice or in the ring-plain, were produced by a variety of sub-Plinian eruptions, some of which produced some of the thickest fall deposits in Taranaki's history (Whitehead, 1976; Alloway et al., 1995).
- The most recent sub-Plinian eruption produced the AD 1655 Burrell Lapilli (Druce, 1966; Neall, 1972), which ejected 1.7 x 10^6 m^3 of block-and-ash flow deposits and surge deposits 150 km east–southeast of the summit vent (Druce, 1966; Platz et al., 2007). It was followed by effusive and small explosive events in 1755–1800 AD, producing the Tahurangi Ash (Druce, 1966; Neall, 1972). These included two block-and-ash flow deposits and surge-producing eruptions. The last known eruption of the volcano is represented by the extrusion of the Sisters dome, which occurred in the crater of Taranaki around the year 1800 (Platz et al., 2012). Tephra deposits are typically thickest near the volcanic vent and thin out as the distance increases (Carey, 2005).

2.1.2. Volcanic soils

The soils on Taranaki have predominantly developed from andesitic tephra. The sample sites are located in temperate broadleaved evergreen forests growing on soils developed on andesitic ash belonging to the Burrell formation (1655 AD), which was deposited over older ash (Aitken et al., 1978) (Figure 2.1). The soils are classified as 'Andosols' by the World Reference Base Classification system and as 'Allophanic' soils by the New Zealand classification system (Hewitt & Shepherd, 1997; World Reference Base, 2015). The term 'Andosol' will be used for this type of soil in this thesis, where possible.

Andosols develop mostly from materials linked to volcanic eruptions, which include pyroclastic materials, volcanic ash, pumice, cinders, lahars, volcanic alluvium, loess, and other volcanic ejecta of all compositions (Mizota & Van Reeuwijk, 1989). In this case, volcanic ash refers to materials with a diameter of <2 mm blown out of the crater during eruptions (Buol et al., 2011). Given the high weather ability of the minerals in these materials, mineral alteration is generally faster than that of crystallization (Chesworth, 2008; Weil & Brady, 2017), leading to the formation of short-range-order constituents (SRO) precipitate (e.g., allophane) and organo-Al complexes, which have a high surface area (Takahashi & Dahlgren, 2016). These surfaces provide sites where organic ligands can attach and become protected from decomposition (Hashizume & Theng, 2007; Parfitt, 2009). This is the reason why these soils have the greatest potential for soil carbon (C) accumulation compared with other mineral soil orders (Dahlgren et al., 2004), reaching up to 200 gC kg^{-1} soil (Nanzyo, 2002). Globally, Andosols cover only about 0.8% of the world's ice-free surface area (McDaniel et al., 2012), but they contain approximately 1.8% of the world's total soil C stocks (Matus et al., 2014; World Reference Base, 2015). Andosols are sometimes divided into two types for management purposes: allophanic Andosols

(dominated by allophane, imogolite, and ferrihydrite) and non-allophanic Andosols (dominated by organo-Al complexes) (Takahashi & Dahlgren, 2016). In general, non-allophanic Andosols exhibit greater acidity and Al toxicity to plants, whereas these become attenuated in allophanic Andosols (Takahashi et al., 2008). These two main Andosol types are commonly classified on the basis of the relative abundance of Al associated with organic ligands within the total reactive Al (as inferred from the ratio of sodium pyrophosphate- extractable aluminium and acid oxalate-extractable aluminium or Al_{py}/Al_{ox}). When $Al_{py}/Al_{ox} < 0.5$, the World Reference Base refers to it as a sil-andic Andosol, whereas the opposite occurs with alu-andic Andosols (FAO et al., 2014). Dahlgren et al. (2004) identified the pH threshold value of 4.9 and the leaching condition as the dividing line between the two development pathways for allophanic and non-allophanic Andosols during pedogenic transformation. At pH values below 4.9, organic acids are the predominant proton donors and outcompete OH^- (whose concentration decreases as the soil acidity increases) for Al and Fe ions, thereby facilitating their complexation (Dahlgren et al., 1993; 2004). In such circumstances, organo-Al complexes form preferentially, which consequently reduces the availability of Al for co-precipitating with Si in order to form SRO constituents such as allophane and imogolite (Takahashi & Dahlgren, 2016). In these soils, at pH values above 4.9 (and thus when organic acidity is low), the Al and Si released during the weathering of aluminosilicates tend to polymerize and precipitate to form SRO aluminosilicates such as allophane and imogolite (Dahlgren et al., 2004). Decomposing organic residues, in turn, tend to be chemically stabilised through interactions with the SRO constituents (Yuan et al., 2000) and are also physically protected within the porous structure generated by the allophane clusters (Chevallier et al., 2010) and within microaggregates in wet environments (Buurman et

al., 2007). In terms of the soil OM chemistry, Buurman et al. (2007), Suárez-Abelenda et al. (2015), and Shen et al. (2018) reported that Andosols had a more abundant fraction of microbially processed C than non-Andosols. The environmental conditions have influenced the degree of Andosol development. Lack of water has influenced the hydrolytic reaction of the parent material and, consequently, the formation of SRO components (Buol et al., 2011). Parfitt & Wilson (1985) studied the development of Andosols in different precipitation regimes and discovered that, with fine-grained rhyolitic tephra as the parent material, Andosols containing allophane were overwhelmingly found in areas with high rainfall (although not high enough to decrease the pH 4.9), whereas halloysite dominated in low-rainfall regions. Andosols require a sufficiently thick layer of volcanic ash to form (Brady & Weil, 2017). As the distance from the crater increases, less material is deposited. The relatively thick layer of material in proximal sites can bury the antecedent surface and form multiple buried profiles, whereas the relatively thin layer of materials at medial and distal deposits from successive eruptions can form composite or aggravating profiles (Lowe & Palmer, 2005). Some Andosols may develop from a parent material other than volcanic material, and these soils are commonly known as "non-volcanic" Andosols (Soil Survey Staff, 1999). Garcia-Rodeja et al. (1987) studied the properties of well-drained soils developed from gabbros, amphibolites, and schists under udic moisture and mesic temperature conditions, and found that these soils had similar characteristics to those of “non-allophanic Andosols”. Similarly, soils with andic properties (but not Andosols *senso stricto*) developed from mica schist with quartzite beds and quartz veins have been described in east central Bhutan (Bäumler et al., 2005). In the South Island of New Zealand, soils with andic properties (but not Andosols *senso stricto*) also developed from quartzo-feldspathic sandstones

and siltstones, which have been reported to be dominated by Al-rich allophane (Lowe & Palmer, 2005).

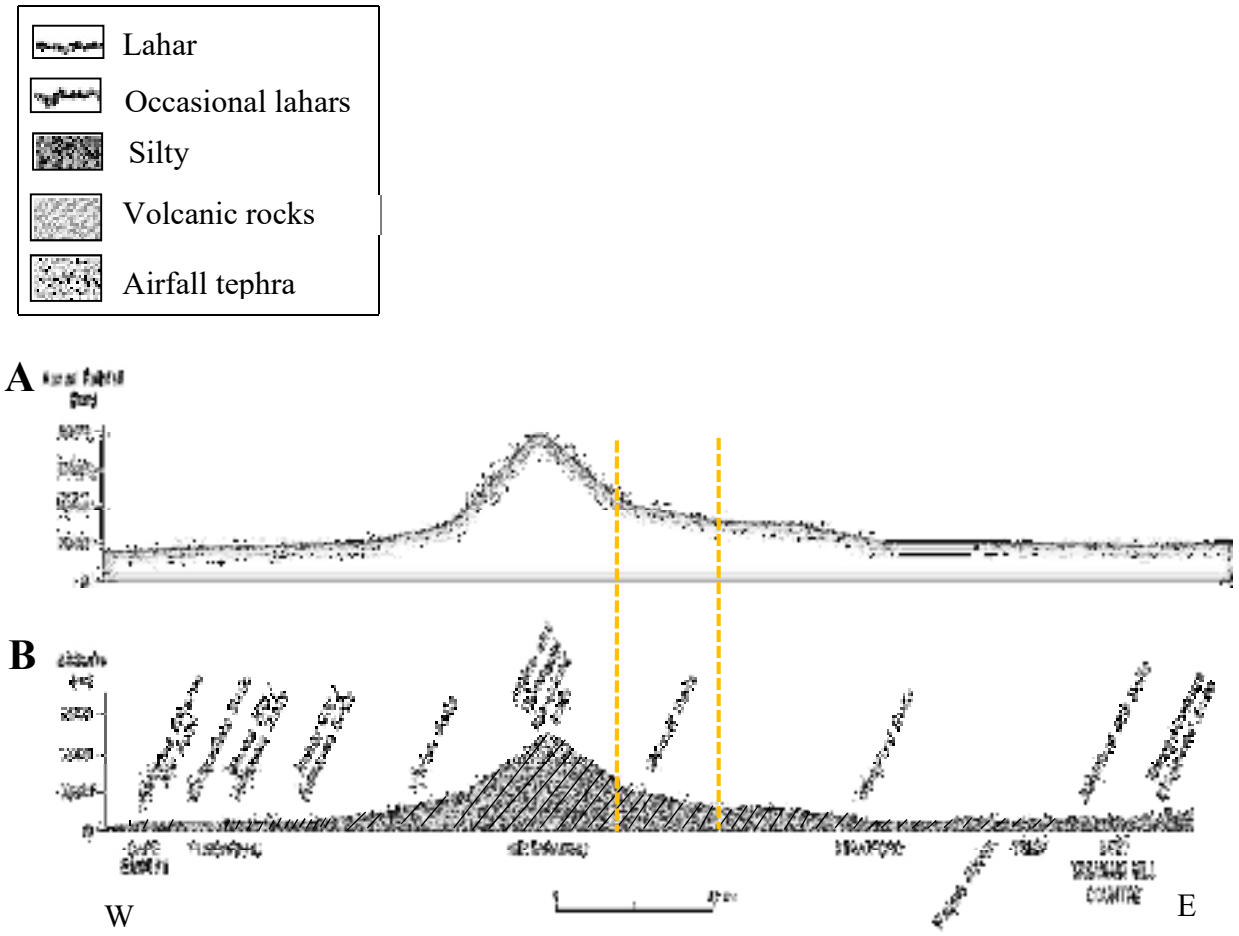

Figure 2.1 (A) Soil and landform and (B) rainfall cross-section from Cape Egmont to the eastern Taranaki hill country. Sampling sites for this study are located in the area between the two dotted yellow lines (source: Molloy, 1988).

2.1.3 Vegetation structures and types

The eruptions of the mountain over the past 10 000 years have led to the development of the present soils and vegetation (Clarkson, 1986). The Burrell Lapilli eruption events destroyed the forest and disrupted the canopy, thus giving rise to secondary successions which were first dominated by *Coriaria pteridoides* W.R.B., but later by dense stands of kamahi (*Weinmannia*

racemosa L.f.). Only in the last 100 years have these *Weinmannia* stands begun to open up, allowing the forest to revert to its pre-eruption state (Mc Glone et al., 1988). In Taranaki, the vegetation changes with altitude. Six major zones are recognized on the eastern flank of Mt. Taranaki, consisting of lowland forest (460–760 m asl), montane forest (760–1100 m asl), subalpine scrub and shrubland (1100–1300 m asl), subalpine and alpine tussock land (1400–1500 m asl) (Clarkson, 1986). Within the forest area (lowland and montane), which is the area which this thesis is focused on, the canopy and emergent species are dominated by native broadleaved evergreen trees such as *Weinmannia*, (almost 80% of the canopy) and, to a less extent, by rata (*Metrosideros robusta* A. Cunn) and tawa (*Beilschmiedia tawa* A. Cunn), whereas mountain totara (*Podocarpus cunninghamii* Colenso) is more abundant at higher altitudes. The understorey trees are mainly mahoe (*Melicytus ramiflorus* J.R. Forst), toro (*Myrsine salicina* Hew. ex Hook), and mountain horopito (*Pseudowintera colorata* (Raoul) Dandy). At higher altitudes, epiphytic filmy ferns (*Hymenophyllum spp.*), mosses, lichen, and liverworts are abundantly found, reflecting the colder and much wetter environment in these sites (Clarkson, 1986).

2.1.4 The reasons why Taranaki was chosen as a study site

Studies on the effect of temperature on soil C cycling and stocks are challenged by the fact that thermo-sequence generally co-vary with other environmental factors (Eliasson et al., 2005; Braakhekke, 2007; Bradford et al., 2008). Appropriate field experiments are challenging to conduct and understand, whereas gradient studies are limited by the inability to control for variables other than temperature (Conant et al., 2011). An attempt to overcome these difficulties was made by Giardina et al. (2014), who investigated changes in the soil C pools and fluxes along a highly constrained mean annual temperature (MAT) gradient (from 13 to 18^{o}C) in the

tropical wet montane forest of Hawaii, where factors other than temperature that affected the ecosystem processes (i.e., soil, vegetation and plant-available soil moisture) were relatively similar. The Taranaki region in New Zealand offers a similar opportunity to that of Giardina et al. (2014). In comparison with Hawaii, Taranaki has a lower MAT gradient range (7.3–10.5^{o}C) under a common and non-limiting precipitation regime (>3000 mm annually) (NIWA, 2022), with a similar soil type (Andosols) and vegetation type (broadleaved evergreen trees) along the gradient. In terms of soil C storage, it has been assumed that the Taranaki Forest region is in a steady state because, with the exception of the Burrell Lapilli eruption (approximately 350 years ago), no studies have documented major damage caused by floods, windstorms, humans, or animals that have dramatically altered the structure of the forest.

Furthermore, the Taranaki sites show a different trend in the changes in soil mineralogy compared with Giardina et al. (2014), with a greater amount of SRO constituents at warmer sites, although this is only apparent below a depth of 30 cm. These differences allowed a cross-site examination of the generalisation of previous findings that whole-ecosystem warming has accelerated soil C cycling but had no impact on the soil C stocks (Giardina et al., 2014), which was the main objective of this study.

The soils in this study are Andosols and are similar to those investigated by Giardina et al. (2014). Andosols are characterised by having a large amount of SRO constituents (e.g., allophane, imogolite, and ferrihydrite) and being rich in C (Litton et al., 2011; Shen et al., 2018). The high C stocks of Andosols are related to the greater ability of these constituents to interact with organic ligands, forming organo-mineral complexes and offering a greater protection against decomposition than soils in which other clay-type constituents are present. Given their large C stocks, they might also have a greater liability than other soils when subject to

environmental changes (Kov et al., 2018; Shen et al., 2018). However, the influence of temperature on soil C cycling and stocks in these soils with abundant organo-mineral complexes is not yet well understood (Conant, Drijiber et al., 2008).

All these factors combine to provide an excellent natural laboratory experiment for studying the influence of altitude-related temperature changes in soil C fluxes and stocks, and also for monitoring the changes in the composition of OM.

2.2 An overview of soil C

2.2.1 Soil C: A component of soil OM

According to the classic concept of soil OM (now outdated), plant litter decomposes into a range of organic compounds, which then recombine to form "humic substances". This framework has being challenged since contemporary analytical techniques have failed to discover “humic substances” (Lehmann & Kleber, 2015). According to the most recent concept (the soil continuum model), soil OM is considered to be a continuum of decaying organic compounds originating from plant inputs (such as leaf litter, roots, and root exudates) and soil organisms (e.g., the biomass and necromass of animals and microorganisms) (Cotrufo et al., 2015; Lefevre et al., 2017) that decompose into smaller and more oxidised water-soluble molecules and then interact with the soil’s reactive surfaces (Lehmann & Kleber, 2015).

Soil OM contains roughly 55–60% C by mass. Except in soils where inorganic forms of soil C are present, this C makes up the majority of the entire soil C stock (FAO & ITPS, 2015). Soil C can be classified into different pools depending on its physical and chemical stability (FAO & ITPS, 2015; O’Rourke et al., 2015):

- Fast pool (labile or active pool): Decomposition results in a large proportion of the initial biomass being lost in 1–2 years after the addition of fresh C to the soil.
- Intermediate pool: C that has been partially stabilised on mineral surfaces and/or protected within aggregates, with turnover times ranging from 10 to 100 years.
- Slow pool (refractory or stable pool): A highly stabilised C that enters a period of very slow turnover, ranging from 100 to >1000 years.

Pyrogenic C is another slow soil C pool, found in many ecosystems and formed from biomass that has been partially carbonised (pyrolysed) during wildfires (Schmidt & Noack, 2000). Some of this material has a highly condensed aromatic chemical structure known as "pyrogenic carbon" or "black carbon" that is resistant to microbial decay and lasts for a long time in soils (Lehmann & Kleber, 2015).

Soil C sequestration and soil health are influenced by the proportion of labile C to total soil C rather than the total C pool itself (Blair et al., 1995; Datta et al., 2010; Duval et al., 2018). Evidence suggests that the labile C fraction can be used as a proxy for other important chemical and physical characteristics of the soil. For instance, the percentage of aggregates smaller than 0.125 mm in the surface crust after laboratory-simulated rain indicated that this fraction was the primary factor controlling aggregate breakdown in ferrosols (non-cracking red clays) (Bell et al., 1998). To date, the temperature sensitivity of the recalcitrant C fraction is an intriguing research topic because it decomposes very slowly while having a greater proportion relative to labile carbon, so that a small increase in C fluxes from this fraction has a significant effect on global warming (Smith et al., 2008).

2.2.2 Soil C: A crucial part of the global carbon cycle

Soil C is a component of the much larger global carbon cycle, which includes C cycling through the soil, vegetation, ocean, and atmosphere. The soil C pool is estimated to store 1700 PgC in the first metre of soil, which is more carbon than contained by the atmosphere (~870 PgC) and terrestrial vegetation (~450 PgC) combined (Figure 2.2) (IPCC, 2021). Therefore, increasing soil C stocks could be a feasible strategy for removing C (0.79–1.54 PgC yr^{-1}) from the atmosphere, thus mitigating climate change (Fuss et al., 2018; Shukla et al., 2019). For this reason, soil C preservation has gained increasing attention in recent years (Paustian et al., 2016; Rumpel et al., 2018; Amelung et al., 2020).

Growing evidence has suggested that increasing temperatures can speed up the influx and outflux of C. The significant impact of rising CO_2 concentrations on the Earth's greening has been highlighted in a recent study (Zhu et al., 2016). Crowther et al. (2016) reported that global soil C stocks will decrease by 30–203 PgC under 1°C of warming. Under Representative Concentration Pathway 6.0 (Pachauri & Meyer, 2014), the global mean surface temperature is predicted to rise by 1.4°C to 3.1°C compared with 1986–2005 by the end of the 21st century if additional CO_2 emissions mitigation measures are not taken. However, it is still unclear to what extent future warming trends will counterbalance or outweigh these influences.

It is exceedingly challenging to predict the cumulative effects of climate change on soils, given the complex interactions among temperature and moisture, increased productivity, and an increased decomposition rate, as well as regional and soil type differences (FAO & ITPS, 2015; Keesstra, 2016). Anthropogenic increases in atmospheric CO_2 may lead to increased net primary productivity (NPP) if nutrient and water shortages do not occur, which is the main source of carbon inputs to the soil. However, increased soil C inputs may ultimately have a negative

feedback on atmospheric CO_2 levels (van Groenigen et al., 2014; Amundson et al., 2015). The theory of progressive nutrient limitation states that the supply of soil nutrients, particularly nitrogen, will limit NPP responses to elevated CO_2. However, it is unclear whether increases in NPP will result in increased soil C storage.

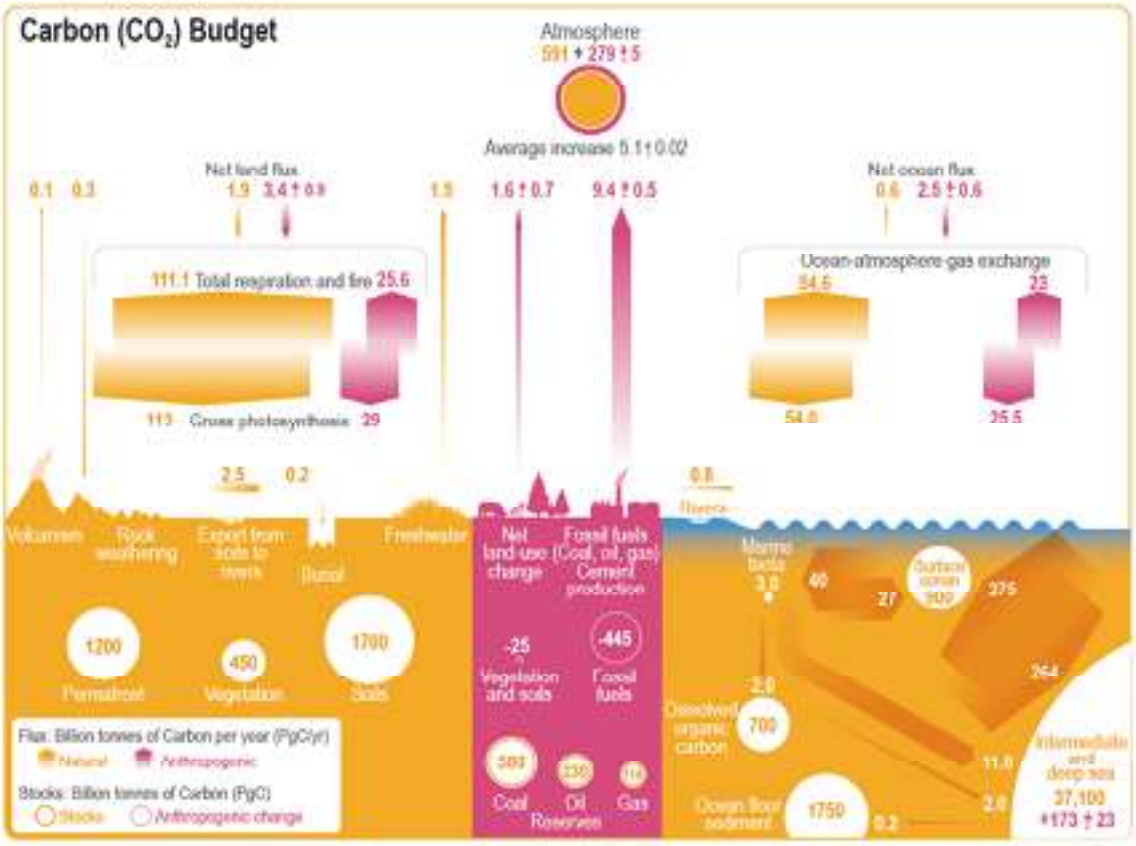

Figure 2.2 Global carbon (CO_2) budget (2010–2019) (IPCC, 2021). Yellow arrows indicate the estimated yearly carbon fluxes (in PgC yr^{-1}) associated with the natural carbon cycle prior to the industrial, around 1750. The pink arrows reflect mean anthropogenic fluxes from 2010 to 2019. The rate of carbon accumulation in the atmosphere is equal to net land-use change emissions, including land management (called LULUCF in the main text) plus fossil fuel emissions, minus land and ocean net sinks (plus a small budget imbalance). Circles with yellow numbers indicate pre-industrial carbon stocks in PgC. Circles with pink numbers indicate anthropogenic changes to these stocks (cumulative anthropogenic fluxes) since 1750.

2.2.3 The role of soil C as a sink and source of CO_2 emissions

Soils can serve as a C sink or source, which is mostly depending on their properties, land use management, and climatic conditions (Eglin et al., 2010; Weissert et al., 2016). Given that global soil C stocks represesent about 1700 PgC for the topmost 1 m (IPCC, 2021), even a small change in the stock of soil C can have a significant impact on the level of CO_2 in the atmosphere. Among anthropogenic sources, land use and the transition from natural to agricultural ecosystems have been and continue to be significant sources of CO_2 emissions. Unsustainable cropping intensification has been found to reduce soil C stocks by 30–60% (Kopittke et al., 2017). In New Zealand, the intensification of dairy pastures has resulted in a decline in the C stocks of Allophanic soils by -1.37 kgC m^{-2} in the top 30 cm of the soil profile and by -0.7 kgC m^{-2} in soil at depth between 30–60 cm (Schipper et al., 2014). On the other hand, agricultural amendments (e.g., organic and inorganic fertiliser applications) are widely recognised to boost crop and pasture yields (Chen et al., 2018), resulting in an increase in C inputs derived from plant tissues (e.g., shoots, reproductive organs, and root biomass) and exudates (Liu, et al., 2018). This increases soil C storage (Chen et al., 2018; Eze et al., 2018; Mathew et al., 2020). It is worth noting that over time only a very small proportion of C inputs become protected in the soil, and this is depending on soil properties and environmental conditions (Castellano et al., 2015). The positive correlation between microbial activity and temperature is anticipated to enhance soil OM decomposition rate, reduce C storage, and exacerbate global warming (Birgander, et al., 2018; Walker et al., 2018). But, on the other hand, warming is known to boost forest production (Grant, 2014) and, consequently, detrital carbon inputs to soils (Lyu et al., 2019; Giardina et al., 2014). Soil geochemistry and physical properties influence below-ground processes, including the processing and stabilisation of organic inputs to soil (Luo et al., 2017).

These complex mechanisms result in inconsistent outcomes within research. To date, the effect of rising temperatures, collectively with environmental factors, on soil OM decomposition remains debatable.

2.3 Soil OM decomposition

Decomposition plays a very significant environmental role and is a key process in soil C and nutrient cycling (Bot & Benites, 2005). Organic matter degradation is mainly mediated by the soil biota and, to a large extent, by microbes, with extracellular enzymes playing a key role in solubilizing soil organic molecules through oxidation and depolymerisation (Li et al., 2015). Once the organic molecules are small enough, microbes can ingest them and use them for growth and energy. Throughout these activities, microorganisms contribute to the release of CO_2 into the atmosphere through respiration (Metcalfe et al., 2011). Through digesting (microbial catabolism) and breaking down (ex vivo modification) plant detritus (the primary external C input) the resulting small plant-derived or freshly generated microbe-derived OM molecules have a higher ability to interact with soil particles (Liang et al., 2017). Interactions with the mineral–soil surface are essential to shelter them from decomposition (Cotrufo et al., 2015; Crowther, Sokol et al., 2015; Kleber et al., 2015).

2.3.1 Plant litter quality and quantity

Differences in the quantity and quality of plant litter and root functional traits (such as root architecture, morphology, physiology, chemical composition, and symbiotic associations) create different effects on soil OM decomposition (Blagodatskaya & Kuzyakov, 2008; Dignac et al., 2017; Hervé et al., 2019). The decomposition rate is faster with organic materials with a low C:N ratio than with a high C:N ratio (Bot & Benites, 2005; dos Reis Martins & Angers, 2015).

Nutrient-rich leaves generally decompose more quickly than woody materials because of their abundance of labile compounds and less complex macromolecules (Reich et al., 1997). Indeed, root litter decomposition is generally 30% slower than leaf decomposition (Birouste et al., 2012; Freschet et al., 2013). Furthermore, only a small amount of aboveground litter is deposited into the mineral soil (Garten, 2009), where interactions with inorganic particles contribute to protecting OM molecules (Garcia-Pausas et al., 2012; Poirier et al., 2014; Prieto et al., 2016). The rate at which OM inputs decompose depends on their quality. The chemical composition (e.g., N content, lignin) of above- and belowground litter inputs, as well as root exudates, varies considerably among plant species and affects the OM decomposition rate on time scales ranging from a year to a decade (Jones et al., 2009; Machinet et al., 2011; Birouste et al., 2012). It is well known that a high lignin content (as in woody material) is associated with a build-up of particulate C in the soil (Chapin et al., 2011; Cotrufo et al., 2015) and enhances the contribution of plant residue to the intermediate soil C pool.

The initial rate of decomposition of plant residues is typically accelerated by high N levels, which also cause a build-up of microbial residues in the soil. High N levels in plant residues slow down the specific decomposition of lignin as the enzymes needed for its decomposition are released by microbes under no-growth conditions (Dignac et al., 2002; Berg et al., 2010; dos Reis Martins & Angers, 2015).

2.3.2 Soil texture and aeration

Decomposition is mostly regulated by aerobic microorganisms, which require oxygen as an electron acceptor. Loosely structured and well-drained soils allow sufficient air into the soil to enhance the rate of soil OM decomposition, although anoxic conditions can develop at microsites

within aggregates. In compacted soils, clayey soils, and poorly drained soils, the flow of oxygen through soil pores might be impaired, especially after rain (Hervé et al., 2019). In a poorly aerated environment, where anaerobic microbes use weaker electron acceptors, soil OM tends to decompose more slowly and, under very reduced conditions, it may tend to accumulate as the input rate tends to be larger than the output. Soil aeration is increased when the soil is physically disturbed, as this breaks soil aggregates and facilitates the access of O_2 to microbial communities (Haynes, 1986; West & Post, 2002). The texture of the soil significantly affects its aeration, in addition to affecting the presence of the reactive sites to which C attaches and, consequently, the OM decomposition rate. This partially explains why, under similar climate and drainage conditions, the soil C content in fine-textured soils has been found to be around four times larger than that in coarse-textured soils (Power & Prasad, 1997). Fine-textured soils often have a larger amount of organo-mineral complexes than coarse-textured soils, and these complexes make C more resistant to decomposition (Six et al., 2002; Jindaluang et al., 2013). Inaccessibility caused by a narrow pore neck and binding to reactive surfaces limits the supply of decomposable substrate.

2.3.3 Soil pH

Biomass production and soil OM decomposition are impaired by salinity, toxicity, and extreme soil pH values. Highly acidic or alkaline soils provide adverse conditions for microorganisms to flourish, resulting in a decrease in soil OM decomposition rate (Macías & Camps-Arbestain, 2020). However, under such conditions, particularly under highly alkaline conditions, plant growth is also severely impaired and plant detritus input decreases (Primavesi, 1984 as cited in Jungkunst et al., 2012). A low pH promotes the formation of tight inner-sphere bonds between C

and mineral surfaces with a varying charge (e.g., Fe oxides; clay mineral borders, allophane, imogolite). The formation of inner-sphere complexes becomes weaker as the pH increases, favouring the formation of outer-sphere complexes. Moreover, H-bonds linking C and Fe oxides and clay minerals become weaker as the soil pH increases (Kleber et al., 2015).

2.3.4 Soil moisture

At a high moisture content, there is an increase in plant biomass as long as the conditions do not impair root respiration, thus increasing plant residues and the associated soil C (Linn & Doran, 1984; Bot & Benites, 2005). The flux of CO_2 from soils is mostly derived from root and microbial respiration, and both are subject to water constraints. The optimum soil moisture for aerobic microbial activity is typically 60% of field capacity (Linn & Doran, 1984). The decay rate reduces when the moisture content falls below 30–50% of field capacity. Further, drought decreases the thickness of soil water films, thus hampering the diffusion of extracellular enzymes and reducing the supply of substrates at reaction microsites. The decay rate also decreases with a very high moisture content (>100% of field capacity) as a result of O_2 restriction of pore spaces (Haynes, 1986). The diffusion of O_2 in water is 10 000 times lower than that in air, thus causing anaerobic decomposition via smaller and usually slower degradative enzymatic pathways.

2.3.5 Soil clay type

The type of clay in the soil has a major impact on the decomposition of soil OM, and on the mechanisms through which it is preserved, because each type of clay has specific characteristics. A 2:1 clay mineral with an interlayer lattice structure, such as vermiculite, has a large surface area that improves water retention, cation exchange capacity, and aggregate formation and keeps microbial metabolites protected from decomposers; whereas a 1:1 clay, such as kaolinite, has a

low water retention capacity and weakly protects C metabolite from the decomposition process (Fissore et al., 2016). Additionally, highly reactive Al and Fe compounds, such as allophane and ferrihydrite, decrease the decomposition rate of the organic ligands attached to them (Miltner & Zech, 1998).

2.3.6 Weathering

The ability of soils to protect C can differ widely, depending on the degree of soil development (Doetterl et al., 2015). Humid environments under warm conditions favour mineral weathering and the formation of reactive surfaces in young soils (Chaplot, 2010; Doetterl et al., 2016). In the early stages of soil formation (100–3000 yr) in highly weatherable materials, such as basalt, andesite, gabbros, and amphibolites, under humid temperate conditions and free drainage, SRO constituents are formed. In less weatherable parent materials, 2:1 clay mineral form, and their content increases from the early stages to the intermediate stages of weathering (35 000 yr). At the late stages of weathering (300 000–3 000 000 yr), 1:1 mineral is formed as silicon is lost from the system. Nutrient availability is high in young soils and soils at the intermediate stages of weathering and decreases in highly evolved soils. All this has implications for soil C preservation and microbial activity. Moreover, erosion processes can lead to the removal of weathered material, changing the mineral matrix in which biological processes take place as fresh material becomes exposed, and drastically changes the geochemical conditions for C stabilisation (Doetterl et al., 2016). Finally, it should be noted that, at a geological time scale (and also at a shorter time scale in highly weatherable materials), CO_2 has had a key role on mineral weathering through its dissolution in water (and the subsequent formation of carbonic acid). This has been the main driving force controlling the Earth's climate throughout history and

is now being considered as a potential technology for mitigating climate change through enhanced weathering (Hartmann et al., 2013; Beerling et al., 2020).

2.4 Soil C preservation

Carbon is originally fixed from the atmosphere by plants into living C. Its detritus is subsequently modified *ex vivo* and/or biosynthesised *in vivo* by soil biota, and it can be preserved in long-lasting pools in the soil (Lefevre et al., 2017, Liang et al., 2017). Many variables influence this, including the chemical and physical interactions of C with inorganic constituents, and the numerous types of microbial metabolism involved in C turnover (Plaza et al., 2013; Stockmann et al., 2013; Kleber et al., 2015; Liang et al., 2017). At greater depths, decomposition rates may be slower and mean residence durations longer as a result of the decreased ratio of soil C to reactive mineral surfaces, which supports the chemical preservation of soil C (Kane, 2015). In general, C is retained in the soil via the following mechanisms: (i) chemical protection, (ii) physical protection, (iii) intrinsic "chemical recalcitrance" (basically related to the presence of pyrogenic C) (Mikutta et al., 2006; Plaza et al., 2013; Stockmann et al., 2013), and (iv) environmental conditions (e.g., waterlogging conditions) (Six et al., 2006; Kane, 2015).

2.4.1 Selective preservation of recalcitrant OM compounds

A common assumption in older numerical C models was that the stable soil C is composed of organic detritus with inherent "chemical recalcitrance," or resistance to breakdown (Lützow et al., 2006). Historically, it was considered that the litter decomposition rate was inversely correlated with the C/N ratio, lignin content, and lignin/N ratio, and favourably correlated with N concentration (Kleber, 2010). With the exception of carbonised C, there is now strong evidence that, under optimal conditions, the microbial community has the ability to breakdown persistent

compounds more rapidly than was previously believed. The carbonised C is rich in condensed aromatic C and can remain longer in the soil because it is not a favoured substrate for serving the energy requirements of microorganisms (Lehmann and Joseph, 2015; Lehmann and Kleber, 2015). This new perspective on soil C dynamics claims that C persists in soil not due to intrinsic features of C, but rather due to physical, chemical, and biological factors. (Dungait et al., 2012; Kleber, 2010; Schmidt et al., 2011).

2.4.2 Physical protection

Conceptually, soil aggregation and the arrangement of aggregates, according to the aggregate hierarchy model developed by Oades & Waters (1991), are known to limit access of OM decomposers to their substrates (Gregorich & Janzen, 2000). Physical protection occurs when the OM is encapsulated within soil micro- and macroaggregates, rendering them inaccessible to decomposers and, in some cases, reducing the amount of O_2 available (Keiluweit et al., 2017). The accessibility of occluded organic molecules is largely determined by the aggregates' specific surface area and pore characteristics (size, shape, and distribution) (Pulleman & Marinissen, 2004; Dungait et al., 2012). Asano & Wagai (2014) found that in Andosols, aggregates followed the hierarchy model at the micron and submicron levels. This has been supported by the results of Chevallier et al. (2010) and Huang et al. (2016). The latter proved the fractal pore structure (Figure 2.3A) of allophane clusters and the associated pore system that is responsible for entrapping and stabilising C. Filimonova et al. (2016), using xenon isotope and nuclear magnetic resonance technology (^{129}Xe magnetic resonance technology), proposed that the presence of four types of pores in allophane-rich soils was important for C adsorption: Type I or micropores (pores between primary allophane nanospherules; 0.92 nm in diameter), Type II or meso- or

macropores (pores between allophane aggregates), Type III or ultra-micropores (pores of allophane wall perforations; 0.6 nm in diameter), and Type IV (interiors of primary allophane spherule) (Figure 2.3B), although the latter is quite unlikely (Benny Theng, Landcare Research, pers. comm.).

A **B**

Figure 2.3 (A) Schematic illustration of the adsorption model of allophane-rich soil by ^{129}Xe nuclear magnetic resonance showing Type I, Type II, Type III, and Type IV (Filimonova et al., 2016), (B) Adsorption of DNA in the fractal pore structure of allophane spherules (Huang et al., 2016).

2.4.3 Chemical and biochemical protection

The microbial decomposition of the OM adsorbed on mineral surfaces requires greater effort than what is needed to decompose non-adsorbed organic ligands, as pre-existing connections need to be disrupted for microbes to have access to their substrate (Kaiser & Guggenberger, 2003; Oades, 2013). The type of bonding can include ligand exchange reactions, polyvalent cation bridges, H-bonding, and van der Waals interactions (Kaiser & Guggenberger, 2003). Organic ligands chemically interact with mineral surfaces and metal cations to generate organo-mineral complexes that are resistant to microbial degradation. Amorphous constituents (e.g., allophane, Al and Fe oxyhydroxides) with a high surface area and broken end bonds at their

surface edges can form strong bonds with C and chemically protect it against further microbial decomposition (Kögel-Knabner et al., 2008; Kleber et al., 2015; Wagai et al., 2015) (Figure 2.4). The concept behind these interactions postulates the existence of a separate zonal sequence, akin to an "onion-type" structure, in which the strength of chemical bonding decreases as the distance from the mineral surfaces increases (Figure 2.5) (Hargety et al., 2014; Kleber et al., 2015). The formation of connections between C (especially microbially produced N-rich OM) (Possinger et al., 2020; Kopittke et al., 2020) and C-free mineral surfaces happens via strong bonding (e.g., covalent bonding) in the inner zone (the contact zone, Layer 1 in Figure 2.5). The type of interaction shifts from covalent bonds to van der Waals bonding or electrostatic binding in the outer layers (Layer 2 in Figure 2.5), where the cations (e.g., Ca^{2+}, Mg^{2+}, Al^{3+}, and Fe^{3+}) operate as bridges between organic ligands (Kleber et al., 2007). Despite the widespread acceptance of this "membrane-like bilayer" structure, more direct and nanoscale evidence is required to support it.

Biochemical protection is particularly associated with charred materials containing condensed aromatic C formed through the thermal degradation of plant material (Nguyen & Lehmann, 2009). As well as condensed aromaticity, charred soil C can have strong associations and bonding with minerals, making them stable and preventing decomposition (Brodowski et al., 2005). Because of these characteristics, the C in charred soil OM is preserved from decomposition (Swift, 2001).

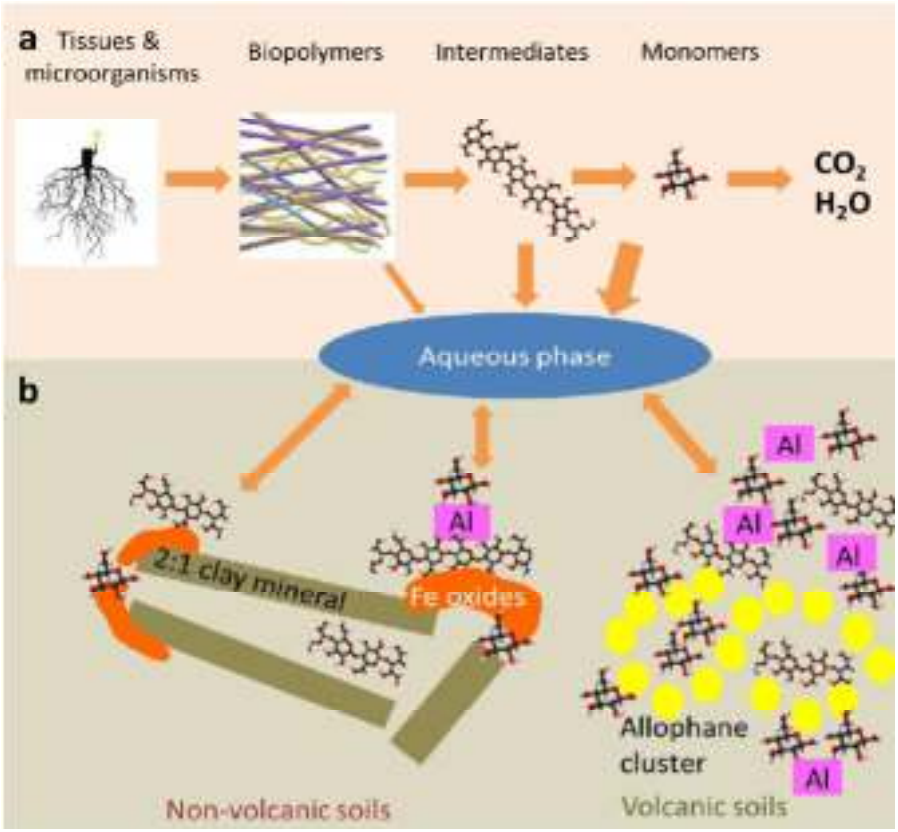

Figure 2.4 Schematic diagram of the formation of organo-mineral associations. (a) Soil continuum model of the nature of soil organic matter. (b) Chemical and physical protection of organic ligands by a mineral or metal (e.g., Al). These are more abundant in soils derived from volcanic materials (e.g., an Andosol, as shown on the right). Source: Marta Camps Arbestain, modified from Kleber et al. (2015).

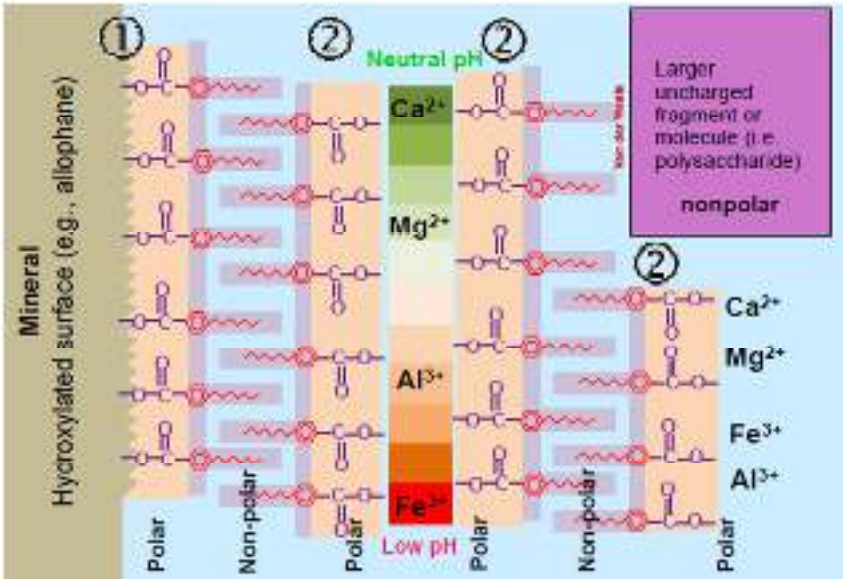

Figure 2.5 The "member-like bilayer model" of organo-mineral/metal interactions. Diagram courtesy of Marta Camps-Arbestain, adapted from Peter Buurman's course (the original authorship is attributed to Markus Kleber).

2.4.4 Soil microorganisms

There is growing evidence that soil microorganisms are crucial to the preservation of soil C, as (i) microbial extracellular enzymes attack and degrade plant litter, the major external source of C, into smaller and more soluble plant-derived OM molecules (microbial catabolism, *ex vivo* modification), and (ii) microorganisms degrade plant-derived C and create novel microbial-derived C, through a cell uptake–biosynthesis– growth–death process (microbial anabolism, *in vivo* turnover) (Liang et al., 2017). Microorganisms engage in these processes by releasing CO_2 into the atmosphere (via respiration), which is the main source of CO_2 from terrestrial ecosystems worldwide (Metcalfe et al., 2011). Additionally, the smaller, newly generated OM molecules produced by microbes or plants often have a higher capacity to interact with inorganic components, which aids in the stabilisation of OM (Kleber et al., 2015).

The C sequestration process can be visualised as a microbial funnel, through which microbes digest labile C, and the fraction that passes through is able to be preserved in the soil (Melillo et al., 2011; Bradford et al., 2013; Crowther, Thomas et al., 2015). Under this paradigm, soil microbes act not only as the primary mediators of OM decomposition but also as primary agents for C preservation (Figure 2.6) (Tang & Riley, 2015). Further, this dual function raises the possibility of soil OM decomposition and stabilisation being hastened by warming, shifting stocks toward proportionally more protected forms of C that are less sensitive to rising temperatures. The protection of C has been linked to: (i) the existing physical distance between the microbial biomass and the C molecules, (ii) the amount of reactive surfaces available in inorganic constituents where chemical interactions with OM molecules occur, (iii) the diversity and structure of microorganisms, and (iv) the proportion of C inputs (Sokol & Bradford, 2019). Microbe-derived C requires more metabolic investment than plant-derived C to decompose and has a more heterogeneous spatial distribution within the soil (which occurs at increasing soil depths), which reduces the likelihood of microbes coming into contact with organic substrates. As a result, the microbes' ability to decompose OM becomes hampered by the increase in functional complexity (e.g., molecular, spatial, and temporal complexity) (Lehmann et al., 2020).

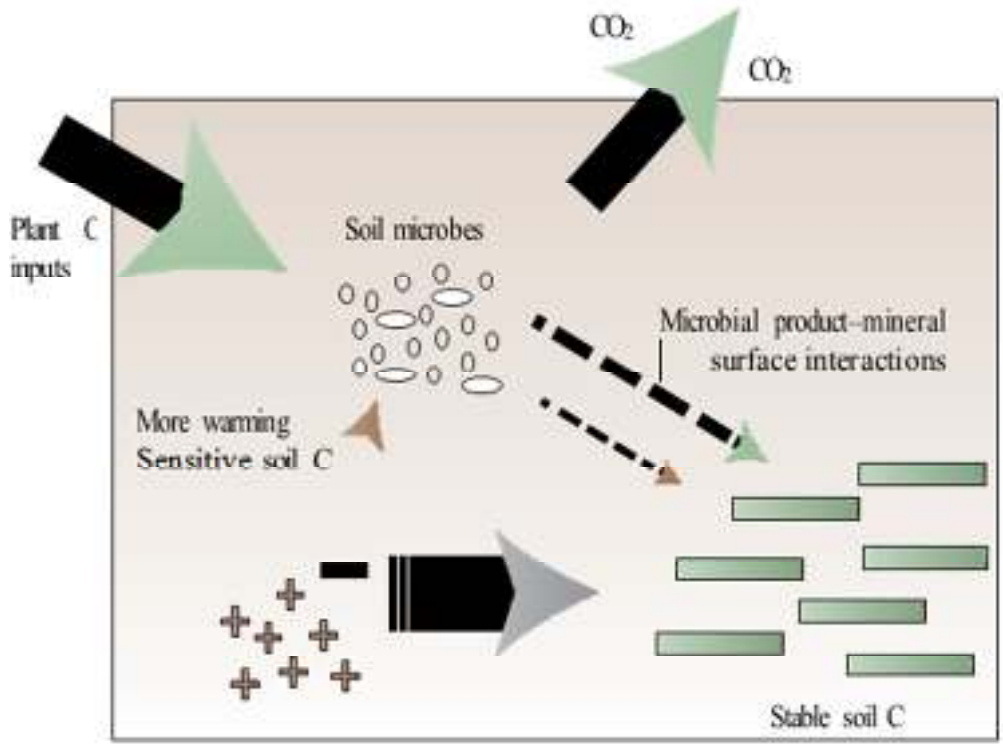

Figure 2.6 The dual role of soil microbes as the mediators of soil OM decomposition and stabilisation. A new understanding of how soil C is built emphasizes that plant C inputs where soil microbes develop result in an increase in sequestered soil C stocks. The grey arrow depicts this general movement of soil C from more to less temperature-sensitive pools under warming, via the microbial funnel into microbial product-mineral complexes. Source: Tang & Riley (2015).

2.5 Relationship between temperature and soil C storage

2.5.1 Effects of rising temperature on soil C storage

Climatic conditions, particularly temperature and precipitation, are the main components controlling soil OM abundance and storage on both global and regional scales (Deb et al., 2015; Wiesmeier et al., 2019). The relationship between global warming and soil C is complex, and there is disagreement about the potential feedback between soil C and global warming. Although increasing temperatures may increase plant production, thereby increasing C inputs to the soil, it will also tend to increase the microbial decomposition of soil C (Keesstra, 2016). In fact, there is

strong empirical support for the idea that rising temperatures will stimulate the net loss of soil C to the atmosphere, driving a positive land C–climate feedback that could accelerate climate change (Crowther et al., 2016; Nottingham et al., 2020). Crowther et al. (2016) have estimated that 1^{o}C of warming will reduce worldwide soil C reserves by 30–203 Pg. Without additional efforts to mitigate CO_2 emissions, by the end of the 21st century, the global mean surface temperature is expected to increase by 1.4^{o}C to 3.1^{o}C relative to 1986–2005 under Representative Concentration Pathway 6.0 (Pachauri & Meyer, 2014). While, some research also reported that no significant effect of temperature on either bulk soil C stocks or the turnover of C fractions (Giardina et al., 2014; Carey et al., 2016). As a result, it is critical to comprehend the potential response of these C stocks to global warming. However, the mechanisms that regulate soil C sequestration are still unclear, and the ability to extrapolate from short-term empirical investigations to long-term forecasts of global C balances remains uncertain (Rustad, 2006).

Many studies have documented that C-rich soils, such as wetlands and permafrost, where microbial decomposition is decelerated by the absence of O_2 and liquid water, respectively, are those most susceptible to warming (Davidson et al., 2012; Carvalhais et al., 2014; FAO & ITPS, 2015). As warming occurs, thawing generates an increase in liquid water, and temperature limitations on the catalytic activities of intracellular and extracellular microbial enzymes are lifted, hastening the decomposition of soil OM and the associated release of CO_2. A geographical relationship between soil C stocks and temperature has been reported by Jones, Hiederer et al. (2005), where the largest C stocks were found at the highest latitudes, indicating that the relationship between climate and soil C stocks is inversely related to latitudinal gradients of NPP, and suggesting that decomposition rates change faster as a function of temperature than NPP. This imbalance in the temperature sensitivity between NPP and OM decomposition

suggests that soil C stocks will decline in response to warming, as warming-induced C emissions from soils will be greater than C fixation by plant growth, and soils will become a net source of atmospheric CO_2. Consequently, most mathematical models predict that rising temperature will lead to considerable losses of soil C and cause strong positive feedback on the atmospheric CO_2 concentration (Kirschbaum, 2000). Furthermore, many studies have reported that the rate of soil OM decomposition decreases with increasing altitude because of a decline in temperature and a general increase in precipitation, which may favour waterlogging conditions in some specific landscape positions (Tashi et al., 2016), although the work of Tan and Wang (2016) drew a contradictory conclusion regarding this correlation. The general principle is that rate of OM decomposition declines with elevation because of a reduction in temperature but it is, to some extent, also affected by changes in the vegetation and soil properties (Sierra & Causeret, 2018).

There have been divergent views regarding the decline in soil OM decomposition in volcanic soils as the altitude increases, as some authors have attributed it to physical protection by minerals or inorganic constituents in Andosols and a decline in microbial activity (Naafs et al., 2004; Li et al., 2016), whereas others have attributed it to a decrease in soil temperature as the elevation increases (Zimmermann & Bird, 2012; Dieleman et al., 2013; Wang et al., 2016). Understanding the relationship between these biotic and abiotic factors will help us to predict the future of soil C in highland areas under global warming (Frey et al., 2013; Sanderman et al., 2016).

2.5.2 Temperature sensitivity (Q_{10}) of soil OM decomposition

Understanding the temperature sensitivity of bulk soil C and its fractions is a key aspect in determining the feedback between the global C balance and rising temperature. The temperature

sensitivity, as expressed by the Q_{10} value, is a measure of the rate of change in a biological or chemical system to an increase in temperature of 10°C. The Arrhenius function is a formula for determining the temperature dependence of the rates of chemical reactions. It was developed from the equation proposed by van't Hoff, who stated that a change in the equilibrium constant of chemical reactions could be attributed to a change in the temperature. Chemical reactions often require activation energy (E_a) to proceed. Hence, the equation is: $k = Ae^{-E_a/RT}$, where k is the constant of the reaction rate, E_a is the required activation energy, R is the gas constant, T is the temperature (in Kelvin), and A is the exponential factor. This function forecasts that the Q_{10} of chemical reactions will decrease with an increase in the temperature (Davidson & Janssens, 2006).

There is much disagreement in the literature about the Q_{10} of labile and preserved soil C. Both labile and preserved soil C have been reported to be temperature-sensitive (Fang et al., 2005); however, some authors have reported that the rate of decomposition of the preserved soil C is more sensitive to temperature than the labile substrate (Knorr et al., 2005; Conant, Steinweg et al., 2008; Karhu et al., 2010; Lefèvre et al., 2014). In contrast, some researchers have concluded that preserved soil C is temperature-insensitive (Giardina & Ryan, 2000; Melillo et al., 2002). Enzymatic depolymerisation is considered to be one of the primary reasons for expecting labile soil C decomposition rates to increase with short-term rises in temperature, especially in the low-temperature range (Kirschbaum, 2006; Lawrence & Neff, 2009; Wallenstein & McMahon, 2009; Wallenstein et al., 2010). To date, the temperature sensitivity of the more recalcitrant forms of soil C remains a subject of debate. Many environmental constraints affect the intrinsic temperature sensitivity of soil C, reducing its apparent temperature sensitivity. Conant et al. (2011) argued that attention should be paid to investigating how temperature influences the

various factors regulating the decomposability of soil OM. Furthermore, previous studies have reported that the Q_{10} of topsoil is greater than that of subsoil. This is a result of the subsoil's decreased microbial abundance and increased soil C protection (Qin et al., 2019). In the subsoil, the ratio of OM to minerals decreases as the depth increases, whereas the proportion of organo-mineral complexes increases (Dungait et al., 2012; Blagodatskaya et al., 2014). This contradicts the findings of Bosatta & Ågren (1999) and Craine et al. (2010), who found that the Q_{10} value of subsoil layers is greater than that of topsoil layers. This is because the enzymatic degradation of biochemically resistant substrates (lower soil C quality) requires more activation energy and should be more temperature-sensitive than the decomposition of more labile substrates. Temperature is therefore considered to be the most influential factor controlling the soil OM's decomposition rate, and hence there is a need to understand the temperature sensitivity of soil C so that we can predict the effects of global warming on soil C stocks more accurately (Meyer et al., 2018).

2.6 Approaches to modelling soil OM decomposition

Because of the significance of soil OM decomposition to ecosystem function and climate change, several models have been developed to describe its dynamics. More than 250 different models of soil OM decomposition have been proposed since the 1930s, the majority of which share similar mathematical frameworks (Manzoni & Porporato, 2009). Soil C modelling approaches are constantly evolving. A model of soil OM decomposition should ideally be based on a mechanistic understanding of the soil dynamics. It should use soil C pools based on data and function on more than one scale. However, no single model has met all of these requirements to date (Campbell & Paustian, 2015). Models for conceptualizing the decomposition of soil C are

classified as either theory-driven or data-driven. The theory-driven models can be represented by the Q-model. The Q-model depicts decomposition as C atoms with a quality feature that changes over time. The model uses the concept of activation energy and links C quality to temperature (viewed as an intrinsic property) (Wetterstedt, 2010). The end result is usually a mathematical formula that can be converted into a computer model by software packages such as SOILR in R programming software (Sierra, 2012). In a data-driven method, the model is directly fed with data, or is transformed into simple correlations and functions that serve as frameworks. Linking these components requires abstract perception. The CENTURY model is an example of a data-driven model (Parton et al., 1987).

The majority of investigations into the kinetics of OM decomposition in the soil have identified C pools with various mean residence times (MRTs) in the soil. The MRT, which is the inverse of the decomposition rate, reflects both the pool's inherent reactivity and the ambient constraints. It has been agreed that using conceptual pools in soil C models to predict changes in soil C reserves is better than treating the soil as a single uniform pool, though the measurement of the MRTs and sizes of these pools may be inaccurate (Trumbore, 2000; Jones McConnell et al., 2005; Powlson, 2005). Specifically, the CENTURY and ROTH-C (Parton et al., 1987; Jenkinson, 1990) models separate soil C into conceptual pools, including decomposable plant residues close to the surface of the soil and three pools containing C in the mineral soil, with MRTs ranging from years to millennia. The decomposition of plant debris on the soil surface is dependent on climate functions and indices of the substrate's decomposability (Melillo et al., 1982). The three C pools, from the most labile to the most resistant to decomposition, are called fast, slow, and passive in CENTURY; in ROTH-C, they are denoted as “microbial biomass”, “humified organic matter”, and “inert”, respectively (Trumbore et al., 1996; Six et al., 2002).

The CENTURY and ROTH-C models are still in use; they are useful because they account for the dynamics of soil OM and view soil OM as containing C pools that decompose at different times (Blankinship et al., 2018). Another useful model is the SOMic model (Woolf & Lehmann, 2019), which considers microbial interactions with mineral-associated organic matter and removes the need for an intrinsically slow-cycling soil C pool while still predicting long-term experimental data.

2.7 Conclusions and research gaps

To fully comprehend the feedback of the soil C balance to climate change, it is crucial to investigate the long-term effect of temperature rise on soil C fluxes, stocks, and fractions under natural temperature gradient, such as that offered in the Taranaki region, which allows a space-for-time substitution approach. This literature review emphasises the need to pay close attention to the current research gaps listed below:

- Despite extensive study being undertaken to examine the effect of rising temperatures on soil C stocks, the interplay between temperature and soil geochemistry and their combined impacts on soil C stocks, fractions, as well as the amount and quality of soil OM composition remain poorly understood.
- Although the effect of rising temperatures on soil C stocks and fluxes has been extensively researched, less is known about the dynamics of soil OM composition, notably carbohydrates, as influenced by temperature. This knowledge might assist in assessing the influence of temperature on the turnover of soil C.
- Despite the temperature sensitivity (Q_{10}) of soil OM decomposition has been extensively estimated, in most instances, this information has been generated from short-term

incubations, which is unlikely to capture the long-term rising temperatures effects (Conant et al., 2011).

- Despite the fact that the spatial and temporal variations of temperature sensitivity of soil OM decomposition have been investigated extensively, the responses of different OM compositions to elevated temperatures remain poorly quantified.

CHAPTER 3

THE CONTROL OF SOIL GEOCHEMISTRY AND TEMPERATURE GRADIENT ON SOIL CARBON OF VOLCANIC SOILS UNDER A TEMPERATE NATIVE FOREST

Abstract

Field studies on the impact of warming on the carbon (C) cycle are challenged by the covariance of temperature with other environmental properties. Here, we investigated the changes in soil geochemistry within a quasi-thermo-sequence and their influence on soil C content, stocks, fractions, and composition. For this, we characterised C-rich volcanic soils in the forest of Mt. Taranaki (New Zealand) down to 85 cm depth at four elevations (1024, 880, 680, and 512 m above sea level) with mean annual temperatures of 7.3, 8.2, 9.1, and 10.5^{o}C (hereafter referred to as T7, T8, T9, and T10), respectively. The presence of reactive aluminium (Al) along the transect is influenced by the temperature gradient, which, in turn, covaries with rainfall and the particle size of tephra). The proportion of organo-Al complexes out of the total reactive Al significantly (P <.05) decreased as the temperature increased (e.g., from approximately 100% to 50%) whereas the allophane content increased (e.g., from 0.6% to 4.6%). Below 10 cm, the soil C content is greater in soil layers that are rich in organo-Al complexes (r = 0.91; P <.05), peaking in low-temperature sites, but the total soil C stocks down to 85 cm depth are not significantly different (P >.05) across sites (ranging from 153 to 176 MgC ha^{-1}). The amount of unprotected C (estimated as the C present in the residue after extraction with diluted hydrofluoric acid) decreased significantly (P <.05) as the temperature increased (the weighted averages at T7 and T10 were 33 and 26 g kg^{-1}, respectively). The fact that at colder elevation sites (T7 and T8), the soil profiles are richer in well-preserved plant material (as identified using pyrolysis gas chromatography mass spectrometry (GC/MS) and in organo-Al complexes, as opposed to soils at warmer elevation sites (T9 and T10), which have more microbially processed organic carbon and a higher fraction of protected C forms along with a greater abundance of short-range order Al

constituents, reveals that the mechanisms through which organic matter is preserved down to 85 cm depth differ with temperature. The results reveal how the interactions of climatic and geochemical factors control the mechanisms through which soil C is preserved. Thus, these factors should be considered in models that project soil C changes over time under different climate scenarios.

3.1 Introduction

Soil organic matter (OM) is a primary terrestrial carbon (C) pool. The amount of soil C stored in the top 1 m of the soil is estimated to be around 1700 PgC, which is more than the C present in the atmosphere (~870 PgC) and terrestrial plants (~450 PgC) combined (IPCC, 2021). One of the main factors affecting soil C dynamics is the climate (Deb et al., 2015). In fact, global warming may drive the net loss of soil C into the atmosphere through the influence of temperature on the decomposition of microbial OM (Keesstra et al., 2016), resulting in a positive terrestrial C–climate feedback loop (Crowther et al., 2016). Numerous mathematical models have projected a linear relationship between soil C loss and temperature (Jones et al., 2005; Friedlingstein et al., 2006; Cox et al., 2013). However, an increase in global temperatures may also cause an increase in plant production and thus in C inputs to the soil, where water and nutrients are not limiting. This can explain the inconsistency of recent research into the responses of OM decomposition to warming, as these studies have yielded conflicting results, including positive (Fang et al., 2005; Hicks Pries et al., 2018), neutral (Giardina et al., 2014; Carey et al., 2016), and negative responses (Bradford et al., 2008). The balance between C inputs and C outputs may be influenced by plants' nutrient acquisition patterns, given that plants may

increase their biomass by mining soil OM for nutrients and thus decrease soil C storage (e.g., the priming effect) (Terrer et al., 2021).

By and large, studying the response of soil C fluxes to temperature changes is challenging, and measurements in the laboratory and in situ are not always consistent (Carey et al., 2016; Xu et al., 2019). One of the difficulties often encountered in studies in natural thermo-sequence is that the temperature changes co-vary with the biotic and abiotic factors (Davidson & Janssens, 2006; Carvalhais et al., 2014), and with spatial and temporal variations (Lindahl et al., 2007; Fiener et al., 2015), which also influence the soil's properties and, ultimately, its geochemistry (Doetterl et al., 2015). Andosols are soils that are common in volcanic regions and rich in reactive surfaces, and can exemplify the abovementioned challenges. They predominantly contain aluminium (Al) in the form of organo-Al complexes and/or short-range order (SRO) constituents (e.g., allophane and imogolite) (Takahashi & Dahlgren, 2016), onto which organic ligands can attach and become protected from decomposition (Hashizume & Theng, 2007; Parfitt, 2009). Organo-Al complexes and SRO constituents are considered together as organo-mineral associations and are believed to follow a discrete zonal sequence referred to as the membrane-like bilayer (Kleber et al., 2007; Li et al., 2022). In the outer zone, also referred to as the kinetic zone, cations (e.g., Al) act as bridges between organic ligands (Kleber et al., 2007) with the exchange rate of organic molecules (and their decomposition) being faster than in the inner layer closer to the minerals' surface (Kögel-Knabner et al., 2008). Therefore, the susceptibility of organic ligands in these organo-mineral associations differs depending on the relative abundance of SRO constituents vs. that of Al cations, which is, in turn, strongly dependent on the climatic conditions. Temperature, under high rainfall and good drainage, increases the rate of physical and chemical weathering of the volcanic parent material, which is key in the formation of reactive Al (Macías & Camps-

Arbestain, 2020). The formation of allophane vs. organo-Al complexes is strongly defined by the pH of the system, with more acidic pH values favouring the formation of the latter (i.e., hydroxyls are less able to compete with organic ligands for Al cations) (Dahlgren et al., 2004). The interaction of temperature and soil geochemistry and their combined impacts on the quantity and quality of soil C are still poorly understood. This study therefore aimed to investigate the influence of temperature and soil geochemistry on soil C stocks, fractions, and the composition of isolated pools in Andosols along a quasi-thermo-sequence of a volcano, namely Mt. Taranaki in New Zealand. Taranaki provides an excellent natural laboratory to study the effects of temperature, which changes by around 3.2^{o}C along a mean annual temperature (MAT) gradient, with a uniform parent material and native vegetation cover; the precipitation is >3000 mm throughout the year (thus not limiting either vegetation growth or mineral weathering) and increases with elevation. We hypothesised that: (i) the forms of reactive Al (i.e., SRO constituents vs. organo-Al complexes) would differ along the thermo-sequence, with a greater abundance of SRO constituents in warmer elevation sites (i.e., lower altitudes) as opposed to organo-Al complexes at colder elevation sites (i.e., higher altitudes), where the weathering rate is slower; (ii) under warmer conditions, C is likely to be more microbially processed as opposed to colder conditions, where the plants' fingerprints are more evident as OM decomposition rate is slowed down; (iii) as a result, the mechanisms of C preservation along the transect will differ, with C that is more associated with SRO constituents (and more microbially derived) at lower elevations, and with Al cations (and more likely to be plant-derived) at the more leached sites with a higher elevation.

3.2 Material and methods

3.2.1 Site description

The study was conducted in a mature native forest on the eastern flank of Mt. Taranaki in the North Island of New Zealand. Taranaki is an andesitic stratovolcano, the upper cone of which has been rebuilt by frequent eruptions in the last 7000 years after a sector collapse (Alloway et al., 1995; Zernack et al., 2011). Four sampling sites were chosen, with elevations ranging from 512 to 1024 m above sea level (asl) and a difference in elevation of around 200 m between adjacent sampling locations. The MAT ranged from 7.3^{o}C to 10.5^{o}C from high to low altitudes (Figure 3.1), and the mean annual precipitation (MAP) rates exceed 3000 mm per year at all sampling sites (Figure 3.1). Details of the elevation, GPS coordinates, MAT, and MAP are provided in Table 3.1. All sampling sites had the same parent material (Aitken et al., 1978) but had decreasing tephra particle sizes as the distance from the source increased, non-limiting plant-available moisture, and similar native evergreen broadleaf trees (>80% kamahi (*Weinmannia racemosa* L.f.) and mahoe (*Melicytus ramiflorus* J.R & G. Forster)). The soil is formed on andesitic tephra of the Burrell formation deposited in A.D. 1655 (Aitken et al., 1978; Torres-Orozco et al., 2017) and is classified as Allophanic soil from andesitic ash by the New Zealand soil classification system (Hewitt, 2010), and an alu-andic Andosol according to the World Reference Base system (World Reference Base for Soil Resources, 2015). The topography ranges from gentle to steep (Davies & Lambert, 2015); however, in order to minimise the effects of erosion, we selected sampling sites away from streams and gullies. The soils are moderately drained at lower elevations (460–760 m asl), although the water table is always deeper than 0.5 m, and well drained at higher elevations (760–920 m asl) (Aitken et al., 1978). The forest was

assumed to be in a steady-state condition in terms of soil C storage after a series of successions from shrubs to the current native forest since the latest eruption (McGlone et al., 1988; Clarkson, 1990). No studies have documented any major damage caused by natural (floods, windstorms, and animals) or human disturbance (logging) that has resulted in significant changes to the forest's structure.

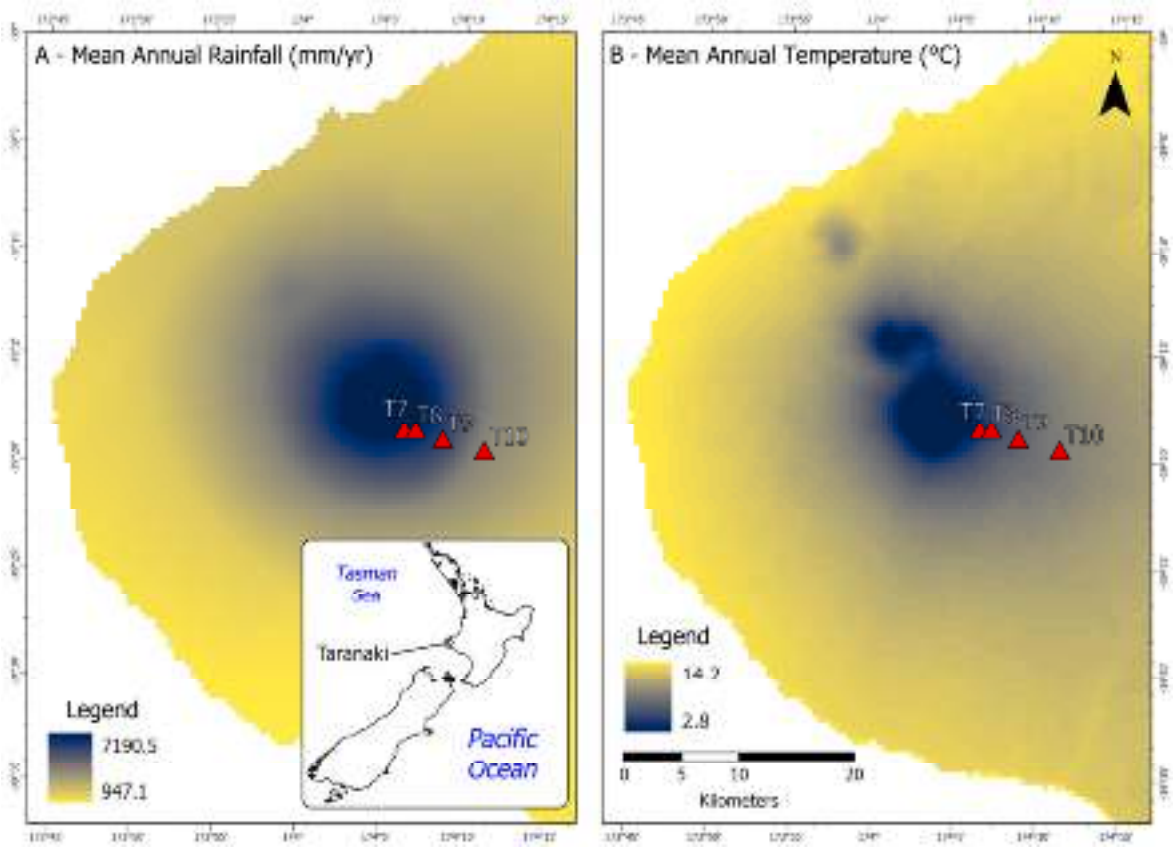

Figure 3.1(A) The mean annual precipitation (MAP) and (B) the mean annual temperature (MAT) of four sampling sites on Mt. Taranaki. This map was created using GIS software based on the latitude, longitude, and elevation of the sampling sites following the method of Tait et al. (2006).

Table 3.1 Elevation and GPS coordinates of the sampling sites on the eastern flank of Mt. Taranaki

Site	Elevation (m asl)	Longitude	Latitude	MAT (^{o}C)	MAP (mm yr^{-1})
T7	1024	39°18'21.00"S	174° 6'27.12"E	7.3	6531
T8	880	39°18'20.46"S	174° 7'8.83"E	8.2	6242
T9	680	39°18'46.43"S	174° 8'47.20"E	9.1	5443
T10	512	39°19'15.82"S	174°11'18.05"E	10.5	3400

3.2.2 Soil sampling and general soil characterisation

Soil samples were taken with a soil core with a 25-mm diameter at four different soil depths (0–10, 10–30, 30–50, and 50–85 cm) with four replicates per site (within an area of ~400 m^2), making a total of 64 soil samples. The soil bulk density was determined by dividing the soil's dry weight by the volume of the soil corer. The soil samples were air-dried to a constant weight and then sieved through a 2-mm mesh. The following characterisations were carried out: pH in water, Olsen P, ammonium oxalate-extractable aluminium (Al_{ox}), iron (Fe_{ox}), and silicon (Si_{ox}), and sodium pyrophosphate-extractable aluminium (Al_{py}), iron (Fe_{py}), and carbon (C_{py}). The methods used for each analysis are provided below. The methods and data for the pH in water, Olsen P, and C_{py} are provided in the Supplementary Information. The iron (Fe_{py}) and aluminium (Al_{py}) in organo-mineral complexes were extracted using 0.1 M sodium pyrophosphate ($Na_4P_2O_7$; pH ~10) as described by Blakemore et al. (1981). Short range order materials (Al, Fe, and Si) were extracted by 0.1 M acid ammonium oxalate (pH=3) (Al_{ox}, Fe_{ox} and Si_{ox}) in a dark room following the method of Blakemore et al. (1981). These values were used to estimate the quantity of SRO constituents (e.g., allophane and Al/Fe oxy-hydroxides) following the method of Mizota & Van Reeuwijk (1989). The concentrations of Al, Fe, and Si in all extractants were

analysed via microwave plasma-atomic emission spectrometer (MP-AES) (4200 MP-AES, Agilent Technologies, Singapore).

3.2.3 Total C content. total nitrogen (N), and soil C stocks

Total C content (equivalent to total OC, given the low pH values) and total N were measured by weighing around 1 g of soil (ground to <100 μm with a tungsten mill) and analysed with a Elementar Vario MACRO (Hanau, Germany). Total soil C stocks (TC_s in Mg ha^{-1}) at fixed depths were calculated by considering the soil C concentration, soil bulk density, and soil depth. Because of the presence of lapilli material (2–64 mm in diameter), particularly at T7 and T8 (at depths of 30–50 cm and 50–85 cm), the total soil C stocks at these depths were calculated after correction for the coarse fragments, following Schwager & Mikhailova (2002) as follows:

$$TC_s = TC_c \times \rho \times D \times (1- \delta_{2mm}/100) \times 10^{-1} \quad (1)$$

where TC_s represents the C stocks (Mg ha^{-1}), TC_c represents the C content (g kg^{-1}), ρ represents the soil bulk density (g cm^{-3}), D represents the thickness of each soil layer (cm), and δ_{2mm} represents the proportion of the coarse fragments on a volume basis (>2-mm mesh) (%). The cumulative soil C stocks at the different depths (0–10, 10–30, 30–50, and 50–85 cm) were estimated on the basis of an equivalent soil mass, following Wendt & Hauser (2013). The soil mass per ha (Mg ha^{-1}) was calculated by multiplying the soil bulk density by the corresponding soil volume. After calculating the soil C stocks and soil masses at specific depths, considering their corresponding bulk densities, the cumulative soil C stocks and soil masses at 0–10, 0–30, 0–50, and 0–85 cm were determined. For depth intervals (0–10, 0–30, and 0–50 cm), the

cumulative soil masses across sites were averaged, whereas for the whole soil interval (0–85 cm depth), the minimum soil mass was considered so that that the C stocks calculated via the cubic spline method of Microsoft Excel could fall within the extrapolation zone. The cumulative soil masses at specific depths considered were as follows: 0–10 cm = 491 Mg ha^{-1}; 0–30 cm = 1687 Mg ha^{-1}; 0–50 cm = 3064 Mg ha^{-1}; and 0–85 cm = 3773 Mg ha^{-1}. The cubic spline function was used to interpolate the cumulative C stocks for each specific soil mass in the soil profile.

3.2.4 Carbon characterisation

3.2.4.1 Hydrofluoric acid treatment

The hydrofluoric acid (HF) treatment aims to isolate the soil C fraction that is not tightly associated with the mineral fraction (Eusterhues, 2007). For this, 30 mL of 2% HF was added to 3 g of air-dried soil (<2-mm mesh) in 50-mL centrifuge tubes and shaken for at least 8 h in an end-over-end shaker at around 50 rpm. The soil suspensions were centrifuged at 23 000g for 10 min (Sorvall RC 6 Plus Superspeed Centrifuge, Thermo Scientific), and the supernatants were removed by a water aspirator. These procedures were repeated six times, and the residual HF in the soil residues was then removed by rinsing at least six times with deionised water until the supernatant reached a pH of >4. Thereafter, the soil residues were re-suspended with deionised water and transferred to a pre-weighed plastic beaker. The suspensions were dried in an oven at 45^{o}C for a week and weighed. The dried soils were ground to <100 μm with a ring grinder. Next, the C recovered in the soil residue after the HF treatment ($C_{HF\text{-}residuum}$) was analysed in an Elementar Vario MACRO (Hanau, Germany). The C fraction mobilised by 2% HF ($C_{HF\text{-}mobile}$) was calculated as total C – $C_{HF\text{-}residuum}$ after correction for the water-soluble C that might have

been dissolved during the extraction. The C fraction mobilised by 2% HF is considered to be tightly bound to the surface of the soil's inorganic constituents.

3.2.4.2 Pyrolysis-gas chromatography–mass spectrometry

The molecular fingerprint of soil OM in the $C_{HF\text{-}residuum}$ was identified by pyrolysis-gas chromatography–mass spectrometry (GC-MS) in a Multi-Shot Pyrolyser (EGA/PY-3030D, Frontier Lab). Around 0.5 to 3 mg of each soil sample (depending on the C content of the $C_{HF\text{-}residuum}$) was pyrolysed at 550^{o}C for 12 s. The pyrolysis unit was connected to a GC/MS unit (GCMS QP2010 Ultra, Shimadzu). The injection was carried out in split mode (split ratio: 1:30). The pyrolysis products were separated on a stainless steel capillary column (SH-Rxi-5 ms Crossbond, Shimadzu; 5% diphenyl/95% dimethyl poly siloxane, 30 m, 0.25 mm internal diameter, with a film thickness of 0.50 μm). High-purity helium was used as a carrier gas (flow rate: 1 mL min^{-1}). The initial oven temperature was 40^{o}C, which was maintained for 12 s (the same as the pyrolysis time) and then amplified up to 300^{o}C at a rate of 5^{o}C min^{-1}. The final column temperature was 300^{o}C and was maintained for 16 min. The temperature of the interface between GC and MS was 270^{o}C, and that of the ion source was 230^{o}C. The ionisation energy was set to 70 eV, with a mass change of m/z 45–650 and a cycle time 0.5 s. In total, 109 organic compounds of pyrolysis were identified by the internal NIST library and published sources such as Buurman et al. (2007), Suárez-Abelenda et al. (2015), and Wang et al. (2016). Quantification of the products of pyrolysis was achieved with the Masslab 1.2.7 software (Shimadzu) provided with the equipment. The sum of the total quantified peak area (TQPA) of the primary fragment ion(s) (m/z) was set to 100%, giving the relative contribution of each product of pyrolysis. The products of pyrolysis were grouped into the following compound classes: polysaccharides,

methylene chain compounds (MCC), lignin-derived compounds, monocyclic aromatic hydrocarbons (MAHs), polycyclic aromatic hydrocarbons (PAHs), phenols, and other compounds (Shen et al., 2018).

3.2.5 Data analysis

A statistical analysis of the major soil properties was carried out with IBM SPSS Statistics version 25.0 (IBM Corp., Armonk, New York, USA). A statistical analysis of the pyrolysis-GC/MS products was carried out with Tanagra 1.4.50 (Hastie et al., 2001). One-way ANOVA with Tukey's test was performed to find significant differences (at P <.05) between the treatment means across the levels of a single categorical factor, with all other variables being constant. Principal component analysis (PCA) was performed to maximise the variance of the projected data (i.e., selected soil chemical properties and C fractions). Prior to conducting the PCA, the soil properties (including the different C fractions) were normalised to z-scores to avoid scaling effects. Linear regression analysis was applied to assess the correlation between reactive Al and the total C and C fractions.

3.3 Results

3.3.1 Soil geochemical properties of the soil

The influence of temperature was particularly evident in the topsoil, where the soil pH generally increased with an increase in temperature (from pH 4.9 to 5.5; Supplementary Information; Figure S3.2.1); however, differences were only significant at P <.05 between T10 and the rest of the sites. Across the transect, the topsoil had a significantly lower pH (an average pH of 5.1) (P <.05) than the deepest soil interval (an average pH of 5.5), except at T10. Temperature had also an influence on Al_{ox}. In fact, when we compared specific soil depths among the sites, those of

T10 had higher Al_{ox} values (generally significant at P <.05) than the sites with lower temperatures (e.g., the weighted average down to 85 cm depth at T10 vs. T7 was 18.3 vs. 8.1 g kg^{-1}) (Figure 3.2A). There were no consistent trends in Al_{py} across sites and depths (Figure 3.2.B). At all sampling sites, the top 10 cm had a smaller Al_{py} content than the deeper soil intervals. The second depth interval (10–30 cm) of T7 and T8 showed the greatest Al_{py} content across sites, with values of >12 g kg^{-1}; these differed significantly (P <.05) from those with higher temperatures (T9 and T10).

At all sampling sites, the proportion of organo-chelated Al within the total reactive Al (Al_{py}/Al_{ox}) tended to decrease with increases in temperature and depth (Figure 3.2C). In the first 30 cm, the ratio of Al_{py} to Al_{ox} exceeded 0.6 at all sampling sites. This ratio decreased to <0.6 at the deepest soil interval (50–85 cm), which had the largest Al_{ox} content (significant at P <.05), with a mean value of 17.5 g kg^{-1} compared with the topsoil, which had a mean value of 4.2 g kg^{-1} (Figure 3.2A). At all sites, allophane followed the opposite trend to the Al_{py}/Al_{ox} ratio, increasing with temperature and depth (Figure 3.2D). Site T10 had the highest allophane content at each depth considered; at the deepest soil interval, this was significantly higher (P <.05) than in the rest of the sites. At all sampling sites, the top 30 cm of the soil had the smallest allophane content (0.3% on average), whereas the greatest content was found at the deepest soil interval (4% on average) (Figure 3.2D).

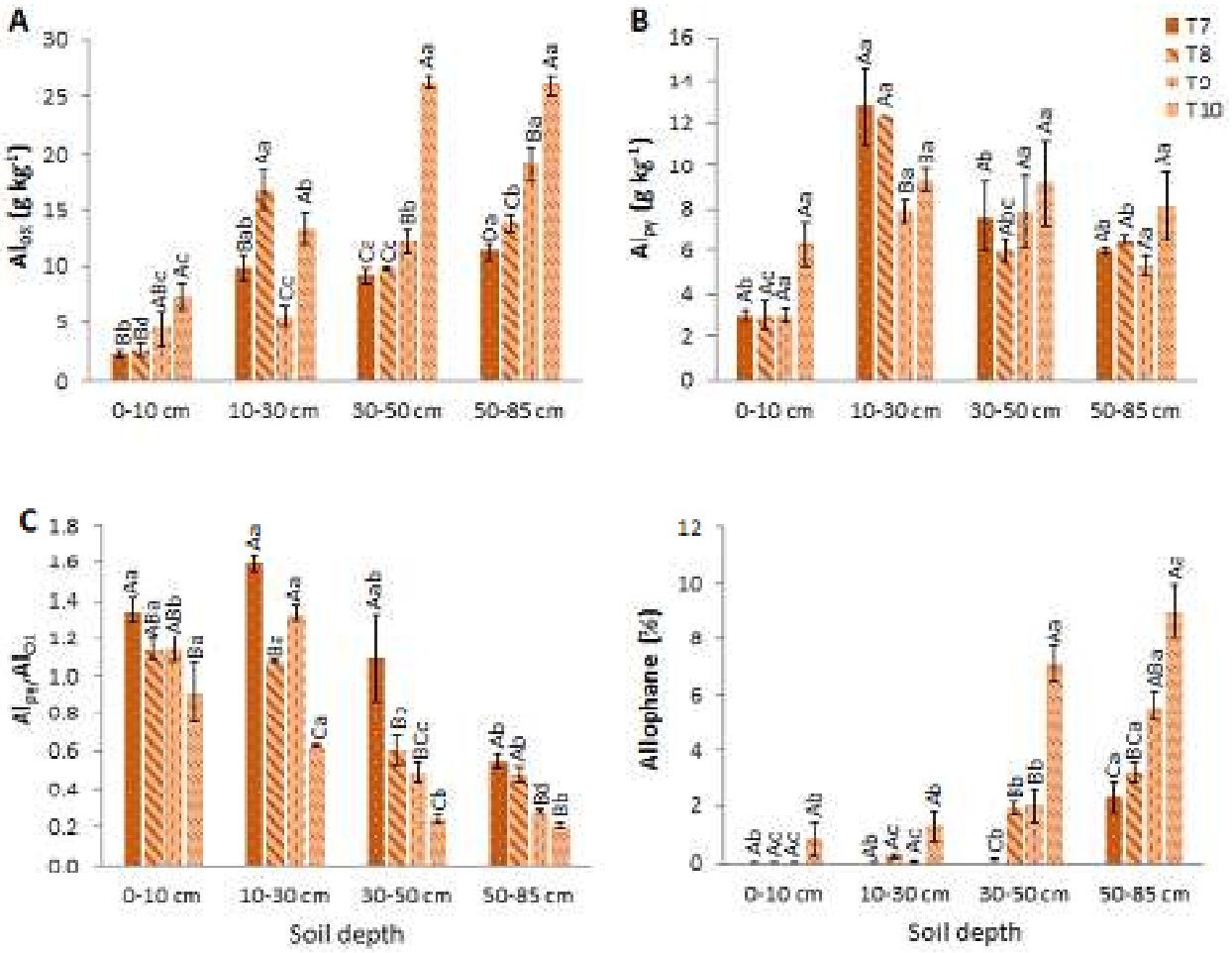

Figure 3.2 The average of: (A) Al_{ox} content, (B) Al_{py} content, (C) Al_{py}/Al_{ox} content, and (D) allophane content of each sampling site and depth. Capital letters indicate differences among the four sites at the same depth, whereas lowercase letters indicate differences among the four different soil depths at the same site. Different letters denote a significant difference according to one-way ANOVA followed by Tukey's test (P <.05). Error bars represent the standard error of the means (n = 4).

3.3.2 Total C content, soil C stocks, and C:N ratio

Overall, at a specific depth, total C content did not show a consistent trend across sites. The average C content in the topsoil (0–10 cm) was twofold larger than that of the deepest soil depth interval (50–85 cm), with mean values of 77.1 g kg^{-1} and 35.4 g kg^{-1}, respectively (Figure 3.3). At T10 and T9, the decrease in total C content from the topsoil to the deepest interval was significant (P <.05). However, at T8 and T7, the topsoil and the next soil interval (10–30 cm)

were not significantly different (P >.05) in C content, whereas C decreased significantly (P <.05) at greater depths. The deepest soil interval (50–85 cm) of T10 showed significantly greater (P <.05) total C content than the sites with lower temperatures (Figure 3.3). At all investigated depths, the bulk soil C:N ratio tended to be higher at colder elevation sites (i.e., T7 and T8 versus T9 and T10). The weighted average of the 0–85 cm depth for T7, T8, T9, and T10 were 14.4, 14.4, 13.2, and 13.1, respectively. However, neither the temperature gradient across sites nor the depth gradient had a significant effect on the C:N ratio (Figure S3.2.2). The total cumulative soil C stocks down to 85 cm did not show significant differences (P >.05) among sites, with values ranging from 153 $\pm$ 11.7 to 176 $\pm$ 10.4 MgC ha^{-1}, although T10 tended to have greater C stocks (Figure 3.3B).

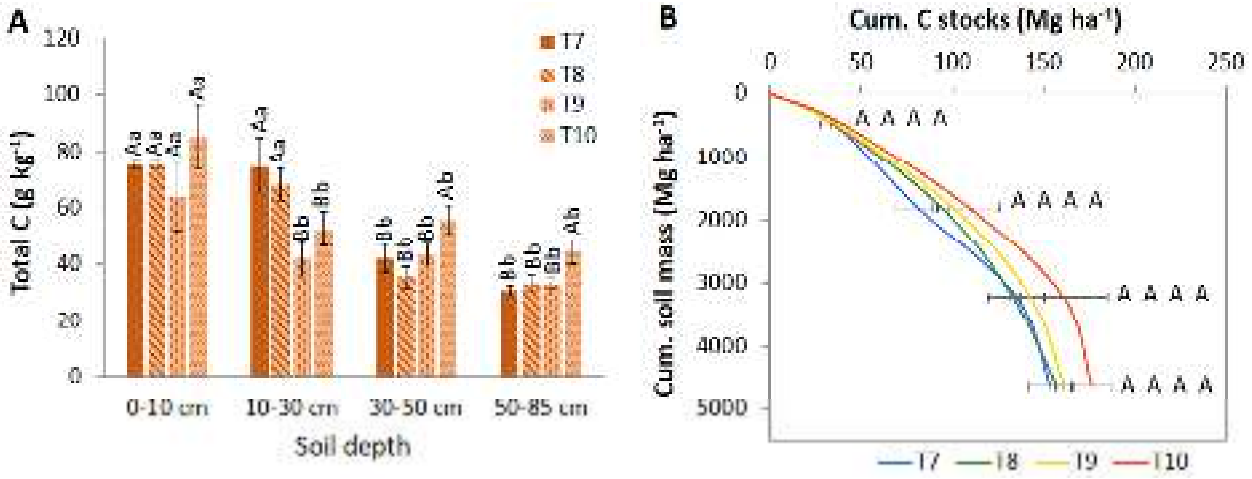

Figure 3.3 (A) The average total C content at each sampling site and depth, and (B) cumulative soil C stocks at four different depths across sites along the Taranaki gradient. Capital letters indicate differences among the four distinct sites at the same depth, whereas lowercase letters indicate differences among the four different soil depths at the same site. Different letters denote a significant difference according to one-way ANOVA followed by Tukey's test (P <.05). Error bars represent the standard error of the means (n = 4).

3.3.3 Characterisation of carbon

At all sampling sites, $C_{HF\text{-}residuum}$, which is the soil C fraction remaining in the soil residue after demineralisation with 2% HF, tended to decrease with an increase in the temperature and consistently declined with depth (Figure 3.4A). At all sampling sites, the largest $C_{HF\text{-}residuum}$ was found in the topsoil (a weighted average of 59.5 g kg^{-1}), which was significantly larger (P <.05) than in the underlying intervals. The smallest value was found at the deepest soil interval (50–85 cm depth), with a weighted average of 9.3 g kg^{-1}, which is six times smaller than that of the topsoil (Figure 3.4A). At all sampling sites, the C fraction that was released by the HF treatment ($C_{HF\text{-}mobile}$) followed the opposite trend (Figure S3.2.3). This fraction has often been associated with the fraction closely bound to the surface of the soil's inorganic constituents, as HF reacts with silicates and oxides to form soluble fluoride complexes (Eusterhues et al., 2007). The proportion of $C_{HF\text{-}mobile}$ within total C tended to increase with increases in temperature and depth (Figure 3.4B). If we compare $C_{HF\text{-}mobile}$/total C at a specific depth across sites, significant differences (P <.05) were mostly found between T7 and T10. At all sampling sites, as expected, the topsoil had the smallest $C_{HF\text{-}mobile}$/total C (ranging from 18.6% to 24.3%) and differed significantly (P <.05) from the deeper soil depth intervals, with the deepest interval having the largest proportion (ranging from 65.3% to 79.1%) (Figure 3.4B). The carbon extracted by with sodium pyrophosphate (C_{py}) (Supplementary Information; Figure S3.2.4) decreased with depth, as expected, but, similar to that for Al_{py}, this decrease was attenuated at low temperatures (T7). and T8) (Figure 3.2B).

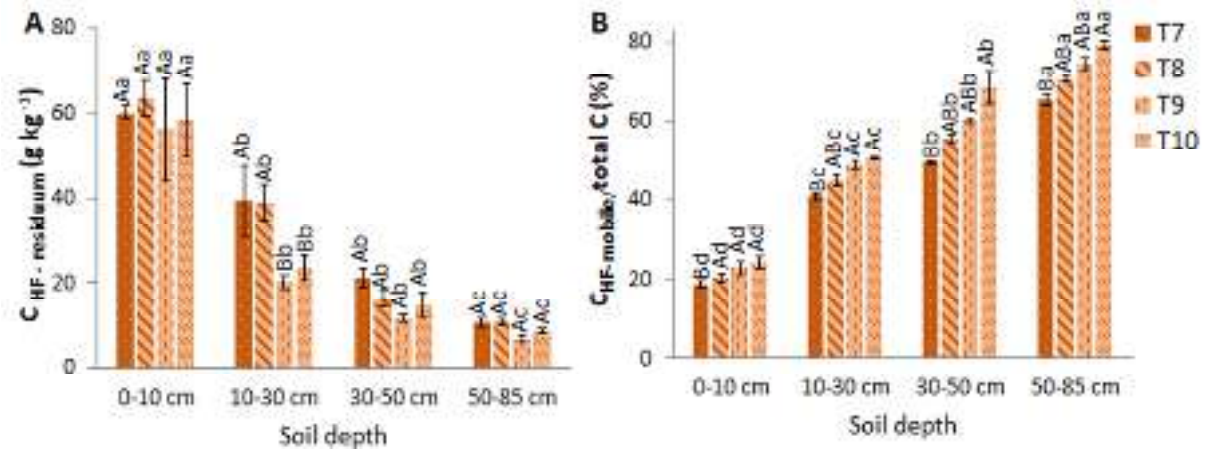

Figure 3.4 The carbon fraction of total C content after demineralisation with 2% HF solution: (A) $C_{HF\text{-}residuum}$ and (B) $C_{HF\text{-}mobile}$/total C in across sites and depths along the Taranaki gradient. Capital letters indicate differences among the four sites at the same depth, whereas lowercase letters indicate the differences among the four different soil depths at the same site. Different letters denote a significant difference according to one-way ANOVA followed by Tukey's test (P <.05). Error bars represent the standard error of the means (n = 4).

3.3.4 Relationship between the total C and C fractions vs. reactive Al

The relationship between total C content and organo-complexed Al (Al_{py}) showed positive correlations (significant at P <.05) at all depths below 10 cm (r = 0.90) (Figure 3.5A), but no significant relationship was found in the topsoil samples (r = 0.01, data not shown). The $C_{HF\text{-}residuum}$ also showed positive correlations with Al_{py} at depths below 10 cm (r = 0.90) (Figure 3.5B). The 10–30-cm depth presented the strongest correlation (r = 0.93) followed by the intervals at 30–50 cm (r = 0.45) and 50–85 cm (r = 0.53) (Figure 3.5B). When we considered the specific soil layers separately across sites, the total C content did not significantly correlate (P >.05) with $Al_{ox,}$ except in the 30–50-cm soil depth (r = 0.57) (Figure S3.2.7). At all depths below 10 cm across sites, the relationship between $C_{HF\text{-}mobile}$ and Al_{ox} was positive and significant at P <.05 (r = 0.49) (Figure 3.5C).

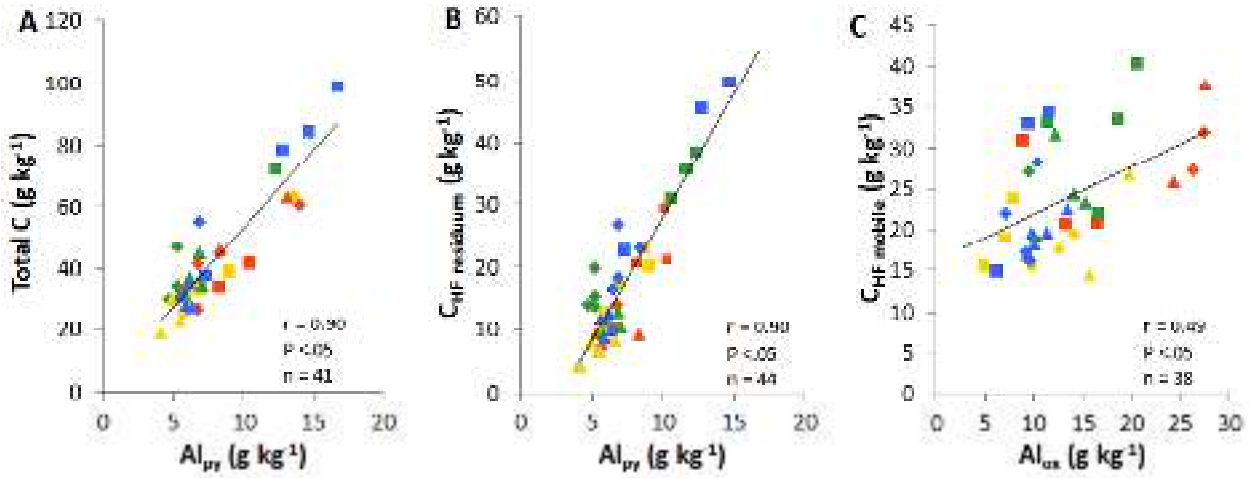

Figure 3.5 Linear regression by depth (excluding the top 10 cm) across sites for: (A) total C content vs. Al_{py}, (B) $C_{HF\text{- residuum}}$ vs. Al_{py}, and (C) $C_{HF\text{-mobile}}$ vs. Al_{ox}. The square, diamond, and triangle indicate depth levels of 10–30 cm, 30–50 cm, and 50–85 cm, respectively; blue, green, yellow, and red indicate the sampling sites (T7, T8, T9, and T10, respectively). The black line is the regression line for all data points < 10 cm.

3.3.5 Characterisation of soil OM composition with pyrolysis-GC/MS

Among the different groups of compounds identified by pyrolysis-GC/MS, carbohydrates, lignin, totarol (a diterpenoid derived from conifer resin), and N-derived compounds had the most distinct patterns across the temperature gradient (Figure 3.6). Methylene chain compounds (MCC) (e.g., alkanes, alkenes, and fatty acids), PAHs, MAHs, phenols, and other compounds were also identified, but, given their weak response to temperature changes, a description of these is provided only in the Supplementary Information (Figure S3.2.6).

The sum of carbohydrates was very high in all topsoil samples, i.e., 55–65% of TQPA. Compounds included acetic acid, furans, furaldehydes, cyclopentenones, 4-hydroxy-5,6-dihydro-(2*H*)-pyran-2-one, and anhydrosugars (e.g., levoglucosan) (Table S.3.2.1). In addition, an unidentified carbohydrate product with a base peak of *m*/*z* 116 was abundant in all samples (ranging from 5 to 15% of TQPA) and is ascribed to plant-derived polysaccharides (Schellekens

et al., 2011; Kaal & Mailänder, 2018). Despite the high overall carbohydrate contribution, there was a clear decrease as the temperature increased at all depths (significant at P <.05). The relative proportion of carbohydrates also showed a decreasing pattern with depth (significant at P <.05), and this decrease was attenuated as the C's mean residence time increased with a drop in the temperature (Figure 3.6A).

The products of lignin (4-vinylphenol, guaiacols, and syringols) accounted for 7.7 ± 2.4% of TQPA, and their abundance followed a similar depth trend (i.e., a decrease) to carbohydrates. However, unlike polysaccharides, the contribution of lignin tended to increase with the temperature (significant at P <.05) (Figure 3.6B). Products with N accounted for 5.3 ± 1.0% of the TQPA (pyrrole, pyridine, acetamide, and diketopiperazines) (Table S.3.2.1). The sum of N compounds tended to increase with an increase in the temperature (significant at P <.05), possibly due to faster decay rates and the resulting microbial necromass pools (Figure 3.6C). At each altitude, the N-containing compounds were highest at the 10–30 cm depth and lowest at the surface (Figure 3.6C). However, caution is required regarding the role of microbial C in the deep range of these soils; the proportion of N compounds in the residue after the HF treatment was only weakly correlated with the C/N ratio of the bulk sample (data not shown), possibly because of bias induced by the HF treatment, which eliminated most of the soil C from the deeper soil intervals.

Finally, the relative proportion of totarol (named after the tōtara tree (*Podocarpus totara*) of New Zealand, from which it was first extracted) was small (<0.4% of TQPA) but showed a marked difference between T7 and all other samples (significant at P <.05) (Figure 3.6D). This minor product also seemed to increase slightly with depth at sites T9 and T8 (significant at P <.05), possibly reflecting changes in the palaeovegetation, because it is unlikely that the increase with

depth could be ascribed to selective preservation of diterpenes. These observations might indicate some legacy of a vegetation signal.

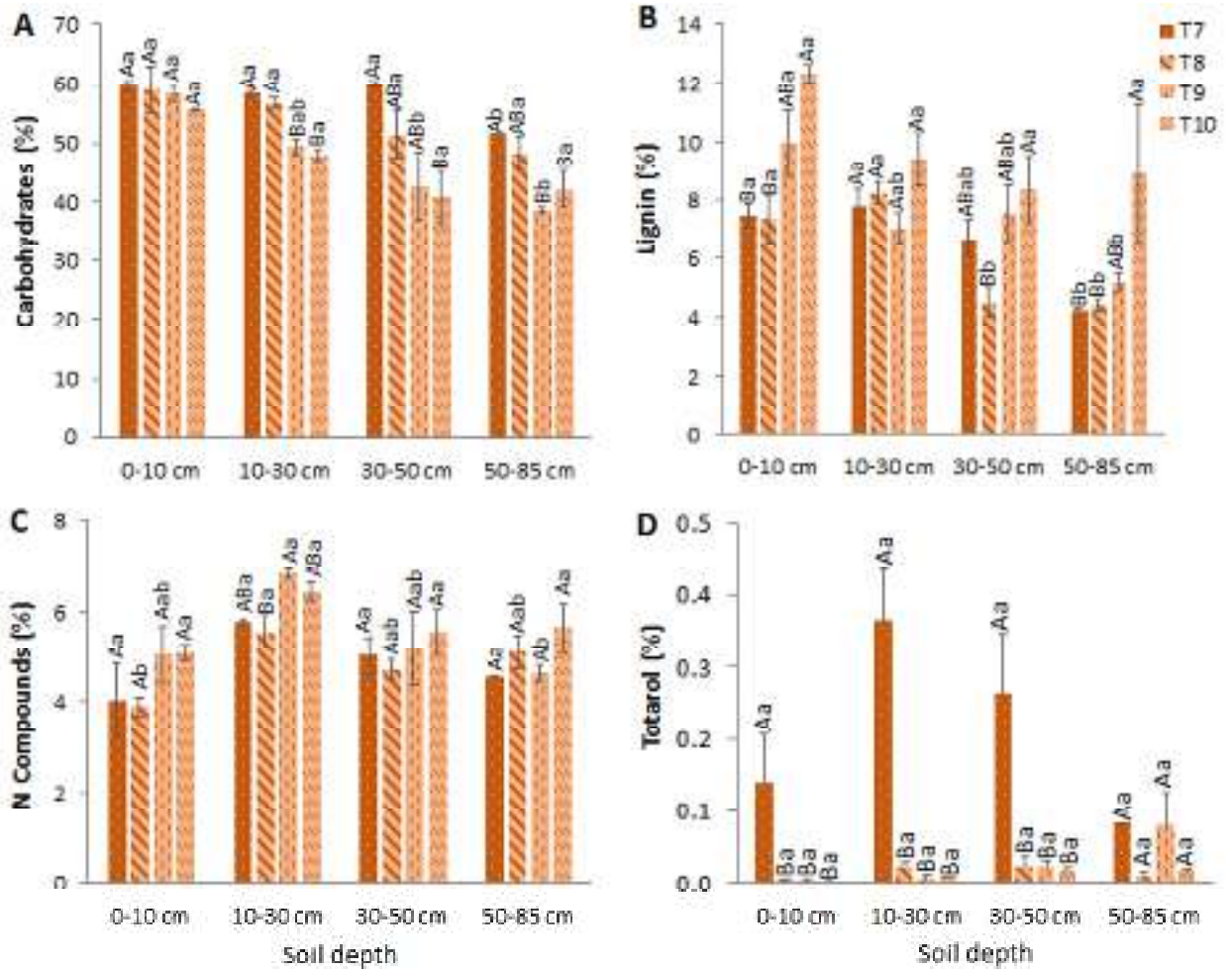

Figure 3.6 Distribution of the groups of the products of pyrolysis (pyrolysis-gas chromatography–mass spectrometry) along the altitudinal gradient on Taranaki. Capital letters indicate the differences among the four sites at the same depth, whereas lowercase letters indicate the differences among the four different soil depths at the same site. Different letters denote a significant difference according to one-way ANOVA followed by Tukey's test (P <.05). Error bars represent the standard error of the means (n = 3).

3.3.6 Principal component analysis

To investigate the underlying structure of the data, PCA was performed on all soil chemical properties and C fractions containing CHF-residuum, $C_{HF\text{-}mobile}$, and C_{py} but excluding pyrolysis-GC-MS results. The four principal components (PCs) accounted for 77.7% of the variability, with PC1 accounting for 41.3% of the variability and PC2 accounting for 19.3% (Figure 3.7A). The factor loadings (Figure 3.7A) showed that PC1 was driven by the total C, total nitrogen (N), the associated C fractions ($C_{HF\text{-}residuum}$, $C_{HF\text{-}mobile}$, and C_{py}), and Olsen-P, with large values plotted close to large Al_{py}/Al_{ox} values and away from the high pH values, and allophane and Si_{ox} contents. On the other hand, PC2 was driven by the presence of organo-metal complexes (represented by Al_{py} and Fe_{py}) and reactive surfaces (e.g., allophane, Al_{ox} + ½ Fe_{ox}), with large values plotting away from large Al_{py}/Al_{ox} values. The factor scores (Figure 3.7B) showed that the combination of depth and temperature could explain the differences in the reactive surfaces, with the deep intervals of warmer sites plotted towards high PC2 values, consistent with a higher pH and the presence of SRO constituents (this being especially evident at 50–85 cm), with the top layers and low temperatures plotted towards more unprotected forms of C and a high Al_{py}/Al_{ox} ratio, and, interestingly, towards high Olsen-P values.

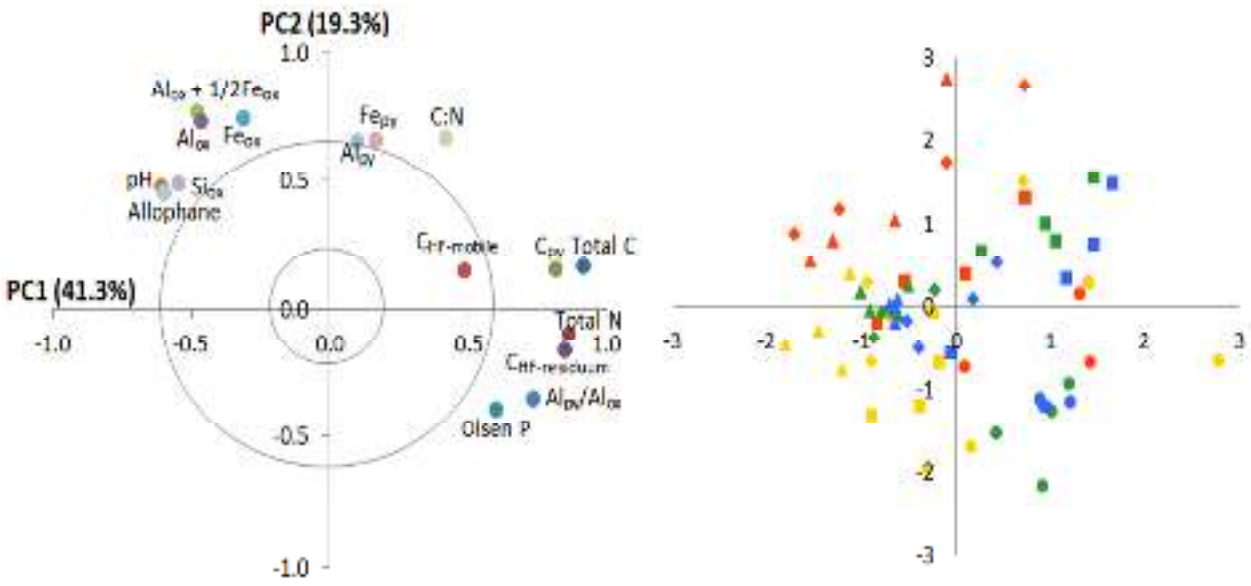

Figure 3.7 (A) The loading of soil chemical properties including the C fractions ($C_{HF\text{-}residuum}$, $C_{HF\text{-}mobile}$, and C_{py}) on the axes of PC1 and PC2 and (B) the factor scores of the data on the axes of PC1 and PC2 from all sampling sites and depths. The circle, rectangle, diamond, and triangle indicate depth levels of 0–10 cm, 10–30 cm, 30–50 cm, and 50–85 cm, respectively. Blue, green, yellow, and red indicate sites T7, T8, T9, and T10, respectively.

A separate PCA was carried out for the biochemical characterisation of the residuum after the HF treatment with pyrolysis-GC/MS, and the details are provided in the Supplementary Information (Figure S3.2.5 and Table S3.2.1). The first four principal components explained 79.0% of the variability, with PC1, PC2, PC3, and PC4 accounting for 56.7%, 9.4%, 7.4%, and 5.5%, respectively. Here, only the scores of PC3 (Figure 3.8) are shown, as these are the most relevant to the response of the soil OM's biochemistry to temperature. PC1 and PC2 reflect the preferential elimination of lignin and polysaccharides over MCC during advanced decay and are controlled by depth. The positive loadings for PC3 (0.5–0.6) correspond to benzene, toluene, phenol, 4-methylphenol, 4-vinylphenol, acetophenone, and biphenyl, reflecting microbial C and lignin (Table S3.2.1). The negative loadings (0.4–0.5) correspond to several carbohydrates, including levoglucosan and the unidentified product, allegedly from intact plant-derived

polysaccharides (e.g., cellulose) (Table S3.2.1). PC3 highlights the enhanced preservation of intact plant-derived polysaccharides when temperatures are low and preferential decomposition of these polysaccharides and the enrichment of microbial C when temperatures are higher. Note that numerous lignin products also have weak (0.3–0.4) positive loadings on PC3, reflecting the preferential decay of polysaccharides over lignin when the temperature increases (Table S3.2.1).

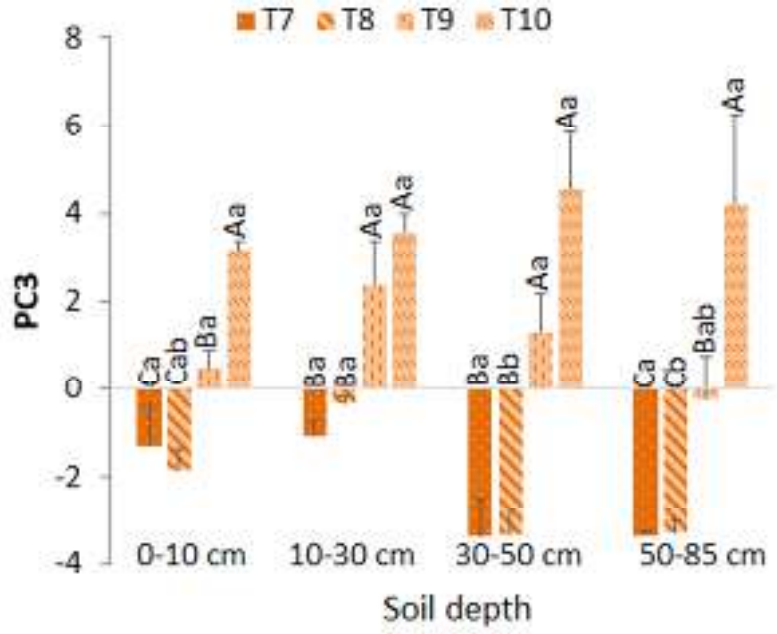

Figure 3.8 PC3 scores of the pyrolysis GC/MS compounds along the altitudinal gradient on Taranaki. Capital letters indicate the differences among the four sites at the same depth, whereas lowercase letters indicate the differences among the four different soil depths at the same site. Different letters denote a significant difference according to one-way ANOVA followed by Tukey's test (P <.05). Error bars represent the standard error of the means (n = 3).

3.4 Discussion

3.4.1 Temperature and soil depth influence the soil's geochemistry

In the two gradients considered (temperature and depth), the soil's geochemistry follows a common pattern, and this is associated with the acidification undergone by the soil as: (i) the temperature increased, accelerating the weathering rate; and (ii) the distance from the weathering

front increased (i.e., the soil layers closer to the soil surface are more acidic). Thus, in both gradients (temperature and soil depth), as the contribution of alkalinity from mineral weathering decreased, so did its ability to counteract the acidity originating from decomposing organic matter (Macías and Camps-Arbestain, 2020). However, it should be noted that the larger particle sizes (and smaller surface area) of the tephra closer to the volcano's summit could have also favoured a slower weathering rate at low temperatures (Qin & Beckingham, 2021), despite the heavier rainfall at higher altitudes. It is well known that as Andosols become more acidic, the decreasing concentration of OH^- makes these anions less able to compete with organic ligands for Al cations (Miyazawa et al., 2013), favouring the formation of organo-Al complexes over those of allophane (Percival et al., 2000; Rasmussen et al., 2006; Takahashi et al., 2012). This was clearly reflected in our study (particularly in the PCA analysis) where, as the pH decreased (either because of the temperature or depth gradient), the allophane content decreased and the ratio of organo-Al complexes to the total amount of reactive Al increased. The peak Al_{py} (used as a proxy for the organo-Al complexes) was reached at a depth of 10–30 cm, away from the influence of the weathering front, but not in the uppermost layer. This is explained by the fact that the interaction of Al cations with organic moieties is favoured by a certain degree of OM processing and oxidation (Kleber et al., 2015), and this is not likely to occur in the fresh plant residues that prevail on the surface of the soils on Taranaki.

3.4.2. Temperature and soil depth influence the fractionation and composition of carbon

The effect of temperature on the fractions and composition of soil C, although less marked than the effect of depth, is distinguishable and consistent. Several key patterns are worth highlighting.

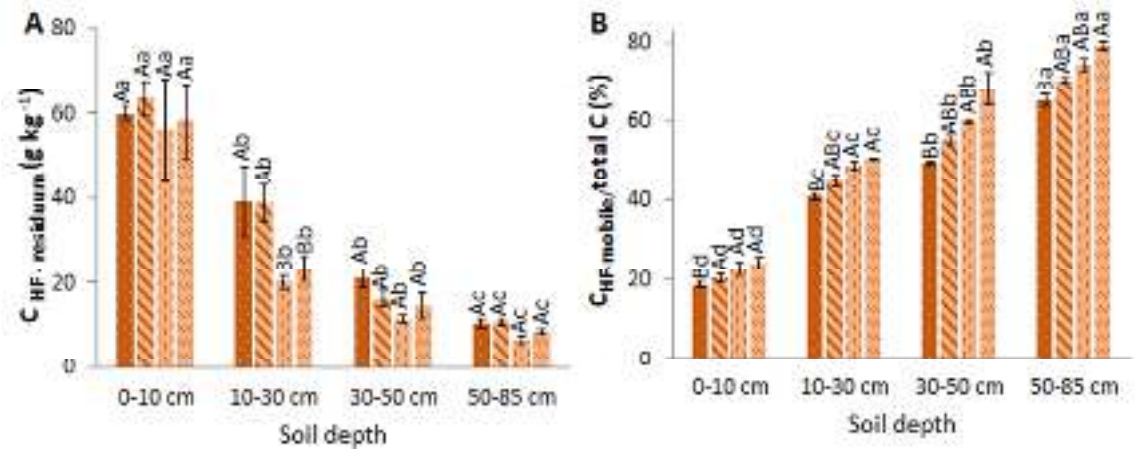

First, at T7 and T8, the decrease in $C_{HF\text{-}residuum}$ with depth is less sharp than at T9 and T10, specifically in the 10–30-cm layer, and this more attenuated decrease in $C_{HF\text{-}residuum}$ is accompanied by a peak in Al_{py} in this soil layer, supporting the more prominent role of Al cations in the preservation of soil C as the environment becomes colder. This is opposed to the trends at T9 and T10, where the low $C_{HF\text{-}residuum}$ at greater depths and the increase in SRO constituents reflect the role of organo-mineral complexes in preserving soil C. These opposing trends (T7 and T8 vs. T9 and T10) are also shown by the effects of decay on the molecular composition of the OM (particularly the carbohydrates), which are less expressed in the deep layers of T7 and T8 soils than T9 and T10 soils, suggesting a temperature-controlled preservation of plant-derived C (preservation in the deeper soil layers enabled by colder conditions). This indicates a long-term temperature-controlled stabilisation mechanism acting on polysaccharides. Thus, the transect made it evident that as the temperature cooled (MAT = <9^{o}C), the soil OM became more stratified and less decomposed, with a weaker interaction with soil minerals. Nevertheless, potential bias in the analysis of OM quality induced by selective solubilisation of mineral-stabilised OM during the HF treatment needs to be addressed to validate these findings. The sharp increase with depth in the C fraction ($C_{HF\text{-}mobile}/C_{total}$) was

expected and was in line with previous studies (e.g., Rumpel et al., 2006; Eusterhues et al., 2007). This increasing pattern is explained by the fact that, at the surface (especially in the 0–10 cm layer), there is a greater amount (and proportion) of plant-derived C and a rich abundance of anhydrosugars and other compounds from fresh plant material. This weakly decomposed (i.e., large molecular weight) and weakly oxidized C pool (i.e., poor in carboxylic functional groups) is less likely to interact with mineral surfaces, as opposed to more microbially processed C (Kleber et al., 2015), namely the one mobilised with HF, which is more abundant at depth. More details on the organo-mineral interactions of the soils under study (particularly the soil of T10) revealed by nanoscale secondary ion mass spectrometry (NanoSIMS) are provided by Li et al. (2022). The increase in the more microbially processed C with depth (as inferred from the increase in the $C_{HF\text{-}mobile}/C_{Total}$ ratio, is paralleled by an increase in the reactive sites (e.g., reactive Al, among others), which favours the preservation of C in organo-mineral interactions (Li et al., 2022). Unfortunately, the data of the N-compounds from pyrolysis-GC/MS cannot be used as fingerprints for microbially derived C, given that it seems likely that the HF treatment selectively removed the N-rich mineral-associated C fraction the residuum remaining after the HF treatment (Figure S3.2.2). However, it is interesting to note that in the 10–30 cm layer at all sites, where the SRO constituents were almost negligible (as indicated by the $Al_{ox} - Al_{py}$ values) but organo-Al complexes are abundant, the presence of N compounds was greater than in the 0–10 cm layer, reflecting the existence of more microbially processed C preserved through either interactions with Al cations or the toxicity that this cation may cause (Scheel et al., 2008). Overall, keeping in mind that the carbohydrate patterns are indicative of the prevailing intact plant remains as their main source (not microbial polysaccharides), it can be concluded that: (i)

all soil samples have large pools of plant-derived soil C; and (ii) a preferential decay of polysaccharides is reflected by the decrease with depth within a soil.

3.4.3. The effects of temperature and soil OM biochemistry on soil C stocks

The data generated in this study clearly show that the existing gradient from low to high temperature affects the soil geochemistry (with the reactive Al transitioning from a greater dominance of Al cations associated with organic ligands at low temperatures to the dominance of Al in SRO constituents at higher temperatures), the soil C fractions (with a trend of organic ligands increasingly associated with minerals as the temperature increased), and the soil OM's biochemistry (with a transition from more plant-derived C to more microbial derived C as the temperature increased). Despite these gradients and the different mechanisms through which C is preserved, soil C stocks did not differ across the temperature gradient. Thus, it is apparent that, at low-temperature sites, although the cold environment slows down mineral weathering and generates a more acidic environment, it also slows down the decomposition of OM (especially plant-derived carbohydrates). Warmer temperatures favour mineral weathering (which, in turn, causes the partial buffering of organic acidity and the formation of SRO constituents) and the decomposition of plant residues, with the generation of microbially processed OM being more prone to interact with mineral surfaces.

When considering the different pools of the four ecosystems, Siregar et al. (unpublished data) have estimated that the turnover rate of unprotected particulate C is approximately 1.4 times faster in warmer sites than in colder sites (Chapter 4, Figure S4.2.5). Although the decay rate is greater at warmer sites, the soil C stocks are not significantly different and even tend to increase. It was observed that as temperatures rose, plant productivity in the forest sites also increased

(Chapter 4, Figure 4.1), thus compensating for the loss of soil C. This indicates that the increase in plant biomass and mineral-associated C with temperature also contributed to the elevated soil C stocks at warmer sites. The Taranaki transect demonstrates that temperature accelerates the decomposition of OM; influences the C stabilisation mechanism by favouring minerals weathering (e.g., SRO constituents), particularly at depth; and increases plant biomass until an optimum temperature is reached.

3.5 Conclusions

This study aimed to deepen our understanding of the effects of temperature on the soil's geochemistry and how this has an impact on the preservation mechanisms of soil C (bulk and fractions). From these results, we can infer that in the short term, with global warming, the soil C stocks of Andosols located at cold temperate sites (with a small presence of SRO constituents and an abundance of organo-metal complexes) will be more susceptible to OM decomposition than those located in warm temperate sites with a greater abundance of SRO constituents. However, it should be kept in mind that the information drawn from this study cannot be fully extrapolated to the effect of global warming on the soil's geochemistry, including soil C. Here, the system and its geochemistry have had centuries to adjust to their specific local conditions (e.g., different weathering rates affecting the chemistry of the system over time), and the C fluxes have reached a new steady state. With warming, there will be an imbalance, with C inputs not equalling C outflux and a mismatch of the system's geochemistry to the new climatic conditions. For example, an increasing occurrence of dry episodes as a result of global warming may favour the formation of halloysite rather than allophane (Parfitt & Wilson, 1985). Halloysite is reported to have a smaller specific surface area and less charge than allophane, and thus has less ability to interact with soil OM (Theng et al., 1982). This study reflects the long-term effects of temperature on the soil's geochemistry and the preservation mechanism of soil C, demonstrating the significance of soil mineralogy for C preservation. This should be incorporated into C models in order to accurately predict future soil C stocks.

Appendix I. Supporting Information for Chapter 3 (SI3)

S3.1 Supporting material and methods

S3.1.1 Soil pH

Five g of air-dried soil was added to a beaker, followed by 12.5 mL of deionized (DI) water. The suspension was stirred vigorously (soil:DI water = 1:2.5, w/v) and left to stand overnight before measuring the pH with a pH electrode.

S3.1.2 Olsen P

Available phosphorus was measured following the method of Olsen et al. (1954) using a 0.5 M $NaHCO_3$ solution (pH adjusted to 8.4). Phosphorus in solution was determined using the phosphomolybdate (blue) method (Murphy & Riley, 1962). The absorbance was then measured with a JENWAY 7315 spectrophotometer (Staffordshire, UK).

S3.1.3 Sodium pyrophosphate-extractable C (C_{py})

To measure soil OM that is associated with metals (mostly aluminum) in the form of organo-metal complexes, sodium pyrophosphate-extractable C was determined following the method of Bascomb (1968). For this, 30 mL of 0.1 M sodium pyrophosphate (pH adjusted ~10) and 0.3 g of air-dried soil (<2 mm) in a 50 mL centrifuge tube were shaken on an end-over-end shaker (ca. 50 r.p.m.) overnight (16 h). The soil suspensions were then centrifuged at 20.000 rpm for 30 min and filtered with a Whatman nylon membrane 0.45 µm. Further, the concentration of C dissolved in the sodium pyrophosphate extractant (C_{py}) was measured by Carbon Analyzer (Shimadzu TOC-VCSH, Shimadzu Corp, Japan). Forty µl of the extracts were injected in the detection chamber. Three injections of the same volume were analysed for each sample.

S3.2 Supporting result

S3.2.1 Soil pH

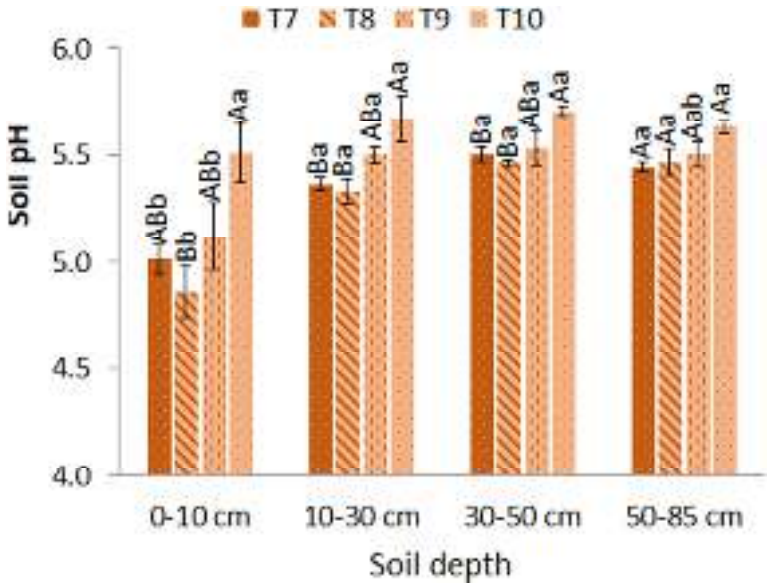

Figure S3.2.1 The average of the soil pH at each sampling site and depth. Capital letters indicate the comparison of four distinct sites at the same depth, whereas small letters indicate the comparison of four different soil depths at the same site. Different letters denote a significant difference according to one-way ANOVA followed by Tukey's test (P <.05). Error bars represent the standard error of the means (n = 4).

S3.2.2 C:N ratio

At all investigated depths, the bulk soil C:N ratio tends to be higher at higher elevation sites (i.e., T7 and T8 versus T9 and T10) (Figure S3.2.2A). However, neither the temperature gradient across sites nor the depth gradient has a significant effect on the C:N ratio. The weighted average of 0–85 cm depths for T7, T8, T9, and T10 is 14.4, 14.4, 13.2, and 13.1, respectively (Figure S3.2.2A). The C:N ratio of $C_{HF\text{-}residuum}$ exhibits a similar trend, with the average weights of 0–85 cm depth being 15.3, 15.1, 14.4 and 14.1 for T7, T8, T9, and T10 (Figure S3.2.2B).

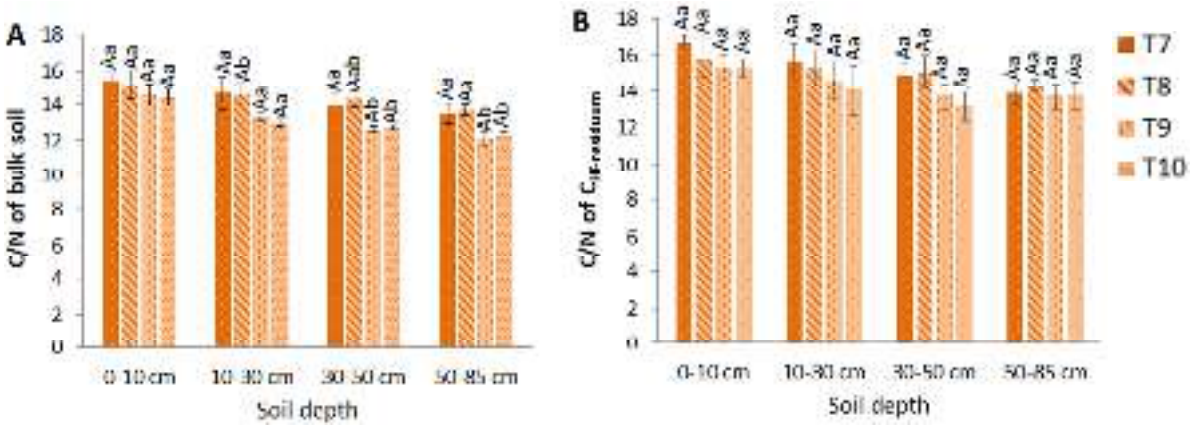

Figure S3.2.2 The average C:N ratio of (A) bulk soil and (B) $C_{HF\text{-}residuum}$ at each sampling site and depth. Capital letters indicate the comparison of four distinct sites at the same depth, whereas small letters indicate the comparison of four different soil depths at the same site. Different letters denote a significant difference according to one-way ANOVA followed by Tukey's test (P <.05). Error bars represent the standard error of the means (n = 4).

S3.2.3 $C_{HF\text{-}mobile}$

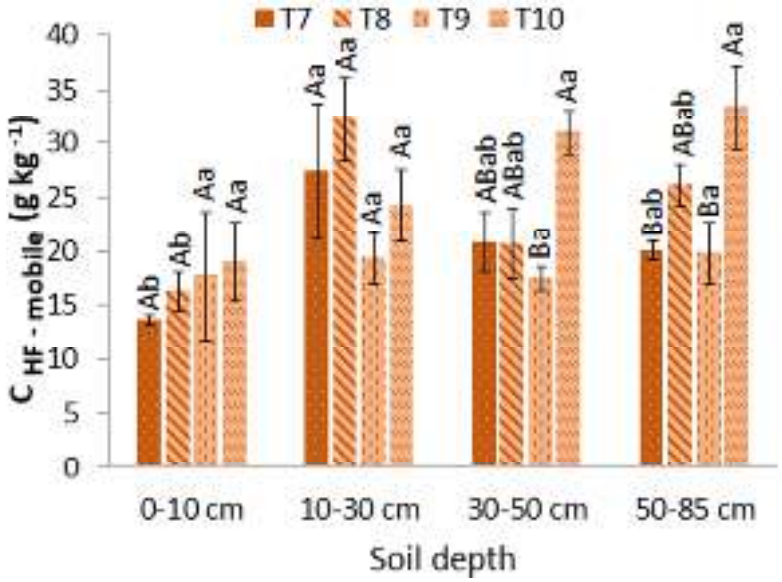

Figure S3.2.3 $C_{HF\text{-}mobile}$ (the organic carbon fraction of total C content that was mobilised by 2% HF solution). Capital letters indicate the comparison of four distinct sites at the same depth, whereas small letters indicate the comparison of four different soil depths at the same site. Different letters denote a significant difference according to one-way ANOVA followed by Tukey's test (P <.05). Error bars represent the standard error of the means (n = 4).

S3.2.4 Sodium pyrophosphate extractable C (C_{py})

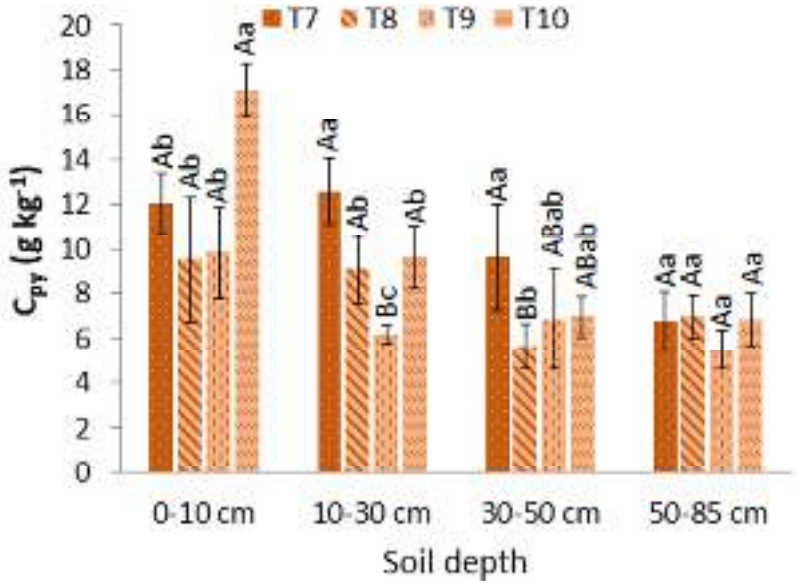

Figure S3.2.4 Pyrophosphate-extractable Carbon (C_{py}) at all sampling sites. Capital letters indicate the comparison of four distinct sites at the same depth, whereas small letters indicate the comparison of four different soil depths at the same site. Different letters denote a significant difference according to one-way ANOVA followed by Tukey's test (P <.05). Error bars represent the standard error of the means (n = 4).

S3.2.5 PCA scores of pyrolysis product group distribution

The PC1 loadings show a clear difference between MCC, MAHs and PAHs, with positive loadings, and polysaccharide and lignin products (except for 4-vinylphenol) with negative loadings (Figure S3.2.5A, Table S3.2.1). The PC1 illustrates that the main source of variation in the dataset is related to the depth variation in decay intensity. PC1 is not clearly different for different altitudes, but nevertheless at depth levels 2 and 3 there seems to be a decrease (better preservation of soil C at higher elevation). This is corroborated by the fact that at T10 only the topsoil has a negative score (best-preserved soil C), at T9 and T8 depth levels 1 and 2 have negative scores, and at T7 depth levels 1, 2 and 3 have negative scores. Hence, even though

decay intensity differences are more strongly affected by depth than by altitude, the effect of elevation (better preservation of soil C at high elevation) is clear especially for soil layers beneath the topsoil.

PC2 yields positive scores for topsoil samples. Positive loadings are found for two lignin products. More informatively, negative loadings of several N-compounds (pyrrole, pyridine, acetamide and diketopiperazines) indicate that PC2 highlights the low abundance of microbial N-rich soil C at the soil surfaces, and highest abundances at the second depth interval (10–30 cm) (FigureS.3.2.5B, Table S3.2.1).

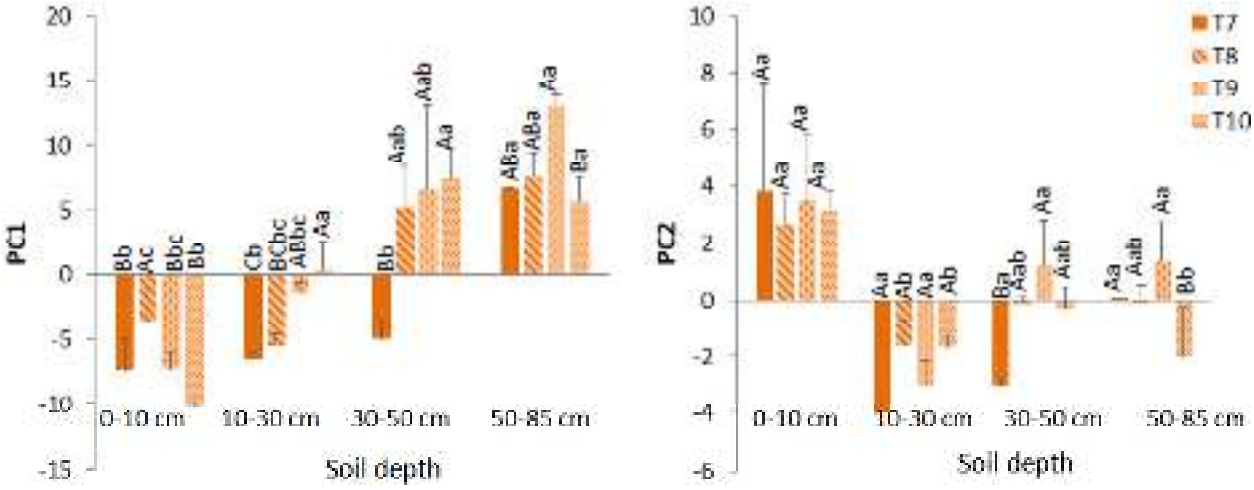

Figure S3.2.5 PC1 and PC2 scores of the Pyrolysis GC/MS compound along the altitudinal gradient on Mount Taranaki. Capital letters indicate the comparison of four distinct sites at the same depth, whereas small letters indicate the comparison of four different soil depths at the same site. Different letters denote a significant difference according to one-way ANOVA followed by Tukey's test (P <.05). Error bars represent the standard error of the means (n = 3).

Table S3.2.3 PC loadings and the Py-GC-MS compound list

RT(min)	m/z	Compound	group	PC1	PC2	PC3
1,767	82+53	2-methylfuran	CARB	-0,66	-0,46	-0,07
2,100	78	Benzene	MAH	0,70	-0,26	0,53
2,142	60	acetic acid	CARB	-0,80	0,10	0,21
2,475	96+95	Dimethylfuran	CARB	-0,72	-0,24	0,09
3,192	91+92	Toluene	MAH	0,49	-0,50	0,60
3,167	79	Pyridine	NCOMP	0,56	-0,63	0,19
3,242	67	Pyrrole	NCOMP	-0,12	-0,69	0,37
4,883	91+106	dimethylbenzene	MAH	0,61	-0,36	0,41
5,083	91+106	dimethylbenzene	MAH	0,73	-0,20	0,11
5,583	91+106	Ethylbenzene	MAH	0,89	-0,31	0,23
5,583	104+78	Styrene	MAH	0,52	-0,55	0,46
4,545	95+96	3/2-furaldehyde	CARB	-0,37	-0,28	-0,04
4,959	59	Acetamide	NCOMP	-0,04	-0,59	0,38
7,508	105+106	Benzaldehyde	OTHER	0,44	-0,26	0,47
8,092	110+109	5-methyl-2-furaldehyde	CARB	-0,21	-0,47	-0,46
8,692	114+58	4-hydroxy-5,6-dihydro-(2H)-pyran-2-one	CARB	-0,38	-0,36	0,11
9,292	94+66	Phenol	PHEN	-0,30	-0,31	0,55
9,575	112	3-hydroxy-2-methyl-2-cyclopenten-1-one	CARB	-0,16	-0,44	-0,45
9,850	113+128	dianhydrorhamnose	CARB	0,17	-0,71	-0,09
10,425	77+105	Acetophenone	OTHER	0,68	-0,05	0,52
11,050	128	Naphthalene	PAH	0,14	-0,62	-0,30
11,075	109+124	Guaiacol	LIG G	-0,82	0,13	0,30
11,458	107+108	4-methylphenol	PHEN	-0,48	-0,28	0,55
14,000	123+138	4-methylguaiacol	LIG G	-0,83	0,39	0,23
14,900	69+57	1,4:3,6-dianhydro-alpha-D-glucopyranose	CARB	-0,71	-0,21	-0,38
16,142	120+91	4-vinylphenol	LIG H	0,55	-0,06	0,59
16,375	137+152	4-ethylguaiacol	LIG G	-0,84	0,36	0,21
16,700	142+115	methylnaphthalene	PAH	0,72	-0,36	0,43
17,117	142+115	methylnaphthalene	PAH	0,64	-0,38	0,47
17,442	150+135	4-vinylguaiacol	LIG G	-0,74	0,30	0,37
18,525	164+149	4-(1-propenyl)guaiacol	LIG G	-0,86	0,23	0,31
19,858	164+149	4-(2-propenyl)guaiacol (cis)	LIG G	-0,87	0,20	0,25
20,942	164+149	4-(2-propenyl)guaiacol (trans)	LIG G	-0,86	0,24	0,24
18,700	137+166	4-propylguaiacol	LIG G	-0,86	0,33	0,26
18,550	154+139	Syringol	LIG S	-0,72	0,50	0,14
18,904	154	Biphenyl	PAH	0,57	-0,28	0,56
20,833	168+153	4-methylsyringol	LIG S	-0,67	0,57	0,15
21,575	116	unidentified carbohydrate product	CARB	-0,40	-0,28	-0,47
22,083	151+166	4-acetylguaiacol	LIG G	-0,69	-0,19	0,26
22,742	167+182	4-ethylsyringol	LIG S	-0,80	0,44	0,11
23,100	60+73	Levoglucosan	CARB	-0,83	0,20	-0,46
32,159	60+73	C16 fatty acid	MCC	-0,50	0,27	0,33
23,133	137+180	4-propan-2-one guaiacol	LIG G	-0,89	0,22	0,15
23,725	180+165	4-vinylsyringol	LIG S	-0,74	0,45	0,21
25,700	194+179	4-(2-propenyl)guaiacol (cis)	LIG S	-0,65	0,46	0,32
26,817	194+179	4-(2-propenyl)guaiacol (trans)	LIG S	-0,66	0,55	0,26
27,700	181+196	4-acetylsyringol	LIG S	-0,77	0,29	0,09
26,933	186+93	Diketodipyrrole	NCOMP	-0,77	-0,34	-0,12
27,100	55+56	prist-1-ene	MCC	0,07	0,13	-0,42
29,550	70+154	Diketopiperazine	NCOMP	-0,49	-0,56	0,37
29,508	181+210	4-(propan-3-one)syringol	LIG S	-0,72	0,46	0,10
31,900	70+194	Diketopiperazine	NCOMP	-0,64	-0,29	0,37

38,592	83+280	unidentified compound	OTHER	0,55	-0,26	-0,48
38,253	175+271	totarol (T)	OTHER	-0,19	-0,38	-0,39
38,525	202+284	dehydroferruginol (T)	OTHER	0,48	0,11	-0,03
45,375	59+72	Cx amide	MCC	0,64	-0,37	-0,08
41,317	58+59	methylketone C23	MCC	0,85	0,14	-0,18
44,333	58+59	methylketone C25	MCC	0,87	0,00	-0,31
45,742	58+59	methylketone C26	MCC	0,95	0,01	0,05
47,142	58+59	methylketone C27	MCC	0,84	-0,04	-0,28
48,458	58+59	methylketone C28	MCC	0,95	0,07	0,09
49,767	58+59	methylketone C29	MCC	0,89	0,11	0,14
51,001	58+59	methylketone C30	MCC	0,93	0,19	0,19
52,233	58+59	methylketone C31	MCC	0,44	0,55	0,35
53,500	58+59	methylketone C32	MCC	0,79	0,25	0,29
55,017	58+59	methylketone C33	MCC	0,74	0,21	0,04
8,017	55+69	alkene C10	MCC	0,93	0,02	0,16
10,858	55+69	alkene C11	MCC	0,97	-0,03	0,00
13,708	55+69	alkene C12	MCC	0,96	0,00	0,13
16,500	55+69	alkene C13	MCC	0,93	-0,03	0,12
19,133	55+69	alkene C14	MCC	0,88	0,08	0,11
21,633	55+69	alkene C15	MCC	0,96	0,00	0,10
26,258	55+69	alkene C17	MCC	0,80	0,12	0,22
28,400	55+69	alkene C18	MCC	0,81	0,01	-0,18
30,417	55+69	alkene C19	MCC	0,70	0,14	0,14
32,292	55+69	alkene C20	MCC	0,74	0,12	0,05
34,258	55+69	alkene C21	MCC	0,70	0,13	-0,20
36,050	55+69	alkene C22	MCC	0,85	0,27	0,10
37,725	55+69	alkene C23	MCC	0,80	0,17	-0,09
39,367	55+69	alkene C24	MCC	0,81	0,42	-0,04
40,959	55+69	alkene C25	MCC	0,93	0,21	0,01
42,475	55+69	alkene C26	MCC	0,88	0,25	0,18
43,950	55+69	alkene C27	MCC	0,87	0,28	0,05
45,358	55+69	alkene C28	MCC	0,91	0,09	0,13
46,783	55+69	alkene C29	MCC	0,74	0,45	0,00
48,058	55+69	alkene C30	MCC	0,89	0,26	0,19
49,383	55+69	alkene C31	MCC	0,75	0,12	-0,36
8,267	57+71	alkane C10	MCC	0,96	-0,02	0,05
11,092	57+71	alkane C11	MCC	0,95	-0,07	0,10
13,933	57+71	alkane C12	MCC	0,77	-0,22	-0,19
16,683	57+71	alkane C13	MCC	0,94	-0,05	-0,01
19,333	57+71	alkane C14	MCC	0,93	0,04	-0,05
21,817	57+71	alkane C15	MCC	0,89	-0,05	-0,01
26,408	57+71	alkane C17	MCC	0,96	0,00	-0,03
28,542	57+71	alkane C18	MCC	0,93	0,07	-0,12
30,567	57+71	alkane C19	MCC	0,95	0,10	-0,07
32,508	57+71	alkane C20	MCC	0,91	0,15	-0,07
34,367	57+71	alkane C21	MCC	0,91	0,20	-0,07
36,142	57+71	alkane C22	MCC	0,92	0,23	-0,03
37,842	57+71	alkane C23	MCC	0,89	0,15	-0,16
39,483	57+71	alkane C24	MCC	0,86	0,07	0,12
41,025	57+71	alkane C25	MCC	0,90	0,23	-0,12
42,575	57+71	alkane C26	MCC	0,92	0,27	0,11
44,042	57+71	alkane C27	MCC	0,89	0,23	-0,01
45,450	57+71	alkane C28	MCC	0,88	0,33	0,14
46,825	57+71	alkane C29	MCC	0,73	0,33	-0,01

48,142	57+71	alkane C30	MCC	0,87	0,34	0,12
49,433	57+71	alkane C31	MCC	0,72	0,11	-0,39
51,867	57+71	alkane C33	MCC	0,68	0,00	-0,37

S3.2.6 Pyrolysis product group distribution

For the MCC, MAHs and PAHs, clear positive depth trends are observed. These MCC do not exhibit a clear trend with temperature at depth levels 1, 2 and 4. MAHs tend to increase with increasing temperature at each depth level except for the topsoil. PAHs do not show a clear trend except for depth level 4 (decrease with altitude). Note that MCC levels increase between depth levels 2 and 3 whereas that of MAHs and PAHs exhibit the largest increment between the topsoil and depth level 2.

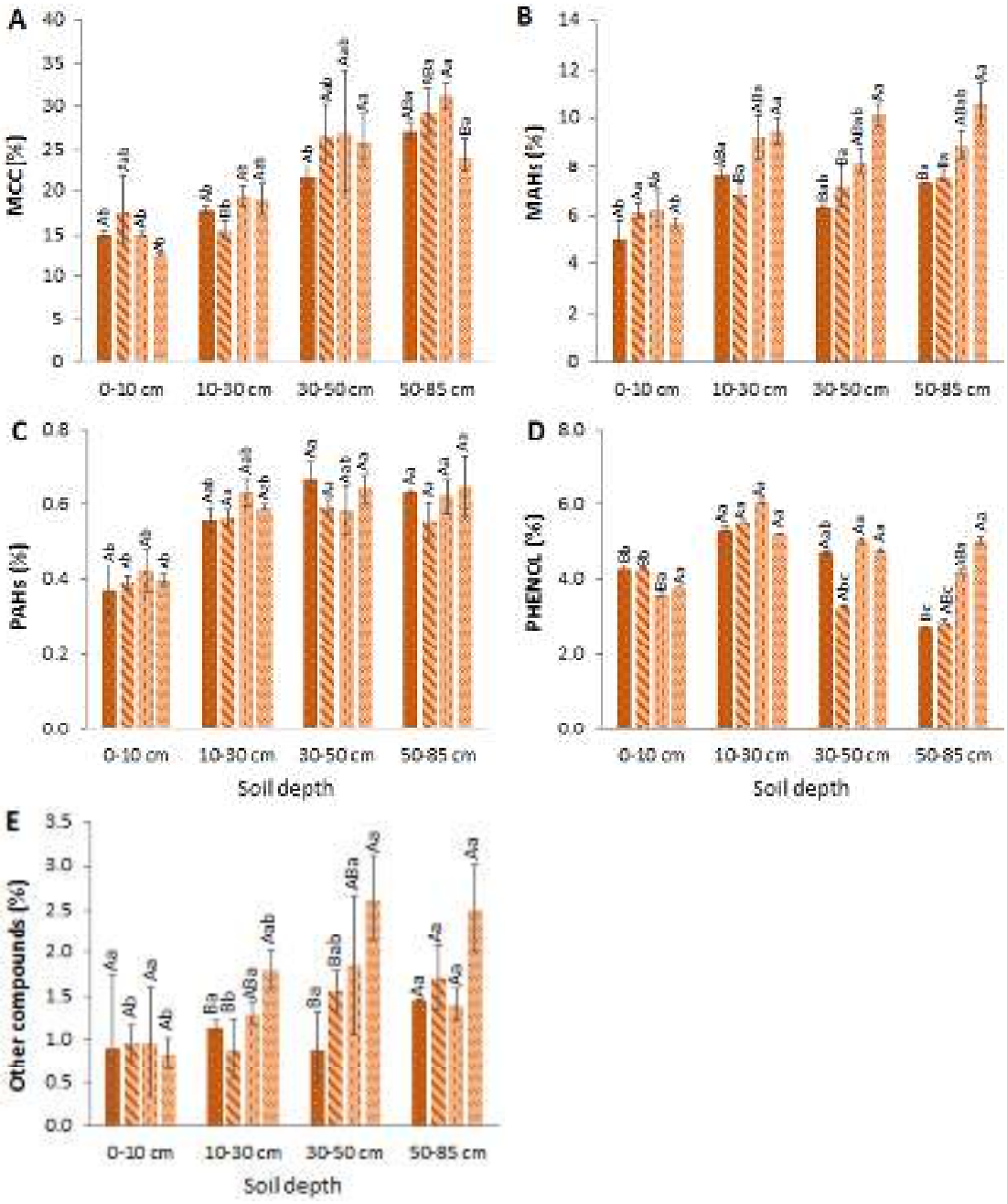

Figure S3.2.6 Pyrolysis product group distribution (Py-GC-MS) along the altitudinal gradient on Mount Taranaki. Capital letters indicate the comparison of four distinct sites at the same depth, whereas small letters indicate the comparison of four different soil depths at the same site. Different letters denote a significant difference according to one-way ANOVA followed by Tukey's test (P <.05). Error bars represent the standard error of the means (n = 3). MCC=methylene chain compounds (aliphatic OM), MAHs/PAHs=monocyclic/polycyclic aromatic hydrocarbons.

S3.2.7 Relationship between total C and reactive Al

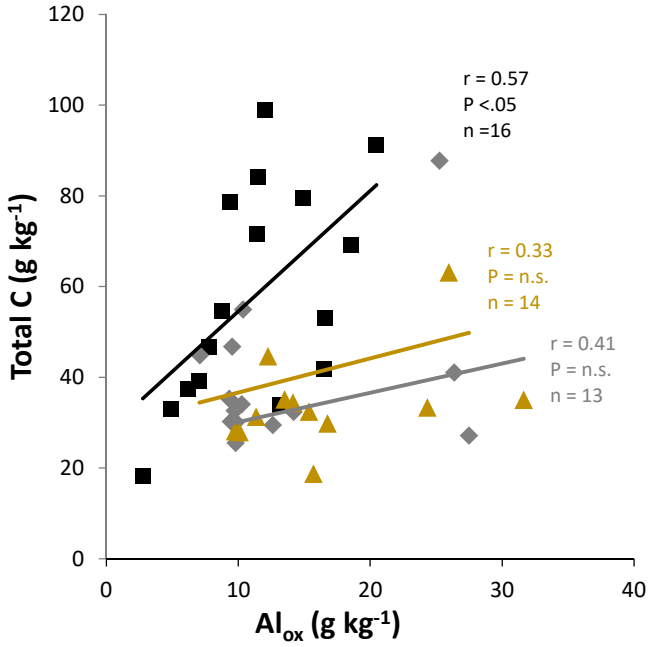

Figure S3.2.7 Linear regression by depth (excluding the top 10 cm) across sites between total C content and $Al_{ox.}$ The coefficient correlation (r), P value (significant at P <.05) and number of replicates (n) are given in the figure in the same colour as the trendline. The rectangle, diamond, and triangle each indicate a depth level: 10–30 cm, 30–50 cm, and 50–85 cm, respectively.

S3.2.8 Al_{ox} + ½ Fe_{ox}

Reactive Al and Fe constituents (as inferred by using Al_{ox}+½Fe_{ox} as proxy) tended to decline as altitude increased, although some exceptions were observed. T10 had a significantly larger Al_{ox}+½Fe_{ox} content (P <.05) than the rest of the sites at each corresponding depth studied. (Figure S3.2.8). The increase being gradual for T10 and T9, and abrupt for T7 and T8 (with a large jump from the 0–10 cm to the 10–30 cm depth). At all sampling sites, Al_{ox}+1⁄2Fe_{ox} content was largest at the deepest interval (50–85 cm) with a mean value of 2.1% compared to that of the topsoil with mean value of 0.63%.

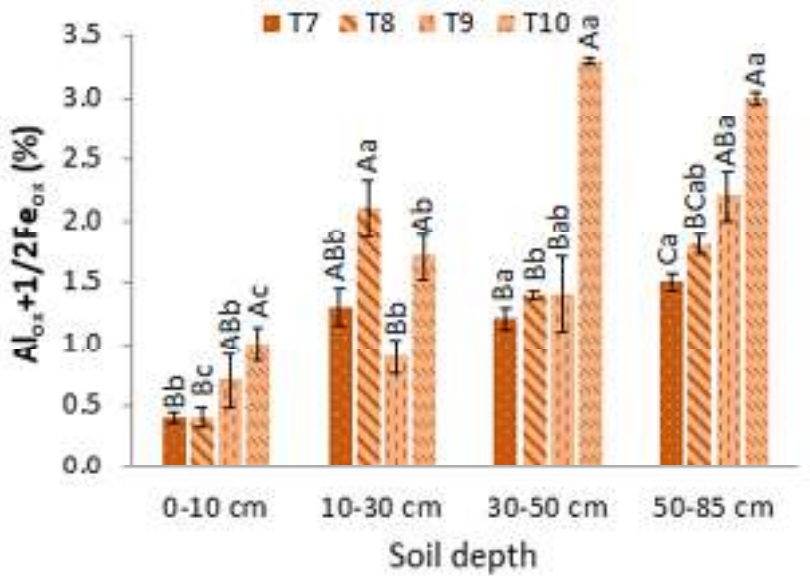

Figure S3.2.8 The average of Al_{ox}+1/2Fe_{ox} content at each sampling site and depth. Capital letters indicate the comparison of four distinct sites at the same depth, whereas small letters indicate the comparison of four different soil depths at the same site. Different letters denote the significant difference according to one-way ANOVA followed by Tukey's test (P <.05). Error bars represent the standard error of the mean (n = 4).

CHAPTER 4

HIGHER TEMPERATURE ACCELERATES THE FLUXES OF SOIL CARBON IN A MATURE MONTANE FOREST WITHOUT DECREASING SOIL CARBON STOCKS

Abstract

The decomposition of soil organic matter (OM) and soil CO_2 efflux are hypothesised to be accelerated under warming in the short term (months to years), thus potentially triggering a positive feedback loop with global warming. However, the extent to which soil carbon (C) responds to temperature rise is still uncertain in the long term (decades to centuries). Here, a space-for-time substitution approach was applied to study the long-term influence of temperature on soil C cycling across a ~3.2^{o}C mean annual temperature (MAT) gradient in a native forest ecosystem. Specifically, four elevation sites at Mt Taranaki (North Island, New Zealand), referred to as T7, T8, T9 and T10 based on their MAT (7.3, 8.2, 9.1 and 10.5^{o}C, respectively) were selected. We: (i) measured aboveground litterfall and soil respiration monthly and forest floor C storage every two months for a year; (ii) estimated the above- and belowground biomass, and belowground C input; and (iii) determined soil C stocks (to 85 cm depth) and semi-quantified the organic matter load as carbohydrates. There was a significant increase (P <.05) in aboveground (from 162 to 214 MgC ha^{-1}) and belowground biomass C (from 21 to 28 MgC ha^{-1}) as the temperature increased (from T7 to T10). This generated an associated increase in: (i) aboveground litterfall (from 1.8 to 2.4 MgC ha^{-1} yr^{-1}, P =.06); (ii) belowground C input (from 7.0 to 8.1 MgC ha^{-1} yr^{-1}, P =.08); (iii) soil respiration rate (from 9.0 to 10.4 MgC ha^{-1} yr^{-1}, P =.08); and (iv) decay intensity, as inferred from the carbohydrate preservation index (P =.09). Soil C stocks also increased with temperature from 153.6 to 176.4 MgC ha^{-1} (P =.06). This study demonstrates that the increase in temperature along this quasi-thermo-sequence at Taranaki increases plants' C input through enhanced gross primary production, which counteracts soil C loss, resulting in no apparent detrimental impact on soil C storage.

4.1 Introduction

Soils retain the largest carbon (C) pool in terrestrial ecosystems, amounting to 1300–1500 PgC in the first 1 m of the soil depth (Harden et al., 2018) and 2400 PgC down to 2 m globally, which is twice the amount of atmospheric C (830 PgC) (Paustian et al., 2016) and forest biomass C (363 PgC) (Pan et al., 2011) combined. The annual C input to the soils through aboveground litterfall and belowground C allocation is about 60 PgC yr^{-1}, which is balanced by a roughly equal amount of C lost to the atmosphere through soil respiration (Houghton, 2007). Because of the positive link between soil respiration and temperature, it has been assumed that rising temperatures would accelerate the rate of soil organic matter (OM) decomposition and decrease soil C storage, thus accelerating global warming (Kirschbaum, 2000; Davidson & Janssens, 2006; Bond-Lamberty & Thomson, 2010). Crowther et al. (2016) estimated that by 2050, 1^{o}C of warming would reduce global soil C stocks (and cause an associated loss as CO_2 carbon to the atmosphere) from 30 $\pm$ 30 to 203 $\pm$ 161 PgC, accounting for approximately 12–17% of the projected anthropogenic CO_2 emissions over this period (Riahi et al., 2011; Ballantyne et al., 2015). However, there are also studies showing that warming has no or even a positive effect on soil C stocks (Lu et al., 2013; Sistla et al., 2013; Blagodatskaya et al., 2016). These mixed results could be partly ascribed to the transient nature of the soil C response to warming (Smith et al., 2008). Therefore, more studies on the long-term effects of warming on soil C stocks are needed to reduce the uncertainty associated with the prediction of future climate–soil C feedback.

Most laboratory and field experiments subjected to artificial warming are insufficient for determining the long-term response of soil C stocks because they are often short-lived relative to the mean residence time of slowly cycling soil C pools, making it difficult to forecast changes in stable soil C pools (Powlson, 2005). Moreover, these experiments often overwhelmingly focus

on soil C losses, and fail to capture of contemporary changes in fresh C inputs under warming. Some investigations have used a space-for-time substitution approach to study the long-term warming effects on soil C. However, these studies are often confounded by variables other than temperature (Conant et al., 2011). An attempt to overcome these difficulties was made by Giardina et al. (2014) who investigated changes in the C pools and fluxes along a highly constrained mean annual temperature (MAT) gradient (from 13 to 18^{o}C) in the tropical wet montane forest of Hawaii, where the factors other than temperature affecting ecosystem processes (e.g., soil, vegetation and plant-available soil moisture) were relatively similar. These authors reported no significant effect of temperature on either bulk soil C stocks or the turnover of C fractions, with warming mostly increasing the belowground C inputs and accelerating the cycling of incoming plant-derived C, thus providing no evidence that a warmer temperature will have a direct impact on soil C stocks by accelerating bulk C decomposition.

The soils investigated by Giardina et al. (2014) developed from volcanic materials and are classified as Andosols. These soils are characterised by having large contents of short-range order (SRO) constituents (e.g., allophane, imogolite and ferrihydrite) and being rich in C (Litton et al., 2011; Shen et al., 2018). The high C stocks of Andosols are related to the greater ability of these constituents to interact with soil C, forming organo-mineral complexes and offering greater protection against decomposition than soils in which other clay-type constituents are present. Given their large soil C stocks, they might also have a greater liability than other soils when subject to environmental changes (Kov et al., 2018; Shen et al., 2018). However, the influence of temperature on soil C cycling and stocks in soils with abundant organo-mineral complexes is not yet well understood (Conant et al., 2008) and requires not only the study of C fluxes and stocks, but also the monitoring of changes in soil C composition with the use of specific molecular

markers. Carbohydrates are a primary source of plant C input into soils and are a key form of C that is stabilised by soil minerals (Kiem & Kögel-Knabner, 2003). They can be synthesised by both plants and microorganisms (Kögel-Knabner, 2002). Plant-derived carbohydrate molecules are utilised as a primary C source by soil microorganisms. However, microbial-derived carbohydrates are synthesised through anabolic processes and form organo-mineral associations that can be stabilised against further microbial decomposition (Miltner et al., 2012). It has been observed that altered turnover of soil C corresponds to a change in soil carbohydrate abundance and a shift in its composition (Kiem & Kögel-Knabner, 2003). Therefore, knowledge of the abundance and composition of soil carbohydrates might assist in assessing the influence of temperature on the turnover of soil C.

The Taranaki region in New Zealand offers a similar opportunity to that of Giardina et al. (2014), as it has a highly constrained MAT gradient. In comparison with Hawaii, the Taranaki sites have a lower temperature range (7.3–10.5^{o}C) and are covered by a temperate rainforest. Moreover, the Taranaki sites show a different trend in the change of soil mineralogy compared with Giardina et al. (2014), with a greater amount of SRO constituents at warmer sites, although this is only apparent below 30 cm depth. These differences allow a cross-site examination of the generality of previous findings that whole-ecosystem warming accelerates soil C cycling but has no impact on the soil C stocks (Giardina et al., 2014), which was the main objective of this study. For this, soil C pools (and carbohydrate abundance and composition), plant biomass C pools and soil C fluxes at four forest sites along the Taranaki temperature gradient were quantified. We hypothesised that an increase in temperature under conditions of no water deficit: (i) would increase aboveground and belowground plant growth and litterfall, thus increasing C inputs to soil; (ii) which would drive a greater efflux of CO_2 to the atmosphere, and therefore greater

microbial processing of soil C; and (iii) would not lead to a loss of soil C stocks, as the increase in soil CO_2 efflux would be counteracted by the increase in soil C input. Given that warming experiments have primarily been conducted in North America, Europe, and China, with few studies conducted in the Southern Hemisphere (van Gestel et al., 2018) , this research will contribute further to worldwide datasets through the addition of data from the Southern Hemisphere, which are needed to project C storage based on modelling.

4.2 Materials and Methods

4.2.1 Site description

The study was conducted in a mature native forest on the eastern flank of Mt. Taranaki, North Island, New Zealand. Four sampling sites were chosen, with elevations ranging from 512 to 1024 m above sea level (asl) with a difference of at least a 200-m elevation between each of the sites. The sites have a thermo-sequence with a MAT of 7.3, 8.2, 9.1 and 10.5^{o}C and are referred to as T7, T8, T9 and T10, respectively (Chapter 3, Figure 3.1B). The mean annual precipitation rates exceeded 3000 mm yr^{-1} at all sampling sites (Chapter 3, Figure 3.1A and Chapter 3, Table 3.1). All sampling sites had identical parent material, moisture (constant plant-available moisture) and native evergreen broadleaf trees (>80% with kamahi (*Weinmannia racemosa* L.f.) and mahoe (*Melicytus ramiflorus* J.R & G. Forster). The soil was formed on andesitic tephra from the Burrell lapilli eruption that occurred in AD 1655 (Aitken et al., 1978). It is classified as Allophanic soil by the New Zealand soil classification system (Hewitt, 2010) and an alu-andic Andosol according to the World Reference Base system (World Reference Base for Soil Resources, 2015). Despite all soils fulfilling the requirements needed to be classified as alu-andic Andosols, there is a gradient of reactive forms of aluminium (Al) across the transect below 30

cm depth, as inferred from values of allophane, which increase with temperature (e.g., the weight average between 30 and 85 cm depth at T10 vs. T7 is 8.04 vs. 2.29 g kg^{-1}) (Chapter 3, Figure 3.2D). However, there is no significant difference between 0 and 30 cm. The topography ranges from gentle to steep (Davies & Lambert, 2015). Soils are moderately well drained at lower elevations (460–760 m asl), with the water table always deeper than 0.5 m, and well drained at higher elevations (760–920 m asl) (Aitken et al., 1978). The native forest was assumed to be in a steady state in terms of soil C storage after achieving an advanced stage of succession since the last eruption (Knowles & Beveridge, 1982). No studies have documented major damage caused by natural (e.g., floods, windstorms and animals) or human disturbance (e.g., logging) that could have resulted in significant changes to the forest's structure. As explained in Chapter 5, most of the C efflux from soil organic matter (OM) decomposition occurs in the 0–15 cm depth interval, which also receives the majority of above- and belowground C inputs. As a result, the investigation of soil C cycling in this chapter focuses on the 0–15 cm layer rather than the entire soil profile, as soil OM decomposition between at the deeper soil intervals was estimated to be minimal in proportion.

4.2.2 Aboveground live and belowground biomass C

At all sampling sites, canopy trees were surveyed in 400-m^2 subplots. Kamahi (*Weinmannia racemosa* L.f.), tawa (*Beilschmiedia tawa* (A. Cunn) Kirk)) and mountain totara (*Podocarpus cunninghamii* Hooibr. ex Endl), particularly at T7, dominated the canopy, which ranged in height from 20 to 30 m. Mahoe (*Melicytus ramiflorus* J.R & G. Forster) dominated the understorey trees, with a height range of 10–15 m. Tree ferns (*Hymenophyllum spp.* Sm) were prevalent at the two highest sites, where the weather conditions were colder and wetter. Aboveground

biomass (AGB) C was estimated by the allometric equations developed by Beets et al. (2012) for indigenous tree species in New Zealand. The allometric equations differentiated between stems with a diameter at breast height (DBH) of ≥0.10 m and <0.10 m (1.3 m above the ground). Belowground biomass (BGB) C (roots) was estimated with robust conversion factors established from a systematic review (Mokany et al., 2006). For all targeted trees, DBH was measured with a diameter tape (Larjavaara and Muller-Landau, 2013).

4.2.3 Forest floor

At all sampling sites, material from the forest floor was collected every 2 months from four square plots measuring 0.5 m × 0.5 m. The collected forest floor material was dried in an oven at 65^{o}C to a constant weight. The material was then separated into leaf material, or twig, branch and bark material, and each component were weighed. The C content of each component of the forest floor material was analysed using Elementar Vario MACRO equipment (Hanau, Germany).

4.2.4 Aboveground litterfall C

Litterfall was collected monthly, and the information generated was used to calculate the rate of C from aboveground litterfall (F_{AC}), which included dead leaves and small branches <10 cm in diameter at different stages of decomposition that accumulated on the forest floor. Five litter traps were placed at each sampling site. One trap had a collection surface of 1 m × 1 m (Figure S4.1.1) but for the other four, it was 0.4 m × 0.6 m. After collection, the litterfall biomass was dried at 65^{o}C to a constant weight. The C content of each litterfall component was analysed with an Elementar Vario MACRO (Hanau, Germany), and the total C content was weight averaged.

Through a visual observation, coarse woody debris was estimated to be ≤5% of the F_{AC} input at each sampling site and was not considered in this study.

4.2.5 CO_2 efflux from the soil surface

A static chamber made from polyvinyl chloride collars (diameter: 230 mm; height: 250 mm) was used to sample CO_2 efflux from the soil surface (Fs). At each site, four static chambers were inserted about 50 mm into the ground (Figure S4.1.2A). At the time of sampling, the chambers were closed by a lid with a batten to turn and lock the lid in position. Gas sampling was carried out at 0, 30 and 60 min with four replicates at each site. A 25-mL syringe with a three-way tap was connected to the sampling tube of the chamber (Figure S4.1.2B). The syringe was pumped many times to achieve adequate mixing of the gas in the chamber before collecting the sample in the 25-mL syringe and then transferring it to a 12.5-mL evacuated gas vial. CO_2 gas sampling was carried out every month for 1 year (April 2019–March 2020). The previous studies of Bahn et al. (2010a) and Litton et al. (2011) reported similar patterns in F_S measured monthly over 1 year versus the daily F_S, which closely mirrored the seasonal patterns in soil temperature, indicating that monthly measurements can be used to predict the annual F_S. The air temperature was recorded every 30 min with a Tinytag Plus 2 data logger (Gemini Data Loggers Ltd., West Sussex, UK), which was set up at each site during the research period (Figure S4.1.3).

The concentration of CO_2 (parts per million (ppm)) in the 12.5-mL evacuated gas vials was measured with a gas analyser fitted with a CO_2 transducer (Analytical Development Co, Hoddesdon, UK) using N_2 as a carrier gas at a flow rate of 35 mL min^{-1}. The gas analyser was calibrated with a 0.5% CO_2 β-standard (BOC Ltd., Auckland, New Zealand) and the linear signals over the standard range were recorded with an HP 3396A integrator. The concentration

of the CO_2 slope (α_v) in each vial was determined over time (T0, T30 and T60). The density of CO_2 (ρ) was derived from the ideal gas law:

$$P \times V = n \times R \times T \quad (1)$$

$$\rho = P \times M/(R \times T) \quad (2)$$

where P is the atmospheric pressure (Pa), V is the volume (m^3), n is moles (mol), R is the gas constant (8.3145 m^3 Pa mol^{-1} K^{-1}, T is air temperature (K), ρ is the density (kg m^{-3}) and M is the molar concentration (g mol^{-1}). The CO_2 fluxes were calculated as $F_S = \rho \times \alpha_v \times V_c$, where V_c is the volume of the chamber. The unit was then converted to MgC ha^{-1} mo^{-1} by multiplying F_S x 12/44 (C atomic weight/CO_2 molecular weight) × 60 (min) × 24 (h) x 30 (d).

4.2.6 Approaches used to estimate belowground C

Total belowground carbon allocation (F_{BC}) is defined as the annual total C allocated from AGB to BGB to produce and maintain roots, mycorrhizae and other symbionts, as well as root exudates (Giardina et al., 2004). The forest at the sampling sites was considered to be in a steady state. Under this assumption, the amount of C that enters the soil (above- and belowground detritus input) yearly is approximately equal to the annual C loss, or:

$$F_S = F_{AC} + F_{BC} \quad (3)$$

where F_S is the CO_2–C efflux from the soil surface, F_{AC} is the C input from aboveground litterfall (mostly leaves and small branches) and F_{BC} is the C input from belowground sources.

This approach is coupled with the assumption that annual changes in soil C storage are negligible in undisturbed forests (Nadelhoffer et.al., 1998; Gower et al., 1996). Carbon losses through erosion and leaching were minor, as supported by the values of cold-water extractable C (C_{H2O}) obtained at these sites, despite the large amount of water draining through the soil (Figure S4.2.1) (Richter et al., 1999). According to visual observations, coarse woody debris was estimated to be ≤5% of aboveground litterfall C, or approximately ≤0.1 MgC ha^{-1} mo^{-1}, and was considered to be negligible in this study. The annual F_{BC} can therefore be estimated as the annual soil respiration minus the annual detritus input from AGB decomposition, or:

$$F_{BC} = F_S - F_{AC} \quad (4)$$

4.2.7 Determination of total C content, soil C stocks and carbohydrate loads

Method and data for calculating the total C content and soil C stocks are detailed in Chapter 3.

4.2.7.1 Carbohydrate abundance and carbohydrate preservation index

The abundance and composition of soil carbohydrates were used to assess the influence of temperature on the turnover of soil C via pyrolysis gas chromatography mass spectrometry (GC/MS) (methods see Chapter 3, 3.2.4.2). Pyrolysis-GC/MS analysis of hydrofluoric acid-treated soil samples was conducted following Wang et al. (2016) and Shen et al. (2018). The abundance of each pyrolytic product of carbohydrates was roughly measured as its relative proportion to the total quantified peak area (%TQPA). The abundance of total carbohydrates was

therefore calculated as the sum of the abundances of all identified pyrolytic products of carbohydrates. We also proposed a carbohydrate preservation index (CPI) to indicate the change in the composition of carbohydrates. The index was based on the observation that an accelerated turnover of soil C is expected to decrease the ratio of plant-derived carbohydrates to total carbohydrates. We used anhydrosugars, which are the pyrolytic product of cellulose, as a biomarker of plant-derived carbohydrates. The CPI was thus calculated as the ratio of the relative abundance of anhydrosugars to that of total carbohydrate products. A lower CPI value indicated a faster soil C turnover.

4.2.8 Data analysis

Statistical analysis was carried out in IBM SPSS Statistics version 25.0 (IBM Corp, Armonk, New York, USA). One-way ANOVA with Tukey's test was performed to find significant differences (at P <.05) between the treatment means across the levels of a single categorical factor, with all other variables being constant. A statistical analysis of the pyrolysis-GC/MS products (i.e., carbohydrates abundance and CPI) was carried out with Tanagra 1.4.50 (Hastie et al., 2001). The correlation between two variables was evaluated by linear regression analysis. Data are presented as the mean $\pm$ 1 SE (standard error).

4.3 Results

4.3.1 Plant productivity

The highest AGB C was found at T10 with a mean value of 214.2 $\pm$ 13.2 MgC ha^{-1}, which differed significantly (P <.05) from T8 and T7 with mean values of 177.4 $\pm$ 10.2 and 162.4 $\pm$ 11.8 MgC ha^{-1}, respectively (Figure 4.1A). The highest estimated BGB C was also found at T10, with a mean value of 27.8 $\pm$ 13.2 MgC ha^{-1}, which differed significantly (P <.05) from T8 and

T7, with a mean value of 23.0 ± 12.1 and 21.1 ± 11.8 MgC ha^{-1}, respectively (Figure 4.1A). The forest floor C stock tended to decrease with an increase in temperature (Figure 4.1B). T7 had the highest forest floor C stock at 3.1 ± 0.3 MgC ha^{-1} (P =.08), whereas T10 had the lowest at 2.9 ± 0.3 MgC ha^{-1} (Figure 4.1B).

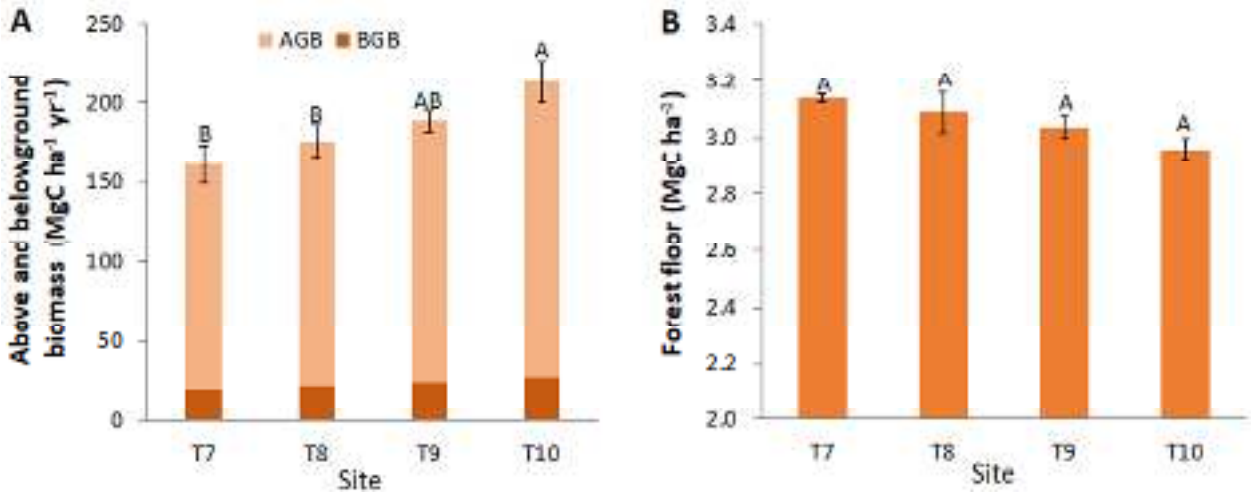

Figure 4.1 (A) The mean value of aboveground biomass (ABG) and belowground biomass (BGB) C (roots), (B) forest floor C stocks along the thermo-sequence in Taranaki. Different letters denote significant differences among sampling sites according to one-way ANOVA followed by Tukey's test (P <.05). Error bars represent the standard error of the mean (n = 4).

4.3.2 Carbon fluxes

Figure 4.2A shows the distribution of all measured F_{AC} values when plotted against the corresponding temperatures at each sampling time (r = 0.77, P <.05). When averaged on the basis of MAT, F_{AC} at the lowest temperature site (T7) had a mean value of 1.8 ± 0.2 MgC ha^{-1} mo^{-1}, which was smaller (P =.06) than that at T10, with a mean value of 2.4 ± 0.1 MgC ha^{-1} mo^{-1}, with a strong positive correlation between these mean values and the MAT at each site (r = 0.96, P <.05) (Figure 4.2B).

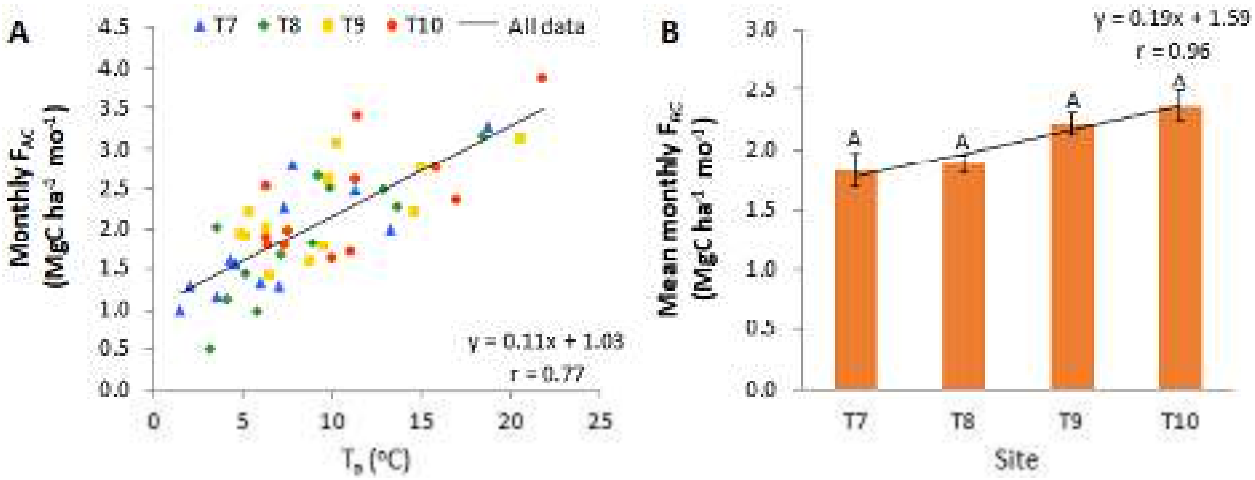

Figure 4.2 (A) The relationship between individual values of aboveground litterfall C (F_{AC}) and temperature at sampling time (r = 0.77, P <.05) measured monthly over a 1-yr research period, (B) the relationship between average monthly F_{AC} and mean annual temperature (MAT) (r = 0.77, P <.05) along the thermo-sequence in Taranaki. Different letters denote significant differences among sampling sites according to one-way ANOVA followed by Tukey's test (P <.05). Error bars represent the standard error of the mean (n = 5).

The monthly soil respiration (Fs) showed a clear seasonal pattern (Figure 4.3A), as expected. The peak was observed in summer (December–February), with an average rate of 13.3 MgC ha^{-1} mo^{-1}, and the lowest was in the winter (June–August) with an average rate of 8.4 MgC ha^{-1} mo^{-1} (Figure 4.3A). Soil respiration from all sites was strongly correlated to temperature over a wide temperature range throughout the year (r = 0.96, 0.92, 0.89 and 0.89, for T7, T8, T9 and T10, respectively; significant at P <.05) (Figure 4.3B). As the distance between points of different experiment is minor, the data from all sites can be fitted well with a single curve (r = 0.91, P <.05) (Figure 4.3B). The mean monthly Fs also showed a strong positive correlation with MAT (r = 0.99, P <.05) (Figure 4.3C). The Fs at the lowest temperature site (T7) had a mean value of 9.1 $\pm$ 0.8 MgC ha^{-1} mo^{-1}, which was smaller (P =.08) than the Fs at T10, which had a mean value of 10.4 $\pm$ 0.4 MgC ha^{-1} mo^{-1} (Figure 4.8C). As expected, the F_{AC} had a strong positive correlation with Fs (r = 0.83, P <.05) (Figure S4.2.2).

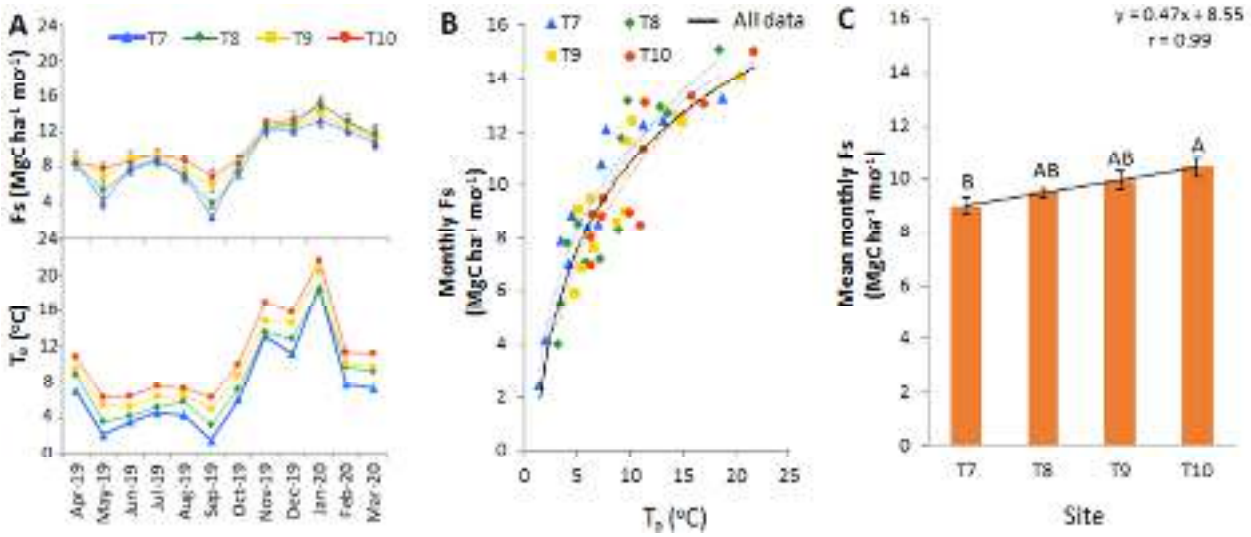

Figure 4.3 (A) Monthly average air temperature (Ta, bottom graph) and soil respiration (Fs, top graph), which mirror the seasonal temperature along the thermo-sequence in Taranaki, with summer (December–February) having the highest value and winter (June–August) having the lowest, (B) monthly relationship between Fs (individual values of replicates) and Ta over a 1-yr research period (r = 0.96, 0.92, 0.89, 0.89 and 0.91 for T7, T8, T9, T10 and all data, respectively; significant at P <.05, (C) monthly mean Fs at each sampling site. Different letters denote significant differences according to one-way ANOVA followed by Tukey's test (P <.05). Error bars represent the standard error of the mean (n = 4).

The estimated monthly average F_{BC} (estimated as $F_{BC} = Fs - F_{AC}$) tended to increase with increasing temperature, with F_{BC} at T7 being lower (P =.08) than at T10, with mean values of 7.2 $\pm$ 0.1 MgC ha^{-1} mo^{-1} and 8.1 $\pm$ 0.4 MgC ha^{-1} mo^{-1}, respectively (Figure 4.4).

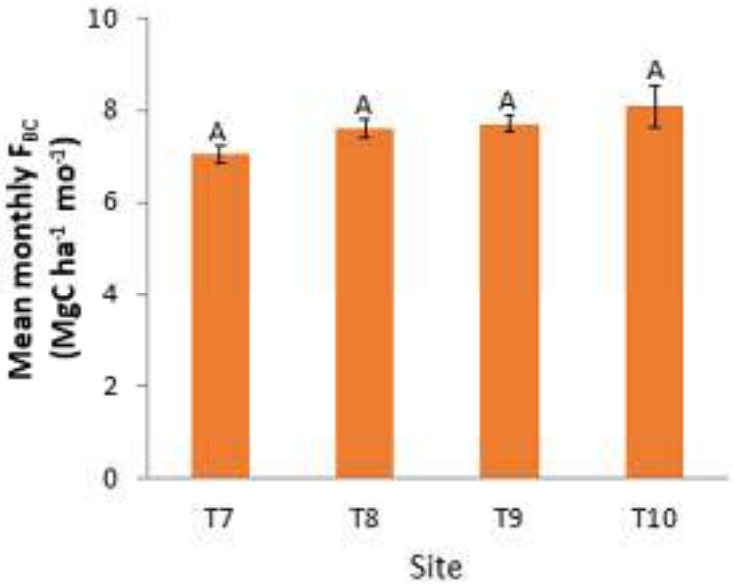

Figure 4.4 The annual average total belowground carbon (F_{BC}) at each sampling site across a ~3.2°C mean annual temperature gradient in Taranaki. Different letters denote significant differences among sampling sites according to one-way ANOVA followed by Tukey's test (P <.05). Error bars represent the standard error of the mean (n = 4).

4.3.3 Soil C content, C stocks and carbohydrate preservation index

When the soil C contents were compared (Figure 4.5.A), significant differences (P <.05) across sites were found for all the subsoil layers. Specifically, the C content of T7 and T8 showed an accumulation of soil C down to at least 30 cm depth, consistent with their larger forest floor, as opposed to T9–T10, where the content quickly dropped below the top layer (Figure 4.5A). This is consistent with the larger forest floor in the sites at higher altitudes (Figure 4.1B). The total cumulative soil C stocks calculated on an equivalent soil mass basis down to 85 cm depth tended to rise with an increase in temperature, ranging from 153.6 $\pm$ 11.7 to 176.4 $\pm$ 10.4 MgC ha^{-1} between T7 and T10, however no significant differences (P >.05) observed across sites at the depths considered (Figure 4.5B).

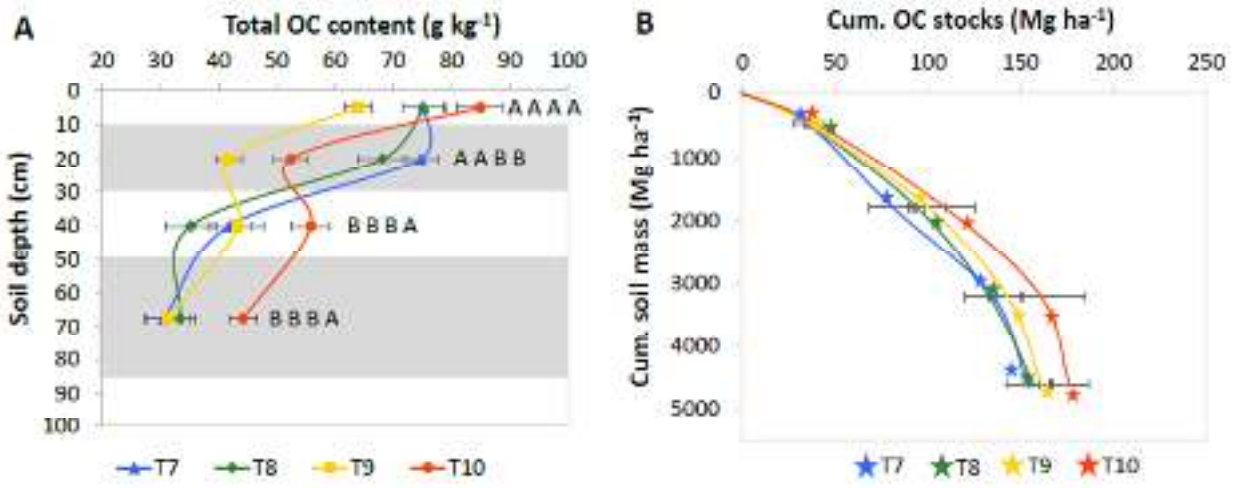

Figure 4.5 (A) Total carbon (C) content and (B) cumulative soil C stocks at four different sites and depths along the thermo-sequence in Taranaki. Different letters, read to represent the sites in the legend, denote significant differences among sampling sites according to one-way ANOVA followed by Tukey's test (P <.05). Error bars represent the standard error of the means (n = 4).

Information about the pyrolysis-GC/MS results from these sites is provided elsewhere (Chapter 3, Figure 3.2.6 and Figure SI S3.2.6). Here, we focus only on the pattern of carbohydrates (quantity and quality) across the transect at different soil depths. The products from carbohydrates made the largest contribution to the pyrolysis signal, accounting for 51.6 ± 8.4% of total quantified peak area. The abundance of total carbohydrates tended to decrease as the annual mean temperature increased across the gradient and decreased with depth at each specific site (Figure 4.6A). The CPI also showed a decreasing pattern as the annual mean temperature increased at the same soil depth, with an exception at the soil depth interval of 0–10 cm (Figure 4.6B), suggesting a faster decay rate at warmer sites. The CPI also showed a clear decrease with depth (P <.05), especially at T10. These results suggested that both the abundance and composition of carbohydrates were influenced by both the MAT and soil depth.

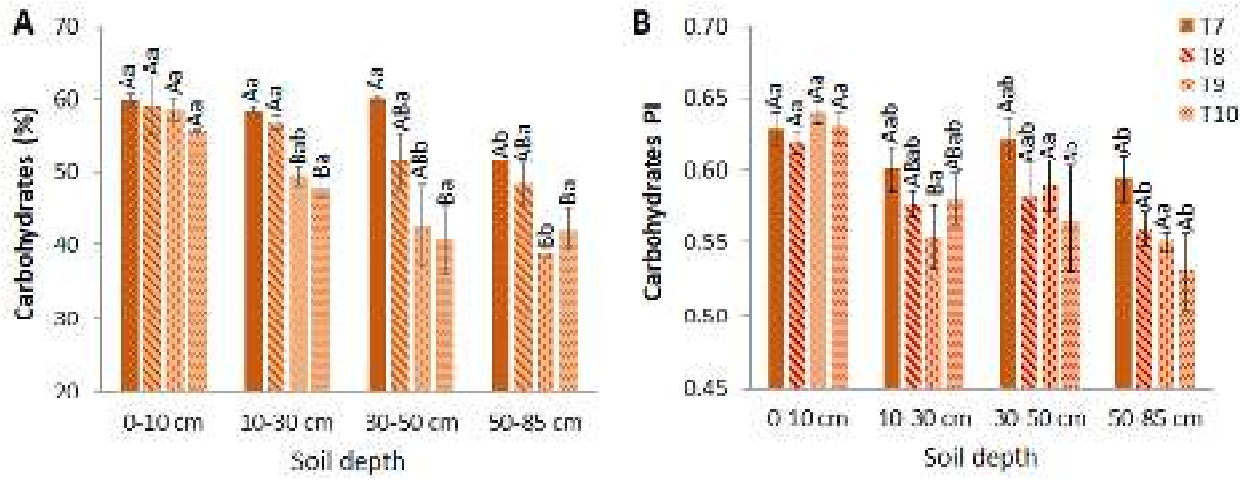

Figure 4.6 Carbohydrates and carbohydrate preservation index (CPI) along the thermo-sequence in Taranaki. Capital letters show a comparison among the four soil depths at the same site, whereas small letters represent a comparison of the four different sites at the corresponding depth. Different letters denote a significant difference according to one-way ANOVA followed by Tukey's test (P <.05). Error bars represent the standard error of the mean of two to four replicates.

4.3.4 Carbon budget at each temperature considered

The above and belowground C biomass increased with temperature and this resulted in an increase in F_{AC} and F_{BC}, which accelerated soil respiration (Fs) along the thermo-sequence in Taranaki. From the lowest (T7 = 7.3°C) to the highest MAT (T10 = 10.5°C), C stocks in AGB increased from 162.0 $\pm$ 11.8 to 214.2 $\pm$ 3.1 MgC ha^{-1}, whereas those in BGB (root biomass) increased from 21.1 $\pm$ 8.4 to 27.8 + 11.2 MgC ha^{-1}. F_{AC} increased by 29% from 1.8 $\pm$ 0.2 to 2.4 $\pm$ 0.1 MgC ha^{-1} mo^{-1}, whereas F_{BC} increased by 15%, from 7.0 $\pm$ 0.1 to 8.1 $\pm$ 0.4 MgC ha^{-1} mo^{-1} (Figure 4.7). The Fs tended to increase as temperature rose. Fs at T7 was 9.0 $\pm$ 0.8 MgC ha^{-1} mo^{-1} and it was Fs 10.4 $\pm$ 0.4 MgC ha^{-1} mo^{-1} at T10. Estimated belowground C input (F_{BC}) was the largest contributor to total Fs, accounting for about three-quarters of total soil CO_2 efflux, with F_{AC} contributing the other quarter. Soil C stocks tended to increase from 153.6 $\pm$ 11.7 MgC ha^{-1} at T7 to 176.4 $\pm$ 10.4 MgC ha^{-1} at T10. The forest floor C stocks, which represent the smallest C

pool considered, showed the reverse pattern, declining from 3.2 $\pm$ 0.3 MgC ha^{-1} at T7 to 2.9 $\pm$ 0.3 MgC ha^{-1} at T10 (Figure 4.7).

The summary diagram shows dissolved organic C leaching, but we did not measure the exact value due to the difficulty of measuring this component inside the forest. However, we noticed that the area has a high precipitation rate. As a result, cold water extractable-C (C_{H2O}) was measured to estimate DOC leaching. Cold C_{H2O} accounts for approximately 0.09% of the total C content (Figure S4.2.1). Given that the concentrations of DOC leachate are typically smaller than the C_{H2O} concentration, the DOC leachate concentration can be much smaller. Therefore, it is most likely negligible. Our estimate is equivalent to that of Jiang et al. (2020), who estimated that mature forest leachate contained 0.07% soil C. In addition, our F_{AC} just considers litterfall without measuring coarse woody debris (CWD). Based on visual observation, CWD was estimated at around $\leq$5% of aboveground litterfall C, or 0.1 MgC ha^{-1} $month^{-1}$. Given that CWD is very slowly released due to its lignin composition, the amount of C efflux from this component could be even lower than these estimates suggest. Additionally, under steady state conditions, the quantity of carbon input from the wood will be released into the atmosphere at the same rate, resulting in no change in the carbon stock. Therefore, we believed that this lack of measurement would not change the pattern that we observed.

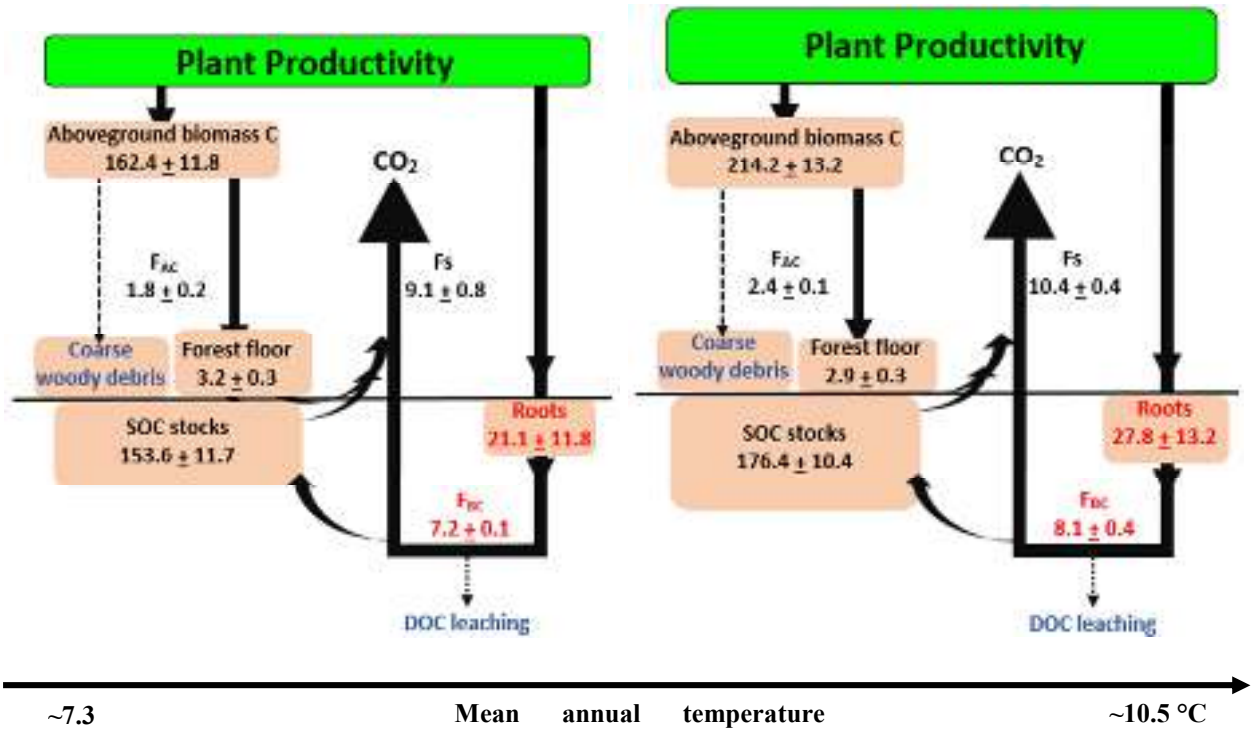

Figure 4.7 A summary of the response of a mature native forest ecosystem to an increasing ~3.2°C MAT gradient in Taranaki, New Zealand. Coarse woody debris and dissolved organic C (DOC) leaching are in blue font, indicating that they are considered to be negligible.

4.4 Discussion

4.4.1 Temperature increased above- and belowground C inputs to the ecosystem

Taranaki, with its ~3.2°C MAT gradient along the altitude while maintaining a uniform parent material and soil geochemistry (at a soil depth of 0–30 cm), native vegetation cover and excess precipitation, proved to be a suitable natural laboratory for studying the effects of temperature changes on soil C cycling. The F_{BC} and F_{AC} both increased by 1.5 MgC ha^{-1} yr^{-1} from the site with the lowest MAT (T7) to the site with the highest MAT (T10). These results are consistent with previous findings observed along an elevation gradient by Joshi et al. (2003) and Sheikh et al. (2009) who found that temperature plays a role in increasing plant growth until optimum temperature is attained.

The increase in plant C input is attributed to the increase in the productivity of the forest system at lower elevations (i.e., warmer sites) (Figure 4.1A), which, in turn, leads to enhanced rates of litterfall and belowground C flux rates (Pietikäinen et al., 2005; Koch et al., 2007). The increasing trend of plant productivity at lower altitudes can be attributed to several temperature-driven processes. First of all, total tree density and basal area are greater at sites with a higher MAT. Second, higher temperatures (until an optimum is reached) have been shown to increase enzyme activity and the photosynthetic rate in the leaves, and thus the AGB (Luo et al., 2009; Zhang et al., 2013; Baig et al., 2015). Thirdly, root growth can be enhanced by warmer temperatures through an increase in the metabolic activity of root cells and by promoting the development of lateral roots, thereby generating greater root biomass (McMichael & Burke, 1998; Puhe, 2003; Repo et al., 2004).

Additionally, the lower forest productivity at low-temperature sites may also be, to some extent, associated with increased cloud cover, which reduces irradiance and inhibits photosynthesis by fully exposed solar leaves (Mulkey et al., 1996; Graham et al., 2003). The observation that the C:N ratio was lower at warmer sites (Chapter 3, Figure S3.2.2) suggests a greater N mineralisation potential (Joshi et al., 2003; Lu et al., 2013), which may also contribute to the greater plant productivity at warmer sites by alleviating the N limitation that is often encountered by forest ecosystems (LeBauer & Treseder, 2008).

4.4.2 Temperature increased the microbial processing of C and soil CO_2 efflux

The forest floor mass declined as MAT increased (from 3.1 to 2.9 MgC ha^{-1}), which can be attributed to the faster decomposition of the forest floor at the warmer sites. In line with the forest floor mass and the litterfall rates (turnover rate=litterfall/forest floor mass) (Chapin et al.,

2011), we estimated the turnover rates for unprotected particulate C (i.e., C that is not associated with the mineral fraction) to increase by 1.4-fold from the coolest to the warmest site (Figure S4.2.3). The slower decomposition rate of the forest floor was also reflected by the greater abundance of carbohydrates and the higher CPI in this soil layer at the colder sites (Figure 4.6). In particular, the higher CPI suggested that a larger proportion of plant-derived carbohydrates remained at colder sites because of a lesser degree of decomposition.

Our results show that warmer temperatures not only accelerate the cycling of litterfall on the forest floor and belowground C but also the cycling of bulk soil C. Slower decomposition at the colder sites than at the warmer sites could be supported by the presence of a more "mor" type of C at the colder sites rather than a "mull" type of C (Labaz et al., 2014), as illustrated by the pattern of soil C contents down the soil profile, as the C contents at T7 and T8 showed a thicker A1 horizon (that is, a less drastic drop in soil C with depth) than at warmer sites (T9 and T10). The finding that bulk C cycling is accelerated in mineral soil horizons is opposed to the results from Giardina et al. (2014), where no effect of temperature on the bulk soil C and its fractions was reported. These somewhat conflicting results can be partly explained by the different techniques used to gauge the turnover of soil C. Giardina et al. (2014) took advantage of radiocarbon-based measurements to suggest that <5% of the total soil respiration was derived from soil C turnover. However, they also conceded that the actual contribution of soil C decomposition could be underestimated because radiocarbon measurements were less powerful at capturing the dynamics of fast-cycling soil C pools. In contrast, our results suggest that pyrolysis-GC/MS is able to capture the subtle alterations in soil C composition in response to different MAT along the temperature gradient. Both the abundance of carbohydrate-related pyrolysis products and CPI tended to decrease as the temperature increased, suggesting a

generally faster decomposition of plant-derived carbohydrates at a higher MAT. The decreasing pattern seemed to be more prominent in the deeper soil intervals, with warming accelerating the degradation of plant-derived C at depth, thus indicating that C cycling in subsoils is also sensitive to warming. This agrees with a previous finding that subsoil carbon cycling was as sensitive as that in surface soils to increased temperature in a whole-soil warming experiment (Ofiti et al., 2021).

The F_S–temperature curves across the altitude gradient showed a logarithmic shape as the temperature increased, which differed from the exponential relationship between respiration and temperature often observed in previous warming experiments (i.e., Kirschbaum, 2004). Notably, the observed temperature in this study was air temperature, not soil temperature. The lag between air and soil temperatures may modify the shape of the temperature response curve of soil respiration. In addition, our results also suggest that other factors beyond soil temperature may play a role in influencing soil respiration. The factors that have been reported to confound the effect of temperature on soil respiration include, non-exclusively, soil moisture, changes in soil C composition and accessibility, shifts in soil microbial and enzymatic activities (Trivedi et al., 2018), and belowground C allocation (Bahn et al., 2010b). Although precipitation was high at all sites and soil moisture was not a limiting factor for the growth of plants and soil microorganisms, high soil moisture may reduce CO_2 effluxes by lowering CO_2 diffusivity through the soil profile (Hashimoto & Komatsu, 2006). The increase in precipitation over winter will cause greater leaching and loss of the nutrients needed for plant and microbial growth (Macías and Camps-Arbestain, 2020), creating a lower soil respiration than predicted by an exponential temperature–respiration relationship. Furthermore, it is well documented that the time lag between photosynthesis and allocation to BGB and soil respiration is highly variable depending on the

transport distance (plant height and phloem path length), root depth, plant physiology and growth stage, and environmental conditions (Davidson & Holbrook, 2009; Kuzyakov & Gavrichkova, 2010; Mencuccini & Hölttä, 2010). This may induce variations in the temperature and soil respiration curves among studies.

4.4.3 Higher temperatures did not cause a loss of soil C stocks

Along the thermo-sequence, we observed that soil C stocks did not decrease or even tend to increase at warmer sites, despite the associated increase in soil respiration. This is attributed to the greater C gains achieved through increased C inputs from both F_{AC} and F_{BC} at warmer sites, as mentioned above. The enhanced C inputs counteracted the C loss from soil respiration, resulting in no significant change in C storage along the Taranaki thermo-sequence.

Our findings align with those of Giardina et al. (2014) and Ziegler et al. (2017), but not with those of Conant et al. (1998) and Garten & Hanson (2006). However, the study of Conant et al. (1998) was carried out across different ecosystems, from a low-elevation desert to a high-elevation pine forest, where there were large differences in the amount of C in the litterfall, with the least in the desert and the greatest in the pine forest. The work of Garten & Hanson (2006) was conducted in sites where the vegetation types and soil moisture conditions were not uniform along the elevation gradients. The differences in environmental variables other than temperature may confound the real effects of warming on soil C cycling. The lack of change in soil C stocks in this study also contradicts previous findings that reported significant C losses from warming the entire soil profile by 4^{o}C for 4.5 years (Soong et al., 2021). This discrepancy can be attributed to two reasons. First of all, the whole-soil warming experiment heated the soil only and was not able to warm the whole ecosystem, so the effects of warming on NPP, litterfall, and

belowground C allocation were not examined. With increased soil respiration and constant plant C input, soil C loss was not surprising. Secondly, the soil was heated for 4.5 years and mainly addressed the short-term effects of warming, which contrasts with our experiments that focused on the long-term effects of warming on soil C stocks.

In our study, the accelerated OM decomposition with warming may have led to an increase in microbial-derived C, which is more susceptible to being preserved through organo-mineral interactions. This could be inferred from the proportion of 2% hydrofluoric acid (HF) - solubilised C within the total C (Chapter 3; Figure 3.4B), which showed that more microbial-derived C was bound to the reactive sites of soil minerals at warmer temperature sites and increased with depth. This could partly explain the larger C stocks at warmer sites, corroborating the previous finding by Shen et al. (2018), which was carried out in the same study area. The organo-mineral complexes provide chemical stabilising mechanisms, where organic ligands adhere to mineral surfaces, limit the substrate availability to bacteria, and allow C to persist (Six et al., 2002; Hartley et al., 2021). However, this is likely to have had a minor effect, given that the significant difference in the amount of reactive Al was observed only below 30 cm and, as noted in Chapter 5, most of the C efflux from soil OM decomposition occurs in the 0–15 cm soil depth interval, which also receives the majority of above- and belowground C inputs (Baldock & Skjemstad, 2000; Kleber et al., 2015).

4.5 Conclusion

The Taranaki region has been demonstrated to be an ideal location for testing the long-term effects of temperature on rapid C fluxes. Our results clearly show that warming influenced the acceleration of the rapid C fluxes (litterfall and total belowground C fluxes) in this forest

ecosystem, and the cycling of bulk soil OM decomposition. Moreover, there was an increase in C inputs from plant production (above- and belowground) which, in turn, increased C losses but also increased C gains, resulting in no significant change in C storage along the thermo-sequence. This finding indicates that long-term warming alone might not influence C storage, providing that the other environmental conditions (e.g., shifts in vegetation, atmospheric CO_2 concentration, and precipitation) are maintained under global warming.

Appendix II. Supporting Information for Chapter 4 (SI4)

S4.1 Supporting materials and methods

S4.1.1 Litterfall traps

Figure S4.1.1 Litterfall trap size 1 m × 1 m was set up at each sampling site.

S4.1.2 Respiration chambers

Figure S4.1.2 (A) Four respiration chambers were inserted ca. 50 mm randomly into the soil (litter layer intact) at each sampling site, (B) A 25 mL syringe was connected to the chamber pipe for taking the gas sampling.

S4.1.3 Temperature logger

Figure S4.1.3 A temperature logger was installed to record air temperature at a 30 min interval during the research period at each sampling site.

S4.1.4 Cold Water extractable-C (C_{H2O})

Cold water extractable-C (C_{H2O}) was measured to estimate potential dissolved organic C (DOC) leaching, given that this is the fraction of DOC that is easily transferred into the soil solution (Stutter, et al., 2007), although given that soil structure disruption occurs during the extraction, it may contain DOC in macropores and micropores, and overestimate DOC in the leachate (Zsolnay, 1996). Cold C_{H2O} was determined following the method described by Curtin et al. (2015). For this, 3 g of soil samples from the deepest soil depths (50–85 cm) were first extracted with 18 mL of DI water (soil: DI water = 1:6, w/w) at room temperature (20 $\pm$ 1^{o}C) (Ghani, et al., 2003). The soil-water suspension (in 50 mL centrifuge tubes) was shaken for 1 h on an end-over-end shaker (ca. 50 r.p.m.) and then centrifuged (ca. 4500 g) for 20 min. The supernatant was filtered through filter paper (Whatman no. 42) into separate tubes. Organic C in the cold-

water extracts was analysed using a Total Organic Carbon Analyzer (Shimadzu TOC-VCSH, Shimadzu Corp, Japan). For total C analysis, 40 µl of the extracts were injected into the detection chamber in triplicates.

S4.2 Supporting results

S4.2.1 Cold Water extractable-C (C_{H2O})

Across all sampling sites, C_{H2O} did not show a consistent pattern. T7 has the highest content of C_{H2O}, amounting to 381.4 mg kg^{-1}, followed by T10, T9, and T8, which amounted to 325.9, 295.2, and 187.9 mg kg^{-1}, respectively (Figure S4.2.1). A significant difference (P <.05) was only found between T7 and T8 (Figure S4.2.1).

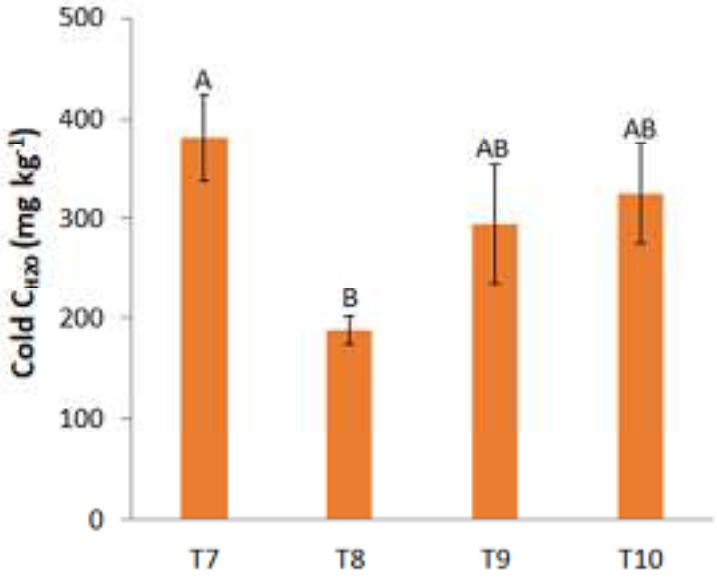

Figure S4.2.1 The average of the C_{H2O} at each sampling site. Different letters denote the significant difference between sampling sites according to one-way ANOVA followed by Tukey's test (P <.05). Error bars represent the standard errors (n = 4).

S4.2.2 Relationship between Fs and F_{AC}

As expected, the F_{AC} had a strong positive correlation with soil respiration (Fs) with r = 0.83 (P <.05) and fit to a linear model with Fs = 3.49F_{AC} ± 2.49 (Figure S4.2.2). Despite the strong correlation, there were a couple of measurements at low temperatures that diverted from the main group of data. This was due to the variation in temperature during the measurement. In fact, F_{AC} was positively correlated (significant at P <.05) with temperature, as shown by Figure 4.8A.

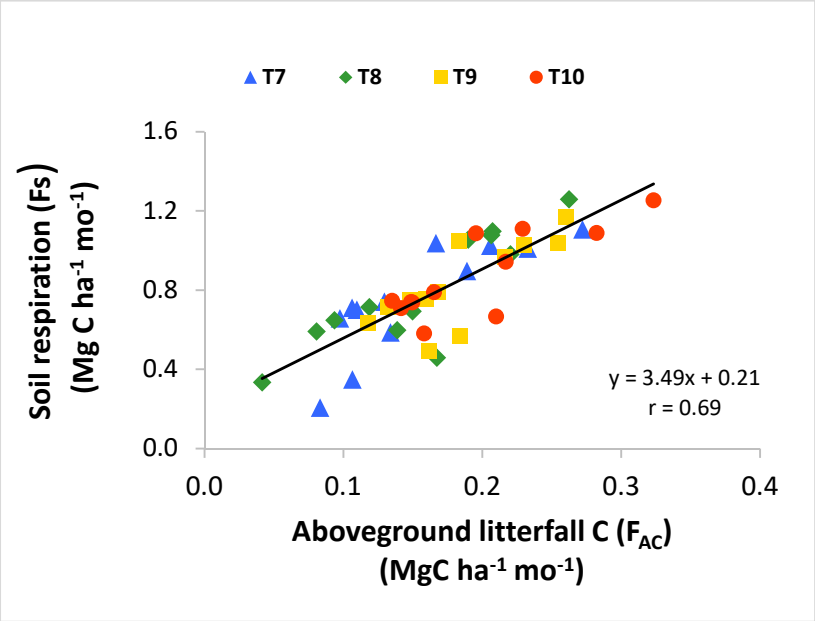

Figure S4.2.2 Linear regression analysis between Fs and F_{AC}. A linear curve fitted independently to all sampling sites with Fs = 3.45F_{AC} + 2.49, r = 0.83, significant at P <.05. The measurement was carried out monthly over a one-year research period.

S4.2.3 Turnover rate

The turnover rates of unprotected particulate C (i.e., C that is not associated with the mineral fraction), as estimated from the forest floor mass and the litterfall rates (turnover rate=litterfall/forest floor mass) (Chapin et al., 2011) increased by 1.4-fold from the coolest to the warmest site (Figure S4.2.3).

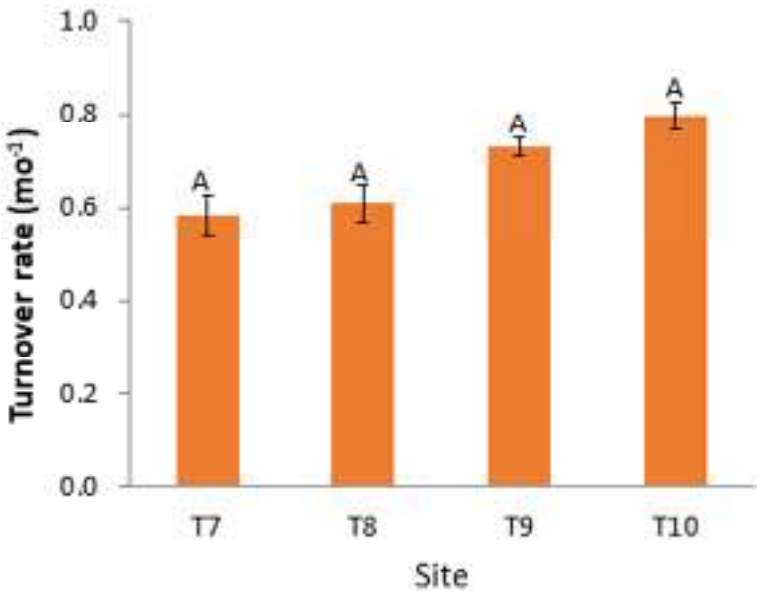

Figure S4.2.3 The turnover rate of unprotected particulate C (i.e., OC that is not associated with the mineral fraction) at each sampling site. Different letters denote the significant difference between sampling sites according to one-way ANOVA followed by Tukey's test (P <.05). Error bars represent the standard errors (n = 4).

CHAPTER 5

TEMPERATURE SENSITIVITY OF SOIL ORGANIC MATTER DECOMPOSITION ACROSS A THERMO-SEQUENCE IN A TEMPERATE MONTANE FOREST

Abstract

The lack of knowledge on the long-term effect of elevated temperature on the temperature sensitivity of soil organic matter (OM) decomposition (Q_{10}) obscures the accurate prediction of the soil carbon (C) cycle feedback to global warming. Here, a space-for-time substitution approach was used in Mount Taranaki (a stratovolcano located in the west coast of New Zealand's North Island) to investigate the long-term effect of elevated temperature on Q_{10} and to explore the factors regulating the response of Q_{10}, by taking advantage of the existing highly constrained mean annual temperature (MAT) gradient (from 7.3 to 10.5^{o}C), with other factors affecting soil OM turnover being similar. Soil samples from the MAT gradient were incubated in the laboratory at several controlled temperatures (5, 15, 25, 35^{o}C). Q_{10} values of cumulative CO_2 efflux and of three C pools derived from a three-component model were estimated and coupled with a comprehensive set of soil geochemical properties and soil OM molecular composition data using multivariate analysis. Results showed that all Q_{10} values decreased (from 1.8 to 1.5) as MAT increased across the temperature gradient. However, redundancy analysis and structural equation modelling revealed that Q_{10} values of cumulative CO_2 efflux and distinct C pools were differentially regulated by soil C availability, OM molecular composition, and OM-mineral interactions. These findings suggest that Q_{10} of soil OM decomposition tends to attenuate under centennial-scale warming, which should be accounted in Earth System Models in order to accurately project soil C cycle-warming feedback.

5.1 Introduction

Soil organic matter (OM) is the greatest terrestrial C pool, containing more C than the world's vegetation (450 PgC) and atmosphere (870 PgC) combined (IPCC, 2021). About 60 PgC is

released to the atmosphere annually through soil respiration, which is largely contributed by soil OM decomposition (Paul, 2014). Given its importance in the global C cycle, the response of soil OM decomposition to global warming represents a vital determinant of C cycle-climate feedback (Davidson & Janssens, 2006; Mao et al., 2022). Global mean surface temperature by the end of the 21st century under Representative Concentration Pathways 6.0 is expected to range from 1.4^{o}C to 3.1^{o}C above the temperature at the beginning of the century (Pachauri & Meyer, 2014). Such global warming magnitude was estimated to drive a net loss of *ca.* 55 Pg organic C from the upper soil horizons via enhanced OM decomposition rate (Crowther et al., 2016). However, this estimate has a large uncertainty primarily because of the lack of universal agreement on an appropriate function of the temperature sensitivity of soil OM decomposition (Q_{10}). Therefore, it has received considerable attention in ongoing efforts to better quantify this critically important parameter and to identify the key factors regulating Q_{10} (Kirschbaum, 2010; Giardina et al., 2014; Meyer et al., 2018; Qin et al., 2019).

The temperature sensitivity of soil OM decomposition has been extensively estimated, but mainly based on incubation experiments. Results suggest that Q_{10} is both spatially and temporally variable (Qin et al., 2021; Mao et al., 2022). For example, incubations with soils collected from broadly geographical regions show that Q_{10} varies horizontally across space (Qin et al., 2021; Mao et al., 2022). There are also studies showing that Q_{10} differs vertically along soil depths (Li et al., 2020; Li et al., 2021). In addition, growing evidence has shown that Q_{10} changes over time, which often displays a transient pattern with Q_{10} increasing initially and decreasing after a certain period (Karhu et al., 2010; Dacal et al., 2020). However, those results are primarily derived from short-term incubation and field experiments and unlikely to capture much information about the long-term effect of warming (Conant et al., 2011). Long-term field

studies are therefore indispensable to advance our understanding of long-term response of soil OM decomposition to warming. A recent study found that Q_{10} in a Spanish dryland ecosystem decreased after warming for 10 years compared to the onset of the experiment (Dacal et al., 2020). Yet in a global synthesis of 27 temperature manipulation studies covering nine biomes and over 20 years of warming, Q_{10} was found unaltered under warming (Carey et al., 2016). Moreover, in a 26-year field-based warming experiment from a mid-altitude forest, Melillo et al. (2017) identified four phases of soil OM decomposition response to warming, suggesting Q_{10} changed inconsistently within the experimental duration. These inconsistent findings may reflect the transitory state of soil C cycling at the non-equilibrium stage of warming perturbation (Walker et al., 2018) and, therefore, demand experiments of longer duration. However, to our knowledge, warming experiments longer than several decades are sparse largely because they are difficult to implement (Conant et al., 2011). Consequently, our understanding about the long-term warming effect on Q_{10} is still limited. An alternative way for moving forward is to use a space-for-time substitution approach, such as an MAT gradient, to study the long-term elevated temperature effects on Q_{10} of soil OM decomposition across sites along altitude gradients or over broad latitudinal scales, although this approach is sometimes criticised due to the difficulty to separate the effect of elevated temperature from those of precipitation and vegetation shifts, along with their impacts on soil pedogenesis (Conant et al., 2011).

The temperature sensitivity of soil OM decomposition is also dependent on soil OM components (Qin et al., 2019). New paradigms consider soil OM as a continuum of progressively decomposing organic compounds, which form myriad interactions with minerals and decomposers (Lehmann & Kleber, 2015; Lehmann et al., 2020). Such complex nature confers different soil OM components with contrasting resistances to decomposition and thus diverse Q_{10}

values (Lehmann et al., 2020). Clearly, an averaged Q_{10} value for soil OM as a whole masks the responses of different OM components to elevated temperature and may lead to an erroneous prediction of future soil C loss (Qin et al., 2019). Several studies have attempted to solve this issue by isolating soil C pools with different turnover times using pool-based models and estimating Q_{10} for each pool (Qin et al., 2019; Mao et al., 2022). Such a manner not only greatly improves our understanding of the temperature sensitivity of different soil OM components, but also provides mechanistic insights into specific factors regulating Q_{10} of each OM component.

Ultimately, the large variation of Q_{10} can be attributed to the multiple mechanisms controlling soil OM persistence, which can be grouped roughly in two categories, including: (i) chemical recalcitrance conferred by molecular structures of soil OM (e.g., condensed aromatic C structures in pyrogenic C); and (ii) environmental constraints, particularly the physicochemical protection by forming mineral-OM associations (i.e., mineral adsorption and aggregation) (Davidson & Janssen, 2006; Conant et al., 2011; Lehmann & Kleber, 2015). Theoretically, according to the kinetic theory, Q_{10} increases as the molecular structure is more recalcitrant (Davidson & Janssen, 2006; Conant et al., 2011) and, therefore, as OM decomposition proceeds and recalcitrant molecules become residually enriched over time, Q_{10} increases. On the other hand, when forming mineral-OM associations, soil OM is protected by minerals from decomposition due to the limited accessibility/availability to decomposers. In this scenario, Q_{10} becomes less dependent on molecular structure of OM, but rather controlled by the release kinetics of OM from mineral surfaces and/or the destruction of aggregate matrixes (Conant et al., 2011). These two mechanisms are not mutually exclusive and often act interactively yet with altered relative importance for different OM components and under different circumstances (Conant et al., 2011). Therefore, disentangling their relative contribution and identifying factors

that drive the shifts in the contribution may improve our understanding of Q_{10} changes under warming.

Mount Taranaki in the west coast of the New Zealand's North Island has a highly constrained MAT gradient (~3.2^{o}C range), with other factors affecting soil OM turnover (i.e. precipitation, soil and vegetation types) being relatively similar. Therefore, this study can help overcome the shortcomings of common cross-site studies and offer an ideal site to investigate the long-term effect of elevated temperature on Q_{10} of soil OM decomposition and to explore the factors regulating the change in Q_{10}. Two hypotheses were tested: (i) temperature sensitivity of soil OM decomposition decreases as MAT increases across the temperature gradient; (ii) temperature sensitivities of distinct OM components differs in responses to elevated temperature and the responses are driven by contrasting mechanisms. We collected soils from the MAT gradient and conducted a 330-d laboratory incubation experiment at a series of temperatures. The incubation results were fitted by a three-component model to derive three C pools with distinct decomposition rates followed by calculating their corresponding Q_{10} values. These values were then coupled with a set of comprehensive soil geochemical properties and OM molecular composition data using multivariate analysis to gain mechanistic insights into biogeochemical drivers of Q_{10} changes. As the major part of C is stored in deep soils (Lorenz & Lal, 2005; Rolando, 2021) and sensitivity to warming might change with depth (Hicks Pries et al., 2017), we also examined the long-term effect of elevated temperature on Q_{10} across soil depths.

5.2 Material and methods

5.2.1 Study area

The study was carried out on the eastern flank of Mount Taranaki. We selected four sites at elevations ranging from 512 to 1024 m asl with a difference of at least a 200-m elevation between each of the sites. The thermosequence from lowest to the highest altitude have MATs of 7.3, 8.2, 9.1, and 10.5^{o}C (and are referred to as T7, T8, T9, and T10), respectively (Chapter 3, Figure 3.1). Rainfall is received throughout the year and is considered adequate to prevent moisture limitations (>3000 mm per year at all sites) (Chapter 3, Figure 3.1). The topography ranged from gentle to steep (Davies & Lambert, 2015). However, to minimise the effects of erosion and leaching, the sampling sites were selected on stable landscapes inside the forest. Soils are moderately well drained at lower elevations (512–680 m asl) and well drained at higher elevations (760–920 m asl) (Aitken, 1978). All four study sites were covered with native broadleaved evergreen trees, consisting of >80% of kamahi (*Weinmannia racemose* L.f.) and mahoe (*Melicytus ramiflorus* J.R. & G. Forster) trees. The soils at all sites had developed from similar parent material, andesitic tephra of the Burrell formation that originated from a volcanic eruption in 1655 A.D. (Tonkin, 1970; Aitken, 1978) and was categorised as alu-andic Andosol based on the World Reference Base system (World Reference Base for Soil Resource, 2015).

5.2.2 Soil sampling

In February 2019, at each specific elevation (T7, T8, T9, T10), we selected a sampling area, where four sampling positions (i.e., replicates) were chosen. At each position, four soil columns down to 40 cm depth (0–5, 10–15, 20–25, and 35–40 cm) were taken using a 50-mm diameter PVC pipe (cylinder) cut into a 5-cm length (Figure SI S5.1.1A). The soil columns were carefully

pounded into the soils to minimise soil disturbance as much as possible. A total of 256 soil columns (4 elevations × 4 positions/elevation × 4 soil columns/position × 4 depths/column) were then transported to the laboratory while being kept at a storage temperature <5^{o}C in preparation for the subsequent incubation. For soil chemical analyses, a fifth column was collected from each position using the same cylinders and at identical depth intervals, resulting in a total of 64 additional 5-cm soil columns. These were air-dried until they reached a constant weight and then sieved through a 2-mm mesh and used to determine the following soil analyses: total C content and stocks (methods see Chapter 3, 3.2.3), pH in water (methods see Chapter 3, SI S3.1.1), aluminum (Al_{py}) in organo-mineral complexes (methods see Chapter 3, 3.2.2), short range order (SRO) materials (Al_{ox}, Fe_{ox}, and Si_{ox}) to estimate the quantity of SRO constituents (e.g., allophane and Al/Fe oxy-hydroxides (Al_{ox} + 1/2Fe_{ox})) (methods see Chapter 3, 3.2.2), sodium pyrophosphate-extractable C (C_{py}) (methods see Chapter 3, S3.1.3), cold water extractable-C (C_{H2O}) (methods see Chapter 4, S4.1.4). Data for these soil chemical analyses are provided in Table S5.2.1 in the Supplementary Information. Soil OM composition (i.e., carbohydrates, N compounds, lignin, methylene chain compounds (MCC), monocyclic aromatic hydrocarbons (MAHs), and polycyclic aromatic hydrocarbons (PAHs)) was characterised using Py-GC/MS (methods see Chapter 3, 3.2.4.2) after a hydrofluoric acid (HF) treatment (methods see Chapter 3, 3.2.4.1) in soil samples taken at 0–10, 10–30, and 30–50 cm in an earlier sampling, and the data were included in RDA and SEM to reveal the factors regulating Q_{10s}. The OM composition data from depths 0–10, 10–30, 10–30, and 30–50 cm were then utilised for depths 0–5, 10–15, 20–25, and 35–40 cm, respectively (data see Chapter 3, Table SI S3.2.1).

5.2.3 Soil incubation

Soil samples were incubated without further disturbance, with the exception of several samples collected from high-elevation sites that contained considerable coarse fragments (i.e., pumice). For those containing coarse fragments (<15% of the incubated cylinders), the soils were sieved through a 2-mm mesh and repacked carefully according to the bulk densities of the soils. Prior to incubation, the base of the soil columns was taped with perforated plastic film. Then soil columns were watered and brought to field capacity to ensure consistent moisture content and had the base resealed with unperforated plastic film thereafter (Figure S5.1.1B). A total number of 256 soil columns plus four blanks, thus in total 260 samples, were prepared for the incubation. The blanks were columns without soil but taped with plastic film on both sides. Each soil column was placed in a 500 ml jar for incubation. To maintain a humid environment, five ml of water acidified to a pH of ~1.5 with diluted HNO_3 was added to the bottom of the incubation jars to minimise CO_2 solubility in water. The acidified water was replenished when needed. All samples were then acclimatised for 48 h at room temperature in the dark (Tucker et al., 2013) before being placed into different temperature-controlled cabinets for their incubations (Figure S5.1.1C). Twenty ml of 0.25 M NaOH solution was added to a plastic vial (35 ml) and placed in the jar to trap CO_2 emitted from microbial respiration (Figure S5.1.1D). 260 samples were incubated at 5, 15, 25, and 35°C for 330 days (Figure S5.1.1E).

5.2.4 Determination of CO_2 emission

During the first week of the incubation, the plastic vial, containing 20 ml of 0.25 M NaOH solution, was exchanged daily to measure the respired CO_2. From the second to the fourth week, the vial was removed every three days. After the fourth week, the vials were removed weekly

until the eighth week. Thereafter, the vials were exchanged fortnightly. The amount of CO_2 absorbed was determined by measuring the electrical conductivity (EC) of the NaOH solution in the vials using an EC meter and following a modified method of Woo et al. (2016). Carbon dioxide (CO_2) trapped was calculated using a linear model:

$$y = -1.9555x + 91.882 \quad (1)$$

where y = CO_2 (ml CO_2/g soil); x = EC of the NaOH solution (ms/cm) with an R^2 of 0.9982

Equation (1) was obtained from a standard curve generated by injecting six known standards of CO_2 with concentration of 0.5, 2.6, 5.5, 11, 22, and 33 ppm. Those standards were put into 500-ml jars containing 20 ml of 0.25 M NaOH solution in a plastic vial and left to equilibrate for 24 hours at 25 ^{o}C prior to EC measurement.

5.2.5 Modelling C pools

We used a three-pool exponential C decay model to fit the data and to determine the effects of temperature on the decomposition of discrete soil C pools (Bauer et al., 2008; Herath et al., 2015):

$$C_{tot} = C_f + C_i + C_s \quad (2)$$

where C_{tot} is total C in an incubated sample and $C_f, C_i \; and \; C_s$ are the amounts in notional fast, intermediate and slow pools. Each pool was assumed to decay exponentially during the incubation so that:

$$C_i = C_{i,0} e^{-\tau_i t} \quad (3)$$

where *i* refers to one of the three notional pools, $C_{i,0}$ is the initial amount of C in pool *i* at the start of the incubation, *t* is time in days and τ_i is a decay constant for pool *i*.

The C loss at time *j*, as ΔC_j, can then be calculated as:

$$\Delta C_j = \left(C_{f,j-d} + C_{i,j-d} + C_{s,j-d}\right) - \left(C_{f,j} + C_{i,j} + C_{s,j}\right) \quad (4)$$

$C_{f,j-d}$, $C_{i,j-d}$ *and* $C_{s,j-d}$ are the amounts of C remaining in the three pools at time *j-d,* where *j* is the incubation day and *d* the number of days since the previous measurement had been taken. It corresponds to the time over which CO_2 could accumulate before measurement. Correspondingly, $C_{f,j} + C_{i,j} + C_{s,j}$ are the amounts of C remaining in the three pools at time *j*.

In the model, the initial C_{tot} was constrained to the measured amount of soil C stocks (MgC ha^{-1}) in each sample measured at the beginning of the incubation. The C loss through respiration measured by the measured CO_2 release rates ΔC_j at different times during the incubation and was used to the proportions of C in the three notional pools and their decay constants. For each incubation, there were therefore five independent variables, consisting of the three time constants, and two parameters to determine the proportion in the three notional pools, with the extra constraint that the sum of the pools had to add to the total measured.

5.2.6 Estimation of temperature sensitivity (Q_{10s})

The cumulative C loss of each incubation temperature (i.e., 5, 15, 25, and 35^{o}C) was determined by adding the observed C loss over a 330 day incubation period. Further, the $Q_{10\text{-cum}}$ was

estimated using a first-order exponential equation where we fitted the changes in CO_2 emission rate with the incubation temperatures following the method of Qin et al. (2021):

$$R=Ae^{(BT)} \quad (5)$$

where R is the cumulative CO_2 release rate (MgC ha^{-1} yr^{-1}) at a given temperature, T is the incubation temperature (°C). A and B are fitted parameters. Subsequently, the values from the fitted B were then used to calculate the $Q_{10\text{-cum}}$ (Mikan et al., 2002; Ricketts et al., 2020):

$$Q_{10\text{-}cum}=e^{(10B)} \quad (6)$$

Using the decay rate of each C pools (fast, intermediate, slow) at each incubation temperatures (i.e., 5, 15, 25, and 35°C) obtained from the C modelling, the temperature sensitivity of $Q_{10\text{-fast}}$, $Q_{10\text{-intermediate}}$, $Q_{10\text{-slow}}$ was estimated using a first-order exponential equation where we fitted the changes in decay rate with the incubation temperatures following the method of Qin et al (2021). The exponential equation adopted was:

$$\pi_{(f)}=A_f e^{(BfT)} \quad (7)$$

$$\pi_{(i)}=A_i e^{(BiT)} \quad (8)$$

$$\pi_{(s)}=A_s e^{(BsT)} \quad (9)$$

where π is the decay rate of the three notional C pools (% d^{-1}), *f*, *i*, and *s* are the fast, intermediate, and slow pools, respectively, *T* is the incubation temperature (°C). *A* and *B* are fitted parameters. Subsequently, the values from the fitted B were then used to calculate the Q_{10} for each C pool (Mikan et al., 2002; Ricketts et al., 2020):

$$Q_{10(f)}=e^{(10Bf)} \quad (10)$$

$$Q_{10(i)}=e^{(10Bi)} \quad (11)$$

$$Q_{10(s)}=e^{(10Bs)} \quad (12)$$

5.2.7 Statistical analysis

We examined the observed temperature sensitivity of cumulative C loss ($Q_{10\text{-cum}}$) and the Q_{10s} for the three notional C pools (fast, intermediate, and slow) using One-way ANOVA with Tukey's test to find significant differences (at $P < .05$) between the treatment means across the levels of a single categorical factor, with all other variables being constant. A canonical ordination-based redundancy analysis (RDA) (Borcard et al., 2011) was also conducted to explicitly explore the relationships between $Q_{10\text{-cum}}$, Q_{10s} for the three notional C pools ($Q_{10\text{-fast}}$, $Q_{10\text{-intermediate}}$, $Q_{10\text{-slow}}$) and the explanatory matrix. The explanatory matrix includes a suite of variables including mean annual temperature (MAT), soil pH, soil C stock, allophane, $Al_{ox} + 1/2Fe_{ox}$, $C_{HF\text{-mobile}}$, C_{py}, and OM molecular composition (i.e., carbohydrate, N compound, lignin, MCC, MAHs, and PAHs). The RDA was performed on standardised Q_{10} values and explanatory variables using the RDA function in R package vegan.

We performed structural equation modelling (SEM) to further clarify the complex interconnections among predictors. We classified the predictor variables into six groups: 1) MAT, 2) soil depths, 3) soil pH, 3) C availability (i.e., soil C stocks, water extractable C (C_{H2O})), 4) reactive mineral surface (e.g., allophane, Al_{ox} + 1/2Fe_{ox}), 5) molecular structure of OM (i.e., carbohydrates, N-compounds, lignin, MCC, MAHs, PAHs). We ran the principal components analysis (PCA) using: (i) soil C stocks, and C_{H2O}; (ii) allophane, and Al_{ox} + 1/2Fe_{ox}; (iii) $C_{HF\text{-}mobile,}$ and C_{py}; and (iv) carbohydrates, N compounds, lignin, MCC, MAHs, and PAHs. The first principal component (PC1) of these analyses (which explained >50.5% of the variance, as shown in Table S5.2.2) was then represented as C availability, reactive surfaces, mineral associated-C and OM molecular structure, respectively, into the subsequent SEM (Figure 5.6). The SEM analyses were performed using the IBM SPSS Amos 26.0. We considered the hypothetical model pathways based on well-known relationships among the explanatory variables using the generalised least squares, and we obtained the final models with a nonsignificant Chi-squared test (P >.05), high $\chi 2$ goodness-of-fit index (GFI >.85), low root mean square error of approximation (RSME <.08).

5.3 Results

5.3.1 CO_2 effluxes and cumulative CO_2 emission

Regardless of sites across the temperature gradient (T7, T8, T9, T10) and temperatures of incubation (5, 15, 25, 35^{o}C), there was a rapid CO_2 emission during the initial days of the incubation and this decreased thereafter (data from the 25^{o}C incubation as an example in Figure 5.1 and that for the other incubation temperatures presented in Figure S5.2.1 in Supplementary Information). The top layer (0–5 cm depth) was the soil layer that had the largest CO_2 efflux, as

expected. The CO_2 efflux decreased with depth, and the decrease was more pronounced from 0–5 cm to deeper soil layers. Also, as expected, as the incubation temperature increased, CO_2 efflux increased for all soil samples, with the increase being consistent during the throughout period of incubation. At the same incubation temperature and the same soil depth, no significant difference (P >.05) was detected between any two elevation sites in the same time period, suggesting that the MAT had a negligible effect on soil C efflux in our study sites.

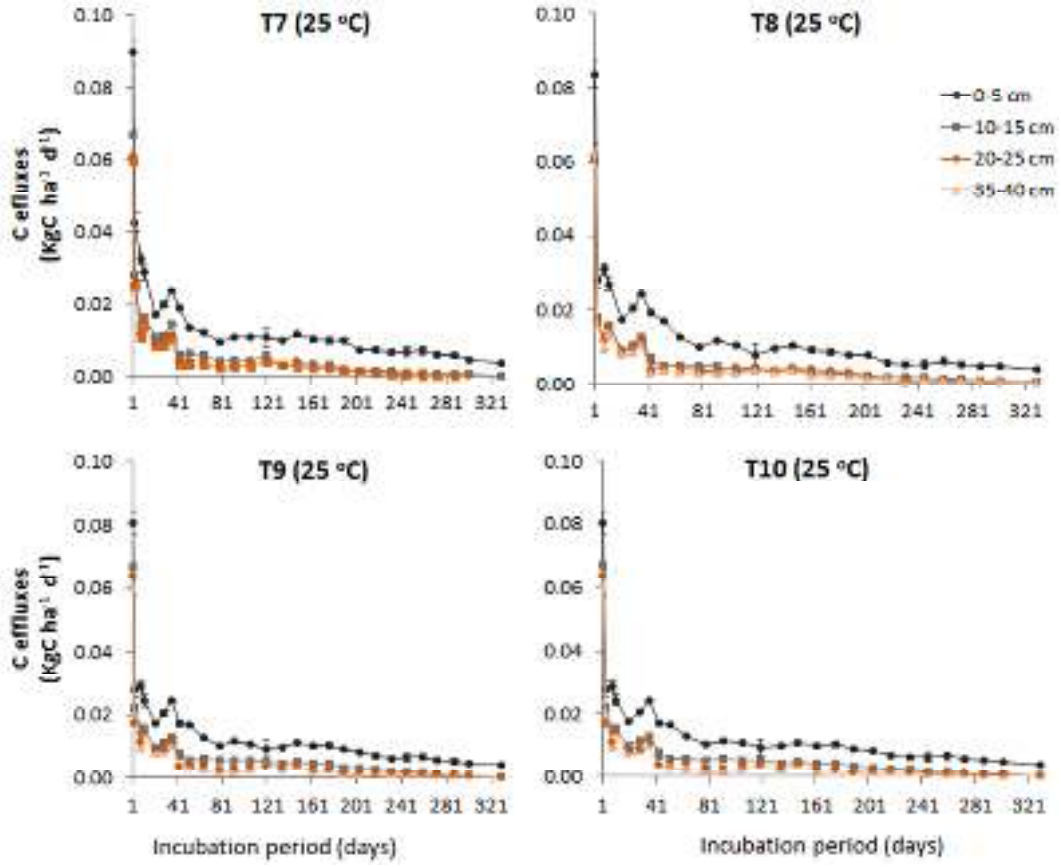

Figure 5.1 Soil C effluxes at different sites at a 25°C incubation temperature during 330 days of incubation.

The enhancing effect of elevated incubation temperature on CO_2 emission was also evident when the cumulative C efflux during the 330-day incubation was normalised based on the initial total

C content (abbreviated as C efflux/total C) of each soil sample (Figure 5.2). Mean values of cumulative C efflux/total C ranged from 0.52 – 1.68%, 0.20 – 0.80%, 0.18 – 0.66% and 0.13 – 0.46% for 0–5 cm, 10–15 cm, 20–25 cm and 35–40 cm layers, respectively (Figure 5.2). The cumulative C efflux/total C increased 3 to 4 times in incubations at 35°C in comparison to incubations at 5°C for all soil depths. Cumulative C efflux/total C tended to increase as the elevation increased, with T7 having a generally larger value than the rest of sites. There were significant differences (P <.05) between T7 and T10 at depths of 10–15 cm at 35°C, 20–25 cm at 25 and 35°C, and 35–40 cm at 35°C (Figure 5.2).

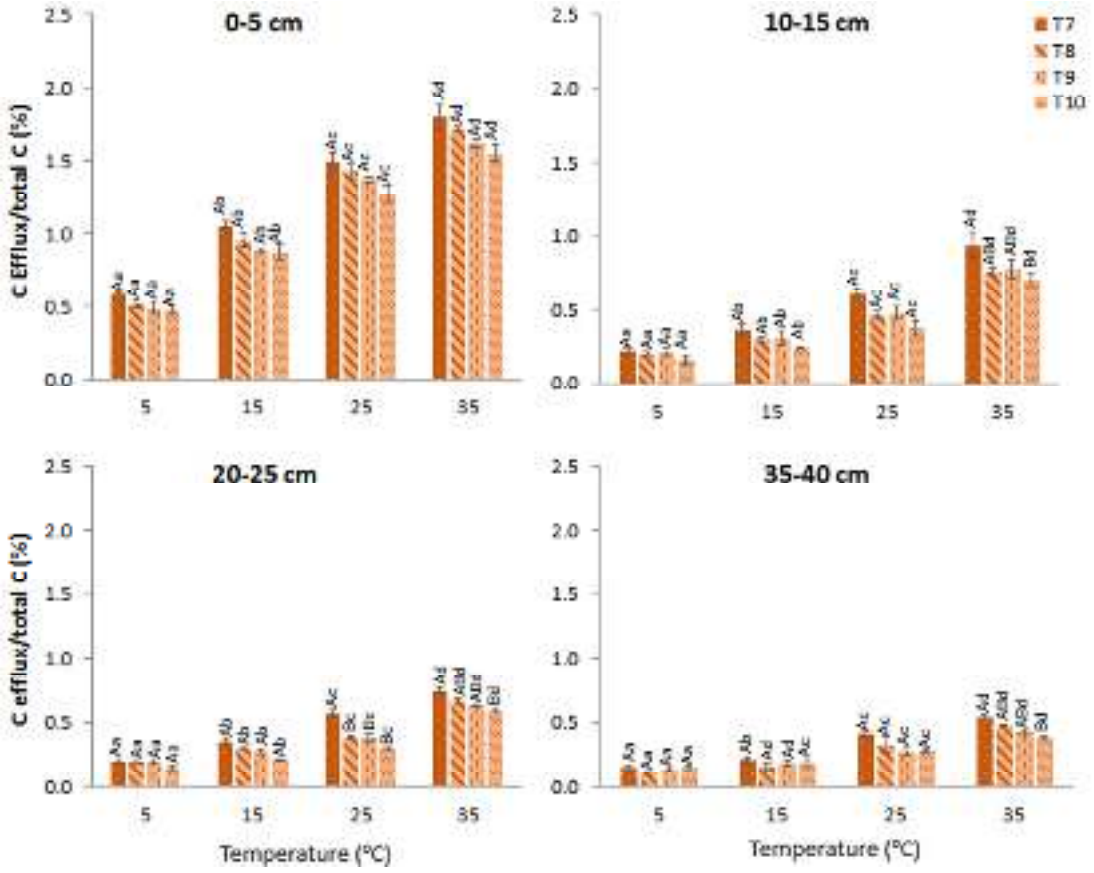

Figure 5.2 Cumulative C efflux (%initial total C content) of soils collected at four different sites and depths across a mean annual temperature gradient. Capital letters indicate differences among the four sites at the same temperature, whereas lowercase letters indicate differences among the four different incubation temperatures at the same site. Different letters denote a significant difference according to

one-way ANOVA followed by Tukey's test (P <.05). Error bars represent the standard error of the means (n = 4).

5.3.2 Model-derived soil OM pools and their decomposition rates

The three-pool model fitted soil OM decomposition dynamics well across all incubation temperatures, regardless of sites and soil depths. The soil OM was dominated by the slow pool, accounting for approximately ~96% of total soil C stocks. The fast pool and intermediate C pool contained estimates ~3% and ~1% of total soil C stocks, respectively (Table 5.1). The proportions of the three C pools (fast, intermediate, and slow pool) did not differ significantly (P >.05) either across the thermo-sequence (T7, T8, T9, T10) or incubation temperatures (5, 15, 25, 35^{o}C), indicating that the C pool sizes were temperature independent. In contrast, at all sampling sites and depths, the decomposition rates of the three notional C pools (fast, intermediate, and slow) increased significantly (P <.05) with the incubation temperatures (Figure 5.3). At 5^{o}C and 35^{o}C, the decomposition rate of the fast pool in the topsoil was 2.5 and 12.3% d^{-1}, respectively, while the intermediate pool at 0.02 and 0.06% d^{-1}, and in the slow pool at 1.4×10^{-5} and 6.9×10^{-5} % d^{-1} (Figure 5.3). When comparing sites (T7, T8, T9, and T10), the OM decomposition rates of the three notional C pools tended to decrease as MAT increased. At the same site, the decomposition rate also decreased with soil depth (Figure 5.3).

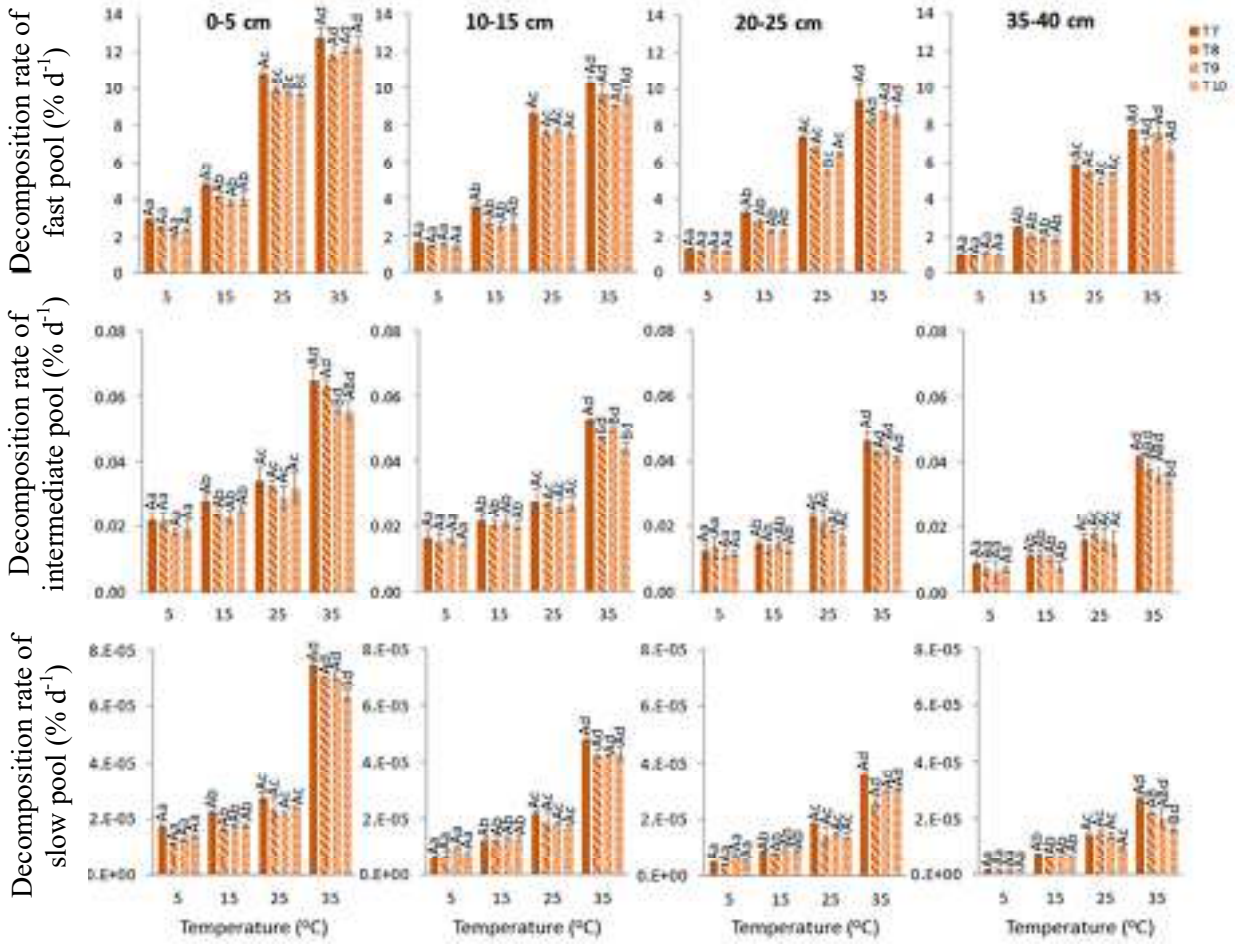

Figure 5.3 The decomposition rates of soil organic matter (OM) of three notional C pools in response to temperature rise in all sampling sites and depths studied. Capital letters indicate the comparison of four distinct sites at the same depth, whereas small letters indicate the comparison of four different soil depths at the same site. Different letters denote the significant difference according to one-way ANOVA followed by Tukey's test (P <.05). Error bars represent the standard error of the mean (n = 4).

Table 5.4 Proportion of the three notional C pools to initial soil C stocks (%) across sites and depths.

Notional C pools	Depth (cm)	T7 %	T8 %	T9 %	T10 %
Fast C pool	0–5	3.39 ± 0.04	3.17 ± 0.07	3.18 ± 0.05	3.06 ± 0.04
	10–15	2.47 ± 0.01	2.33 ± 0.05	2.33 ± 0.02	2.49 ± 0.08
	20–25	2.43 ± 0.01	2.23 ± 0.04	2.25 ± 0.06	2.54 ± 0.04
	35–40	2.18 ± 0.06	2.18 ± 0.05	2.04 ± 0.02	2.20 ± 0.07
Intermediate C pool	0–5	1.09 ± 0.02	1.13 ± 0.04	1.23 ± 0.02	1.24 ± 0.02
	10–15	1.10 ± 0.04	1.32 ± 0.01	1.13 ± 0.01	1.21 ± 0.01
	20–25	0.78 ± 0.01	0.98 ± 0.04	0.97 ± 0.03	0.78 ± 0.01
	35–40	1.03 ± 0.05	1.01 ± 0.01	1.22 ± 0.03	1.03 ± 0.04
Slow C pool	0–5	95.52 ± 0.02	95.71 ± 0.04	95.59 ± 0.02	95.69 ± 0.02
	10–15	96.43 ± 0.01	96.35 ± 0.01	96.54 ± 0.01	96.30 ± 0.03
	20–25	96.79 ± 0.01	96.80± 0.04	96.78 ± 0.03	96.68 ± 0.01
	35–40	96.78 ± 0.01	96.82 ± 0.01	96.74 ± 0.03	96.77± 0.04

5.3.3 Temperature sensitivity (Q_{10s}) in response to elevated MAT

Q_{10} value of the cumulative C efflux ($Q_{10\text{-cum}}$) over 330 days of incubation tended to decrease as MAT increased, with T7 having the highest $Q_{10\text{-cum}}$ compared to the rest of the sites at all depths considered. Specifically, $Q_{10\text{-cum}}$ of T7 differed significantly (P <.05) with T10 at the two deepest soil intervals, while there was no observed significant difference (P >.05) at the two upper soil intervals (Figure 5.4). Further, the $Q_{10\text{-cum}}$ tended to increase as depth increased, but significant differences were only observed between the topsoil and the deepest soil interval (35–40 cm) across sites (Figure 5.4). Besides $Q_{10\text{-cum}}$, the Q_{10s} value of the three-pool C fractions ($Q_{10\text{-fast}}$,

$Q_{10\text{-intermediate}}$, and $Q_{10\text{-slow}}$) were also estimated. The slow pool, in particular, had the greatest Q_{10} (average = 2.64), followed by $Q_{10\text{-fast}}$ (average = 2.06) and $Q_{10\text{-intermediate}}$ (average = 1.61) (Figure 5.4). Both $Q_{10\text{-fast}}$ and $Q_{10\text{-slow}}$ tended to decrease with elevated MAT, while $Q_{10\text{-intermediate}}$ showed a minor variation. Further, the $Q_{10\text{-fast}}$ and $Q_{10\text{-slow}}$ tended to increase with depth, whereas the $Q_{10\text{-intermediate}}$ showed in the opposite direction; nonetheless, no statistically significant differences were observed (P >.05).

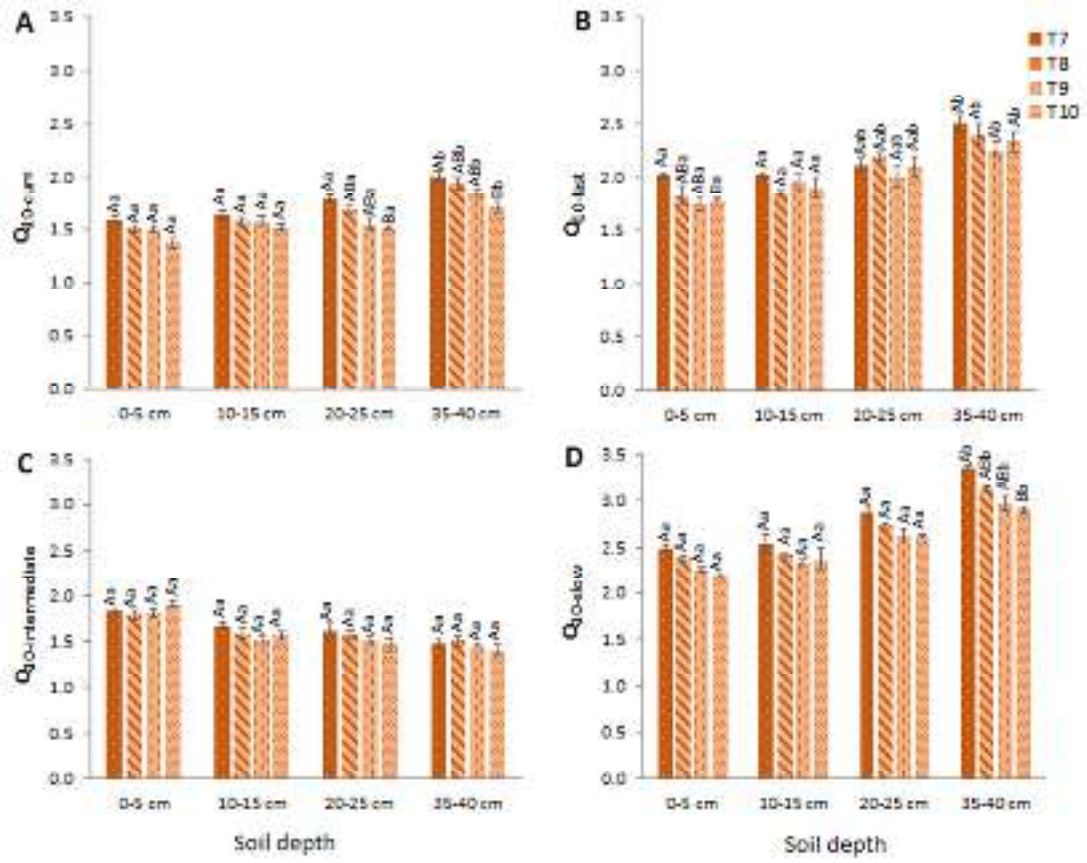

Figure 5.4 Temperature sensitivity of cumulative CO_2 efflux ($Q_{10\text{--cum}}$) and the three- pool C fractions ($Q_{10\text{--fast}}$, $Q_{10\text{--inteermediate}}$, $Q_{10\text{-slow}}$) measured across sites and depths during a 330-day incubation period. Capital letters indicate the comparison of four distinct sites at the same depth, whereas small letters indicate the comparison of four different soil depths at the same site. Different letters denote the significant difference according to one-way ANOVA followed by Tukey's test (P <.05). Error bars represent the standard error of the mean (n = 4).

5.3.4 Redundancy analysis (RDA) and structural equation modelling (SEM)

The RDA explained 64% of the overall variance in the data, with the first two canonical axes contributing 52% and 12%, respectively (Figure 5.5). This result revealed that the RDA had captured the significant linear trends/relationships in the data and could successfully explain the data. Q_{10} values of the cumulative C efflux and those of model-derived C pools showed significant correlations with different explanatory variables, including the molecular composition of soil OM and environmental constraints (i.e., interactions with minerals). More specifically, $Q_{10\text{-slow}}$ appeared to have a strong and positive correlation with the abundances of PAHs, MAHs, MCC and soil C stocks (SOCs), while it correlated negatively with lignin, C_{H2O} and C_{py}. $Q_{10\text{-slow}}$ also showed no correlation with the abundance of carbohydrates. $Q_{10\text{-cum}}$ correlated well with $Q_{10\text{-slow}}$ and exhibited similar relationships with the explanatory variables of $Q_{10\text{-slow.}}$ In contrast, $Q_{10\text{-fast}}$ had a strong positive correlation with the abundance of carbohydrates and a negative correlation with the abundance of N compounds, the allophane content, and $C_{HF\text{-mobile.}}$ Furthermore, $Q_{10\text{-intermediate}}$ correlated positively with C_{H2O} and the abundance of lignin but showed negative relationships with the abundance of PAHs, MAHs, and MCC (Figure 5.5). It also had a negative correlation with the SRO constituent contents.

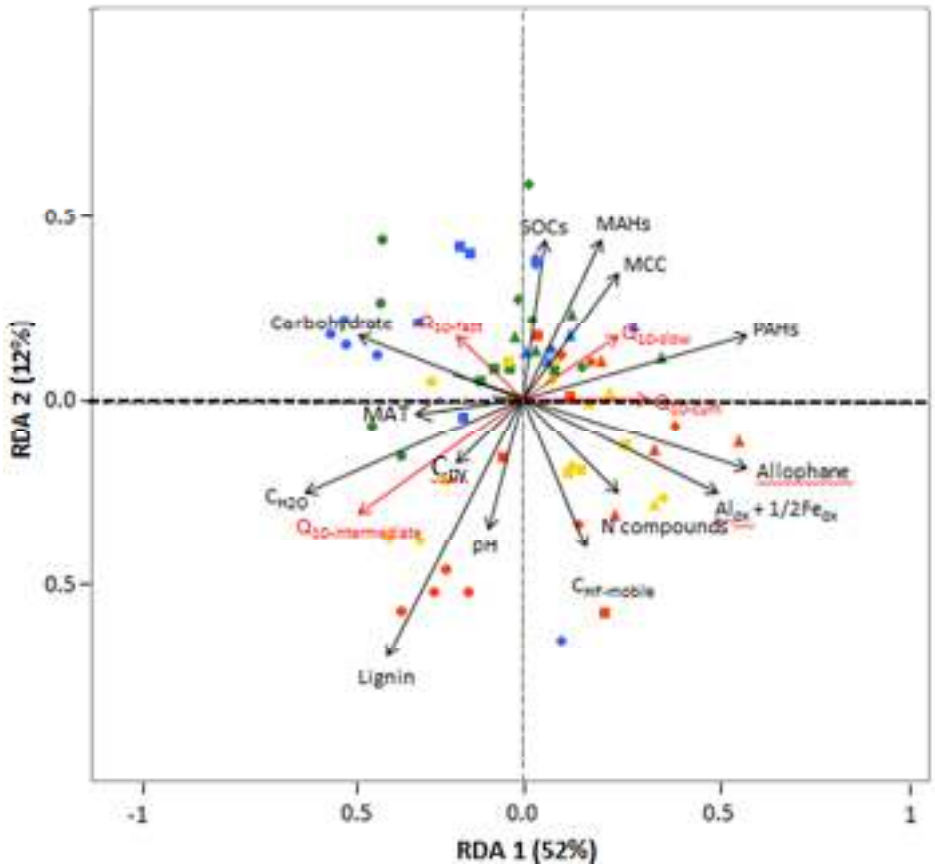

Figure 5.5 Redundancy analyses demonstrating the relationships between Q_{10} metrics and a set of explanatory variables. The first and second RDA axes explained 52% and 12% of the variability in Q_{10} data, respectively. The circle, rectangle, diamond, and triangle indicate depth levels of 0–5 cm, 10–15 cm, 20–25 cm, and 35–40 cm, respectively. Blue, green, yellow, and red indicate sites T7, T8, T9, and T10, respectively.

The SEM analysis was run considering the direct and indirect effects of MAT, soil depth, soil pH, C_{H2O} (i.e., an index for C availability), the molecular structure of soil OM, the reactive surface (i.e., allophane, Al_{ox} + 1/2Fe_{ox} as proxies), and mineral-associated C ($C_{HF\text{-}mobile}$, C_{py}). These variables could account for 53%, 77%, 49%, and 72% of the total variance of $Q_{10\text{-}cum}$, $Q_{10\text{-}fast}$, $Q_{10\text{-}intermediate}$, and $Q_{10\text{-}slow}$, respectively (Figure 5.6). Soil depth tended to have a direct effect on all Q_{10} values, indicating that depth-dependent geochemical conditions have a strong

influence on Q_{10} of soil OM decomposition. For $Q_{10\text{-cum}}$, molecular structure presented the strongest direct effect (the path coefficient was 0.48), while the direct effects of other variables were relatively weak and insignificant (Figure 5.6). $Q_{10\text{-fast}}$ was predominantly and negatively influenced by reactive mineral surfaces and mineral associated-C, and positively influenced by C availability (the path coefficients were -0.64, -0.20 and 0.44, respectively). $Q_{10\text{-intermediate}}$ was predominantly regulated by C availability (the path coefficient was 0.41). $Q_{10\text{-slow}}$ was primarily controlled by the molecular composition of soil OM (the path coefficient was 0.89). MAT showed no direct effects on any Q_{10} values, but it indirectly influenced $Q_{10\text{-fast}}$ via its effect on reactive mineral surface and mineral associated-C.

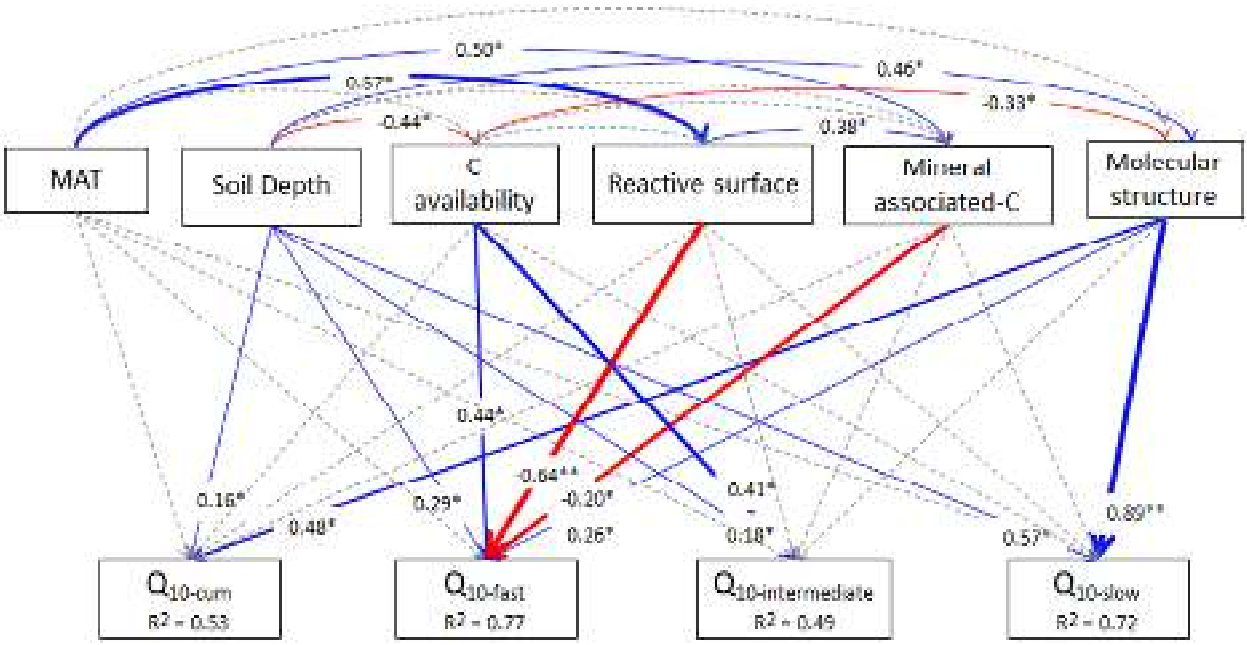

Figure 5.6 Structural equation modelling (SEM) of the controlling factors on Q_{10s}. C availability, reactive surface, mineral associated C and molecular structure represented the first axis of principal component analysis (PCA) of (i) soil C stock, water extractable-C (C_{H2O}), (ii) allophane and Al_{ox} + 1/2Fe_{ox}, and (iii) $C_{HF\text{-}mobile}$ and C_{py}, (iv) carbohydrates, N compounds, lignin, MCC, MAHs, and PAHs, respectively. The significant (P <.05) and insignificant (P >.05) correlations are represented by the solid and dashed lines, respectively, and are displayed in blue for positive correlations and red for negative correlations. The path width is proportional to the strength of the correlations. Numbers adjacent to the path are standardised path coefficients with asterisks indicating their significance (P <.05, ** P <.01). The proportion of variance explained (R^2) are shown alongside the box of the endogenous variables.*

5.4 Discussion

5.4.1 Lower temperature sensitivity (Q_{10}) of soil OM decomposition at warmer sites

The accurate projection of soil C-climate feedback under future warming requires an improved understanding of the temperature sensitivity (Q_{10}) of soil OM decomposition. Although previous incubation and field warming experiments have provided invaluable information on the magnitude, variability, and regulators of Q_{10}, such information might only be relevant to short-term responses of OM decomposition to elevated temperatures (Conant et al., 2011). Instead, it is the response of soil OM decomposition on time scales from decades to centuries that is likely

more relevant to the Earth's climate system (Trumbore & Czimczik, 2008; Walker et al., 2018). However, the dearth of warming experiments at a comparable time scale leaves the changes of Q_{10} under prolonged temperature rise an open question (Conant et al., 2011; Carey et al., 2016). Therefore, our investigation of the Q_{10} pattern along the highly constraint MAT gradient along the Taranaki slope complements previous experimental warming studies by providing a proxy for the response of Q_{10} of soil OM decomposition to centennial-scale temperature rise. Our data support the first hypothesis by showing that $Q_{10\text{-cum}}$ tended to decrease as MAT increased (Figure 5.4A). As other factors such as precipitation (i.e., in excess of evapotranspiration), vegetation type and soil C content that affect soil OM decomposition are relatively similar in the Taranaki slope, our results provide more compelling evidence for the negative Q_{10}-temperature relationship than previous space-for-time substitution studies which have other factors confounding the temperature effect (Davidson and Janssens, 2006; Conant et al., 2011). These results suggest that Q_{10} of soil OM decomposition is inclined to attenuate over a centennial scale under elevated temperature. Overlooking the attenuation may overestimate the soil C feedback to global warming.

The decrease in $Q_{10\text{-cum}}$ of soil OM decomposition as MAT increases has been commonly observed in forest ecosystems across broad latitudinal and elevational gradients (Zheng et al., 2009; Zhou et al., 2009; Li, Nie et al., 2020; Mao et al., 2022). Indeed, the negative relationship can be predicted by the Arrhenius equation that describes the relationship between the decomposition rate of OM and temperature (Davidson & Janssens, 2006; Schipper et al., 2014). The reason is related to the smaller relative increase in the fraction of molecules that have sufficient energy to react under a higher temperature. Additionally, the negative relationship can be also partly explained by the enhanced protection of soil OM by SRO constituents at warmer

sites, as suggested by the greater amount of reactive surfaces at the same soil depth of the warmer sites (Table S5.2.1), which reduces the accessibility of OM to microorganisms (Conant et al., 2011). Alternatively, the acclimation of microbial physiology, microbial community structure and enzyme conformation to a higher MAT may also contribute to the observed decrease in Q_{10} at warmer sites (Bradford, 2013); however, this warrants confirmation in future research.

In contrast to Mao et al. (2022), the decrease in Q_{10} as MAT increases along the Taranaki temperature gradient cannot be solely explained by the pattern of OM recalcitrance. There was a remarkably consistent decrease in carbohydrate abundance with elevated temperature (Chapter 3, Figure 3.2.6). It is noted that carbohydrates under our study largely consisted of intact plant remnants, such as levoglucosan (Chapter 3, Table S3.2.1). The greater abundance of carbohydrates suggests more labile and less recalcitrant C prevailed at colder sites compared to warmer sites. According to the kinetic theory, we should expect to observe an increased in Q_{10} at warmer sites due to the associated increase in chemical recalcitrance of OM. However, it was not the case, presumably due to the greater organo-mineral interactions at warmer sites, which might reduce the microbial decomposer's ability to access C substrate, thus reducing Q_{10}.

The decrease of Q_{10} with an increase in temperature was observed at all studied soil depths (Figure 5.4A). The extent of Q_{10} decrease across the thermo-sequence, from the colder to the warmer sites, was more pronounced at a deeper soil depth, consistent with Li, Pei et al. (2020) and Mao et al. (2022). Detailed explanation will be discussed in the following subsection. These results suggest that: (i) OM decomposition in deep soil might be more sensitive to warming than that in shallow soil; yet (ii) OM decomposition in deep soil might “acclimate” to long-term elevated temperature to a larger extent than that in shallow soil. Furthermore, the observation

that $Q_{10\text{-cum}}$ tended to rise as depth increased was consistent with previous findings (Li et al., 2020; Mao et al., 2022). Such results could be partially explained by the greater proportion of chemical recalcitrant C (as represented by MAHs, PAHs, and MCC) at depth (Chapter 3, Figure S3.2.6). It is generally accepted that compounds with a greater chemical recalcitrance have higher intrinsic temperature sensitivity (Davidson & Janssens, 2006). Although our results also showed that organo-mineral interactions increased with depth, the enhanced interactions could unlikely outcompete the importance of the molecular recalcitrance in regulating the variation of Q_{10}. This is also reflected from the SEM analysis which showed that the molecular structure rather than reactive surfaces posed a direct effect on $Q_{10\text{-cum}}$.

5.4.2 Factors driving changes in temperature sensitivity of soil OM decomposition

The three C-pool model allowed us to effectively extract information about Q_{10} of soil C pools with distinct decay rates. In general, Q_{10} of each model-derived soil C pool also tended to decrease with elevated MAT, although some exceptions were observed; for instance, at soil depths of 0–5 cm and 10–15 cm in $Q_{10\text{-intermediate}}$ (Figure 5.4). However, for $Q_{10\text{-slow}}$ showed the most consistent decline, while $Q_{10\text{-intermediate}}$ and $Q_{10\text{-fast}}$ showed minor modifications. These results support the first half of the hypothesis (ii) that the responses of Q_{10} of distinct C pools differed under elevated temperature. Both RDA and SEM were used to explore factors driving changes in Q_{10} of soil OM decomposition along the Taranaki temperature gradient. Both analyses clearly demonstrated that $Q_{10\text{-cum}}$ and Q_{10} of separate C pools were regulated by distinct mechanisms, in accordance with the second half of hypothesis (ii).

As the slow C pool accounted for ~96% of total soil C stocks, $Q_{10\text{-cum}}$ and $Q_{10\text{-slow}}$ were controlled by similar factors. RDA results showed that both Q_{10s} did not have correlation with

labile C (i.e. carbohydrates) and positively correlated with the more recalcitrant C (in particular, PAHs which is likely related to pyrogenic OC formed by forest fires (Buurman et al., 2007) (Figure 5.5), indicating $Q_{10\text{-cum}}$ and $Q_{10\text{-slow}}$ were regulated by the chemical recalcitrance of OM. In contrast, the RDA results revealed that $Q_{10\text{-fast}}$ was negatively correlated with SRO constituents (Figure 5.5), suggesting that the fast C pool is dominated by unprotected OM. This is corroborated by SEM data that C availability posed a strong and direct effect on $Q_{10\text{-fast}}$ while SRO constituents and mineral-associated C had negative effects on $Q_{10\text{-fast}}$. It has been well-documented that the majority of labile OM is unprotected by minerals and hence more accessible to microbes (Schmidt et al., 2011). Surprisingly, there was a discrepancy between RDA and SEM results in the effects of molecular composition of OM on $Q_{10\text{-fast}}$. $Q_{10\text{-fast}}$ positively correlated to the labile compounds (i.e. carbohydrates) in RDA, whereas it was positively regulated by the chemical recalcitrance of OM according to SEM. Such a discrepancy might be attributed to the difference in underlying mathematics between the two methods. The molecular composition of OM was considered by incorporating the separate OM groups (e.g. carbohydrates, N compounds, lignin, MCC, MAHs, and PAHs) in RDA; while SEM was run after extracting the primary variation of all OM groups using PCA (Fig. S5.2.2), and specifically, using the PC1. Given that the PC1 only extracted 50.5% of the variability, the subsequent SEM analysis is based on a portion of information regarding molecular structure. This might have resulted in a different evaluation of the relationship between $Q_{10\text{-fast}}$ and molecular structure. Intuitively, RDA provides a more direct method to see the relationship between individual explanatory variables and the Q_{10s}, whereas SEM is more efficient at showing the overall picture of a large group of data. These differences can be observed in the standardised path coefficient values, where the path coefficient of molecular structure for $Q_{10\text{-fast}}$ is smaller than $Q_{10\text{-slow}}$ and

$Q_{10\text{-cum}}$. This indicates that the molecular structure has a stronger influence on $Q_{10\text{-slow}}$ and $Q_{10\text{-cum}}$ than $Q_{10\text{-fast.}}$

$Q_{10\text{-intermediate}}$ had the lowest values among all Q_{10}. Such low values of Q_{10} could be explained by the strong environmental constraints to decomposition (Davidson and Janssens, 2006; Conant et al., 2011). We infer the constraints are mainly related to mineral protection of OM from microbial decomposition according to the following lines of evidence. Firstly, RDA results showed that $Q_{10\text{-intermediate}}$ positively correlated to C_{H2O} (i.e. an index of C availability) and negatively correlated with allophane and Al_{ox} + $1/2Fe_{ox}$ (Figure 5.5). Secondly, SEM results indicated that $Q_{10\text{-intermediate}}$ was only significantly controlled by C availability. It is also noted that in SEM there was lack of direct negative effects of reactive mineral surface and mineral associated-C on $Q_{10\text{-intermediate}}$, which seems to contradict the above inference that $Q_{10\text{-intermediate}}$ was related to mineral protection of OM. Causes for divergence between RDA and SEM results have been described above. Yet, we reconcile this apparent contradiction by the observation that OM decomposition is regulated by the amount of OM release from mineral surfaces rather than the amounts of reactive mineral surfaces and mineral associated-C (Li et al., 2022). The release of OM has been shown dependent on the strength of mineral-OM associations, soil pH and competing ligands (Kaiser & Guggenberger, 2000; Kothwala et al., Li et al., 2020).

Although our study has extensively discussed the factors regulating Q_{10} pertaining to soil OM composition and OM stabilisation mechanisms, there are also some obvious limitations. First of all, we did not explicitly discuss the shifts in microbial properties that could influence Q_{10} of soil OM decomposition (Bradford, 2013). Secondly, since the experiments were conducted in the laboratory without fresh C input, our results did not take account the interactions between

continuous C input on Q_{10} under elevated temperature. These limitations should be considered in future research.

5.5 Conclusions

Our investigation of the Q_{10} pattern along the highly constraint MAT gradient along the Taranaki slope has provided evidence for that: (i) Q_{10} of soil OM decomposition is inclined to attenuate over a centennial scale under elevated MAT; and (ii) Q_{10} values of the bulk soil OM and the distinct C pools were differentially regulated by soil C availability, OM molecular composition, and OM-mineral interactions. These results suggest that the temporal and spatial variation of both the OM molecular structure and the environmental constraints that control OM decomposition should be adequately taken into account in Earth system models, in order to accurately predict soil C dynamics in response to global warming. However, our data also demonstrated that the effects of OM molecular structure and the environmental constraints on Q_{10} largely intertwined. Recent physical fractionation protocols to separate soil OM into the particulate and mineral-associated OM may represent a promising step forward to the quantitative disentanglement of the long-term effects of various drivers underlying Q_{10} changes.

Appendix III. Supporting Information for Chapter 5 (SI5)

S5.1 Supporting materials and methods

Figure S5.1.2: Pictorial representation of the steps: A) Soil sampling to a 40 cm depth at 5cm intervals, B) Soils in columns ready to be irrigated to bring moisture content to field capacity, C) Soils acclimatised in the dark at room temperature after field capacity and prior to incubation, D) Jar with the soil column and NaOH solution in a P35 plastic vial ready for incubation, E) Samples in incubation temperature/chamber.

S5.2 Supporting results

S5.2.1 Carbon effluxes

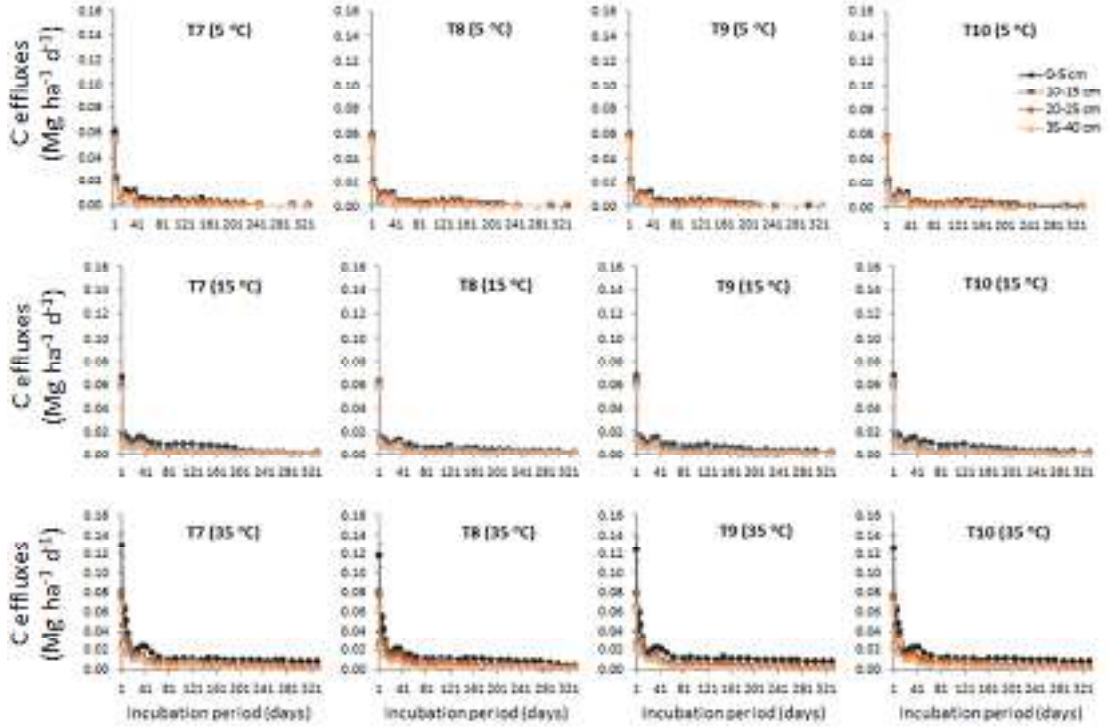

Figure S5.2.1 C effluxes from all sampling sites: T7, T8, T9, T10 at four distinct depths during 5, 15, and 35^{o}C incubation temperatures.

S5.2.2 Principal component analysis

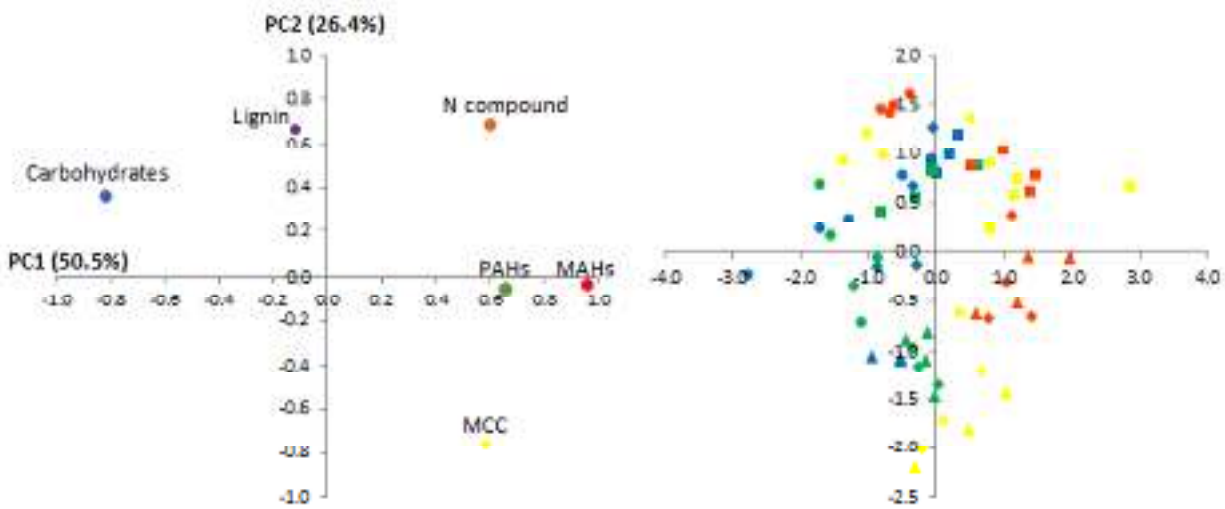

Figure S5.2.2 (A) The loading of soil OM composition on the axes of PC1 and PC2 and (B) the factor scores of the data on the axes of PC1 and PC2 across sites and depths along the Taranaki gradient. The circle, rectangle, diamond, and triangle indicate depth levels of 0–5 cm, 10–15 cm, 20–25 cm, and 35–40 cm, respectively. Blue, green, yellow, and red indicate sites T7, T8, T9, and T10, respectively. Methylene chain compounds (MCC), monocyclic aromatic hydrocarbons (MAHs), and polycyclic aromatic hydrocarbons (PAHs)).

Table S5.2.1 Selected chemical properties of four sampling sites and depths along the Taranaki gradient

Site	Depth (cm)	pH	Total C (g kg^{-1})	C stocks (Mg ha^{-1})	C_{py} (g kg^{-1})	Allophane (%)	$Al_{ox}+1/2Fe_{ox}$ (%)	C_{H2O} (mg kg^{-1})	C_{HF_mobile} (g kg^{-1})
T7	0-5	4.2	179.1	31.3	3.3	0.0	0.2	1349.1	30.5
	10-15	5.1	61.5	23.1	8.8	0.1	0.6	651.0	33.8
	20-25	5.3	81.8	24.0	18.2	0.2	0.8	571.1	52.9
	35-40	5.4	63.3	27.5	15.4	1.4	1.1	381.4	48.7
T8	0-5	4.2	170.9	47.9	3.8	0.0	0.4	2057.9	28.4
	10-15	5.0	77.3	26.8	18.2	0.4	0.8	920.0	42.3
	20-25	5.1	97.6	22.6	13.1	0.5	1.2	592.5	65.8
	35-40	5.5	32.1	16.3	7.5	2.7	1.4	187.9	24.8
T9	0-5	4.5	164.3	38.6	4.2	0.1	0.3	2112.9	28.7
	10-15	4.9	81.7	23.9	16.8	0.1	1.0	794.6	45.6
	20-25	5.2	65.7	20.9	16.6	2.8	1.4	356.3	44.4
	35-40	5.5	80.1	18.2	14.7	5.0	1.5	295.2	61.8
T10	0-5	5.1	140.8	34.3	13.0	0.3	0.6	1844.8	21.4
	10-15	5.7	31.4	27.8	3.7	0.6	0.9	562.2	15.9
	20-25	5.8	56.1	21.2	13.0	1.2	1.6	466.6	36.6
	35-40	5.7	57.8	17.2	12.0	4.2	2.4	325.9	44.3

Table S5.2.2 Total variance of the first component analysis (PCA 1) of the reactive mineral surface, mineral associated-C, and OM composition across sites and depths along the Taranaki gradient.

Grouped Variables	1^{st} principle component (PC1) (%)
Reactive mineral surface	85
Mineral associated-C	68
OM composition	50

CHAPTER 6
OVERALL SUMMARY AND RECOMMENDATIONS FOR FUTURE RESEARCH

6.1 Overall summary

As a result of the effect of temperature on microbial OM decomposition, it is predicted that global warming will result in a net loss of soil C and an accompanying loss of CO_2 into the atmosphere. Given that soils store at least three times as much carbon (C) as is found either in the atmosphere or in living plants, soils have an enormous potential sources or sinks for atmospheric C. Therefore, it is critical to investigate the effect of temperature rise on soil C cycling and stocks and the underlying mechanism, particularly in Andosols that retain high soil C stocks due to the abundance of short-range order (SRO) constituents (e.g., allophane, imogolite, and ferrihydrite), which are able to interact with soil C, forming organo-mineral complexes and offering protection against OM decomposition. The study of the response of soil C fluxes to temperature changes is challenging because temperatures co-vary with biotic and abiotic factors, along with spatial and temporal variations. Furthermore, where water and nutrients are not limited, an increase in global temperature may also result in an increase in plant productivity and, consequently, in C inputs to the soil. All of these factors can account for the discrepancy in the recent studies on the responses of OM decomposition to warming. This thesis investigated the effect of temperature rise on soil C cycling, fractions, and stocks under natural MAT gradient (~3.2^{o}C) in Mt. Taranaki, where other factors affecting the ecosystem (i.e., soil parent material, vegetation type, precipitation exceeding 3000 mm per year, thus not limiting either vegetation and microbial growth or mineral weathering) are relatively similar.

The findings from this study contribute to provide a deeper understanding of how global warming affects soil C cycling, fractions and stocks by examining the long-term effect of temperature rise (i.e., field experiment) and warming (i.e., soil incubation in laboratory

experiment). Therefore, it enables a more accurate estimation of future soil C stocks in order to mitigate global warming.

6.1.1 Temperature (and soil depth) influences soil geochemistry

The rate of mineral weathering is accelerated by temperature, which in turn partially regulates soil acidification. Colder elevation sites (T7 and T8) favour slower mineral weathering, resulting in a lesser contribution of alkalinity (OH^-) to partially buffer acidification. As the amount of OH^- decreases, these anions are less able to compete with organic ligands for Al cations. This makes organo-Al complexes more likely to form than allophane at T7 and T8. This is in contrast to the warmer elevation sites (T9 and T10), where higher temperatures accelerate the mineral weathering rate, hence increasing the concentration of OH^- and generating the partial buffering of organic acidity. It has been reported that higher pH range favour the formation of SRO constituents (i.e., allophane). This finding confirms the hypothesis that: (i) the forms of reactive Al (i.e., SRO vs. organo-Al complexes) differ along the thermo-sequence, with a greater abundance of SRO at warmer sites (i.e., lower elevation) as opposed to organo-Al complexes at colder sites (i.e., higher elevations), where weathering rate is slower (Chapter 3). Further, the increase in the more microbially-processed C with temperature and depth (as inferred by the increase in the $C_{HF\text{-}mobile}$/C total) is paralleled by an increase in reactive sites (e.g., reactive Al among others), indicating that the preservation of C favours organo-mineral interactions. This increasing pattern is accompanied by the fact that, at the surface (especially at the 0–10 cm layer) of T7 and T8, there is a larger proportion of plant-derived C (i.e., carbohydrates) than at the surface of T9 and T10. This weakly decomposed (i.e., large molecular weight) and weakly oxidized C pool (i.e., poor in carboxylic functional groups) is less likely to interact with mineral

surfaces as opposed to more microbially-processed C at warmer sites. These findings confirm the hypotheses (ii) that under warmer conditions, C is likely to be more microbial processed as opposed to colder conditions, where plant fingerprints are more evident (Chapter 3); and (iii) as a result, the mechanisms of C preservation along the transect differ, with a C more associated with SRO constituents (and more microbial-derived) at lower elevation sites, and with Al cations (and more plant-derived) at the more leached higher elevation sites (Chapter 3).

6.1.2 Higher temperatures did not cause a loss of soil C stocks

An in-depth understanding of the long-term effect of temperature rise on soil C cycling and stocks was obtained through a one-year field experiment. It is observed that bulk soil C stocks did not decrease (in fact, it tended to increase), despite the associated increase in soil respiration at warmer elevation sites. This is attributed to the greater C gains achieved from both above and belowground biomass at warmer sites, which offset the C loss from soil respiration, resulting in no significant change in C storage along the Taranaki gradient. Our results show that: (i) warming accelerated the fast C fluxes such as the cycling of litterfall and total belowground C fluxes in the forest ecosystem. This is confirmed by the fact that the forest floor mass decreased as MAT increased, whereas the turnover rates for unprotected particulate C (i.e., C that is not associated with the mineral fraction) increased, indicating that OM decomposed more rapidly at warmer sites; (ii) warming influenced the cycling of the bulk soil C, as reflected by the change in carbohydrate content and composition along the transect. Specifically, the greater proportion of carbohydrates and the higher carbohydrates preservation index (CPI) remained at colder elevation sites are due to a lesser degree of decomposition (Figure 4.6). This is opposed to the results from Giardina et al. (2014) working on a warmer transects where they reported no effect

of temperature on the bulk soil C and their fractions. In our study, the accelerated OM decomposition with warming may have led to an increase in microbial-derived C, which is more susceptible to being preserved through organo-mineral interactions. This could be inferred from the proportion of $C_{HF\text{-}mobile}/C_{total}$, which was parallel with the increase of reactive sites of soil minerals at warmer sites and with depth. This could partly explain the larger C stocks at warmer sites. These results confirm the hypotheses that: (i) an increase in temperature under conditions of no water deficit would increase aboveground and belowground plant growth and litterfall, thus increasing C inputs to soil; (ii) which would drive a greater efflux of CO_2 to the atmosphere, and therefore greater microbial processing of soil C; (iii) and would not lead to a significant change of soil C stocks, as the increase in soil CO_2 efflux would be counteracted by the increase in soil C input.

6.1.3 Temperature sensitivity (Q_{10}) of soil OM decomposition decreases at warmer sites with different driving factors

An in-depth understanding of how warming impact the pattern of Q_{10} of soil OM decomposition was obtained through a 330-days of incubation of soils along the Taranaki gradient. Our findings confirm the first hypothesis by demonstrating that Q_{10} decreased as MAT increased, which is consistent with previous studies in forest ecosystems across broad latitudinal and elevational gradients (Zheng et al., 2009; Zhou et al., 2009; Li, Nie et al., 2020; Mao et al., 2022). The reason for this is related to a smaller relative rise in the fraction of molecules with enough energy to react at higher temperatures. Furthermore, the negative association can be explained in part by increased soil mineral protection of soil OM in warmer sites, as evidenced by a greater proportion of reactive surfaces (i.e., allophane and $Al_{ox} + 1/2Fe_{ox}$ as proxy) at the same soil depth

at warmer sites, reducing OM accessibility to microbes (Conant et al., 2011). Furthermore, the three C-pool model effectively extracted distinct soil C pools with various rates of decomposition. Although some exceptions were observed, the Q_{10} of each model-derived soil C pool generally tended to decline with increased MAT as well, supporting the first half of hypothesis (ii), which states that the responses of Q_{10} in distinct C pools varied under high temperature. RDA and SEM analyses demonstrated that $Q_{10\text{-cum}}$ and $Q_{10\text{slow}}$ were controlled by similar factors as the slow C pool accounted for ~96% of total soil C stocks. Specifically, RDA results showed that both $Q_{10\text{s}}$ did not correlate with labile C (i.e. carbohydrates) and but positively correlated with the more recalcitrant C (in particular, PAHs which is likely related to pyrogenic OC formed by forest fires) (Buurman et al., 2007), indicating $Q_{10\text{-cum}}$ and $Q_{10\text{-slow}}$ were strongly regulated by the chemical recalcitrance of OM. In contrast, the RDA results revealed that $Q_{10\text{-fast}}$ was negatively correlated with reactive surfaces (e.g., allophane and Al_{ox} + 1/2Fe_{ox}), suggesting that the fast C pool is dominated by unprotected OM, as expected. This is corroborated by SEM data that C availability posed a strong and direct effect on $Q_{10\text{-fast}}$ while reactive surface and mineral-associated C had negative effects on $Q_{10\text{-fast}}$. Furthermore, RDA results showed that $Q_{10\text{-intermediate}}$ positively correlated to C_{H2O} and negatively correlated with reactive surface of soil minerals. While SEM results indicated that $Q_{10\text{-intermediate}}$ was only significantly controlled by C availability. These findings show that in order to effectively forecast soil C dynamics in response to global warming, the temporal and spatial variation of both the OM molecular structure and the environmental constraints that govern OM decomposition should be adequately considered within Earth system models.

6.1.4 Highlights of this thesis

1. Temperature affects the soil geochemistry with reactive Al transitioning from a greater dominance of Al cation associated with organic ligands at low temperature to that of Al in SRO constituents at higher temperature (Chapter 3).
2. Temperature affects the soil C fractions with a trend of organic ligands increasingly associated with minerals as temperature increases (Chapter 3).
3. Temperature affects soil OM biochemistry with a transition from more plant-derived C to more microbial derived C as temperature increases (Chapter 3).
4. Warming influenced the acceleration of the rapid C fluxes (litterfall and total belowground C fluxes), and the cycling of bulk soil OM decomposition (Chapter 4).
5. The C stocks at warmer sites did not decrease but even tend to increase due to the increase in plant biomass and the increase in mineral associated C, thus counteract the C loss (Chapter 4).
6. Q_{10} of soil OM decomposition is inclined to diminish on a centennial scale under higher MAT (Chapter 5).
7. Q_{10} values of bulk soil OM and the three notional C pools (fast, intermediate, slow) were differently controlled by soil C availability, OM molecular composition, and OM-mineral interactions (Chapter 5).

6.2 Recommendations for future work

The study conducted in this thesis investigated the effect of temperature rise on soil C cycling, stocks, and fractions under natural MAT gradient in a C-rich Andosol and considering the role of elevation (and thus temperature gradient), depth gradient, soil geochemistry (i.e., the form of

reactive Al and Fe), and molecular fingerprint of soil OM in the $C_{HF\text{-}residuum}$ using pyrolysis-gas chromatography–mass spectrometry (GC-MS). There are research areas on the effect of temperature on soil C cycling and stocks that still require a better understanding, and thus future work could consider the following topics:

- The role of microorganisms in soil OM decomposition

A growing body of evidence reveals that microbial properties (e.g., biomass, community composition, and metabolic pathways) not only regulate the decomposition of soil OM (Liang et al., 2017; Wang et al., 2021) but also its response to warming (Karhu et al., 2014). Uncertainty remains as to whether microbes will adapt to warming or alter their composition. In future research, it would be essential to explore the response of microbial properties to a scenario of warming and elevated CO_2.

- The role of soil aggregates in soil C preservation

In the present study we only examine the effect of soil mineral protection (i.e., the forms of reactive Al and Fe) in regulating soil OM decomposition. It has been reported that soil aggregates exert important control over the stabilisation of soil C (Qin et al., 2019; Kpemoua et al., 2022). Given that Andosols are also characterised by a high micro-aggregates stability (in addition to the well-known chemical interaction of reactive Al with organic ligands), in the future studies, it will be useful to investigate the effect of aggregate protection in governing the response of soil OM decomposition to global warming in Andosols.

- The role of enzyme activity in soil OM mineralisation

It is notable that the soil enzymes secreted or released by microorganisms, roots and soil fauna play a critical role in OM decomposition, in which enzymatic depolymerisation and oxidation jointly modify insoluble and/or macromolecular OM to a smaller size and to more oxidised and

water-soluble OM. Some recent studies reported that, compared with microbial abundance and diversity, enzyme activity had a more important role in controlling soil OM mineralisation (Tan et al., 2021; Xu et al., 2020). We thus advise investigating the effect of temperature on soil enzyme activity on soil OM decomposition.

- A large-scale evidence with meta-analysis

In future studies, it will be important to carry out a meta-analysis of the effect of temperature rise on soil C fluxes and stocks across and within biome types. This could help to prove the universality of the effect of temperature rise on C preservation in soils.

REFERENCES

Aitken, J. F., Campbell, I. B., & Wilde, R. H. (1978). Soils of Stratford County, North Island, New Zealand. New Zealand Soil Bureau, Department of Scientific and Industrial Research.

Alloway, B., McComb, P., Neall, V., Vucetich, C., Gibb, J., Sherburn, S., & Stirling, M. (2005). Stratigraphy, age, and correlation of voluminous debris-avalanche events from an ancestral Egmont Volcano: Implications for coastal plain construction and regional hazard assessment. *Journal of The Royal Society of New Zealand*, 35, 229–267. https://doi.org/10.1080/03014223.2005.9517782

Alloway, B., Neall, V. E., & Vucetich, C. G. (1995). Late Quaternary (post 28,000-year B.P.) tephrostratigraphy of northeast and central Taranaki, New Zealand. *Journal of the Royal Society of New Zealand*, 25(4), 385–458. https://doi.org/10.1080/03014223.1995.9517496

Amelung, W., Bossio, D., de Vries, W., Kögel-Knabner, I., Lehmann, J., Amundson, R., Bol, R., Collins, C., Lal, R., Leifeld, J., Minasny, B., Pan, G., Paustian, K., Rumpel, C., Sanderman, J., van Groenigen, J. W., Mooney, S., van Wesemael, B., Wander, M., & Chabbi, A. (2020). Towards a global-scale soil climate mitigation strategy. *Nature Communications*, 11(1–10). https://doi.org/10.1038/s41467-020-18887-7

Amundson, R., Berhe, A. A., Hopmans, J. W., Olson, C., Sztein, A. E., & Sparks, D. L. (2015). Soil and human security in the 21st century. *Science*, 348(6235), 3–4. https://doi.org/10.1126/science.1261071

Asano, M., & Wagai, R. (2014). Evidence of aggregate hierarchy at micro- to submicron scales in an allophanic andisol. *Geoderma*, 216, 62–74. https://doi.org/10.1016/j.geoderma.2013.10.005

Bahn, M., Janssens, I., Reichstein, M., Smith, P., & Trumbore, S. (2010b). Soil respiration across scales: Towards an integration of patterns and processes. *The New Phytologist*, 186, 292–296. https://doi.org/10.1111/j.1469-8137.2010.03237.x

Bahn, M., Reichstein, M., Davidson, E.A., Grünzweig, J., Jung, M., Carbone, M. S., Epron, D., Misson, L., Nouvellon, Y., Roupsard, O., Savage, K., Trumbore, S. E., Gimeno, C., Curiel Yuste, J., Tang, J., Vargas, R., & Janssens, I. A. (2010a). Soil respiration at mean annual temperature predicts annual total across vegetation types and biomes. *Biogeosciences*, 7, 2147–2157.

Baig, S., Medlyn, B. E., Mercado, L. M., & Zaehle, S. (2015). Does the growth response of woody plants to elevated CO_2 increase with temperature? A model-oriented meta-analysis. *Global Change Biology*, *21*(12), 4303-4319.

Baldock, J. A., & Skjemstad, J. O. (2000). Role of the soil matrix and minerals in protecting natural organic materials against biological attack. *Organic Geochemistry*, 31(7–8), 697–710. https://doi.org/10.1016/S0146-6380(00)00049-8

Ballantyne, A. P., Andres, R., Houghton, R., Stocker, B. D., Wanninkhof, R., Anderegg, W., Cooper, L. A., DeGrandpre, M., Tans, P. P., Miller, J. B., Alden, C., & White, J. W. C. (2015). Audit of the global carbon budget: Estimate errors and their impact on uptake uncertainty. *Biogeosciences*, 12(8), 2565–2584. https://doi.org/10.5194/bg-12-2565-2015

Bascomb, C. L. (1968). Distribution of pyrophosphate-extractable iron and organic carbon in soils of various groups. *Journal of Soil Science*, 19(2), 251–268

Batjes, N. H. (1996). Total carbon and nitrogen in the soils of the world. *European journal of soil science*, 47(2), 151-163.

Bauer, J., Kirschbaum, M.U.F., Weihermüller, L., Huisman, J.A., Herbst, M., Vereecken, H. (2008). Temperature response of wheat decomposition is more complex than the common approaches of most multi-pool models. *Soil Biology and Biochemistry*, 40, 2780–2786.

Bäumler, R., Caspari, T., Totsche, K. U., Dorji, T., Norbu, C., & Baillie, I. C. (2005). Andic properties in soils developed from nonvolcanic materials in Central Bhutan. *Journal of Plant Nutrition and Soil Science*, 168(5), 703–713. https://doi.org/https://doi.org/10.1002/jpln.200521793

Beerling, D. J., Kantzas, E. P., Lomas, M. R., Wade, P., Eufrasio, R. M., Renforth, P., Sarkar, B., Andrews, M. G., James, R. H., Pearce, C. R., Mercure, J.-F., Pollitt, H., Holden, P. B., Edwards, N. R., Khanna, M., Koh, L., Quegan, S., Pidgeon, N. F., Janssens, I. A., Banwart, S. A. (2020). Potential for large-scale CO2 removal via enhanced rock

weathering with croplands. *Nature*, 583(7815), 242–248. https://doi.org/10.1038/s41586-020-2448-9

Beets, P. N., Kimberley, M. O., Oliver, G. R., Pearce, S. H., Graham, J. D., & Brandon, A. (2012). Allometric equations for estimating carbon stocks in natural forest in New Zealand. *Forests*, 3, 818–839. https://doi.org/10.3390/f3030818

Bell, M. J., Moody, P. W., Connolly, R., & Bridge, B. J. (1998). The role of active fractions of soil organic matter in physical and chemical fertility of Ferrosols. *Soil Research*, 36, 809–819.

Berg, B., Davey, M., De Marco, A., Emmett, B. M., F., Hobbie, S., Johansson, M., Liu, C., McClaugherty, C., Norell, L., Rutigliano, F., Vesterdal, L., & De Santo, A. (2010). Factors influencing limit values for pine needle litter decomposition: A synthesis for boreal and temperate pine forest systems. *Biogeochemistry*, 100(1–3), 57–73. https://doi.org/10.1007/s10533-009-9404-y

Birgander, J., Olsson, P. A., & Rousk, J. (2018). The responses of microbial temperature relationships to seasonal change and winter warming in a temperate grassland. *Global change biology*, *24*(8), 3357-3367.

Birouste, M., Kazakou, E., Blanchard, A., & Roumet, C. (2012). Plant traits and decomposition: Are the relationships for roots comparable to those for leaves? *Annals of Botany*, 109(2), 463–472. https://doi.org/10.1093/aob/mcr297

Blagodatskaya, E., Blagodatsky, S., Khomyakov, N., Myachina, O., & Kuzyakov, Y. (2016). Temperature sensitivity and enzymatic mechanisms of soil organic matter decomposition along an altitudinal gradient on Mount Kilimanjaro. *Scientific Reports*, 6(February), 1–11. https://doi.org/10.1038/srep22240

Blagodatskaya, E., & Kuzyakov, Y. (2008). Mechanisms of real and apparent priming effects and their dependence on soil microbial biomass and community structure: Critical review. *Biology and Fertility of Soils*, 45(2), 115–131. https://doi.org/10.1007/s00374-008-0334-y

Blagodatskaya, E., Zheng, X., Blagodatsky, S., Wiegl, R., Dannenmann, M., & Butterbach-Bahl, K. (2014). Oxygen and substrate availability interactively control the temperature

sensitivity of CO2 and N2O emission from soil. *Biology and Fertility of Soils*, 50(5), 775–783.

Blair, G., Lefroy, R. D. B., & Lisle, L. (1995). Soil carbon fractions based on their degree of oxidation, and the development of a carbon management index for agricultural systems. *Crop & Pasture Science*, 46, 1459–1466.

Blakemore, L. C. (1981). Methods for chemical analysis of soils. Scientific Report 10A New Zealand Soil Bureau.

Blankinship, J. C., Berhe, A. A., Crow, S. E., Druhan, J. L., Heckman, K. A., Keiluweit, M., Lawrence, C. R., Marín-Spiotta, E., Plante, A. F., Rasmussen, C., Schädel, C., Schimel, J. P., Sierra, C. A., Thompson, A., Wagai, R., & Wieder, W. R. (2018). Improving understanding of soil organic matter dynamics by triangulating theories, measurements, and models. *Biogeochemistry*, 140(1), 1–13. https://doi.org/10.1007/s10533-018-0478-2

Bond-Lamberty, B., & Thomson, A. (2010). Temperature-associated increases in the global soil respiration record. *Nature*, 464(7288), 579–582. https://doi.org/10.1038/nature08930

Borcard, D., Gillet, F., & Legendre, P. (2011). *Numerical ecology with R* (Vol. 2, p. 688). New York: Springer.

Borggaard, O. K. (1988). Phase identification by selective dissolution techniques. In Iron in soils and clay minerals (pp. 83-98). Springer, Dordrecht.

Braakhekke W. G. D. B. (2007). Modelling decomposition of standard plant Al material along an altitudinal gradient: A re-analysis of data of Couteaux et al. (2002). *Soil Biology and Biochemistry*, 39(99–105).

Bradford, M. A., Davies, C. A., Frey, S. D., Maddox, T. R., Melillo, J. M., Mohan, J. E., Reynolds, J. F., Treseder, K. K., & Wallenstein, M. D. (2008). Thermal adaptation of soil microbial respiration to elevated temperature. *Ecology Letters*, 11(12), 1316–1327. https://doi.org/10.1111/j.1461-0248.2008.01251.x

Bradford, M. A., Keiser, A. D., Davies, C. A., Mersmann, C. A., & Strickland, M. S. (2013). Empirical evidence that soil carbon formation from plant inputs is positively related to

microbial growth. *Biogeochemistry*, 113(1–3), 271–281. https://doi.org/10.1007/s10533-012-9822-0

Brodowski, S., Amelung, W., Haumaier, L., Abetz, C., & Zech, W. (2005). Morphological and chemical properties of black carbon in physical soil fractions as revealed by scanning electron microscopy and energy-dispersive X-ray spectroscopy. *Geoderma*, *128*(1–2), 116–129. https://doi.org/10.1016/j.geoderma.2004.12.019

Bosatta, E., & Ågren, G. I. (1999). Soil organic matter quality interpreted thermodynamically. *Soil Biology and Biochemistry*, *31,475*, 1889–1891. https://doi.org/10.1016/S0038-0717(99)00105-4

Buol, S., Southard, R., Graham, R., & McDaniel, P. (2011). *Soil genesis and classification*. Wiley. https://doi.org/10.1002/9780470960622

Buurman, P., Peterse, F., & Almendros Martin, G. (2007). Soil organic matter chemistry in allophanic soils: A pyrolysis-GC/MS study of a Costa Rican Andosol catena. *European Journal of Soil Science*, *58*(6), 1330–1347. https://doi.org/10.1111/j.1365-2389.2007.00925.x

Campbell, E. E., & Paustian, K. (2015). Current developments in soil organic matter modeling and the expansion of model applications: A review. *Environmental Research Letters*, 10(12), 123004. https://doi.org/10.1088/1748-9326/10/12/123004

Carey, J. C., Tang, J., Templer, P. H., Kroeger, K. D., Crowther, T. W., Burton, A. J., Dukes, J. S., Emmett, B., Frey, S. D., Heskel, M. A., Jiang, L., Machmuller, M. B., Mohan, J., Panetta, A. M., Reich, P. B., Reinschj, S., Wang, X., Allison, S. D., Bamminger, C., … Tietema, A. (2016). Temperature response of soil respiration largely unaltered with experimental warming. Proceedings of the National Academy of Sciences of the United States of America, 113(48), 13797–13802. https://doi.org/10.1073/pnas.1605365113

Carey, S. N. (2005). Understanding the physical behavior of volcanoes. In G. G. J. Ernst & J. Marti (Eds.), Volcanoes and the environment (pp. 1–54). Cambridge University Press. https://doi.org/10.1017/CBO9780511614767.002

Carvalhais, N., Forkel, M., Khomik, M., Bellarby, J., Jung, M., Migliavacca, M., ... & Reichstein, M. (2014). Global covariation of carbon turnover times with climate in terrestrial ecosystems. *Nature*, 514(7521), 213-217.

Castellano, M. J., Mueller, K. E., Olk, D. C., Sawyer, J. E., & Six, J. (2015). Integrating plant litter quality, soil organic matter stabilisation, and the carbon saturation concept. *Global change biology*, 21(9), 3200-3209.

Chapin, F.S., Matson, P.A., Vitousek, P. M. (2011). Decomposition and ecosystem carbon budgets. In: F.S. Chapin, P.A Matson, & P.M. Vitousek (Eds.), *Principles of terrestrial ecosystem ecology.* Springer US.

Chaplot, V., Bouahom, B., & VALENTIN, C. (2010). Soil organic carbon stocks in Laos: spatial variations and controlling factors. *Global Change Biology*, 16(4), 1380–1393. https://doi.org/https://doi.org/10.1111/j.1365-2486.2009.02013.x

Chen, Y., Camps-Arbestain, M., Shen, Q., Singh, B., & Cayuela, M. L. (2018). The long-term role of organic amendments in building soil nutrient fertility: a meta-analysis and review. *Nutrient Cycling in Agroecosystems*, 111(2), 103-125.

Chesworth, W. (2006). Encyclopedia of Soil Science. In AAS/Division for Extreme Solar Systems Abstracts. Springer.

Chevallier, T., Woignier, T., Toucet, J., & Blanchart, E. (2010). Organic carbon stabilisation in the fractal pore structure of Andosols. Geoderma, 159(1), 182–188. https://doi.org/10.1016/j.geoderma.2010.07.010

Clarkson, B. D. (1990). A review of vegetation development following recent (< 450 years) volcanic disturbance in North Island, New Zealand. *New Zealand journal of ecology*, 59-71.

Clarkson B. D. (1986). Vegetation of Egmont National Park, New Zealand. Department of Scientific and Industrial Research.

Conant, R. T., Drijiber, R. A., Haddix, M. L., Parton, W. J., Paul, E. A., Plante, A. F., Six, J., & Steinweg, J. M. (2008). Sensitivity of organic matter decomposition to warming varies with its quality. *Global Change Biology*, 14(4), 868–877. https://doi.org/10.1111/j.1365-2486.2008.01541.x

Conant, R.T., Klopatek, J.M., Malin, R.C., Klopatek, C.C. (1998). Carbon pools and fluxes along an elevation gradient in northern Arizona. *Biogeochemistry*, *43*, 43–61.

Conant, R. T., Ryan, M. G., Ågren, G. I., Birge, H. E., Davidson, E. A., Eliasson, P. E., Evans, S. E., Frey, S. D., Giardina, C. P., Hopkins, F. M., Hyvönen, R., Kirschbaum, M. U. F., Lavallee, J. M., Leifeld, J., Parton, W. J., Steinweg, J. M., Wallenstein, M. D., Wetterstedt, J. Å. M., & Bradford, M. A. (2011). Temperature and soil organic matter decomposition rates – Synthesis of current knowledge and a way forward. *Global Change Biology*, 17(11), 3392–3404. https://doi.org/10.1111/j.1365-2486.2011.02496.x

Conant, R. T., Steinweg, J. M., Haddix, M. L., Paul, E. A., Plante, A. F., & Six, J. (2008). Experimental warming shows that decomposition temperature sensitivity increases with soil organic matter recalcitrance. *Ecology*, 89(9), 2384–2391.

Cotrufo, M. F., Soong, J. L., Horton, A. J., Campbell, E. E., Haddix, M. L., Wall, D. H., & Parton, W. J. (2015). Formation of soil organic matter via biochemical and physical pathways of litter mass loss. *Nature Geoscience*, 8(10), 776–779. https://doi.org/10.1038/ngeo2520

Cox, P. M., Pearson, D., Booth, B. B., Friedlingstein, P., Huntingford, C., Jones, C. D., & Luke, C. M. (2013). Sensitivity of tropical carbon to climate change constrained by carbon dioxide variability. *Nature*, 494(7437), 341-344.

Craine, J.M., Fierer, N., & McLauchlan, K. (2010). Widespread coupling between the rate and temperature sensitivity of organic matter decay. *Nature Geoscience*, *3*, 854–857. https://doi.org/10.1038/ngeo1009

Crowther, T. W, Carey, J. C., & Machmuller, M. B. (2016). Quantifying global soil carbon losses in response to warming. *Nature, 540*(7631), 104–108. https://doi.org/10.1038/nature20150

Crowther, T. W., Sokol, N. W., Oldfield, E. E., Maynard, D. S., Thomas, S. M., & Bradford, M. A. (2015). Environmental stress response limits microbial necromass contributions to soil organic carbon. *Soil Biology and Biochemistry*, *85*, 153–161. https://doi.org/10.1016/j.soilbio.2015.03.002

Crowther, T. W., Thomas, S. M., Maynard, D. S., Baldrian, P., Covey, K., Frey, S. D., van Diepen, L. T. A., & Bradford, M. A. (2015). Biotic interactions mediate soil microbial feedbacks to climate change. *Proceedings of the National Academy of Sciences*, *112*(22), 7033–7038. https://doi.org/10.1073/pnas.1502956112

Crowther, T. W., Todd-Brown, K. E. O., Rowe, C. W., Wieder, W. R., Carey, J. C., Machmuller, M. B., Snoek, B. L., Fang, S., Zhou, G., Allison, S. D., Blair, J. M., Bridgham, S. D., Burton, A. J., Carrillo, Y., Reich, P. B., Clark, J. S., Classen, A. T., Dijkstra, F. A., Elberling, B., … Bradford, M. A. (2016). Quantifying global soil carbon losses in response to warming. *Nature*, *540*(7631), 104–108. https://doi.org/10.1038/nature20150

Curtin, D., Beare, M. H., Qiu, W., & Chantigny, M. H. (2015). Temperature Dependence of Organic Matter Solubility: Influence of Biodegradation during Soil-Water Extraction. *Soil Science Society of America Journal*, 79(3), 858-863.

Dacal, M., García-Palacios, P., Asensio, S., Cano-Díaz, C., Gozalo, B., Ochoa, V., & Maestre, F. T. (2020). Contrasting mechanisms underlie short-and longer-term soil respiration responses to experimental warming in a dryland ecosystem. *Global Change Biology*, 26(9), 5254-5266.

Dahlgren, R. A., Saigusa, M., & Ugolini, F. C. (2004). The Nature, Properties and Management of Volcanic Soils (Vol. 82). Academic Press. https://doi.org/10.1016/S0065-2113(03)82003-5

Dahlgren, R., Shoji, S., & Nanzyo, M. (1993). Mineralogical characteristics of volcanic ash soils. In S. Shoji (Ed.), Volcanic Ash Soils Genesis, Properties and Utilization (Vol. 21, pp. 101–143). Elsevier.

Datta, S., Rattan, R., & Chandra, S. (2010). Labile soil organic carbon, soil fertility, and crop productivity as influenced by manure and mineral fertilizers in the tropics. *Journal of Plant Nutrition and Soil Science*, 173, 715–726. https://doi.org/10.1002/jpln.200900010

Davidson, E. A., & Holbrook, N. M. (2009). Is temporal variation of soil respiration linked to the phenology of photosynthesis? In: A. Noormets (Ed.), BT - Phenology of ecosystem processes: Applications in global change research (pp. 187–199). Springer. https://doi.org/10.1007/978-1-4419-0026-5-8

Davidson, E. A., & Janssens, I. A. (2006). Temperature sensitivity of soil carbon decomposition and feedbacks to climate change. *Nature*, *440*, 165–173. https://doi.org/10.1038/nature04514

Davidson, E. A., Samanta, S., Caramori, S. S., & Savage, K. (2012). The dual Arrhenius and Michaelis–Menten kinetics model for decomposition of soil organic matter at hourly to

seasonal time scales. *Global Change Biology*, *18*(1), 371–384. https://doi.org/10.1111/j.1365-2486.2011.02546.x

Davies, R., & Lambert, R. E. (2015). Under the Mountain – How a volcanic peak has influenced the culture, ecology and landscape history of Taranaki, New Zealand.

Deb, S., Bhadoria, P. B. S., Mandal, B., Rakshit, A., & Singh, H. B. (2015). Soil organic carbon: Towards better soil health, productivity and climate change mitigation. *Climate Change and Environmental Sustainability*, *3*(1), 26–34. https://doi.org/10.5958/2320-642x.2015.00003.4

Dieleman, W. I. J., Venter, M., Ramachandra, A., Krockenberger, A. K., & Bird, M. I. (2013). Soil carbon stocks vary predictably with altitude in tropical forests: Implications for soil carbon storage. *Geoderma*, 204–205, 59–67. https://doi.org/10.1016/j.geoderma.2013.04.005

Dignac, M. F., Derrien, D., Barre, P., Barot, S., Cécillon, L., Chenu, C., ... & Basile-Doelsch, I. (2017). Increasing soil carbon storage: mechanisms, effects of agricultural practices and proxies. A review. *Agronomy for sustainable development*, *37*(2), 1-27.

Dignac, M.-F., Kögel-Knabner, I., Michel, K., Matzner, E., & Knicker, H. (2002). Chemistry of soil organic matter as related to C/N in Norway spruce forest (*Picea abies* (L) Karst.) floors and mineral soils. *Plant Nutrition and Soil Science*, *165*(3), 281–289. https://doi.org/10.1002/1522-2624(200206)165:3<281:AID-JPLN281>3.0.CO;2-A

Doetterl, S., Berhe, A. A., Arnold, C., Bodé, S., Fiener, P., Finke, P., Fuchslueger, L., Griepentrog, M., Harden, J. W., Nadeu, E., Schnecker, J., Six, J., Trumbore, S., Van Oost, K., Vogel, C., & Boeckx, P. (2018). Links among warming, carbon and microbial dynamics mediated by soil mineral weathering. *Nature Geoscience*, *11*(8), 589–593. https://doi.org/10.1038/s41561-018-0168-7

Doetterl, S., Berhe, A. A., Nadeu, E., Wang, Z., Sommer, M., & Fiener, P. (2016). Erosion, deposition and soil carbon: A review of process-level controls, experimental tools and models to address C cycling in dynamic landscapes. *Earth-Science Reviews*, *154*, 102–122. https://doi.org/10.1016/j.earscirev.2015.12.005

Doetterl, S., Stevens, A., Six, J., Merckx, R., Van Oost, K., Casanova Pinto, M., Casanova-Katny, A., Muñoz, C., Boudin, M., Zagal Venegas, E., & Boeckx, P. (2015). Soil carbon

storage controlled by interactions between geochemistry and climate. *Nature Geoscience*, *8*, 780–783. https://doi.org/10.1038/ngeo2516

Dos Reis Martins, M., & Angers, D. A. (2015). Different plant types for different soil ecosystem services. *Geoderma*, *237*, 266–269. https://doi.org/10.1016/j.geoderma.2014.09.013

Druce, A. P. (1966). Tree-ring dating of recent volcanic ash and Lapilli, Mt. Egmont. *New Zealand Journal of Botany*, *4*(1), 3–41. https://doi.org/10.1080/0028825X.1966.10443951

Dungait, J. A. J., Hopkins, D. W., Gregory, A. S., & Whitmore, A. P. (2012). Soil organic matter turnover is governed by accessibility not recalcitrance. *Global Change Biology*, 18(6), 1781–1796. https://doi.org/10.1111/j.1365-2486.2012.02665.x

Duval, M. E., Galantini, J. A., Martínez, J. M., & Limbozzi, F. (2018). Labile soil organic carbon for assessing soil quality: influence of management practices and edaphic conditions. *Catena*, 171, 316–326. https://doi.org/10.1016/j.catena.2018.07.023

Eglin, T., Ciais, P., Piao, S. L., Barre, P., Bellassen, V., Cadule, P., Chenu, C., Gasser, T., Koven, C., Reichstein, M., & Smith, P. (2010). Historical and future perspectives of global soil carbon response to climate and land-use changes. *Tellus B: Chemical and Physical Meteorology*, *62*(5), 700–718. https://doi.org/10.1111/j.1600-0889.2010.00499.x

Eliasson, P. E., McMurtrie, R. E., Pepper, D. A., Strömgren, M., Linder, S., & Ågren, G. I. (2005). The response of heterotrophic CO_2 flux to soil warming. *Global Change Biology*, *11*(1), 167–181. https://doi.org/https://doi.org/10.1111/j.1365-2486.2004.00878.x

Eusterhues, K., Rumpel, C., & Kögel-Knabner, I. (2007). Composition and radiocarbon age of HF-resistant soil organic matter in a Podzol and a Cambisol. *Organic Geochemistry*, *38*(8), 1356–1372. https://doi.org/10.1016/j.orggeochem.2007.04.001

Eze, S., Palmer, S. M., & Chapman, P. J. (2018). Soil organic carbon stock in grasslands: Effects of inorganic fertilizers, liming and grazing in different climate settings. *Journal of environmental management*, *223*, 74-84.

FAO, Bot, A., & Benites, J. (2005). The importance of soil organic matter: Key to drought-resistant soil and sustained food production. *FAO Soils Bulletin 80 (Vol. 1, p. 95).*

FAO, International Soil Reference and Information Centre (ISRIC), The International Unit of Soil Sciences (IUSS). (2014). *World reference base for soil resources 2014 international soil classification system for naming soils and creating legends for soil maps. World Soil Resources Reports No. 106*. FAO.

FAO and ITPS. (2015). Status of the world's soil resources (SWSR) – main report. FAO and Intergovernmental Technical Panel on Soils. https://doi.org/ISBN 978-92-5-109004-6

Fang, C., Smith, P., Moncrieff, J. B., & Smith, J. U. J. N. (2005). Similar response of labile and resistant soil organic matter pools to changes in temperature. *Nature, 433(7021)*, 57–59.

Fiener, P., Dlugoß, V., & Van Oost, K. (2015). Erosion-induced carbon redistribution, burial and mineralisation—Is the episodic nature of erosion processes important? *Catena*, *133*, 282–292. https://doi.org/10.1016/j.catena.2015.05.027

Filimonova, S., Kaufhold, S., Wagner, F. E., Häusler, W., & Kögel-Knabner, I. (2016). The role of allophane nano-structure and Fe oxide speciation for hosting soil organic matter in an allophanic Andosol. *Geochimica et Cosmochimica Acta*, *180*, 284–302. https://doi.org/10.1016/j.gca.2016.02.033

Fissore, C., Jurgensen, M. F., Pickens, J., Miller, C., Page-Dumroese, D., & Giardina, C. (2016). Role of soil texture, clay mineralogy, location, and temperature in coarse wood decomposition – A mesocosm experiment. *Ecosphere*, *7*, 1–13. https://doi.org/10.1002/ecs2.1605

Freschet, G. T., Cornwell, W. K., Wardle, D. A., & Elumeeva, T. G. (2013). Linking litter decomposition of above- and below-ground organs to plant–soil feedbacks worldwide. *Journal of Ecology, 101 (4)*, 943–952. https://doi.org/10.1111/1365-2745.12092

Frey, S. D., Lee, J., Melillo, J. M., & Six, J. (2013). The temperature response of soil microbial efficiency and its feedback to climate. *Nature Climate Change, 3*(4), 395–398.

Friedlingstein, Pierre, Peter Cox, Richard Betts, Laurent Bopp, Werner von Bloh, Victor Brovkin, Patricia Cadule et al. "Climate–carbon cycle feedback analysis: results from the C4MIP model intercomparison." *Journal of climate* 19, no. 14 (2006): 3337-3353.

Fuss, S., Lamb, W. F., Callaghan, M. W., Hilaire, J., Creutzig, F., Amann, T., Beringer, T., De Oliveira Garcia, W., Hartmann, J., Khanna, T., Luderer, G., Nemet, G. F., Rogelj, J., Smith, P., Vicente, J. V., Wilcox, J., Del Mar Zamora Dominguez, M., & Minx, J. C. (2018). Negative emissions – Part 2: Costs, potentials and side effects. *Environmental Research Letters*, *13*(6), 1–47. https://doi.org/10.1088/1748-9326/aabf9f

Garcia-Pausas, J., Casals, P., Rovira, P., Vallecillo, S., Sebastià, M.-T., & Romanyà, J. (2012). Decomposition of labelled roots and root-C and -N allocation between soil fractions in mountain grasslands. *Soil Biology and Biochemistry*, *49*, 61–69. https://doi.org/10.1016/j.soilbio.2012.02.015

Garcia-Rodeja, E., Silva, B. M., & Macías, F. (1987). Andosols developed from non-volcanic materials in Galicia, NW Spain. *Journal of Soil Science*, *38*(4), 573–591. https://doi.org/10.1111/j.1365-2389.1987.tb02156.x

Garten, C. T. (2009). A disconnect between O horizon and mineral soil carbon – Implications for soil C sequestration. *Acta Oecologica*, *35*(2), 218–226. /https://doi.org/10.1016/j.actao.2008.10.004

Garten, C. T., & Hanson, P. J. (2006). Measured forest soil C stocks and estimated turnover times along an elevation gradient. *Geoderma*, *136*(1–2), 342–352. https://doi.org/10.1016/j.geoderma.2006.03.049

Ghani, A., Dexter, M., & Perrott, K. W. (2003). Hot-water extractable carbon in soils: a sensitive measurement for determining impacts of fertilisation, grazing and cultivation. *Soil biology and biochemistry*, *35*(9), 1231-1243.

Giardina, C. P., Binkley, D., Ryan, M. G., Fownes, J. H., & Senock, R. S. (2004). Belowground carbon cycling in a humid tropical forest decreases with fertilization. *Oecologia*, *139*(4), 545–550. https://doi.org/10.1007/s00442-004-1552-0

Giardina, C. P., Litton, C. M., Crow, S. E., & Asner, G. P. (2014). *Warming-related increases in soil CO_2 efflux are explained by increased below-ground carbon flux. Nature Climate Change, 4, 822–827* https://doi.org/10.1038/NCLIMATE2322

Giardina, C. P., & Ryan, M. G. (2000). Evidence that decomposition rates of organic carbon in mineral soil do not vary with temperature. *Nature*, *404*(6780), 858–861.

Gower, S. T., Pongracic, S., & Landsberg, J. J. (1996). A global trend in belowground carbon allocation: Can we use the relationship at smaller scales? *Ecology*, 77(6), 1750–1755.

Graham, E. A., Mulkey, S. S., Kitajima, K., Phillips, N. G., & Wright, S. J. (2003). Cloud cover limits net CO_2 uptake and growth of a rainforest tree during tropical rainy seasons. *Proceedings of the National Academy of Sciences of the United States of America*, *100*(2), 572–576. https://doi.org/10.1073/pnas.0133045100

Grant, R. F. (2014). Nitrogen mineralisation drives the response of forest productivity to soil warming: Modelling in ecosys vs. measurements from the Harvard soil heating experiment. *Ecological modelling*, *288*, 38-46.

Gregorich, E. G., & Janzen, H. H. (2000). Decomposition. In M.E. Sumner (Ed.), *Soil Science* (pp. C107–C120). CRC Press.

Hagerty, S. B., Van Groenigen, K. J., Allison, S. D., Hungate, B. A., Schwartz, E., Koch, G. W., ... & Dijkstra, P. (2014). Accelerated microbial turnover but constant growth efficiency with warming in soil. *Nature Climate Change*, *4*(10), 903-906.

Harden, J. W., Hugelius, G., Ahlström, A., Blankinship, J. C., Bond-Lamberty, B., Lawrence, C. R., Loisel, J., Malhotra, A., Jackson, R. B., Ogle, S., Phillips, C., Ryals, R., Todd-Brown, K., Vargas, R., Vergara, S. E., Cotrufo, M. F., Keiluweit, M., Heckman, K. A., Crow, S. E. … Nave, L. E. (2018). Networking our science to characterize the state, vulnerabilities, and management opportunities of soil organic matter. *Global Change Biology*, *24*(2), e705–e718. https://doi.org/10.1111/gcb.13896

Hartley, I. P., Hill, T. C., Chadburn, S. E., & Hugelius, G. (2021). Temperature effects on carbon storage are controlled by soil stabilisation capacities. *Nature Communications*, *12*(1), 6713. https://doi.org/10.1038/s41467-021-27101-1

Hartmann, J., West, A. J., Renforth, P., Köhler, P., De La Rocha, C. L., Wolf-Gladrow, D. A., Dürr, H. H., & Scheffran, J. (2013). Enhanced chemical weathering as a geoengineering strategy to reduce atmospheric carbon dioxide, supply nutrients, and mitigate ocean acidification. *Reviews of Geophysics*, *51*(2), 113–149. https://doi.org/10.1002/rog.20004

Hashimoto, S., & Komatsu, H. (2006). Relationships between soil CO_2 concentration and CO_2 production, temperature, water content, and gas diffusivity: Implications for field studies through sensitivity analyses. *Journal of Forest Research*, *11*(1), 41–50. https://doi.org/10.1007/s10310-005-0185-4

Hashizume, H., & Theng, B. K. G. (2007). Adenine, adenosine, ribose and 5′-AMP adsorption to allophane. *Clays and Clay Minerals*, *55*(6), 599–605. https://doi.org/10.1346/CCMN.2007.0550607

Hastie, T., Tibshirani, R., Friedman, J. H., & Friedman, J. H. (2009). *The elements of statistical learning: Data mining, inference, and prediction* (Vol. 2). Springer.

Haynes, R. (1986). The decomposition process: Mineralisation, immobilisation, humus formation and degradation. In K.C. Cameron (Ed.), *Mineral nitrogen in the plant–soil system* (pp. 52–109.

Hervé, P., Tiegs, S. D., Grellier, S., Wantzen, K. M., & Isselin-Nondedeu, F. (2019). Combined effects of vegetation and drought on organic-matter decomposition in vernal pool soils. *Wetlands*, *39*(2), 321–327. https://doi.org/10.1007/s13157-018-1091-9

Hewitt, A. E. (2010). New Zealand soil classification. *Landcare research science series*, (1).

Hewitt, A. E., & Shepherd, T. G. (1997). Structural vulnerability of New Zealand soils. *Soil Research*, *35 (3)*, 461–474.

Herath, H.M.S.K., Camps-Arbestain, M., Hedley, M., Kirschbaum, M.U.F., Wang, T., & Van Hale, R. (2015). Experimental evidence for sequestering C with biochar by avoidance of CO 2 emissions from original feedstock and protection of native Soil Organic Carbon. *Global Change Biology Bioenergy*, 7, 512-526.

Hicks Pries, C. E., Castanha, C., Porras, R., Phillips, C., & Torn, M. S. (2018). Response to comment on "The whole-soil carbon flux in response to warming." *Science (New York, N.Y.)*, *359*(6378), 1420–1423. https://doi.org/10.1126/science.aao0457

Holmgren, G. G. S. (1967). A rapid citrate-dithionite extractable iron procedure. *Soil Science Society of America Journal*, *31*(2), 210–211. https://doi.org/10.2136/sssaj1967.03615995003100020020x

Houghton, R. A. (2007). Balancing the global carbon budget. *Annual Review of Earth Planet Science, 35*(1), 313-347.

Huang, Y. T., Lowe, D. J., Churchman, G. J., Schipper, L. A., Cursons, R., Zhang, H., Chen, T. Y., & Cooper, A. (2016). DNA adsorption by nanocrystalline allophane spherules and nanoaggregates, and implications for carbon sequestration in Andisols. *Applied Clay Science*, *120*, 40–50. https://doi.org/10.1016/j.clay.2015.11.009

IPCC, 2021: Chapter 5. In: Climate Change 2021: The Physical Science Basis. Contribution of Working Group I to the Sixth Assessment Report of the Intergovernmental Panel on Climate Change [Canadell, J.G., P.M.S. Monteiro, M.H. Costa, L. Cotrim da Cunha, P.M. Cox, A.V. Eliseev, S. Henson, M. Ishii, S. Jaccard, C. Koven, A. Lohila, P.K. Patra, S. Piao, J. Rogelj, S. Syampungani, S. Zaehle, and K. Zickfeld, 2021: Global Carbon and other Biogeochemical Cycles and Feedbacks. In Climate Change 2021: The Physical Science Basis. Contribution of Working Group I to the Sixth Assessment Report of the Intergovernmental Panel on Climate Change [Masson-Delmotte, V., P. Zhai, A. Pirani, S.L. Connors, C. Péan, S. Berger, N. Caud, Y. Chen, L. Goldfarb, M.I. Gomis, M. Huang, K. Leitzell, E. Lonnoy, J.B.R. Matthews, T.K. Maycock, T. Waterfield, O. Yelekçi, R. Yu, and B. Zhou (eds.)]. Cambridge University Press, Cambridge, United Kingdom and New York, NY, USA, pp. 673–816, doi: 10.1017/9781009157896.007

Intergovernmental technical panel on soils (ITPS). (2015). Status of the world's soil resources (SWSR)—Main report. Food and Agriculture Organization of the United Nations and Intergovernmental Technical Panel on Soils.

Jenkinson, D. S. (1990). The turnover of organic carbon and nitrogen in soil. *Philosophical Transactions: Biological Sciences. 329*(1255), 361–368.

Jindaluang, W., Kheoruenromne, I., Suddhiprakarn, A., Singh, B. P., & Singh, B. (2013). Influence of soil texture and mineralogy on organic matter content and composition in physically separated fractions soils of Thailand. *Geoderma*, *195–196*, 207–219. https://doi.org/10.1016/j.geoderma.2012.12.003

Jones, C., McConnell, C., Coleman, K., Cox, P., Falloon, P., Jenkinson, D., & Powlson, D. (2005). Global climate change and soil carbon stocks: Predictions from two contrasting models for the turnover of organic carbon in soil. *Global Change Biology*, *11*(1), 154–166. https://doi.org/10.1111/j.1365-2486.2004.00885.x

Jones, D. L., Nguyen, C., & Finlay, R. D. (2009). Carbon flow in the rhizosphere: Carbon trading at the soil–root interface. *Plant and Soil*, *321*(1), 5–33. https://doi.org/10.1007/s11104-009-9925-0

Jones, R. J. A., Hiederer, R., Rusco, E., & Montanarella, L. (2005). Estimating organic carbon in the soils of Europe for policy support. *European Journal of Soil Science*, *56*(5), 655–671. https://doi.org/10.1111/j.1365-2389.2005.00728.x

Joshi, A. B., Vann, D. R., Johnson, A. H., & Miller, E. K. (2003). Nitrogen availability and forest productivity along a climosequence on Whiteface Mountain, New York. *Canadian Journal of Forest Research*, *33*(10), 1880–1891. https://doi.org/10.1139/x03-105

Jungkunst, H., Krüger, J. P., Heitkamp, F., Erasmi, S., Fiedler, S., Glatzel, S., & Lal, R. (2012). Accounting more precisely for peat and other soil carbon resources. In R. Lal (Ed.), *Recarbonization of the biosphere* (pp. 127–157). Springer, Dordrecht. https://doi.org/10.1007/978-94-007-4159-1_7

Kaal, J., & Mailänder, S. (2018). Molecular properties of soil organic matter in dark buried colluvium from South Germany show abundance of fire residues from Early Neolithic vegetation clearance and slash and burn agriculture. *Analytical Pyrolysis Letters*, 1–10.

Kaiser, K., & Guggenberger, G. (2000). The role of DOM sorption to mineral surfaces in the preservation of organic matter in soils. *Organic geochemistry*, *31*(7-8), 711-725.

Kaiser, K., & Guggenberger, G. (2003). Mineral surfaces and soil organic matter. European *Journal of Soil Science*, 54(2), 219–236. https://doi.org/10.1046/j.1365-2389.2003.00544.x

Kane, D., & Solutions, L. L. C. (2015). Carbon sequestration potential on agricultural lands: a review of current science and available practices. *National Sustainable Agriculture Coalition Breakthrough Strategies and Solutions, LLC*, 1-35.

Karhu, K., Fritze, H., Tuomi, M., Vanhala, P., Spetz, P., Kitunen, V., & Liski, J. (2010). Temperature sensitivity of organic matter decomposition in two boreal forest soil profiles. *Soil Biology and Biochemistry*, *42*(1), 72–82. https://doi.org/10.1016/j.soilbio.2009.10.002

Keesstra, S. D., Bouma, J., Wallinga, J., Tittonell, P., Smith, P., Cerdà, A., ... & Fresco, L. O. (2016). The significance of soils and soil science towards realization of the United

Nations Sustainable Development Goals. *Soil*, *2*(2), 111–128. https://doi.org/10.5194/soil-2-111-2016

Keiluweit, M., Wanzek, T., Kleber, M., Nico, P., & Fendorf, S. (2017). Anaerobic microsites have an unaccounted role in soil carbon stabilisation. *Nature Communications*, *8(1)*, 1771.

Kiem, R., & Kögel-Knabner, I. (2003). Contribution of lignin and polysaccharides to the refractory carbon pool in C-depleted arable soils. *Soil Biology and Biochemistry*, *35*(1), 101–118. https://doi.org/10.1016/S0038-0717(02)00242-0

Kirschbaum, M. U. F. (2000). Will changes in soil organic carbon act as a positive or negative feedback on global warming? *Biogeochemistry*, *48*(1), 21–51. https://doi.org/10.1023/A:1006238902976

Kirschbaum, M. U. F. (2004). Soil respiration under prolonged soil warming: Are rate reductions caused by acclimation or substrate loss? *Global Change Biology*, 10(11), 1870–1877. https://doi.org/10.1111/j.1365-2486.2004.00852.x

Kirschbaum, M. U. (2006). The temperature dependence of organic-matter decomposition—Still a topic of debate. *Soil Biology and Biochemistry*, 38(9), 2510–2518.

Kirschbaum, M. U. (2010). The temperature dependence of organic matter decomposition: seasonal temperature variations turn a sharp short-term temperature response into a more moderate annually averaged response. *Global Change Biology*, 16(7), 2117-2129.

Kleber, M. (2010). What is recalcitrant soil organic matter?. *Environmental Chemistry*, 7(4), 320-332.

Kleber, M., Eusterhues, K., Keiluweit, M., Mikutta, C., Mikutta, R., & Nico, P. S. (2015). Mineral–organic associations: Formation, properties, and relevance in soil environments. *Advances in Agronomy*, 130, 1–140.

Kleber, M, Sollins, P., & Sutton, R. (2007). A conceptual model of organo-mineral interactions in soils: Self-assembly of organic molecular fragments into zonal structures on mineral surfaces. *Biogeochemistry*, *85*(1), 9–24. https://doi.org/10.1007/s10533-007-9103-5

Klingenfuß, C., Roßkopf, N., Walter, J., Heller, C., & Zeitz, J. (2014). Soil organic matter to soil organic carbon ratios of peatland soil substrates. *Geoderma*, *235–236*, 410–417. https://doi.org/10.1016/j.geoderma.2014.07.010

Knorr, W., Prentice, I. C., House, J. I., & Holland, E. A. (2005). Long-term sensitivity of soil carbon turnover to warming. *Nature*, *433*(7023), 298–301. https://doi.org/10.1038/nature03226

Knowles, B., & Beveridge, A. E. (1982). Biological flora of New Zealand 9. *Beilschmiedia tawa* (A. Cunn.) Benth. et Hook. F. ex Kirk (Lauraceae) *tawa*. *New Zealand Journal of Botany*, *20*(1), 37–54. https://doi.org/10.1080/0028825X.1982.10426403

Koch, O., Tscherko, D., & Kandeler, E. (2007). Temperature sensitivity of microbial respiration, nitrogen mineralisation, and potential soil enzyme activities in organic alpine soils. *Global Biogeochemical Cycles*, *21*(4), GB4017. https://doi.org/10.1029/2007GB002983

Kögel-Knabner, I. (2002). The macromolecular organic composition of plant and microbial residues as inputs to soil organic matter. *Soil Biology and Biochemistry*, 34(2), 139–162. https://doi.org/10.1016/S0038-0717(01)00158-4

Kögel-Knabner, I., Guggenberger, G., Kleber, M., Kandeler, E., Kalbitz, K., Scheu, S., Eusterhues, K., & Leinweber, P. (2008). Organo-mineral associations in temperate soils: Integrating biology, mineralogy, and organic matter chemistry. *Journal of Plant Nutrition and Soil Science*, 171(1), 61–82. https://doi.org/https://doi.org/10.1002/jpln.200700048

.

Kopittke, P. M., Dalal, R. C., Hoeschen, C., Li, C., Menzies, N. W., & Mueller, C. W. (2020). Soil organic matter is stabilised by organo-mineral associations through two key processes: The role of the carbon to nitrogen ratio. *Geoderma*, *357*, 1–24.

Kopittke, P. M., Dalal, R. C., Finn, D., & Menzies, N. W. (2017). Global changes in soil stocks of carbon, nitrogen, phosphorus, and sulphur as influenced by long-term agricultural production. *Global change biology*, *23*(6), 2509-2519.

Kothawala, D. N., Moore, T. R., & Hendershot, W. H. (2009). Soil properties controlling the adsorption of dissolved organic carbon to mineral soils. *Soil Science Society of America Journal*, *73*(6), 1831-1842.

Kov, R., Camps-Arbestain, M., Calvelo Pereira, R., Suarez-Abelenda, M., Shen, Q., Garbuz,. S., Vázquez, F.M. (2018). A farm-scale investigation of the organic matter composition and soil chemistry of Andisols as influenced by land use and management. *Biogeochemistry*, *140,* 65–79. https://doi.org/10.1007/s10533-018-0473-7

Kpemoua, T. P., Barré, P., Chevallier, T., Houot, S., & Chenu, C. (2022). Drivers of the amount of organic carbon protected inside soil aggregates estimated by crushing: A meta-analysis. *Geoderma*, *427*, 116089.

Kuzyakov, Y., & Gavrichkova, O. (2010). Review: Time lag between photosynthesis and carbon dioxide efflux from soil: A review of mechanisms and controls. *Global Change Biology*, 16(12), 3386–3406. https://doi.org/10.1111/j.1365-2486.2010.02179.x

Labaz, B., Galka, B., Bogacz, A., Waroszewski, J., & Kabala, C. (2014). Factors influencing humus forms and forest litter properties in the mid-mountains under temperate climate of southwestern Poland. *Geoderma*, 230–231, 265–273. https://doi.org/10.1016/j.geoderma.2014.04.021

Lal, R. (2004). Soil carbon sequestration impacts on global climate change and food security. *Science*, 304(5677), 1623-1627.

Larjavaara, M., & Muller-Landau, H. C. (2013). Measuring tree height: A quantitative comparison of two common field methods in a moist tropical forest. *Methods in Ecology and Evolution*, *4*(9), 793–801. https://doi.org/10.1111/2041-210X.12071

Lawrence, C. R., Neff, J. C. S. J. (2009). Does adding microbial mechanisms of decomposition improve soil organic matter models? A comparison of four models using data from a pulsed rewetting experiment. *Soil Biology and Biochemistry*, *41*, 1923–1934.

LeBauer, D. S., & Treseder, K. K. (2008). Nitrogen limitation of net primary productivity in terrestrial ecosystems is globally distributed. *Ecology*, *89*(2), 371–379. https://doi.org/https://doi.org/10.1890/06-2057.1

Lefevre, C., Rekik, F., Alcantara, V., & Wiese, L. (2017). *Soil organic carbon: The hidden potential*. Food and Agriculture Organization (FAO).

Lefèvre, R., Barré, P., Moyano, F. E., Christensen, B. T., Bardoux, G., Eglin, T., Girardin, C., Houot, S., Kätterer, T., van Oort, F., & Chenu, C. (2014). Higher temperature sensitivity

for stable than for labile soil organic carbon – Evidence from incubations of long-term bare fallow soils. *Global Change Biology*, *20*(2), 633–640. https://doi.org/10.1111/gcb.12402

Lehmann, J., Hansel, C. M., Kaiser, C., Kleber, M., Maher, K., Manzoni, S., Nunan, N., Reichstein, M., Schimel, J. P., Torn, M. S., Wieder, W. R., & Kögel-Knabner, I. (2020). Persistence of soil organic carbon caused by functional complexity. *Nature Geoscience*, *13*(8), 529–534. https://doi.org/10.1038/s41561-020-0612-3

Lehmann, J., & Joseph, S. (Eds.). (2015). *Biochar for environmental management: science, technology and implementation*. Routledge.

Lehmann, J., & Kleber, M. (2015). The contentious nature of soil organic matter. *Nature*, *528*(7580), 60–68. https://doi.org/10.1038/nature16069

Lemenih, M., & Itanna, F. (2004). Soil carbon stocks and turnovers in various vegetation types and arable lands along an elevation gradient in southern Ethiopia. *Geoderma*, *123*(1–2), 177–188. https://doi.org/10.1016/j.geoderma.2004.02.004

Li, J., He, N., Wei, X., Gao, Y., & Zuo, Y. (2015). Changes in temperature sensitivity and activation energy of soil organic matter decomposition in different Qinghai–Tibet Plateau grasslands. *PLoS One*, *10*(7), 1–14. https://doi.org/10.1371/journal.pone.0132795

Li, J., Pei, J., Dijkstra, F. A., Nie, M., & Pendall, E. (2021). Microbial carbon use efficiency, biomass residence time and temperature sensitivity across ecosystems and soil depths. *Soil Biology and Biochemistry*, *154*, 108117.

Li, J., Nie, M., Pendall, E., Reich, P. B., Pei, J., Noh, N. J., ... & Fang, C. (2020). Biogeographic variation in temperature sensitivity of decomposition in forest soils. *Global change biology*, *26*(3), 1873-1885.

Li, J., Pei, J., Pendall, E., Fang, C., & Nie, M. (2020). Spatial heterogeneity of temperature sensitivity of soil respiration: A global analysis of field observations. *Soil Biology and Biochemistry*, *141*, 107675.

Li, L., Vogel, J., He, Z., Zou, X., Ruan, H., Huang, W., Wang, J., & Bianchi, T. S. (2016). Association of soil aggregation with the distribution and quality of organic carbon in soil

along an elevation gradient on Wuyi Mountain in China. *PLoS One*, *11*(3), 1–14. https://doi.org/10.1371/journal.pone.0150898

Li, Y., Wang, T., Camps-Arbestain, M., Suárez-Abelenda, M., & Whitby, C. P. (2020). Lime and/or phosphate application affects the stability of soil organic carbon: Evidence from changes in quantity and chemistry of the soil water-extractable organic matter. *Environmental science & technology*, 54(21), 13908-13916.

Li, Y., Wang, T., Camps-Arbestain, M., & Whitby, C. P. (2022). The regulators of soil organic carbon mineralization upon lime and/or phosphate addition vary with depth. *Science of The Total Environment*, 828, 154378.

Li, Y., Camps-Arbestain, M., Whitby, C. P., Wang, T., Mueller, C. W., Hoeschen, C., & Beare, M. H. (2022). Functional complexity explains the depth-dependent response of organic matter to liming at the nanometer scale. *Geoderma*, *408,* 115560. https://doi.org/10.1016/j.geoderma.2021.115560

Liang, C., Schimel, J. P., & Jastrow, J. D. (2017). The importance of anabolism in microbial control over soil carbon storage. *Nature Microbiology*, *2*, 17105. https://doi.org/10.1038/nmicrobiol.2017.105

Lindahl, B. D., Ihrmark, K., Boberg, J., Trumbore, S. E., Högberg, P., Stenlid, J., & Finlay, R. D. (2007). Spatial separation of litter decomposition and mycorrhizal nitrogen uptake in a boreal forest. *New Phytologist*, *173*(3), 611–620.

Linn, D. M., & Doran, J. W. (1984). Effect of water-filled pore space on carbon dioxide and nitrous oxide production in tilled and nontilled soils. *Soil Science Society of America Journal*, *48*(6), 1267–1272. https://doi.org/10.2136/sssaj1984.03615995004800060013x

Litton, C. M., Giardina, C. P., Albano, J. K., Long, M. S., & Asner, G. P. (2011). The magnitude and variability of soil-surface CO_2 efflux increase with mean annual temperature in Hawaiian tropical montane wet forests. *Soil Biology and Biochemistry*, *43*(11), 2315–2323. https://doi.org/10.1016/j.soilbio.2011.08.004

Liu, Y., Zang, H., Ge, T., Bai, J., Lu, S., Zhou, P., ... & Guggenberger, G. (2018). Intensive fertilization (N, P, K, Ca, and S) decreases organic matter decomposition in paddy soil. *Applied Soil Ecology*, 127, 51-57.

Lorenz, K., & Lal, R. (2005). The depth distribution of soil organic carbon in relation to land use and management and the potential of carbon sequestration in subsoil horizons. *Advances in agronomy*, *88*, 35-66.

Lowe, D. J., & Palmer, D. J. (2005). Andisols of New Zealand and Australia. *Journal of Integrated Field Science*, *2*, 39–65.

Lu, M., Zhou, X., Yang, Q., Li, H., Luo, Y., Fang, C., Chen, J., Yang, X., & Li, B. (2013). Responses of ecosystem carbon cycle to experimental warming: A meta-analysis. *Ecology*, *94*(3), 726–738. https://doi.org/10.1890/12-0279.1

Luo, Y., Sherry, R., Zhou, X., & Wan, S. (2009). Terrestrial carbon-cycle feedback to climate warming: Experimental evidence on plant regulation and impacts of biofuel feedstock harvest. *GCB Bioenergy*, *1*(1), 62–74. https://doi.org/10.1111/j.1757-1707.2008.01005.x

Luo, Z., Feng, W., Luo, Y., Baldock, J., & Wang, E. (2017). Soil organic carbon dynamics jointly controlled by climate, carbon inputs, soil properties and soil carbon fractions. *Global Change Biology*, *23*(10), 4430-4439.

Lützow, M. V., Kögel-Knabner, I., Ekschmitt, K., Matzner, E., Guggenberger, G., Marschner, B., & Flessa, H. (2006). Stabilisation of organic matter in temperate soils: mechanisms and their relevance under different soil conditions–a review. *European journal of soil science*, *57*(4), 426-445.

Lyu, M., Nie, Y., Giardina, C. P., Vadeboncoeur, M. A., Ren, Y., Fu, Z., ... & Xie, J. (2019). Litter quality and site characteristics interact to affect the response of priming effect to temperature in subtropical forests. *Functional Ecology*, *33*(11), 2226-2238.

Machinet, G. E., Bertrand, I., Barrière, Y., Chabbert, B., & Recous, S. (2011). Impact of plant cell wall network on biodegradation in soil: Role of lignin composition and phenolic acids in roots from 16 maize genotypes. *Soil Biology and Biochemistry*, *43*(7), 1544–1552. https://doi.org/10.1016/j.soilbio.2011.04.002

Macías, F., & Camps-Arbestain, M. (2020). A biogeochemical view of the world reference base soil classification system: Homage to Ward Chesworth. In Donald L. Sparks (Ed.), *Advances in Agronomy* (pp. 295–342). Springer.

Manzoni, S., & Porporato, A. (2009). Soil carbon and nitrogen mineralisation: Theory and models across scales. *Soil Biology and Biochemistry*, 41(7), 1355–1379. https://doi.org/10.1016/j.soilbio.2009.02.031

Mao, X., Zheng, J., Yu, W., Guo, X., Xu, K., Zhao, R., ... & Luo, Z. (2022). Climate-induced shifts in composition and protection regulate temperature sensitivity of carbon decomposition through soil profile. *Soil Biology and Biochemistry*, 108743.

Mathew, I., Shimelis, H., Mutema, M., Minasny, B., & Chaplot, V. (2020). Crops for increasing soil organic carbon stocks–A global meta-analysis. *Geoderma*, 367, 114230.

Matus, F., Rumpel, C., Neculman, R., Panichini, M., & Mora, M. (2014). Soil carbon storage and stabilisation in Andic soils. *Catena*, *120*, 102–110.

McDaniel, P. A., Lowe, D. J., Arnalds, O., & Ping, C.-L. (2012). Andisols. In P. M. Huang, Y. Li, & M. E. Summer (Eds.), *Handbook of soil sciences: Properties and processes* (pp. 29–48). CRC Press.

McGlone, M. S., Neall, V. E., & Clarkson, B. D. (1988). The effect of recent volcanic events and climatic changes on the vegetation of Mt. Egmont (Mt. Taranaki), New Zealand. *New Zealand Journal of Botany*, 26(1), 123–144.https://doi.org/10.1080/0028825X.1988.10410105

McMichael, B. L., & Burke, J. J. (1998). Soil temperature and root growth. *HortScience, 33*(6), 947–951. https://doi.org/10.21273/hortsci.33.6.947

Melillo, J. M., Aber, J. D., & Muratore, J. F. (1982). Nitrogen and lignin control of hardwood leaf litter decomposition dynamics stable. *Ecology*, *63*(3), 621–626.

Melillo, J. M., Butler, S., Johnson, J., Mohan, J., Steudler, P., Lux, H., Burrows, E., Bowles, F., Smith, R., Scott, L., Vario, C., Hill, T., Burton, A., Zhou, Y.-M., & Tang, J. (2011). Soil warming, carbon–nitrogen interactions, and forest carbon budgets. *Proceedings of the National Academy of Sciences*, *108*(23), 9508–9512. https://doi.org/10.1073/pnas.1018189108

Melillo, J. M., Frey, S. D., DeAngelis, K. M., Werner, W. J., Bernard, M. J., Bowles, F. P., ... & Grandy, A. S. (2017). Long-term pattern and magnitude of soil carbon feedback to the climate system in a warming world. *Science*, 358(6359), 101-105.

Melillo, J., Steudler, P. A., Aber, J., Newkirk, K., Lux, H., Bowles, F. P., Catricala, C., Magill, A., Ahrens, T., & Morrisseau, S. (2003). Soil Warming and Carbon-Cycle Feedbacks to the Climate System. *Science* (New York, N.Y.), 298, 2173–2176. https://doi.org/10.1126/science.1074153

Mencuccini, M., & Hölttä, T. (2010). The significance of phloem transport for the speed with which canopy photosynthesis and belowground respiration is linked. *New Phytologist*, *185*(1), 189–203. https://doi.org/10.1111/j.1469-8137.2009.03050.x

Metcalfe, D. B., Fisher, R. A., & Wardle, D. A. (2011). Plant communities as drivers of soil respiration: Pathways, mechanisms, and significance for global change. *Biogeosciences*, *8(8)*, 2047–2061.

Meyer, N., Welp, G., & Amelung, W. (2018). The temperature sensitivity (Q10) of soil respiration: Controlling factors and spatial prediction at regional scale based on environmental soil classes. *Global Biogeochemical Cycles*, *32*(2), 306–323. https://doi.org/10.1002/2017GB005644

Mikan, C. J., Schimel, J. P., & Doyle, A. P. (2002). Temperature controls of microbial respiration in arctic tundra soils above and below freezing. *Soil biology and biochemistry*, *34*(11), 1785-1795.

Mikutta, R., Kleber, M., Torn, M. S., & Jahn, R. (2006). Stabilisation of soil organic matter: association with minerals or chemical recalcitrance?. *Biogeochemistry*, *77*(1), 25-56.

Miltner, A., Bombach, P., Schmidt-Brücken, B., & Kästner, M. (2012). SOM genesis: Microbial biomass as a significant source. *Biogeochemistry*, *111*(1–3), 41–55. https://doi.org/10.1007/s10533-011-9658-z

Miltner, A., & Zech, W. (1998). Carbohydrate decomposition in beech litter as influenced by aluminum, iron and manganese oxides. *Soil Biology and Biochemistry*, *30*(1), 1–7. https://doi.org/10.1016/S0038-0717(97)00092-8

Miyazawa, M., Takahashi, T., Sato, T., Kanno, H., & Nanzyo, M. (2013). Factors controlling accumulation and decomposition of organic carbon in humus horizons of Andosols: A case study for distinctive non-allophanic Andosols in northeastern Japan. *Biology and Fertility of Soils*, *49*(7), 929–938. https://doi.org/10.1007/s00374-013-0792-8

Mizota, C., & Van Reeuwijk, L. P. (1989). *Clay mineralogy and chemistry of soils formed in volcanic material in diverse climatic regions*. International Soil Reference and Information Centre (ISRIC).

Mokany, K., Raison, R. J., & Prokushkin, A. S. (2006). Critical analysis of root: Shoot ratios in terrestrial biomes. *Global Change Biology*, *12*(1), 84–96. https://doi.org/10.1111/j.1365-2486.2005.001043.x

Molloy, L. (1988). *Soils in the New Zealand Landscape: The Living Mantle* (2nd ed.). New Zealand Society of Soil Science.

Mulkey, S. S., Kitajima, K., & Wright, S. J. (1996). Plant physiological ecology of tropical forest canopies. *Trends in Ecology & Evolution*, *11*(10), 408–412. https://doi.org/10.1016/0169-5347(96)10043-4

Murphy, J., & Riley, P. (1962). A modified single solution method for the determination of phosphate in natural waters. *Analytica Chimica Acta*, *27*, 31–36.

Naafs, D. F. W., Van Bergen, P. F., Boogert, S. J., & De Leeuw, J. W. (2004). Solvent-extractable lipids in an acid Andic Forest soil: Variations with depth and season. *Soil Biology and Biochemistry*, *36*(2), 297–308. https://doi.org/10.1016/j.soilbio.2003.10.005

Nadelhoffer, K. J., Raich, J. W., & Aber, J. D. (1998). A global trend in belowground carbon allocation: Comment. *Ecology*, *79,* 1822–1825.

Nanzyo, M. (2002). Unique properties of volcanic ash soils. *Global Journal of Environmental Research*, *6*(2), 99–112.

Neall, V. E. (1972). Tephrochronology and tephrostratigraphy of western Taranaki (N108–109), New Zealand. *New Zealand Journal of Geology and Geophysics*, *15*(4), 507–557. https://doi.org/10.1080/00288306.1972.10423983

Neall, V. E., & Stewart, R. B. S. I. (1986). History and petrology of the Taranaki volcanoes. ED. Late Cenozoic volcanism in New Zealand. *Royal Society of New Zealand Bulletin, 23*, 251–263.

Neall, V. E. (1979). *New Plymouth, Egmont and Manaia. 1st ed. Geological map of New Zealand 1:50,000.* NZ Department of Scientific and Industrial Research, Wellington. 19–21.

Nguyen, B. T., & Lehmann, J. (2009). Black carbon decomposition under varying water regimes. *Organic Geochemistry*, *40*(8), 846–853. https://doi.org/10.1016/j.orggeochem.2009.05.004

NIWA. (2022). National and regional climate maps. Taranaki. NIWA. https://niwa.co.nz/climate/national-and-regional-climate-maps/taranaki

Nottingham, A. T., Meir, P., Velasquez, E., & Turner, B. L. (2020). Soil carbon loss by experimental warming in a tropical forest. *Nature*, *584*(7820), 234-237.

Oades, A. J. M. (2013). The retention of organic matter in soils. *Biogeochemistry, 5*(1), 35–70.

Oades, J. M., & Waters, A. G. (1991). Aggregate hierarchy in soils. *Soil Research*, *29*(6), 815–828. https://doi.org/10.1071/SR9910815

Ofiti, N. O. E., Zosso, C. U., Soong, J. L., Solly, E. F., Torn, M. S., Wiesenberg, G. L. B., & Schmidt, M. W. I. (2021). Warming promotes loss of subsoil carbon through accelerated degradation of plant-derived organic matter. *Soil Biology and Biochemistry*, *156*, 108185. https://doi.org/10.1016/j.soilbio.2021.108185

Olsen, S. R. (1954). *Estimation of available phosphorus in soils by extraction with sodium bicarbonate* (No. 939). US Department of Agriculture.

O'Rourke, S. M., Angers, D. A., Holden, N. M., & McBratney, A. B. (2015). Soil organic carbon across scales. *Global Change Biology*, *21*(10), 3561–3574. https://doi.org/10.1111/gcb.12959

Pachauri, R.K., & Meyer, L.A. (Eds.). (2014). *Synthesis Report. Contribution of Working Groups I, II and III to the Fifth Assessment Report of the Intergovernmental Panel on Climate Change*. IPCC.

Pan, Y., Birdsey, R. A., Fang, J., Houghton, R., Kauppi, P. E., Kurz, W. A., Phillips, O. L., Shvidenko, A., Lewis, S. L., Canadell, J. G., Ciais, P., Jackson, R. B., Pacala, S. W., McGuire, A. D., Piao, S., Rautiainen, A., Sitch, S., & Hayes, D. (2011). A large and persistent carbon sink in the world's forests. *Science*, *333*(6045), 988–993. https://doi.org/10.1126/science.1201609

Parfitt, R., & Wilson, A. D. (1985). Estimation of allophane and halloysite in three sequences of volcanic soils, New Zealand. *Catena*, 7, 1–8.

Parfitt, R. L. (2009). Allophane and imogolite: role in soil biogeochemical processes. *Clay Minerals*, *44*(1), 135–155. https://doi.org/10.1180/claymin.2009.044.1.135

Parton, W. J., Schimel, D. S., Cole, C. V., & Ojima, D. S. (1987). Analysis of factors controlling soil organic matter levels in Great Plains grasslands. *Soil Science Society of America Journal*, 51(5), 1173–1179. https://doi.org/10.2136/sssaj1987.03615995005100050015x

Paul, E. A. (Ed.). (2014). Soil microbiology, ecology and biochemistry. Academic press.

Paustian, K., Lehmann, J., Ogle, S., Reay, D., Robertson, G. P., & Smith, P. (2016). Climate-smart soils. *Nature*, *532*(7597), 49–57. https://doi.org/10.1038/nature17174

Percival, H. J., Parfitt, R. L., & Scott, N. A. (2000). Factors controlling soil carbon levels in New Zealand grasslands: Is clay content important? *Soil Science Society of America Journal*, *64*(5), 1623–1630. https://doi.org/10.2136/sssaj2000.6451623x

Piao, S., Wang, X., Park, T., Chen, C., Lian, X. U., He, Y., ... & Myneni, R. B. (2020). Characteristics, drivers and feedbacks of global greening. *Nature Reviews Earth & Environment*, *1*(1), 14-27.

Pietikäinen, J., Pettersson, M., & Bååth, E. (2005). Comparison of temperature effects on soil respiration and bacterial and fungal growth rates. *FEMS microbiology ecology*, *52*(1), 49–58.

Platz, T., Cronin, S. J., Cashman, K. V., Stewart, R. B., & Smith, I. E. M. (2007). Transition from effusive to explosive phases in andesite eruptions – A case-study from the AD1655 eruption of Mt. Taranaki, New Zealand. *Journal of Volcanology and Geothermal Research*, *161*(1–2), 15–34. https://doi.org/10.1016/j.jvolgeores.2006.11.005

Platz, T., Cronin, S. J., Procter, J. N., Neall, V. E., & Foley, S. F. (2012). Non-explosive, dome-forming eruptions at Mt. Taranaki, New Zealand. *Geomorphology*, *136*(1), 15–30. https://doi.org/10.1016/j.geomorph.2011.06.016

Plaza, C., Courtier-Murias, D., Fernández, J. M., Polo, A., & Simpson, A. J. (2013). Physical, chemical, and biochemical mechanisms of soil organic matter stabilisation under conservation tillage systems: A central role for microbes and microbial by-products in C sequestration. *Soil Biology and Biochemistry*, *57*, 124–134. https://doi.org/10.1016/j.soilbio.2012.07.026

Poirier, V., Angers, D. A., & Whalen, J. K. (2014). Formation of millimetric-scale aggregates and associated retention of $_{13}C$–$_{15}N$-labelled residues are greater in subsoil than topsoil. *Soil Biology and Biochemistry*, *75*, 45–53. https://doi.org/10.1016/j.soilbio.2014.03.020

Possinger, A. R., Zachman, M. J., Enders, A., Levin, B. D., Muller, D. A., Kourkoutis, L. F., & Lehmann, J. (2020). Organo–organic and organo–mineral interfaces in soil at the nanometer scale. *Nature communications*, *11*(1), 1-11.

Power, J. F., & Prasad, R. (1997). *Soil fertility management for sustainable agriculture.* CRC Press.

Powlson, D. (2005). Climatology: Will soil amplify climate change? *Nature*, *433*(7023), 204–205.

Prieto, I., Stokes, A., & Roumet, C. (2016). Root functional parameters predict fine root decomposability at the community level. *Journal of Ecology*, https://doi.org/10.1111/1365-2745.12537

Puhe, J. (2003). Growth and development of the root system of Norway spruce (*Picea abies*) in forest stands—A review. *Forest Ecology and Management*, *175*(1), 253–273. https://doi.org/10.1016/S0378-1127(02)00134-2

Pulleman, M., & Marinissen, J. (2004). Physical protection of mineralizable C in aggregates from long-term pasture and arable soil. *Geoderma*, *120(3)*, 273–282.

Qin, F., & Beckingham, L. E. (2021). The impact of mineral reactive surface area variation on simulated mineral reactions and reaction rates. *Applied Geochemistry*, *124*, 104852. https://doi.org/10.1016/j.apgeochem.2020.104852

Qin, S., Chen, L., Fang, K., Zhang, Q., Wang, J., Liu, F., Yu, J., & Yang, Y. (2019). Temperature sensitivity of SOM decomposition governed by aggregate protection and microbial communities. *Science Advances*, 5(7), 1–10. https://doi.org/10.1126/sciadv.aau1218

Qin, S., Kou, D., Mao, C., Chen, Y., Chen, L., & Yang, Y. (2021). Temperature sensitivity of permafrost carbon release mediated by mineral and microbial properties. *Science Advances*, *7*(32), eabe3596.

Rasmussen, C., Southard, R. J., & Horwath, W. R. (2006). Mineral control of organic carbon mineralisation in a range of temperate conifer forest soils. *Global Change Biology*, *12*(5), 834–847. https://doi.org/10.1111/j.1365-2486.2006.01132.x

Reich, P. B., Walters, M. B., & Ellsworth, D. S. (1997). From tropics to tundra: Global convergence in plant functioning. *Proceedings of the National Academy of Sciences*, *94(25)*, 13730–13734.

Repo, T., Leinonen, I., Ryyppö, A., & Finér, L. (2004). The effect of soil temperature on the bud phenology, chlorophyll fluorescence, carbohydrate content and cold hardiness of Norway spruce seedlings. *Physiologia Plantarum*, *121*(1), 93–100. https://doi.org/10.1111/j.0031-9317.2004.00307.x

Riahi, K., Rao, S., Krey, V., Cho, C., Chirkov, V., Fischer, G., Kindermann, G., Nakicenovic, N., & Rafaj, P. (2011). RCP 8.5 – A scenario of comparatively high greenhouse gas emissions. *Climatic Change*, *109*(1), 33–57. https://doi.org/10.1007/s10584-011-0149-y

Richter, D. D., Markewitz, D., Trumbore, S. E., & Wells, C. G. (1999*).* Rapid accumulation and turnover of soil carbon in a re-establishing forest. *Nature, 400*, 56–58. https://doi.org/10.1038/21867

Ricketts, M. P., Matamala, R., Jastrow, J. D., Antonopoulos, D. A., Koval, J., Ping, C. L., ... & Gonzalez-Meler, M. A. (2020). The effects of warming and soil chemistry on bacterial community structure in Arctic tundra soils. *Soil Biology and Biochemistry*, *148*, 107882.

Rolando, J. L., Dubeux, J. C., Souza, T. C. D., Mackowiak, C., Wright, D., George, S., ... & Santos, E. (2021). Organic carbon is mostly stored in deep soil and only affected by land use in its superficial layers: A case study. *Agrosystems, Geosciences & Environment*, *4*(1), e20135.

Rumpel, C., Amiraslani, F., Koutika, L. S., Smith, P., Whitehead, D., & Wollenberg, E. (2018). Put more carbon in soils to meet Paris climate pledges. *Nature*, *564*(7734), 32–34. https://doi.org/10.1038/d41586-018-07587-4

Rumpel, C., Rabia, N., Derenne, S., Quenea, K., Eusterhues, K., Kögel-Knabner, I., & Mariotti, A. (2006). Alteration of soil organic matter following treatment with hydrofluoric acid (HF). *Organic Geochemistry*, *37*(11), 1437-1451.

Rustad, L. E. (2006). From transient to steady-state response of ecosystems to atmospheric CO_2-enrichment and global climate change: Conceptual challenges and need for an integrated approach. *Plant Ecology*, *182*(1–2), 43–62. https://doi.org/10.1007/s11258-005-9030-2

Sanderman, J., Baisden, W. T., & Fallon, S. (2016). Redefining the inert organic carbon pool. *Soil Biology and Biochemistry*, *92*, 149–152. https://doi.org/10.1016/j.soilbio.2015.10.005

Scheel, T., Jansen, B., Wijk, A., Verstraten, J., & Kalbitz, K. (2008). Stabilisation of dissolved organic matter by aluminum: A toxic effect or stabilisation through precipitation? *European Journal of Soil Science*, *59*, 1122–1132. https://doi.org/10.1111/j.1365-2389.2008.01074.x

Schellekens, J., Buurman, P., Fraga, I., & Martínez-Cortizas, A. (2011). Holocene vegetation and hydrologic changes inferred from molecular vegetation markers in peat, Penido Vello (Galicia, Spain). *Palaeogeography, Palaeoclimatology, Palaeoecology*, *299*(1-2), 56-69. https://doi.org/10.1016/j.palaeo.2010.10.034

Schipper, L. A., Parfitt, R. L., Fraser, S., Littler, R. A., Baisden, W. T., & Ross, C. (2014). Soil order and grazing management effects on changes in soil C and N in New Zealand pastures. *Agriculture, Ecosystems & Environment*, *184*, 67-75.

Schipper, L. A., Hobbs, J. K., Rutledge, S., & Arcus, V. L. (2014). Thermodynamic theory explains the temperature optima of soil microbial processes and high Q_{10} values at low temperatures. *Global Change Biology, 20*(11), 3578-3586.

Schmidt, M., & Noack, A. (2000). Black carbon in soils and sediments: Analysis, distribution, implications, and current challenges. *Global Biogeochemical Cycles*, *14*, 777–793.

Schmidt, M. W., Torn, M. S., Abiven, S., Dittmar, T., Guggenberger, G., Janssens, I. A., ... & Trumbore, S. E. (2011). Persistence of soil organic matter as an ecosystem property. *Nature*, *478*(7367), 49-56.

Schuur, E. A. G., McGuire, A. D., Schädel, C., Grosse, G., Harden, J. W., Hayes, D. J., Hugelius, G., Koven, C. D., Kuhry, P., Lawrence, D. M., Natali, S. M., Olefeldt, D., Romanovsky, V. E., Schaefer, K., Turetsky, M. R., Treat, C. C., & Vonk, J. E. (2015). Climate change and the permafrost carbon feedback. *Nature*, *520*, 171–179. https://doi.org/10.1038/nature14338

Schwager, S. J., & Mikhailova, E. A. (2002). Estimating variability in soil organic carbon storage using the method of statistical differentials. *Soil Science*, *167*(3), 194–200.

Sevanto, S., Suni, T., Pumpanen, J., Grönholm, T., Kolari, P., Nikinmaa, E., Hari, P., & Vesala, T. (2006). Wintertime photosynthesis and water uptake in a boreal forest. *Tree Physiology*, *26*, 749–757. https://doi.org/10.1093/treephys/26.6.749

Shen, Q., Suarez-Abelenda, M., Camps-Arbestain, M., Calvelo Pereira, R., McNally, S. R., & Kelliher, F. M. (2018). An investigation of organic matter quality and quantity in acid soils as influenced by soil type and land use. *Geoderma*, *328*, 44–55. https://doi.org/10.1016/j.geoderma.2018.05.006

Sheikh, M. A., Kumar, M., & Bussmann, R. W. (2009). Altitudinal variation in soil organic carbon stock in coniferous subtropical and broadleaf temperate forests in Garhwal Himalaya. *Carbon Balance and Management*, *4*, 6–6. https://doi.org/10.1186/1750-0680-4-6

Shukla, P., Skea, J., Calvo Buendia, E., Masson-Delmotte, V., Pörtner, H., Roberts, D., & Van Diemen, R. (2019). *Climate change and land: An IPCC special report on climate change, desertification, land degradation, sustainable land management, food security, and greenhouse gas fluxes in terrestrial ecosystems.* IPCC.

Sierra, C. A. (2012). Temperature sensitivity of organic matter decomposition in the Arrhenius equation: Some theoretical considerations. *Biogeochemistry*, *108*(1–3), 1–15. https://doi.org/10.1007/s10533-011-9596-9

Sierra, J., & Causeret, F. (2018). Changes in soil carbon inputs and outputs along a tropical altitudinal gradient of volcanic soils under intensive agriculture. *Geoderma*, *320*(February), 95–104. https://doi.org/10.1016/j.geoderma.2018.01.025

Sistla, S. A., Moore, J. C., Simpson, R. T., Gough, L., Shaver, G. R., & Schimel, J. P. (2013). Long-term warming restructures Arctic tundra without changing net soil carbon storage. *Nature*, *497*, 615–618. https://doi.org/10.1038/nature12129

Six, J., Callewaert, P., Lenders, S., De Gryze, S., Morris, S. J., Gregorich, E. G., Paul, E. A., & Paustian, K. (2002). Measuring and understanding carbon storage in afforested soils by physical fractionation. *Soil Science Society of America Journal*, *66*(6), 1981–1987. https://doi.org/10.2136/sssaj2002.1981

Six, J., Conant, R. T., Paul, E. A., & Paustian, K. (2002). Stabilisation mechanisms of soil organic matter: Implications for C-saturation of soils. *Plant and Soil*, *241*, 155–176. https://doi.org/10.1023/A:1016125726789

Six, J., Frey, S. D., Thiet, R. K., & Batten, K. M. (2006). Bacterial and fungal contributions to carbon sequestration in agroecosystems. *Soil Science Society of America Journal*, *70*(2), 555–569. https://doi.org/10.2136/sssaj2004.0347

Smith, P., Fang, C., Dawson, J. J. C., & Moncrieff, J. B. (2008). *Impact of global warming on soil organic carbon* Vol. 97. Academic Press. https://doi.org/10.1016/S0065-2113(07)00001-6

Soil Survey Staff. (1999). *Soil taxonomy: A basic system of soil classification for making and interpreting soil surveys. U.S. Department of Agriculture Handbook 436.* Natural Resources Conservation Service, U.S. Department of Agriculture.

Sokol, N. W., & Bradford, M. A. (2019). Microbial formation of stable soil carbon is more efficient from belowground than aboveground input. *Nature Geoscience*, *12*(1), 46–53. https://doi.org/10.1038/s41561-018-0258-6

Soong, J. L., Castanha, C., Hicks Pries, C. E., Ofiti, N., Porras, R. C., Riley, W. J., Schmidt, M. W. I., & Torn, M. S. (2021). Five years of whole-soil warming led to loss of subsoil carbon stocks and increased CO_2 efflux. *Science Advances*, *7*(21), 1–9. https://doi.org/10.1126/sciadv.abd1343

Stockmann, U., Adams, M. A., Crawford, J. W., Field, D. J., Henakaarchchi, N., Jenkins, M., Minasny, B., McBratney, A. B., Courcelles, V. de R. de, Singh, K., Wheeler, I., Abbott, L., Angers, D. A., Baldock, J., Bird, M., Brookes, P. C., Chenu, C., Jastrow, J. D., Lal, R., Zimmermann, M. (2013). The knowns, known unknowns and unknowns of sequestration of soil organic carbon. Agriculture, *Ecosystems and Environment*, 164(2013), 80–99. https://doi.org/10.1016/j.agee.2012.10.001

Stutter, M. I., Lumsdon, D. G., & Cooper, R. J. (2007). Temperature and soil moisture effects on dissolved organic matter release from a moorland Podzol O horizon under field and controlled laboratory conditions. *European journal of soil science*, 58(5), 1007-1016.

Suárez-Abelenda, M., Ahmad, R., Camps-Arbestain, M., & Herath, S. H. M. S. K. (2015). Changes in the chemical composition of soil organic matter over time in the presence and absence of living roots: A pyrolysis GC/MS study. *Plant and Soil*, *391*(1–2), 161–177. https://doi.org/10.1007/s11104-015-2423-7

Swift, R. (2001). Humic substances and carbon sequestration. *Soil Science.*, *166*, 858–871.

Tait, A., Henderson, R., Turner, R., & Zheng, X. (2006). Thin plate smoothing spline interpolation of daily rainfall for New Zealand using a climatological rainfall surface. *International Journal of Climatology*, *26*(14), 2097–2115. https://doi.org/https://doi.org/10.1002/joc.1350

Takahashi, T., & Dahlgren, R. A. (2016). Nature, properties and function of aluminum–humus complexes in volcanic soils. *Geoderma*, *263*, 110–121. https://doi.org/10.1016/j.geoderma.2015.08.032

Takahashi, T., Kanno, H., & Nanzyo, M. (2012). Factors affecting organic carbon accumulation in humus horizons of volcanic soils from the Tohoku University World Andosol Database: A path analysis. *Pedologist*, *56*(2), 58–62. https://doi.org/10.18920/pedologist.56.2_58

Takahashi, T., Mitamura, A., Ito, T., Ito, K., Nanzyo, M., & Saigusa, M. (2008). Aluminium solubility of strongly acidified allophanic Andosols from Kagoshima Prefecture, southern Japan. *Soil Science and Plant Nutrition*, *54*(3), 362–368. https://doi.org/10.1111/j.1747-0765.2008.00258.x

Tamocai, C., Canadell, J. G., Schuur, E. A. G., Kuhry, P., Mazhitova, G., & Zimov, S. (2009). Soil organic carbon pools in the northern circumpolar permafrost region. *Global Biogeochemical Cycles*, *23*(2), 1–11. https://doi.org/10.1029/2008GB003327

Tan, Q., & Wang, G. (2016). Decoupling of nutrient element cycles in soil and plants across an altitude gradient. *Scientific Reports*, *6*(October), 1–9. https://doi.org/10.1038/srep34875

Tang, J., & Riley, W. J. (2015). Weaker soil carbon–climate feedbacks resulting from microbial and abiotic interactions. *Nature Climate Change*, *5*(1), 56–60. https://doi.org/10.1038/nclimate2438

Tashi, S., Singh, B., Keitel, C., & Adams, M. (2016). Soil carbon and nitrogen stocks in forests along an altitudinal gradient in the eastern Himalayas and a meta-analysis of global data. *Global Change Biology*, *22*(6), 2255–2268. https://doi.org/10.1111/gcb.13234

Terrer, C., Phillips, R. P., Hungate, B. A., Rosende, J., Pett-Ridge, J., Craig, M. E., ... & Jackson, R. B. (2021). A trade-off between plant and soil carbon storage under elevated CO2. *Nature*, *591*(7851), 599-603.

Theng, B. K. G. (1982). Surface properties of allophane, imogolite and halloysite. *Clays Clay Miner.*, *30*, 143-149.

Torres-Orozco, R., Cronin, S. J., Damaschke, M., & Pardo, N. (2017). Diverse dynamics of Holocene mafic-intermediate Plinian eruptions at Mt. Taranaki (Egmont), New Zealand. *Bulletin of Volcanology*, *79*(11), 1-27.

Trumbore, S. (2000). Age of soil organic matter and soil respiration: Radiocarbon constraints on belowground C dynamics. *Ecological Applications*, *10(2)*, 399–411.

Trumbore, S. E., Chadwick, O. A., & Amundson, R. (1996). Rapid exchange between soil carbon and atmospheric carbon dioxide driven by temperature change. *Science*, *272*(5260), 393–396. https://doi.org/10.1126/science.272.5260.393

Trumbore, S. E., & Czimczik, C. I. (2008). An uncertain future for soil carbon. *Science*, *321*(5895), 1455-1456.

Tucker, C. L., Bell, J., Pendall, E., & Ogle, K. (2013). Does declining carbon-use efficiency explain thermal acclimation of soil respiration with warming? *Global Change Biology*, 19, 252-263. 10.1111/gcb.12036

Trivedi, P., Wallenstein, M. D., Delgado-Baquerizo, M., & Singh, B. K. (2018). Microbial modulators and mechanisms of soil carbon storage. In B. K. Singh (Ed.), *Soil carbon storage: Modulators, mechanisms and modelling* (pp. 73–115). Academic Press. https://doi.org/10.1016/B978-0-12-812766-7.00003-2

Turner, M. B., Cronin, S. J., Bebbington, M. S., Smith, I. E. M., & Stewart, R. B. (2011). Integrating records of explosive and effusive activity from proximal and distal sequences: Mt. Taranaki, New Zealand. *Quaternary International*, *246*(1), 364–373. https://doi.org/10.1016/j.quaint.2011.07.006

van Gestel, N., Shi, Z., van Groenigen, K. J., Osenberg, C. W., Andresen, L. C., Dukes, J. S., Hovenden, M. J., Luo, Y., Michelsen, A., Pendall, E., Reich, P. B., Schuur, E. A. G., & Hungate, B. A. (2018). Predicting soil carbon loss with warming. *Nature*, *554*(7693), E4–E5. https://doi.org/10.1038/nature25745

van Groenigen, K. J., Qi, X., Osenberg, C. W., Luo, Y., & Hungate, B. A. (2014). Faster decomposition under increased atmospheric CO_2 limits soil carbon storage. *Science*, *344*(6183), 508–509. https://doi.org/10.1126/science.1249534

Wagai, R., Kajiura, M., Asano, M., & Hiradate, S. (2015). Nature of soil organo-mineral assemblage examined by sequential density fractionation with and without sonication: Is allophanic soil different? *Geoderma*, *241–242*, 295–305.

Wallenstein, M. D., Allison, S. D., & Bradford, M. A. (2010). Soil-carbon response to warming dependent on microbial physiology. *Nature Geoscience*, *3(5)*, 336–340.

Wallenstein, M. D., McMahon, S. K. S. J. (2009). Seasonal variation in enzyme activities and temperature sensitivities in Arctic tundra soils. *Global Change Biology*, *15*, 1631–1639.

Walker, T. W., Kaiser, C., Strasser, F., Herbold, C. W., Leblans, N. I., Woebken, D., ... & Richter, A. (2018). Microbial temperature sensitivity and biomass change explain soil carbon loss with warming. *Nature climate change*, *8*(10), 885-889.

Wang, T., Camps-Arbestain, M., & Hedley, C. (2016). Factors influencing the molecular composition of soil organic matter in New Zealand grasslands. *Agriculture, Ecosystems & Environment*, *232*, 290–301. https://doi.org/10.1016/j.agee.2016.08.016

Weil, R., & Brady, N. (2017). *The Nature and Properties of Soils. 15th ed*. Pearson Education.

Weissert, L. F., Salmond, J. A., & Schwendenmann, L. (2016). Variability of soil organic carbon stocks and soil CO_2 efflux across urban land use and soil cover types. *Geoderma*, *271*, 80–90. https://doi.org/10.1016/j.geoderma.2016.02.014

Wendt, J. W., & Hauser, S. (2013). An equivalent soil mass procedure for monitoring soil organic carbon in multiple soil layers. *European Journal of Soil Science*, *64*(1), 58–65. https://doi.org/10.1111/ejss.12002

West, T. O., & Post, W. M. (2002). Soil organic carbon sequestration rates by tillage and crop rotation. *Soil Science Society of America Journal*, *66*(6), 1930–1946. https://doi.org/10.2136/sssaj2002.1930

Wetterstedt, M. (2010). *Decomposition of soil organic matter of temperature and quality.* (Unpublished doctoral dissertation). Swedish University of Agricultural Science, Uppsala.

Whitehead, S. J. (1976). *Granulometric studies on selected tephra eruptions, North Island, New Zealand.* Dissertation, Massey University, Palmerston North, New Zealand.

Wiesmeier, M., Urbanski, L., Hobley, E., Lang, B., von Lützow, M., Marin-Spiotta, E., van Wesemael, B., Rabot, E., Ließ, M., Garcia-Franco, N., Wollschläger, U., Vogel, H.-J., & Kögel-Knabner, I. (2019). Soil organic carbon storage as a key function of soils – A review of drivers and indicators at various scales. *Geoderma*, *333*, 149–162. https://doi.org/10.1016/j.geoderma.2018.07.026

Woo, S. H., Enders, A., & Lehmann, J. (2016). Microbial mineralization of pyrogenic organic matter in different mineral systems. *Organic Geochemistry*, 98, 18-26.

Woolf, D., & Lehmann, J. (2019). Microbial models with minimal mineral protection can explain long-term soil organic carbon persistence. *Scientific Reports*, *9*(1), 1–8. https://doi.org/10.1038/s41598-019-43026-8

World Reference Base. (2015). *World reference base for soil resources 2014 International soil classification system*. FAO.

World Reference Base for Soil Resources. (2015). World reference base for soil resources, update 2015. World Soil Resources Reports No. 106.FAO.

Xu, W., Yuan, W., Cui, L., Ma, M., & Zhang, F. (2019). Responses of soil organic carbon decomposition to warming depend on the natural warming gradient. *Geoderma*, *343*, 10–18. https://doi.org/10.1016/j.geoderma.2019.02.017

Yuan, G., Theng, B. K. G., Parfitt, R. L., & Percival, H. J. (2000). Interactions of allophane with humic acid and cations. *European Journal of Soil Science*, *51*(1), 35–41. https://doi.org/10.1046/j.1365-2389.2000.00295.x

Zernack, A. V., Cronin, S. J., Neall, V. E., & Procter, J. N. (2011). A medial to distal volcaniclastic record of an andesite stratovolcano: Detailed stratigraphy of the ring-plain succession of south-west Taranaki, New Zealand. *International Journal of Earth Sciences*, *100*(8), 1937–1966. https://doi.org/10.1007/s00531-010-0610-6

Zernack, A. V., Procter, J. N., & Cronin, S. J. (2009). Sedimentary signatures of cyclic growth and destruction of stratovolcanoes: A case study from Mt. Taranaki, New Zealand. *Sedimentary Geology*, *220*(3), 288–305. https://doi.org/https://doi.org/10.1016/j.sedgeo.2009.04.024

Zhang, Y., Cao, K.-F., & Goldstein, G. (2013). Winter photosynthesis of evergreen broadleaf trees from a montane cloud forest in subtropical China. In: T. Kuang, C. Lu, & L. Zhang (Eds.), *Photosynthesis Research for Food, Fuel and the Future* (pp. 812–817). Advanced Topics in Science and Technology in China. Springer. https://doi.org/10.1007/978-3-642-32034-7-173

Zheng, Z. M., Yu, G. R., Fu, Y. L., Wang, Y. S., Sun, X. M., & Wang, Y. H. (2009). Temperature sensitivity of soil respiration is affected by prevailing climatic conditions

and soil organic carbon content: A trans-China based case study. *Soil Biology and Biochemistry*, *41*(7), 1531-1540.

Zhou, T., Shi, P., Hui, D., & Luo, Y. (2009). Global pattern of temperature sensitivity of soil heterotrophic respiration (Q10) and its implications for carbon-climate feedback. *Journal of Geophysical Research: Biogeosciences*, *114*(G2).

Zhu, Z., Piao, S., Myneni, R. B., Huang, M., Zeng, Z., Canadell, J. G., Ciais, P., Sitch, S., Friedlingstein, P., Arneth, A., Cao, C., Cheng, L., Kato, E., Koven, C., Li, Y., Lian, X., Liu, Y., Liu, R., Mao, J., … Zeng, N. (2016). Greening of the Earth and its drivers. *Nature Climate Change*, 6(8), 791–795. https://doi.org/10.1038/nclimate3004

Zimmermann, M., & Bird, M. I. (2012). Temperature sensitivity of tropical forest soil respiration increase along an altitudinal gradient with ongoing decomposition. *Geoderma*, 187–188, 8–15. https://doi.org/https://doi.org/10.1016/j.geoderma.2012.04.015

Zimmermann, M., Meir, P., Bird, M. I., Malhi, Y., & Ccahuana, A. J. Q. (2009). Climate dependence of heterotrophic soil respiration from a soil-translocation experiment along a 3000 m tropical forest altitudinal gradient. *European Journal of Soil Science*, *60*(6), 895–906. https://doi.org/10.1111/j.1365-2389.2009.01175.x

Zsolnay, A. (1996). Dissolved humus in soil waters. In *Humic substances in terrestrial ecosystems* (pp. 171-223). Elsevier Science BV.

Ziegler, S. E., Benner, R., Billings, S. A., Edwards, K. A., Philben, M., Zhu, X., & Laganière, J. (2017). Climate warming can accelerate carbon fluxes without changing soil carbon stocks. *Frontiers in Earth Science*, *5*, 2.

Appendix IV. Statement of contribution doctorate with publications/manuscripts

MASSEY UNIVERSITY
GRADUATE RESEARCH SCHOOL

STATEMENT OF CONTRIBUTION
DOCTORATE WITH PUBLICATIONS/MANUSCRIPTS

We, the candidate and the candidate's Primary Supervisor, certify that all co-authors have consented to their work being included in the thesis and they have accepted the candidate's contribution as indicated below in the *Statement of Originality*.

Name of candidate:	Idri Hastuty Siregar
Name/title of Primary Supervisor:	Marta Camps-Arbestain/Prof. Dr
Name of Research Output and full reference:	
In which Chapter is the Manuscript /Published work:	Chapter 3
Please indicate:	
• The percentage of the manuscript/Published Work that was contributed by the candidate:	70%
and	
• Describe the contribution that the candidate has made to the Manuscript/Published Work:	
The candidate, chief supervisor and co-supervisors designed the experiments. The candidate conducted the experiments, and data analysis with assistance of Dr. Joeri Kaal. Soil Soil sampling and incubation were carried out in collaboration with	
For manuscripts intended for publication please indicate target journal:	
Geoderma	
Candidate's Signature:	Idri Hastuty Siregar Digitally signed by Idri Hastuty Siregar Date: 2023.01.23 15:14:17 +13'00'
Date:	January 23, 2023
Primary Supervisor's Signature:	Marta Camps Arbestain Digitally signed by Marta Camps Arbestain Date: 2023.01.27 11:39:32 +01'00'
Date:	

(This form should appear at the end of each thesis chapter/section/appendix submitted as a manuscript/ publication or collected as an appendix at the end of the thesis)

MASSEY UNIVERSITY
GRADUATE RESEARCH SCHOOL

STATEMENT OF CONTRIBUTION
DOCTORATE WITH PUBLICATIONS/MANUSCRIPTS

We, the candidate and the candidate's Primary Supervisor, certify that all co-authors have consented to their work being included in the thesis and they have accepted the candidate's contribution as indicated below in the *Statement of Originality*.

Name of candidate:	Idri Hastuty Siregar
Name/title of Primary Supervisor:	Marta Camps-Arbestain/Prof. Dr
Name of Research Output and full reference:	
In which Chapter is the Manuscript /Published work:	Chapter 4
Please indicate:	
• The percentage of the manuscript/Published Work that was contributed by the candidate:	70%
and	
• Describe the contribution that the candidate has made to the Manuscript/Published Work:	
The candidate, chief supervisor and co-supervisors designed the experiments. The candidate conducted the experiments, and data analysis with assistance of Dr. Joeri Kaal. Soil Soil sampling and incubation were carried out in collaboration with	
For manuscripts intended for publication please indicate target journal:	
Biogeochemistry	
Candidate's Signature:	Idri Hastuty Siregar Digitally signed by Idri Hastuty Siregar Date: 2023.01.23 15:14:17 +13'00'
Date:	January 23, 2023
Primary Supervisor's Signature:	Marta Camps Arbestain Digitally signed by Marta Camps Arbestain Date: 2023.01.27 11:40:09 +01'00'
Date:	

(This form should appear at the end of each thesis chapter/section/appendix submitted as a manuscript/ publication or collected as an appendix at the end of the thesis)

MASSEY UNIVERSITY
GRADUATE RESEARCH SCHOOL

STATEMENT OF CONTRIBUTION
DOCTORATE WITH PUBLICATIONS/MANUSCRIPTS

We, the candidate and the candidate's Primary Supervisor, certify that all co-authors have consented to their work being included in the thesis and they have accepted the candidate's contribution as indicated below in the *Statement of Originality*.

Name of candidate:	Idri Hastuty Siregar
Name/title of Primary Supervisor:	Marta Camps-Arbestain/Prof. Dr
Name of Research Output and full reference:	
In which Chapter is the Manuscript /Published work:	Chapter 5
Please indicate:	
• The percentage of the manuscript/Published Work that was contributed by the candidate:	60%
and	
• Describe the contribution that the candidate has made to the Manuscript/Published Work:	
The candidate, chief supervisor and co-supervisors designed the experiments. The candidate conducted the experiments, and data analysis with assistance of Dr. Joeri Kaal. Soil Soil sampling and incubation were carried out in collaboration with	
For manuscripts intended for publication please indicate target journal:	
Global Change Biology	
Candidate's Signature:	Idri Hastuty Siregar Digitally signed by Idri Hastuty Siregar Date: 2023.01.23 15:14:17 +13'00'
Date:	January 23, 2023
Primary Supervisor's Signature:	Marta Camps Arbestain Digitally signed by Marta Camps Arbestain Date: 2023.01.27 11:40:39 +01'00'
Date:	

(This form should appear at the end of each thesis chapter/section/appendix submitted as a manuscript/ publication or collected as an appendix at the end of the thesis)